Influence of Composition on Structure and Caesium Volatilisation from Glasses for HLW Confinement

Benjamin Graves Parkinson
B.Sc. (Hons.), M.Sc.

A thesis submitted to the University of Warwick in partial fulfilment of
the requirement for the degree of Doctor of philosophy

Department of Physics November 2007

Contents

List of Figures

Chapter 2

Chapter 3

Chapter 4

Chapter 5

Chapter 6

Chapter 7

Chapter 8

Chapter 9

List of Tables

Chapter 2

Chapter 4

Chapter 6

Chapter 7

Chapter 8

Abbreviations

AS	Asymmetric
BO	Bridging Oxygen
CRN	Continuous Random Network
DTA	Differential Thermal Analysis
EDX	Energy Dispersive analysis of X-rays
HLW	High Level Waste
HT	High Temperature NMR
LLW	Low Level Wastes
LNB	Lithium-Sodium Borosilicate
MAS	Magic Angle Spinning
MRO	Medium-Range Order
MQ	Multiple Quantum
NBO	Non-Bridging Oxygen
ND	Neutron Diffraction
NMR	Nuclear Magnetic Resonance
NNN	Next Nearest Neighbours
R_2O	Alkali Oxide
REDOR	Rotational Double Echo
RF	Radio Frequency
RS	Raman Spectroscopy
S	Symmetric
SNF	Spent Nuclear Fuel
SRO	Short-Range Order
STA	Simultaneous Thermal/Thermogravimetric Analysis
TGA	Thermogravimetric Analysis
VHLW	Vitrified High Level Waste
XRD	X-ray Diffraction

Acknowledgments

I would like to express my thanks to the many people who have assisted both during the course of this PhD and in helping me get to the position of doing a PhD. I am particularly grateful to the following people:-

My supervisor Dr Diane Holland has been a great help, showing amazing patience and encouragement throughout all stages of my work over the last four years. I could not have found a better supervisor and it has been a pleasure working for her. Without Diane's belief and offering of an MSc place four years ago this PhD would not have been possible for me. At this stage therefore I must also thank Professor Pam Thomas for helping to arrange and continue my career in physics here at Warwick University. I would like to thank Mr Charlie Scales and Nexia Solutions for the financial assistance and help.

Many thanks go out to Professor Mark Smith, Dr Andrew Howes, Professor Ray Dupree and the remainder of the Warwick NMR group for their support and guidance. Notable thanks should also go to Dr Alan Wong for his continual help with the Oxygen-17 NMR work in this study and to Mr Thomas Kemp for his unlimited assistance whenever I had 'NMR issues'. I also owe a great deal of thanks to the following technicians who have contributed to much of my PhD work; Mr Keith Briggs, Mr Dave Hammond, Mr Martin Davis, Mr Dan Lee and Mr Steve York. Thank you to Dr Mark Newton and Mr Robin Cruddace of the Warwick Diamond Group for the use of the Raman spectrometer. I am grateful to the remaining members of the Glass-Ceramics and Crystallography groups, most notably Miss Emma Barney, Mr Robin Orman and Mr Dean Keeble for managing to share an office with me!

I would like to thank the various members of my family who have supported my academic ambitions from the very beginning. Being from a family with a limited academic history my desire to become Dr Parkinson could easily have been questioned but I could not have wished for a more supportive family. Throughout all the trials of getting into this position they have always stood by and supported every single decision I have made.

Last but not least, I would like to thank my wife Kate for all her encouragement, help and support from day one of us being together. Without Kate at my side my PhD career would not have been half as successful and enjoyable and because of this she deserves a doctoral title of her own.

Declaration

The work for this thesis was carried out in the Department of Physics at the University of Warwick. The work was completed during the period from October 2004 to September 2007 and, except where specifically acknowledged in the text, is the result of my own independent research and has not been previously submitted at the University of Warwick, or any other institution, in respect of a higher degree. Parts of this thesis have been published or submitted for publication with the following references:

- *The effect of oxide additions on medium-range order structures in borosilicate glasses*, **B G Parkinson**, D Holland, M E Smith, A P Howes & C R Scales, J. Phys.: Condens. Matter **19** (2007)

- *Effect of minor additions on structure and volatilisation loss in simulated nuclear borosilicate glasses*, **B G Parkinson**, D Holland, M E Smith, A P Howes & C R Scales, J. Non-Cryst. Solids, 353 (2007) 4076-4083

- *Quantitative measurements of Q^3 species in silicate and borosilicate glasses using Raman Spectroscopy*, **B G Parkinson**, D Holland, M E Smith, C Larson, J Doerr, M Affatigato, S A Feller, A P Howes & C R Scales, J. Non-Cryst. Solids, (2007) *In-Press.*

The abstracts to each of these publications can be found in Appendix A. It is anticipated that further parts of this thesis will be submitted for publication in due course.

November 2007

Date

B. G Parkinson

Abstract

The problem of high-temperature volatilisation of material from alkali borosilicate glasses, commonly used for the long-term storage of high-level nuclear waste, has been investigated using four mixed-alkali borosilicate glass systems. Each system is based on the mixed alkali borosilicate base-glass (MW) used in the UK and USA, initially being doped with one of three simulated waste oxides in varying quantities; aluminium oxide (0.95 mol%), lanthanum oxide (1.68 mol%) or magnesium oxide (2.55 or 10.2 mol%), before increasing quantities of caesium oxide were added (0-9.66 mol%) [1].

A number of experimental techniques have been employed in this study, including various thermal analysis measurements, nuclear magnetic resonance (MAS NMR) and Raman spectroscopy. From boron-11 and silicon-29 MAS NMR measurements, the fraction of tetrahedral boron (N_4) and silicon Q^3 and Q^4 units (with respective three- and four-bridging oxygen) were resolved and compared against theory [2] and previous experimental measurements [3-6]. Silicon Q^3 fractions resolved from NMR measurements [1] were compared against values obtained from quantitative Raman spectroscopy [7]. This approach is shown to be successful in resolving silicon Q^3 units and therefore would be particularly useful in studies where the presence of large (> 1 mol%) quantities of paramagnetic species in glasses makes NMR difficult. Further detail resolved in the ^{11}B MAS NMR spectra of these glasses also enabled the fraction of reedmergnerite and danburite medium-range order structures to be calculated [8]. The volatilisation of alkali borate and alkali silicate material, identified using EDX measurements, is shown not only to increase as a function of the fraction of Q^3 units but is also affected by the presence of these medium-range order structures, where increasing quantities of danburite units leads to a greater degree of volatility [4,8].

Finally, a number of ^{17}O-enriched mixed-oxide alkali borosilicate systems have been manufactured, using an ^{17}O-enriched silicon oxide precursor obtained through an established hydrolysis reaction of 20% oxygen-17 enriched water with silicon tetrachloride [9]. Subsequent thermal analysis and NMR measurements have shown the oxygen-17 environments of these borosilicate systems to vary significantly

based on the presence of caesium, aluminium or lanthanum in quantities realistic to the modified mixed-alkali borosilicate glasses in the remainder of this study.

[1] B. G. Parkinson, D. Holland, M. E. Smith, A. P. Howes, and C. R. Scales, *J. Non-Cryst. Solids* **353** (2007) 4076-4083.

[2] W. J. Dell, P. J. Bray, and S. Z. Xiao, *J. Non-Cryst. Solids* **58** (1983) 1-16.

[3] G. El-Damrawi, W. Muller-Warmuth, H. Doweidar, and I. A. Gohar, *Phys. Chem. Glasses* **34** (2) (1993) 52-57.

[4] B. G. Parkinson, D. Holland, M. E. Smith, A. P. Howes, and C. R. Scales, *J. Non-Cryst. Solids* **351** (2005) 2425-2432.

[5] J. M. Roderick, *PhD Thesis, Warwick University* (2001).

[6] A. Duddridge, *PhD Thesis, Warwick University* (2004).

[7] B. G. Parkinson, D. Holland, M. E. Smith, C. Larson, J. Doerr, M. Affatigato, S. A. Feller, A. P. Howes, and C. R. Scales, *J. Non-Cryst. Solids* **Accepted, awaiting publication** (2007).

[8] B. G. Parkinson, D. Holland, M. E. Smith, A. P. Howes, and C. R. Scales, *J. Phys.: Condens. Matter* **19** (2007).

[9] J. A. Abys, D. M. Barnes, S. A. Feller, G. B. Rouse, and W. M. Risen Jnr, *Material Research Bulletin* **15** (1980) 1581-1587.

Chapter 1

1 Introduction

1.1 Overview

The use, over the last 50 years, of nuclear energy in both civil power stations and military installations has presented a major problem in the long-term storage of solid and liquid high level nuclear waste (HLW) [1,2]. Currently this waste is stored in government facilities awaiting a more permanent storage solution, with one such solution being for HLW to be stored within glass matrices capable of withstanding the various physical, chemical and radiological complexities that HLW presents [3,4].

A range of possible storage mechanisms have been investigated with glass, glass-ceramics and cements being the main contenders to provide long-term containment solutions to a variety of HLW [5]. Currently, in the USA, France and the UK (BNFL Ltd), HLW is stored within a borosilicate glass network that is favoured over other alternatives because of its chemical and thermal properties, ease of processing and ability to hold large quantities of waste [6]. The process of HLW-glass containment involves calcined HLW being dissolved in molten glass and then being emptied into steel-lined canisters before long-term storage at a geologically safe site.

Although this is a successful storage method, a number of problems remain in the processing technique. One of these, on which this study aims to improve our understanding, is the evaporation of a radioactive caesium-137-containing gas from the HLW-glass melt which then condenses on vents and surrounding outlets [7-15].

1.2 Aim of the work

Although complex in its task, this study will develop our understanding of the thermal and structural origins of caesium-133 volatility in the glass melt. Work carried out prior to this study by the author, on a mixed alkali caesium-sodium-lithium borosilicate glass composition, produced a number of interesting results on changes in structural and thermal character as a function of increasing caesium oxide content [9,16]. Although useful, the glass system used in the initial study was comparatively simple, containing only five oxide components, comparable to other HLW-borosilicate glass systems studied previously by the Warwick Glass-Ceramics group [17-19] with a variety of different nuclear waste simulant additives, to investigate changes in glass structure and corrosion resistance. None of the studies however used caesium oxide as an additive so this study will also expand on previous work by its inclusion into the composition.

By consideration of the complex composition of HLW, three oxides, thought to be important to the volatility problem, were selected to improve the realistic nature of the study, through their significant molar percent contributions to the BNFL waste-form. Those chosen were MgO (in two different starting quantities), Al_2O_3 and La_2O_3. This study therefore will be on four simulated BNFL base-glasses, doped with an initial quantity of MgO, Al_2O_3 or La_2O_3, before adding a range of caesium oxide contents (0-9.66 mol%) to observe the affect which this has on glass volatility.

Multinuclear magic angle spinning nuclear magnetic resonance (MAS NMR), Raman spectroscopy, X-ray diffraction (XRD), and a range of thermal analysis techniques (including differential thermal and thermo-gravimetric analysis) will be used to look at the structural and thermal characteristics of the glass compositions, as a function of a range of caesium oxide content.

Raman spectroscopy will be used to identify structural groups in the range of borosilicate glasses and also to obtain a quantitative measure of the fractions of silicon units, complementary to those obtained from silicon-29 MAS NMR. Although of limited use in previous studies on glasses [20], if successful, this Raman-based approach would be invaluable in the nuclear industry for quantitative structural measurements on borosilicate glasses, which contain large (> 1 mol%) quantities of paramagnetic oxides which significantly affect the ability to use NMR for structural measurements.

Furthering the scope of study, a range of oxygen-17 enriched borosilicate glasses will be made, primarily to study how the combinations of aluminium oxide, lanthanum oxide and magnesium oxide affect glass structure and thermal characteristics and therefore may affect volatility. A body of oxygen-17 work on silicate and borosilicate glasses exists already in the literature [21-26] and this study aims both to refer to that work in order to understand the results obtained and to develop the knowledge base further.

Overall, the aim of this work is three-fold;

- Primarily to identify changes in volatilisation and structure as a function of composition, as well as identifying the oxides present in the volatile phases formed.
- Use of Raman spectroscopy quantitatively on borosilicate glasses to measure the fraction of silicon Q^n units.
- Study of a range of oxygen-17 enriched borosilicate compositions to increase our understanding of the link between volatilisation and borosilicate glass structure, primarily using ^{17}O MAS NMR.

Thesis Structure

This thesis consists of nine chapters, the contents of which are outlined in this section to give an indication of the direction of the work.

Chapter 2 presents the current theory and operation of HLW vitrification highlighting the processes used and an outline of the different storage materials used in industry. The chapter concludes by introducing the problem of material volatilisation, which is central to this study.

Chapter 3 is a review of the theory of glass structure, including models of borosilicate, borate and silicate glasses. This will include previous studies on the structural and physical properties of the glasses.

Chapter 4 outlines the different theory and practice related to the preparation of glass samples and their characterisation using X-ray diffraction (XRD) and thermal analysis techniques.

Chapter 5 introduces theory relating to the experimental techniques used for structural characterisation of the glasses in this study, such as nuclear magnetic resonance and Raman spectroscopy.

Chapter 6 presents results and discussion concerning the preparation of all the standard, non-^{17}O enriched, borosilicate glasses, their characterisation through the use of XRD and thermal analysis techniques - including differential thermal analysis (DTA and STA) and volatilisation mass-loss measurements, to measure the relative volatility of all the glass compositions.

Chapter 7 presents results and discussion related to structural information from the non-^{17}O enriched borosilicate glasses, obtained from density measurements, nuclear magnetic resonance spectroscopy and Raman spectroscopy.

Chapter 8 outlines and discusses all the results collected on the oxygen-17 enriched borosilicate compositions. This will include both characterisation measurements and structural measurements in this single chapter.

Chapter 9 presents overall discussion and conclusions from the experimental work and suggests possibilities for future work on borosilicates.

Note: References will be provided at the end of each chapter.

1.3 References

[1] J. F. Ahearne, *Physics Today* (June Issue) (1997) 24-29.

[2] W. E. Kastenberg and L. J. Gratton, *Physics Today* (1997) 41-46.

[3] A. M. Bevilacqua, N. B. Messi de Bernasconi, D. O. Russo, M. A. Audero, M. E. Sterba, and A. D. Heredia, *J. Nucl. Mater.* **229** (1996) 187-193.

[4] M. G. Mesko and D. E. Day, *J. Nucl. Mater.* **273** (1999) 27-36.

[5] I. W. Donald, B. L. Metcalfe, and R. N. J. Taylor, *J. Mater. Sci.* **32** (1997) 5851-5887.

[6] M. J. Plodinec, *Glass Technol.* **41** (6) (2000) 186-192.

[7] R. P. Tangri, V. Venugopal, D. K. Bose, and M. Sundaresan, *J. Nucl. Mater.* **167** (1989) 127-130.

[8] J. E. Antill, K. A. Peakall, and E. F. Smart, *J. Nucl. Mater.* **56** (1941) 47-60.

[9] B. G. Parkinson, *MSc Thesis, Warwick University* (2004).

[10] M. Asano, T. Kou, and Y. Mizuntani, *J. Non-Cryst. Solids* **112** (1989) 381-384.

[11] M. Asano, T. Kou, and Y. Yasue, *J. Non-Cryst. Solids* **92** (1987) 245-260.

[12] M. Asano and Y. Yasue, *J. Nucl. Mater.* **138** (1986) 65-72.

[13] M. Asano and Y. Yasue, *J. Nucl. Mater.* **151** (1988) 181-188.

[14] D. W. Bonnell, E. R. Plante, and J. W. Hastie, *J. Non-Cryst. Solids* **84** (1986) 268-275.

[15] V. Stolyarova, *J. Nucl. Mater.* **247** (1997) 7-10.

[16] B. G. Parkinson, D. Holland, M. E. Smith, A. P. Howes, and C. R. Scales, *J. Non-Cryst. Solids* **351** (2005) 2425-2432.

[17] J. M. Roderick, *PhD Thesis, Warwick University,* (2001).

[18] A. Duddridge, *PhD Thesis, Warwick University*, (2004).

[19] M. Islam, *PhD Thesis, Warwick University* (2005).

[20] P. McMillan, *Am. Mineral.* **69** (1984) 622-644.

[21] L.-S. Du and J. F. Stebbins, *J. Non-Cryst. Solids* **351** (2005) 3508-3520.

[22] L.-S. Du and J. F. Stebbins, *Solid State Nucl. Mag.* **27** (2005) 37-49.

[23] J. F. Stebbins, S. Zhao, S. K. Lee, and J. V. Oglesby, *J. Non-Cryst. Solids* **293-295** (2001) 67-73.

[24] J. F. Stebbins, J. V. Oglesby, and S. K. Lee, *Chem. Geol.* **174** (2001) 63-75.

[25] L.-S. Du and J. F. Stebbins, *J. Phys. Chem.* **B** (107) (2003) 10063-10076.

[26] L.-S. Du and J. F. Stebbins, *J. Non-Cryst. Solids* **315** (2003) 239-255.

Chapter 2

2 Immobilisation of High Level Nuclear Waste

2.1 Introduction

This chapter will give a relatively brief outline of the practices used in the nuclear industry for dealing with high-level nuclear waste (HLW) for long-term storage. Currently one of the most common methods for the containment of HLW is dissolution in a glass waste form, contained within suitable canisters for long-term storage. It also introduces the problem central to this study; the unwanted volatilisation of material during the vitrification of HLW.

2.2 High-Level Nuclear Waste

In the current climate of cost-effective, environmentally-friendly energy production, the use of nuclear energy has for a long time been a suggested alternative to carbon based methods. Its use on a large scale in the UK and USA though has however been constrained by the problem of having to immobilise the large stockpiles of high-level nuclear waste (HLW) that have already been produced over the previous 50 years, by commercial energy use and nuclear weapons development [1-6].

HLW is actually a by-product of the chemical separation of reusable “un-burnt” uranium and plutonium from *spent nuclear fuel* (SNF) which leaves waste fission products and minor actinides (e.g. Np and Am). Although minimal, the composition of HLW varies between different reactor types, fuel cells and operating conditions. The composition of calcined waste for a Magnox reactor is given in Table 2.1 [7]. Much of the world’s HLW is currently stored in liquid form which, although an accepted short-term solution, is not favourable because of the liquid’s mobile nature, which requires a high degree of maintenance. An improved long-term solution, based on solidification, is to immobilise the radionuclides for further repository storage [8]. It is these two difficult requirements that have been responsible for the lack of any significant development, investment and use of commercial nuclear power over recent years [1-6].

Oxide	Amount (Wt %)	Oxide	Amount (Wt %)
MoO_3	14.4	Sm_2O_3	2.6
ZrO_2	13.9	Rh_2O_3	2.2
Nd_2O_3	13.1	Y_2O_3	1.7
Cs_2O	9.4	TeO_2	1.6
CeO_2	8.5	Rb_2O	1.1
RuO_2	7.8	Pm_2O_3	0.5
BaO	4.6	Eu_2O_3	0.3
La_2O_3	4.2	Sb_2O_3	0.2
Pr_6O_{11}	4.0	Ag_2O	0.1
Te_2O_3	3.8	In_2O_3	0.1
PdO	3.3	Gd_2O_3	0.1
SrO	2.9		

Table 2.1 *Composition by weight % of calcined Magnox fission products [7].*

2.3 HLW Immobilisation

2.3.1 Introduction

The key requirement for the immobilisaton of radioactive materials, and HLW in particular, is that a solid, durable and stable material be formed to make storage and disposal easier than exposed liquid containment. HLW contains a number of highly active fission products such as ^{137}Cs and ^{92}Sr, and radionuclides with long half-lives such as ^{99}Tc and ^{129}I, with half-lives of 2×10^5 and 1×10^7 years respectively [9]. Because of this complex chemical makeup, the processing of the waste stream into a solid form must have three key properties; a low processing temperature – to prevent volatilisation of radionuclides, e.g. $^{137}Cs_2O$ (*cf.* Section 2.3.3), the ability to withstand water corrosion (*cf.* Section 2.4) and the ability to dissolve a range of different waste stream compositions of varying solubility [10-20].

Although an alkali borosilicate glass waste-form is the current choice for the storage of HLW, because of its adaptability towards different processing techniques and high chemical durability, it has by no means been the only glass investigated; phosphate and silicate glasses have also had significant testing [21-24] as well as a wide variety of other solid materials including ceramics and glass-ceramics [9,18,25-33]. Concretes and cements have been investigated and used mainly for the storage of low-level and intermediate-level wastes (LLW and ILW respectively). Originally chosen as the base-glass for HLW immobilisation, silicates were first used due to their high chemical durability but the high temperatures required (typically 1500^{o}C) to produce these materials were too great. Hence boron oxide was added to lower the melting temperature, down to ~1000^{o}C, without significantly affecting the glass network. Further additions of sodium oxide and lithium oxide were made to improve the solubility of the waste, up to ~30 wt%, into the glass network. It has also been found that borosilicate glasses with two, rather than one, alkali oxides, display greater chemical durability (the mixed alkali effect) [34]. A further benefit of using borosilicate glasses is that they are particularly resistant to the effects of radiation when in storage [35] and, importantly, remain thermally stable at the temperatures produced by radiogenic processes (~500^{o}C).

2.3.2 The Vitrification Process

In the UK, British Nuclear Fuels Ltd (BNFL) currently uses a continuous vitrification process (Figure 2.1). The chemical process of vitrification is dissolution, in which the base glass is effectively a solvent into which the HLW dissolves and contributes to the structure of the glass. Many of the constituents of HLW are nitrates, which require conversion into oxides before being able to dissolve into the base glass. Because of this the vitrification process can be carried out in one of two ways.

The first is a one-stage process whereby liquid HLW is fed directly into the melter with the base glass frit whereon the HLW is then dried to evaporate any nitric acid and other aqueous components. The nitrate compounds decompose at approximately 400^{o}C, with the resultant nitrogen oxide gases being released. The remaining residue is then in the form of oxides or salt-melts; this process is known as calcination [30,34,36]. After calcination the combination of residual materials is then fed through to the melter and then to eventual containment.

The second route available takes the option of thermally pre-treating the liquid HLW before it is added to the melter with the base-glass, at a temperature of between 900-1100^{o}C. It is this two-stage route which has been adopted by BNFL. At the end of both routes (after melting) the molten contents of the furnace are poured into canisters (Figure 2.2), typically stainless steel lined with a corrosion resistant overpack, and left to cool. The canisters are then sealed, decontaminated and taken for long-term repository storage in geologically safe sites [8,37].

For further details of the melter requirements and design and for the two process routes the following references are recommended [36,38,39].

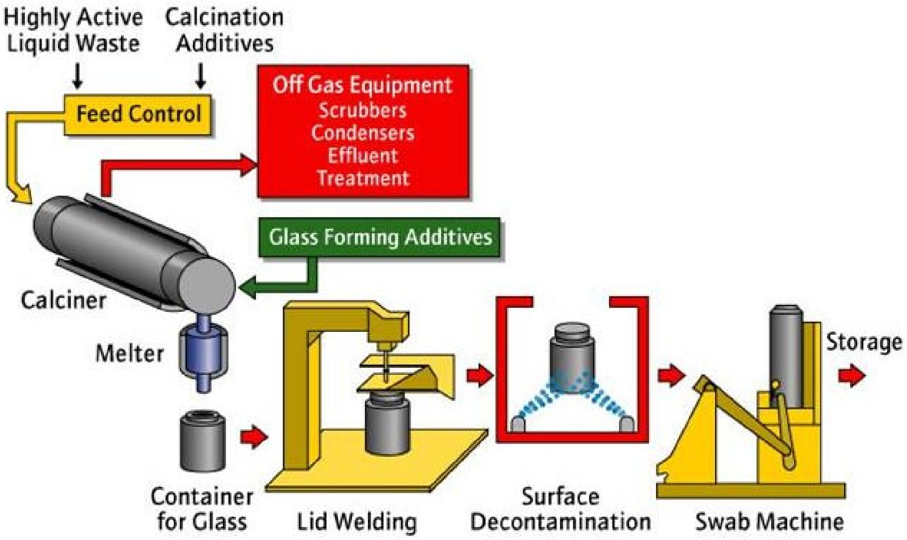

Figure 2.1 *The BNFL Ltd vitrification route [40].*

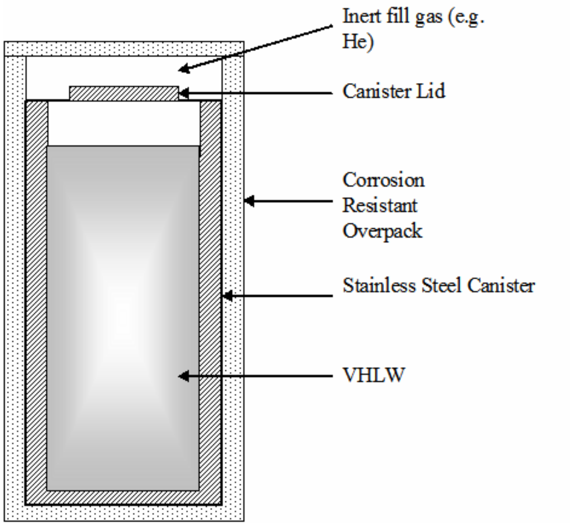

Figure 2.2 *Schematic of the stainless steel canister used for the storage of vitrified HLW [40].*

2.3.3 Volatilisation of Material at the Melt Stage

The problem which is central to this study concerns the issue of unwanted volatilisation of material at the stage where calcined-HLW is added to the melt. Because of the relatively high quantities (> 20 mol%) of Group I oxides, and particularly caesium oxide, within the composition of HLW, a degree of work on the behaviour of caesium within various aspects of nuclear operation has already been carried out by various groups [41-48]. Information from BNFL Ltd indicates that a caesium-containing gas evaporates from the melter at approximately 1000^{o}C, and condenses on vents and outlets around the plant.

Asano *et al.* [45-48] found that, for a variety of (relatively) simple binary and ternary Group I alkali borosilicate systems, with various R (where R is the molar ratio of total alkali oxide to boron oxide content) values (0.87-1.15) and K (where K is the molar ratio of silicon oxide to boron oxide content) value of 3.0, the vapour species which evolved at ~1000^{o}C varied depending on the alkali groups present. $CsBO_2$ and $Cs_2(BO_2)_2$ evolved when only caesium oxide was present in the glass composition, but $NaCs(BO_2)_2$ formed in addition when both caesium and sodium oxides were present. This confirmed the prediction made by Archakov *et al.* [49] that the volatile species were in the form of alkali di-borates.

The study by Bonnell *et al.* [50] on a more complicated glass system, containing a variety of different Group I, II alkali oxides, transition metals and trivalent oxides (Table 2.2) found that, throughout the temperature range 800-1150^{o}C, a similar range of volatile species were formed, including both Li^+, Cs^+ and Na^+, as well as sodium and lithium meta-borate ions. Contrary to prediction however, given the presence of RuO_2 and Re_2O_7 in the initial glass composition, Ru^+, RuO^+, RuO_3^+, RuO_4^+, Re^+, ReO^+, ReO_2^+, ReO_3^+ and $Re_2O_7^+$ were not found, even at high (~1500^{o}C) temperature measurements.

Further work by Stolyarova *et al.* [51], also looking at a simplified glass system, Cs_2O-B_2O_3-SiO_2 , with varying R values and fixed K ($0.11 \leq R \leq 0.83$, $K \sim 0.67$) showed that melts of all the glasses lead to the formation of meta-borate $CsBO_2$ (Cs_2O-B_2O_3) and meta-silicate Cs_2SiO_3 (Cs_2O-SiO_2) units. The vapour produced from the volatilisation of these glasses also contained caesium meta-borate (Cs_2O-B_2O_3), whose formation remained constant over the range of glass compositions analysed. It was proposed that the reaction occurring was that of (2.1);

$$CsBO_2\text{ (liquid) } \rightarrow CsBO_2\text{ (gas)} + Cs_2O \bullet 2BO_2\text{ (gas)} \qquad (2.1)$$

Oxide	Amount (Wt%)	Oxide	Amount (Wt%)
SiO_2	52.00	NiO	1.05
Fe_2O_3	12.96	CaO	1.59
Al_2O_3	4.86	MgO	0.68
B_2O_3	7.26	ZrO_2	0.70
Li_2O	5.10	SrO	0.09
Na_2O	10.13	RuO_2	0.09
Cs_2O	0.10	Re_2O_7	0.10
MnO_2	3.25		

Table 2.2 *Composition of the SNG-1 glass used in the volatilisation study by Bonnell et al. [50].*

A previous study by the author [52,53], took a different approach to those outlined above and focussed on the structural origins of the volatility problem, in a range of mixed-alkali, caesium-containing borosilicate glasses, with different caesium oxide contents ($0 < \text{mol\%}\ Cs_2O < 10$) using both thermal analysis techniques and structural measurements, such as NMR and Raman spectroscopy. This found a non-linear correlation between the mass-loss from the glass and the fraction of silicon Q^3 units (resolved from both ^{29}Si MAS NMR and Raman spectroscopy) as a function of caesium oxide concentration. None of the previous studies [41,45-47,49,50] had conducted any ^{11}B and/or ^{29}Si MAS NMR measurements, so the structural origin of the volatilisation of material at high temperature has not been fully explained. It must be noted that the previous study by the author [53] was not able to identify the exact composition of the volatile species, although EDX measurements indicated the presence of caesium, sodium, boron and silicon.

NMR carried out by Yun and Bray [54], showed that there was preferential association of Na^+ ions with the borate network, due to the free energy of formation of $NaBO_{2(s)}$ units being larger than half that of $Na_2OSiO_{2(s)}$ units. Therefore, volatilisation of Cs^+ and Na^+ ions was thought by Yun and Bray to arise from alkali borate species in the glass, rather than alkali silicate units, since the vapour pressures over the former would be much greater than over the sodium meta-silicate units. The paper also stated that the dissociation of sodium meta-borate is preferred to caesium meta-borate.

Another problem, not addressed in this thesis, with ^{137}Cs-containing HLW is that, due to its high flux of radiation, a large amount of heat is produced in the glass, limiting the loading if the glass transition temperature is not to be exceeded.

2.4 Chemical Durability of Glasses Containing HLW Oxides

The effects of the long-term storage of nuclear waste, whether it be LLW, ILW or HLW, is one of the core concerns in the development and improvement of storage materials [29]. Many factors contribute to this issue, including radiation damage to canisters [35,55-57], pressure, temperature and waste corrosion induced changes to structure [10,42] and finally effects on storage materials of exposure to environmental chemicals, such as water [12,19,30,58-63].

Water corrosion is a highly ranked concern in relation to long-term waste storage, specifically when vitrified waste is stored in geographic locations where it is predicted that exposure to aqueous liquids may occur over the course of 10^4-10^6 years [12,19,30,58-61]. Experimental measurements of aqueous corrosion are complicated, not just by the large timescales over which experiment is required to predict, but also by the wide range of oxide components in different waste streams. This has therefore required studies on simplified glass compositions. The publication by Calestani *et al.* [19] describes the effects that Cs_2O, SrO, U_3O_8 and ZnO all have on leaching (i.e. selected Group I/II and actinide oxides), when vitrified in a common alkali borosilicate base-glass. Work carried out by the Warwick Glass-Ceramics Group, by Roderick, Duddridge and Islam [64-66] also reported leaching of various HLW-simulated borosilicate glasses, including the base-glass MW (Table 2.3), with varying R (the molar ratio of total alkali oxide content to boron oxide content) and K (the molar ratio of silicon oxide to boron oxide) values, MW containing trivalent oxides (Al_2O_3, La_2O_3, Bi_2O_3 and Fe_2O_3) and divalent oxides (CaO, SrO, BaO, ZnO and PbO).

	mol% Na_2O	mol% Li_2O	mol% B_2O_3	mol% SiO_2
MW	10.53	10.29	18.57	60.61

Table 2.3 *Composition of the base-glass MW.*

These studies all used the International Standard Leach Test Procedure (outlined in Chapter 4) which analyses sample weight, leaching of material from glass to water and pH changes over a period of 14 days of exposure to water at 100°C. Roderick [64] showed that chemical resistance of the MW glass was greatly increased by the addition of as little as 2.42 mol% La_2O_3. This result was also observed by Duddridge [65] with the further introduction of either Al_2O_3, Bi_2O_3, Fe_2O_3 and La_2O_3, to the MW system. Measurements of leached material (Na and Li) in the water revealed the amount of sodium and lithium decreased to approximately 5 mg/L, with trivalent oxide levels of > 2 mol%. Sample weight loss was also found to decrease exponentially to 2 %, at similar trivalent oxide contents (Figure 2.3 and Figure 2.4).

Islam's study found that chemical durability decreased upon the addition of BaO, SrO and CaO, with weight-loss increasing as a function of oxide content (Figure 2.5) but decreasing with addition of ZnO and PbO.

It is to be expected that, although the systems in the present study contain additions of Al_2O_3, La_2O_3 or MgO, overall leaching effects are going to be dominated by the presence of Group I alkali oxides, in particular caesium oxide, since the total molar contribution of the Group I oxides is much greater than any of the three additives (20-30 mol% alkali oxide content, compared to ~1-3 mol% additive oxide).

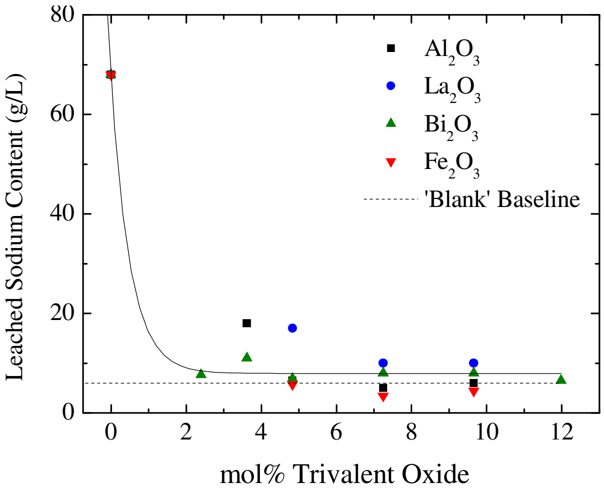

Figure 2.3 *Leached sodium content (g/L) from the range of trivalent oxide MW glasses [65].*

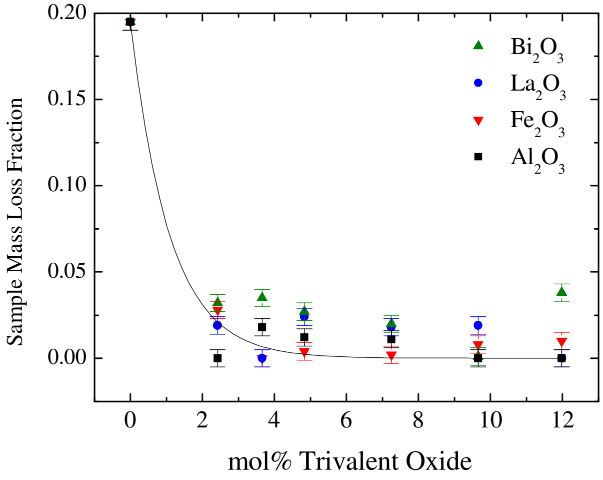

Figure 2.4 *Mass loss (fraction) as a function of trivalent oxide content (mol%) [65].*

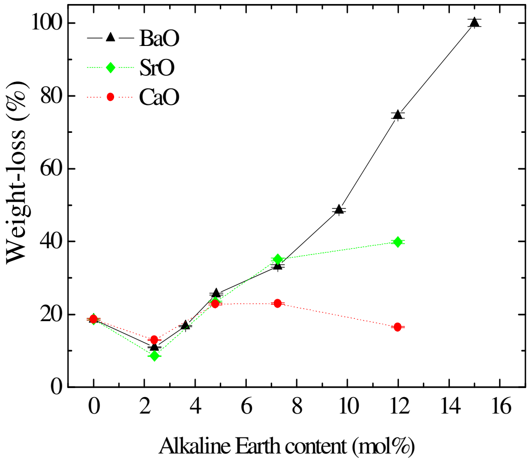

Figure 2.5 *Weight loss (%) of sample after 14 days of leach testing, as a function of alkaline earth content (mol%) [66].*

2.5 References

[1] J. F. Ahearne, *Physics Today* (June Issue) (1997) 24-29.

[2] C. McCombie, *Physics Today* (56-62) (1997).

[3] D. W. North, *Physics Today* (1997) 48-54.

[4] K. D. Crowley, *Physics Today* (June Issue) (1997) 32-39.

[5] F. L. Toth and H.-H. Rogner, *Energy Economics* **28** (2006) 1-25.

[6] S. M. Rashad and F. H. Hammad, *Appl. Energy* **65** (2000) 211-229.

[7] J. A. C. Marples, *Glass Technol.* **29** (6) (1988) 230.

[8] R. C. Ewing and A. Macfarlane, *Science* **296** (2002) 659-660.

[9] R. C. Ewing, *Proc. Natl. Acad. Sci. USA* **96** (1999) 3432-3439.

[10] J.-M. Gras, *C.R. Physique* **3** (2002) 891-902.

[11] B. Haijtink and A. Accary, 603-606.

[12] Y. Linard, T. Advocat, C. Jegou, and P. Richet, *J. Non-Cryst. Solids* **289** (2001) 135-143.

[13] E. S. Lyman, *Public Forum on High-Level Nuclear Waste and Reprocessing Nuclear Fuel Cycle Issues Research Group* (1996).

[14] O. Menard, T. Advocat, J. P. Ambrosi, and A. Michard, *Appl. Geo.* **13** (1998) 105-126.

[15] J. M. Roderick, D. Holland, and C. R. Scales, *Phys. Chem. Glasses* **41** (6) (2000) 392-396.

[16] J.-N. Cachia, X. Deschanels, C. D. Auwer, O. Pinet, J. Pailippou, C. Hennig, and A. Scheniost, *J. Nucl. Mater.* **352** (2006) 182-189.

[17] P. Hrma, J. D. Vienna, B. K. Wilson, T. J. Plaisted, and S. M. Heald, *J. Non-Cryst. Solids* **352** (2006) 2114-2122.

[18] L. L. Hench, D. E. Clark, and J. Campbell, *Nuclear and Chemical Waste Management* **5** (1984) 149-173.

[19] G. Calestani, A. Montenero, E. Ferraguti, G. Ingletto, and M. Bettinelli, *J. Non-Cryst. Solids* **84** (1986) 452-462.

[20] R. K. Mishra, P. Sengupta, C. P. Kaushik, A. K. Tyaki, G. B. Kale, and K. Raj, *J. Nucl. Mater.* **360** (2007) 143-150.

[21] Y. Shih, *Mater. Chem. Phys.* **80** (2003) 299-304.

[22] C. A. Click, R. K. Brow, and T. M. Alam, *J. Non-Cryst. Solids* **311** (2002) 294-303.

[23] S. Prabakar and K. T. Mueller, *J. Non-Cryst. Solids* **349** (2004) 80-87.

[24] T. Okura, T. Miyachi, and H. Monma, *J. Eur. Ceram. Soc.* (2005).

[25] J. Sheng, K. Choi, and M.-J. Song, *J. Nucl. Mater.* **297** (2001) 7-13.

[26] M. G. Mesko and D. E. Day, *J. Nucl. Mater.* **273** (1999) 27-36.

[27] M. J. Plodinec, *Glass Technol.* **41** (6) (2000) 186-192.

[28] P. Hrma, J. V. Crum, D. J. Bates, P. R. Bredt, L. R. Greenwood, and H. D. Smith, *J. Nucl. Mater.* (2005).

[29] I. W. Donald, B. L. Metcalfe, and R. N. J. Taylor, *J. Mater. Sci.* **32** (1997) 5851-5887.

[30] S. V. Raman, *J. Mater. Sci.* **33** (1998) 1887-1895.

[31] S. E. Ringwood, S. E. Kesson, N. G. Ware, W. O. Hibberson, and A. Major, *J. Geochem.* **13** (141) (1979).

[32] S. E. Ringwood, S. E. Kesson, N. G. Ware, W. O. Hibberson, and A. Major, *Nature* **278** (219) (1979).

[33] S. E. Ringwood, S. E. Kesson, N. G. Ware, W. O. Hibberson, and A. Major, *Immobilisation of U.S Defense waste using Synroc process*. (Plenum Press, New York, 1980).

[34] B. Luckscheiter and M. Nesovic, *Waste. Manage.* **16** (7) (1996) 571-578.

[35] D. R. Cousens and S. Myhra, *J. Non-Cryst. Solids* **54** (1983) 345-365.

[36] A. Woodall and J. Maillet, *Nuclear Engineering International* **32** (1987) 44.

[37] W. E. Kastenberg and L. J. Gratton, *Physics Today* (1997) 41-46.

[38] G. Roth and S. Weisenburger, *Nucl. Eng. Des.* **202** (2000) 197-207.

[39] W. Baehr, *IAEA Bulletin* **4** (1989) 43-46.

[40] B. N. F. L. (BNFL).

[41] R. P. Tangri, V. Venugopal, D. K. Bose, and M. Sundaresan, *J. Nucl. Mater.* **167** (1989) 127-130.

[42] J. E. Antill, K. A. Peakall, and E. F. Smart, *J. Nucl. Mater.* **56** (1941) 47-60.

[43] C. Madic, M. Lecomte, P. Baron, and B. Boullis, *Appl. Phys.* **3** (2002) 797-811.

[44] M. L. Lambregts and S. M. Frank, *Microporous and Mesoporous Materials* **64** (2003) 1-9.

[45] M. Asano, T. Kou, and Y. Mizuntani, *J. Non-Cryst. Solids* **112** (1989) 381-384.

[46] M. Asano, T. Kou, and Y. Yasue, *J. Non-Cryst. Solids* **92** (1987) 245-260.

[47] M. Asano and Y. Yasue, *J. Nucl. Mater.* **138** (1986) 65-72.

[48] M. Asano and Y. Yasue, *J. Nucl. Mater.* **151** (1988) 181-188.

[49] I. Y. Archakov, V. L. Stolyarova, and M. M. Shultz, *Rapid Communications in Mass Spectrometry* **12** (1998) 1330-1334.

[50] D. W. Bonnell, E. R. Plante, and J. W. Hastie, *J. Non-Cryst. Solids* **84** (1986) 268-275.

[51] V. L. Stolyarova, S. I. Lopatin, O. L. Belousova, and L. V. Grishchenko, *Glass. Phys. Chem.* **32** (1) (2006) 55-62.

[52] B. G. Parkinson, *MSc Thesis, Warwick University* (2004).

[53] B. G. Parkinson, D. Holland, M. E. Smith, A. P. Howes, and C. R. Scales, *J. Non-Cryst. Solids* **351** (2005) 2425-2432.

[54] Y. H. Yun and P. J. Bray, *J. Non-Cryst. Solids* **27** (1978) 363-380.

[55] M. O. Prado, N. B. Messi, T. S. Plivelic, I. L. Torriani, A. Bevilacqua, M., and M. A. Arribere, *J. Non-Cryst. Solids* **289** (2001) 175-184.

[56] W. Primak, *Nucl. Technol.* **60** (1982).

[57] L. W. Hobbs, F. W. Clinard, S. J. Zinkle, and R. C. Ewing, *J. Nucl. Mater.* **216** (1994) 291-321.

[58] H. Darwish, *Mater. Chem. Phys.* **69** (2001) 36-44.

[59] T. Akai, C. D., D. Masui, and T. Yazawa, *Glass Technol.* **44** (2) (2003) 71-74.

[60] G. Malow and W. Lutze, *J. Non-Cryst. Solids* **67** (1984) 305-321.

[61] P. K. Abraitis, F. R. Livens, J. E. Monteith, J. S. Small, D. P. Trivedi, D. J. Vaughan, and R. A. Wogelius, *Appl. Geo.* **15** (2000) 1399-1416.

[62] B. C. Sales, L. A. Boatner, H. Naramoto, and C. W. White, *J. Non-Cryst. Solids* **53** (1982) 201-226.

[63] H. Li and M. Tomozawa, *J. Non-Cryst. Solids* **195** (1996) 188-198.

[64] J. M. Roderick, *PhD Thesis, Warwick University* (2001).

[65] A. Duddridge, *PhD Thesis, Warwick University* (2004).

[66] M. Islam, *PhD Thesis, Warwick University* (2005).

Chapter 3

3 Glass Theory

3.1 Introduction

This chapter will outline the current theories of glass and glass formation as well as the structural theories developed from nuclear magnetic resonance (NMR), Raman spectroscopy (RS), thermal analysis studies and other selected diffraction studies of borate, silicate and borosilicate glasses.

3.2 Glass definition and properties – glass-forming oxides

For thousands of years the material known as glass has been used for numerous, ever more complex applications. Although silica has always been the most common ingredient of glasses, we now know of many different glass-forming oxides that can be cooled from a high temperature melt in such a way as to produce an amorphous material that cannot be described solely by its chemical composition.

No single theory is suitable for understanding both the physical and chemical nature of a particular glass, although a series of experimental techniques, namely X-ray and neutron diffraction, can be used to verify that a particular glass is amorphous with no long range atomic or molecular order (Figure 3.1). It is from this property that glasses can comfortably be compared to liquids which have been 'locked' into a solid state – a *supercooled liquid*. Obtaining this state and not one of a crystalline order can be explained through a thermodynamic diagram (Figure 3.2).

From Figure 3.2 we can understand the formation of a supercooled liquid through the speed at which a liquid melt cools from B to either C or E. If cooled slowly enough then the melt will begin to crystallize rapidly at T_m and reduce in volume discontinuously, following the route BCD. Alternatively, if the liquid is rapidly cooled (BE) the melt reduces in volume continuously and significantly less and takes the form of a supercooled liquid, before further cooling below the glass transition temperature (T_g) produces a glass (BEF).

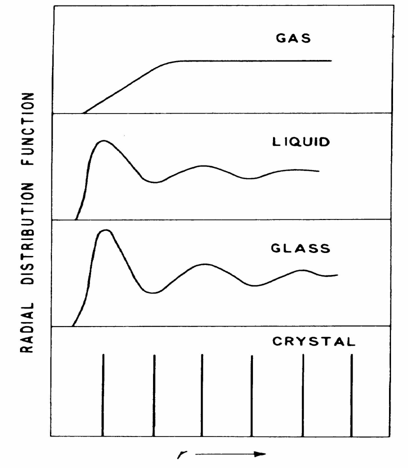

Figure 3.1 *Schematic comparing the degree of long range order, existing between a gas, liquid, glass and crystal [1].*

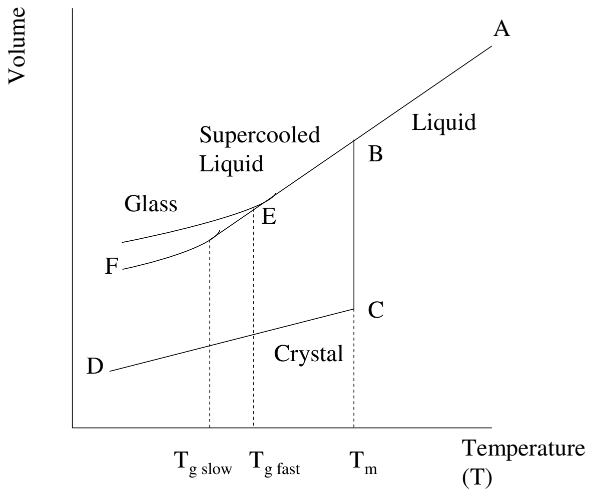

Figure 3.2 *Volume vs. Temperature thermodynamic diagram demonstrating the formation of a supercooled liquid and glass with respect to a crystal structure [1].*

Silica (SiO_2) was and is currently the most commonly used glass forming oxide and is the one which most people recognise as glass. As one of a series of partially covalent oxides ('*network formers*') silica (SiO_2), along with boron oxide (B_2O_3) and phosphorus oxide (P_2O_5), are glass formers by themselves or with other oxides. Oxides other than glass formers exhibit different behaviour.

- Modifiers: Cations forming highly ionic bonds with oxygen. They modify the glass network by breaking bonds, e.g. Group I and II metal oxides
- Intermediates: Cations with more than one ionic bond to oxygen, behaving somewhere in between a glass former and a modifier, e.g. Al_2O_3, La_2O_3, MoO_3. They can form glass when combined with a second component.

3.3 Simple Structural Theories and Observations of Glass Formation

3.3.1 Borates and Borosilicates Structural Theories

The theory which predicts the ability of a chemical composition to form a glass is imprecise, with only a set of rules and guidelines available to help predict glass formation from a liquid state. Much of the problem of finding a complete atomic theory rests in the fact that different compositions require different cooling rates to form a glass, and it is this which ultimately is the cause of the material's physical properties [2]. One of the first to try and find a complete theory was Goldschmidt (1926) with his suggestion that the cation-oxygen radius, r(A-O), was the dominant factor, with glass formation being easiest in the range $0.2 \leq r(A\text{-}O)\ \text{Å} \leq 0.4$ - with tetrahedral packing, favourable with this range of radii, being the key to glass formation. A variety of exceptions to this rule have shown this theory to be incomplete.

Zachariasen (1932) [3] showed that glass-forming silicate compositions possessed network type structures, with no long-range order, instead of the tetrahedral close-packed ones suggested by Goldschmidt. This brought forward the concept of the *continuous random network* (CRN) which contains identical structural units to the related crystalline forms but with random orientations. Zachariasen then proposed a set of rules that set the boundaries for glass formation, these are:

- No oxygen must be linked to more than two cations
- The number of oxygen atoms surrounding the cation must be small (~3-4)
- Oxygen polyhedra share only corners – not edges or faces
- At least three corners per oxygen polyhedron must be shared to form a continuous 3D network.

These are the generally accepted rules for glass formers, though with every rule-based theory exceptions to these rules do exist:

- Oxygen does not always have a coordination number of two
- Although silicon, phosphorus and boron all have co-ordinations of 3 or 4, tellurium, on the other hand has been observed to exist in a coordination of 6
- Certain glasses have networks describable by just 2 dimensions.

The study of glasses has been conducted for several hundred years but still a variety of un-answered questions remain. One of these problems concerns *the borate anomaly* and involves the non-linear relationships of density, acoustic velocity, thermal expansion and the glass transition temperature with content of a second oxide [4-6]. Observed in all alkali-borate glasses ($xR_2O(1-x)B_2O_3$, R: Li, Na, K, Rb, Cs) the borate anomaly has been investigated for a relatively short period, with papers dating back to only the 1960s [7]. This topic, including the structural origins for the anomaly, is discussed in detail in Section 3.4.1.

Borosilicate glasses, a combination of the two-glass forming oxides silica and boron oxide, provide a range of uses in industry. Examples include laboratory equipment, telescope mirrors and, of importance in this study, for the use in long-term storage of high level nuclear waste, due to their easy incorporation of waste radionuclides into their glass structure. Because of this final application, the study into the physiochemical properties of borosilicate glasses has required a wide variety of different experimental approaches, including NMR, thermal analysis techniques, XRD and Raman spectroscopy [8-14].

Research carried out by Roderick *et al.* [15], Plodinec [8], Duddridge [16] and Islam [17], into mixed oxide borosilicate glasses used for nuclear waste storage, focussed on the changes in boron and silicon coordination (*cf.* Sections 3.4.1 and 3.4.2), the glass transition temperature, density and chemical durability; all with respect to changes in alkali and waste simulant contents in the glass. The work by Duddridge [16] is useful in relation to the work in this study, since it focuses on the addition of aluminium oxide, and lanthanum oxide to the BNFL Ltd base glass, but in greater quantities to that found in high level nuclear waste (HLW). Boron and silicon coordination are important factors for caesium volatility (*cf.* Chapter 2), with possible links to the formation of borosilicate superstructural units within the glass (*cf.* Section 3.4.1).

3.3.2 Phase Separation in Glasses

Phase separation in glasses is a property which occurs when the thermodynamics of the glass permit the melt to exist as two separate viscous liquids. The nucleation of droplets of one phase within the matrix of another can be seen when the glass melt is cooled rapidly below its transition temperature (and the two liquids have a high viscosity). This effect can be observed in the solid state in one of two forms – *nucleation-growth or spinodal* (Figure 3.3), and it is this effect which is present in sodium borosilicate glasses at low alkali contents. The importance of phase separation in the solid state lies in the effect it has on the chemical degradation of the HLW mixed alkali borosilicate glasses, making them less chemically resistant over time. Hence, this is an important factor at the stage of selecting a glass composition for HLW vitrification.

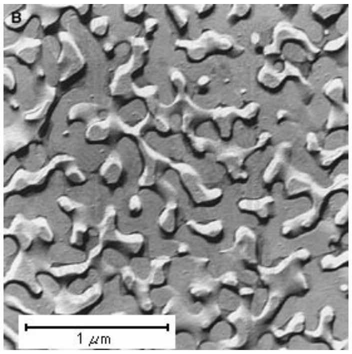

Figure 3.3 *Example of phase separation occurring in a glass [18].*

3.4 Multi-component Glass Theories

Glass structure is non-periodic over long ranges in contrast to that of a crystal. Since reproducible material can be produced, there must be, on some kind of scale, structure existing which is the root of the glass properties.

Physical and chemical reproducibility are vital to the function of borosilicate glasses as waste storage media, given the same starting chemical constituents and thermal history. In this study, the origin of the caesium volatility must be traced to some common structural origin. The identification of the various boron and silicon co-ordinations within a borosilicate glass is one step towards identifying this structure.

3.4.1 Borate Glass Theories – The N_4 Fraction, Superstructures and Multiple Four-Coordinated Boron sites

Boron can exist in five polyhedral units within a glass or crystal structure (Figure 3.4). For this study only the first three units are of any importance, with units f_1, f_2 and f_3 describing the symmetrical three coordinated, four-coordinated and asymmetrical three-coordinated boron units respectively. Addition of a modifier oxide (such as caesium oxide) changes ($B_{3\text{-symmetrical}}$) trigonal planar f_1 units with three bridging oxygen (BO) to charged tetrahedral (B_4) f_2, Further additions of modifier push the f_2 units back to three-coordinated f_3, f_4 and f_5 units with one, two and three non-bridging oxygens (NBOs) respectively.

- f_1 – symmetrical trigonal planar boron unit with all BOs
- f_2 – symmetrical tetrahedral boron unit with all BOs and one alkali ion
- f_3 – non-symmetrical trigonal planar with one NBO and one alkali associated with it
- f_4 – trigonal planar boron unit with two NBOs and two alkali ions
- f_5 – trigonal planar boron unit with three NBOs and three alkali ions.

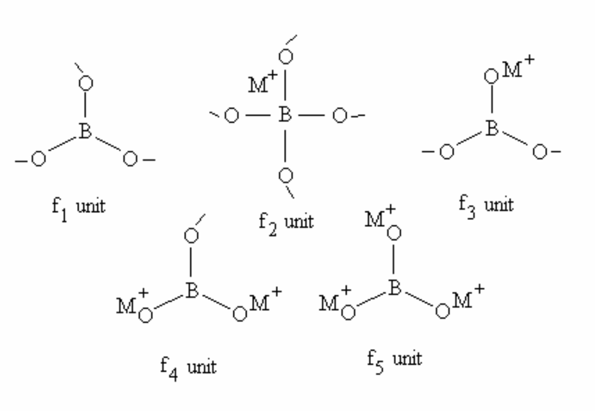

Figure 3.4 *The five possible borate units existing within an alkali borate or borosilicate glass.*

One important factor in the study of the structure of borosilicate glasses is the change in boron coordination with increasing alkali content in the glass. Boron can form two co-ordinations - [BO_3] and [BO_4] - and, in alkali borate glasses, N_4, the ratio of [BO_4] tetrahedrally coordinated boron units to the total amount of borate units in the glass is observed to reach a maximum at a specific concentration of alkali. N_4 was first determined by Silver and Bray [19] using NMR in 1963. They observed a maximum in N_4 at ~30 mol% alkali oxide. The study of N_4 fraction and its dependence on the alkali content is still under investigation and, 30 years later, Clarida *et al.* [4] in 2003, were still trying to determine whether N_4 is dependent on the type of alkali modifier in the glass, with their results suggesting that N_4 is independent of alkali type. The value and temperature dependence [20] of N_4 is also an important consideration in the physics of the mixed-alkali borosilicate glasses since the physical properties - thermal expansion, transition temperature, density and thermal conductivity are dominated by it (*the "borate anomaly"*). Initially two models (Figure 3.5) for N_4 were proposed, with Silver and Bray [19] in 1963 being the first to put forward a quantitative description and then later Beekenkamp [21] in 1966, proposing an alternative theory based on the x/(1−x) form. The origin of this arises from the following equation;

$$xR_2O + (1-x)B_2O_3 \rightarrow 2xR^+[BO_4]^- + 2[1-x][BO_3] \qquad (3.1)$$

whereby the fraction of four-coordinated boron (N_4) is the ratio 2x/2(1−x), i.e. x/(1−x).

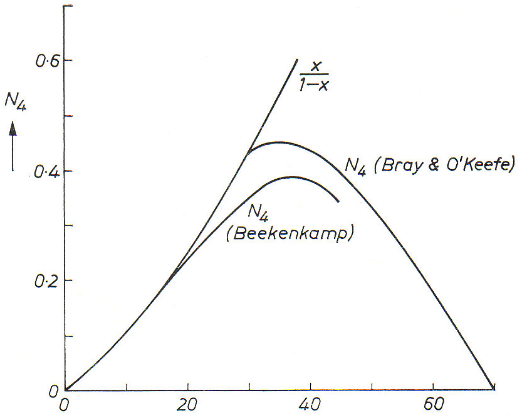

Figure 3.5 *The two main theories predicting the N_4 fraction as a function of alkali content [21]. The function x/(1−x) trend for N_4 proposed by Beekenkamp [21] providing an alternative theory to Silver and Bray [19].*

Beekenkamp's theory was built on several assumptions:

- Various structural units are formed in the glass – [BO_3] and [BO_4] ions, BO and NBOs.

With the conditions that,

- BO_4 units cannot be bound to each other
- NBOs occur in BO_3 triangles only and are absent in BO_4 tetrahedra.

The presence of superstructural units, which do not agree with these rules, in borate and borosilicate glasses meant that the CRN rule was not a requirement for a material to be considered glassy and amorphous. Although consistent to a degree with the observed N_4 variation (Bray and O'Keefe), Beekenkamp's theory is not confirmed by XRD results. Not predicted in the theory was the presence of boroxol rings (Figure 3.6) in vitreous boron oxide (B_2O_3) and alkaline-earth borates [22-26].

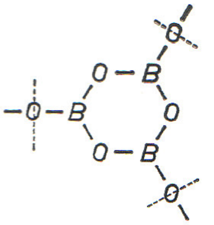

Figure 3.6 *Boroxol ring observed in vitreous B_2O_3 with XRD, not predicted by Beekenkamp [21].*

A study carried out by Zhong and Bray [27] brought into question not only the dependence of N_4 on the type of alkali ion (Figure 3.7) but extended the theory to try and take into account the presence of multiple types of alkali and from this a mechanism for the formation of [BO_3] and [BO_4] co-ordinations.

This data indicated strongly that N_4 is influenced not only by the type of alkali ion but also by the pairings of alkali ions, with the fraction being smaller than the interpolated value for the individual alkali type. On the molecular level an attempt was made to explain this effect by Ingram [28], who suggested that the competition between single and mixed alkali ions e.g. Li_2^{2+} and $(LiK)^{2+}$ was the origin of the formation of [BO_4] up to a certain alkali content and then a reduction in the fraction with increasing alkali past that point. The number of mixed alkali ion pairs was said to increase with the total alkali content and a greater coulombic interaction would favour the bonding of the mixed alkali ion pair with any non-bridging ions, hence reducing N_4 with increasing alkali concentration (Figure 3.8).

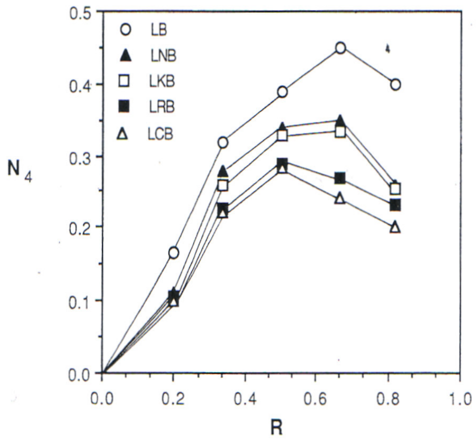

Figure 3.7 *Relationship of N_4 with respect to the binary alkali content in the borate glass [27] (LB – Li_2O-B_2O_3, LNB = Li_2O-Na_2O-B_2O_3, LKB = Li_2O-K_2O-B_2O_3 etc) as measured by Zhong et al. [27] using MAS NMR.*

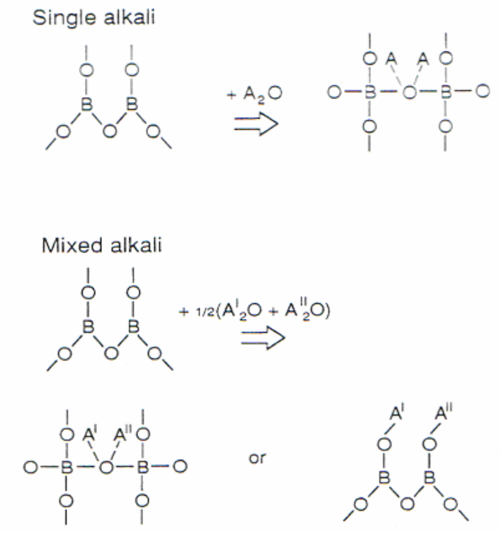

Figure 3.8 *Mechanisms for the production of 3 and 4 coordinated boron [28]. The increase in alkali (A' + A'') content and therefore the increase in the number of non-bridging oxygen favouring alkali-pair ions $(A'A'')^{2+}$ is predicted by Ingram [28] to lead to a decrease in the N_4 fraction as observed. Dashed lines indicate weaker bonds compared to solid lines.*

How N_4 then changes with the introduction of a third alkali and a second glass former is an important consideration with respect to the physical changes of the glass such as T_g, thermal expansion and chemical durability. Finding a model to understand the results of N_4 etc as a function of three alkali types is made all the more difficult through the presence of the silica glass network; in what way will this influence N_4 - will the silicon network be more susceptible to forming alkali-silicate groups than the borate network? How will the silicate-borate networks interact?

Measuring the N_4 fraction is relatively simple and can be represented schematically (Figure 3.9) from the ^{11}B NMR spectra as the fraction of spectrum area produced by four-coordinated boron compared to the total spectrum area, i.e. the total signal produced through three and four-coordinated boron ions (3.2).

$$N_4 = \frac{B_4}{B_3 + B_4}, \tag{3.2}$$

where B_3 and B_4 are the fractions of three- and four-coordinated boron respectively. The fraction of three-coordinated units, B_3, is described by Equation (3.3), and is comprised of the total number of symmetrical and asymmetrical B_3 units present.

$$B_3 = B_{3S} + B_{3AS} \tag{3.3}$$

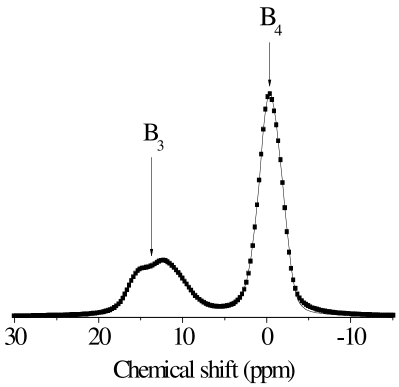

Figure 3.9 *^{11}B MAS NMR spectra for a typical alkali borosilicate glass with [BO_3] and [BO_4] peaks labelled (B_3 and B_4 respectively).*

Four-coordinated boron [BO_4] exists as a spherically symmetric structure (giving a relatively narrow ^{11}B NMR line at ~0 ppm in Figure 3.9) whereas the three-coordinated boron exists in both axially symmetric and asymmetric forms, [BO_{3S}] and [BO_{3AS}] respectively (giving a relatively broad combined ^{11}B NMR line – at ~15 ppm in Figure 3.9).

Recent ^{11}B MAS NMR studies on caesium borates by Kroeker *et al.* [29] and Anguiar [30] have suggested the existence of more than one form of four-coordinated boron, though its structural origin is still unclear. Three possible explanations have been presented; the first being a shift distinction from differences in the second coordination sphere of the observed B_4 sites, the second possibility being differences in network connectivity between trigonal and tetrahedral boron sites. The final explanation and currently the most commonly accepted, is that multiple BO_4 sites in the NMR lineshape arise from individual well defined borate superstructures (Figure 3.10), found to be present in alkali borate glasses and crystals using neutron diffraction and Raman spectroscopy [31-35]. In these superstructures, more than one type of four-coordinated boron environment is thought to exist, providing different four-coordinated boron peaks in the NMR spectra.

Work by Krogh-Moe [36], Bray *et al.* [7,37] and Sinclair and Wright [31,34,38-40] demonstrated the presence of intermediate-range order in borate glasses, in the form of these borate superstructures (Figure 3.10). Ring-like [BO_3]- and [BO_4]-containing structures have been shown to be present in these structures using neutron diffraction and XRD [41,42], as well as Raman spectroscopy [32,35,43,44].

These experimental techniques were primarily used on crystal forms of binary borate glasses, such as alkali meta-, di- and ennea-borates (which contain different specific superstructural units) to obtain signature patterns, such as Raman peak positions, to then compare with borate glass analogues of these compositions, which contain multiple superstructural units. This work continues to date, with Feller *et al.* [45] studying crystal and glass forms of lithium and caesium borate compositions, notably of the meta- and di-borate forms, containing both enriched ^{10}B and ^{11}B, to improve the understanding of both of these compositions using Raman spectroscopy and $^{10/11}B$ NMR.

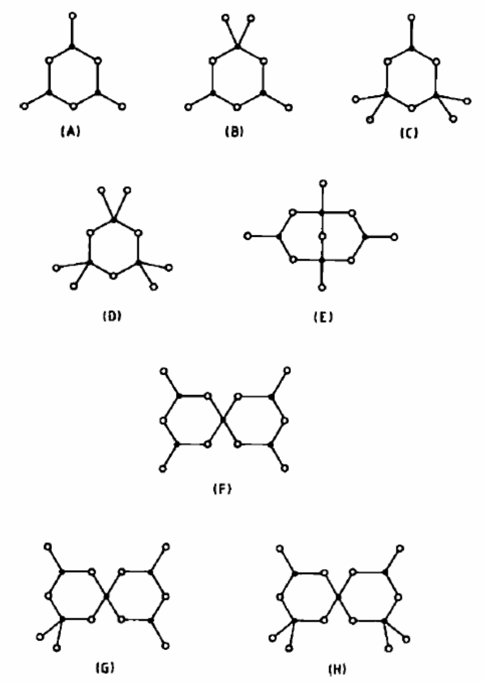

Figure 3.10 *Borate superstructural units; (A) boroxol ring (B) triborate group (C) di-triborate group (D) metaborate group (E) diborate group (F) pentaborate group (G) di-pentaborate (H) tri-pentaborate group [31].*

Borosilicate glasses also have multiple BO_4 units in their NMR spectra. Previously, the lack of any clear asymmetry in the BO_4 region of the ^{11}B MAS NMR lineshape from similar compositions [1,15,16,46], led to only one peak being fitted to the data. This caused no problem in measuring N_4 but work by Stebbins *et al.* [47-50] using ^{11}B MAS and MQMAS NMR techniques, has now shown that there exists more than one form of BO_4 unit in the borosilicate glass network, across a range of samples with R and K values (Figure 3.11). Again, these multiple sites are believed to arise from medium-range (borosilicate, instead of borate) superstructural units in the borosilicate glass network [51-53].

From Figure 3.11 the asymmetry in the BO_4 region of the spectra (10 to −10 ppm) is clearly visible and depends not only on the molar ratio of boron oxide to silicon oxide (K) but also on the molar ratio of alkali oxide to boron oxide (R), for which is it seen that asymmetry reduces as R is increased (for a fixed value of K). For the borosilicate glass compositions in this study, with constant K (=3.2), this asymmetry should therefore still clearly exist but is predicted to be reduced from that shown in Figure 3.11, as R > 1 across all the systems (*cf.* Chapter 4).

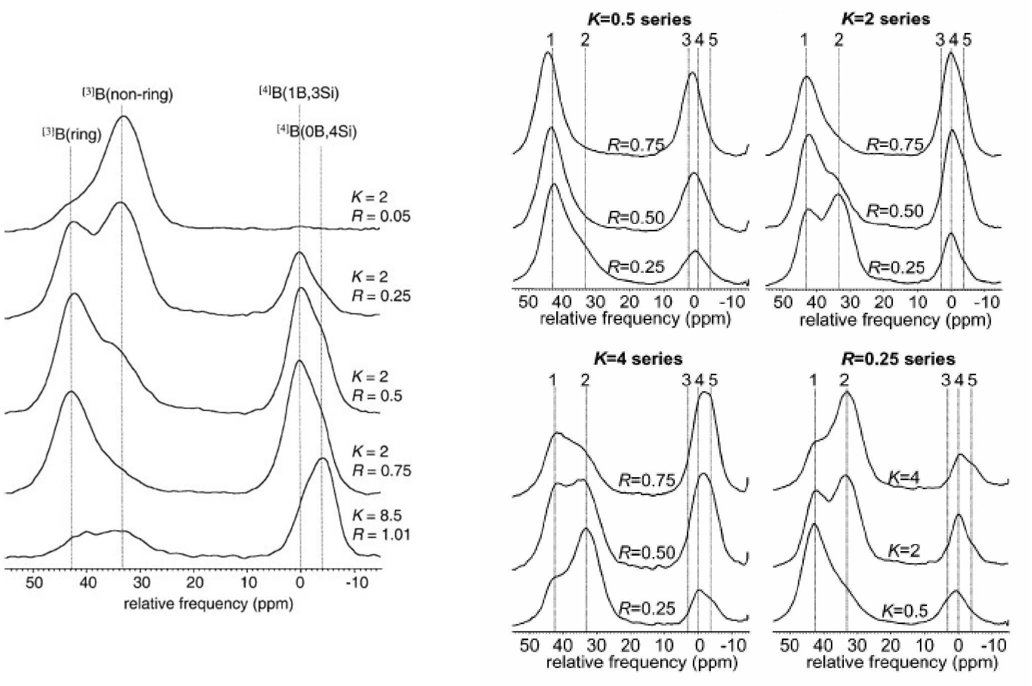

Figure 3.11 *^{11}B 3QMAS NMR spectra for a range of sodium borosilicate glasses of different R and K values. These clearly show asymmetry in the BO_4 peak of the spectra arising from four-coordinated boron sites with different connectivities [48,50].*

Du and Stebbins [47-50] have proposed that up to three different BO_4 sites could be fitted under the BO_4 region of the ^{11}B MAS NMR spectrum; (0B, 4Si), (1B, 4Si) and (2B, 2Si), of increasing unfavourable energetic formation. Resolving of these B_4 peaks [48] showed the sites to be separated by ~1.5 ppm, which is comparable to the observed value in alkali borates of ~1.3 ppm. The borosilicate superstructural units related to the (0B, 4Si), (1B, 4Si) boron sites, have been identified as resembling the units found in reedmergnerite ($NaBSi_3O_8$: Na_2O-B_2O_3:$6SiO_2$) and danburite ($CaB_2Si_2O_8$: CaO-B_2O_3-$2SiO_2$) (Figure 3.12). The reedmergnerite structure contains BO_4 sites connected to four silicon sites (0B, 4Si) and danburite contains BO_4 sites connected to a single boron, and three silicons (1B, 3Si).

These superstructural units are also observable in the Raman spectra of borosilicate glasses at low (< 800 cm^{-1}) wave-numbers. In the original study conducted by the author on a caesium-alkali borosilicate composition [46,54] Raman data showed the presence of reedmergnerite and danburite units, at the positions 489-552 and 782-791 cm^{-1} respectively, based on assignments by Bunker [55].

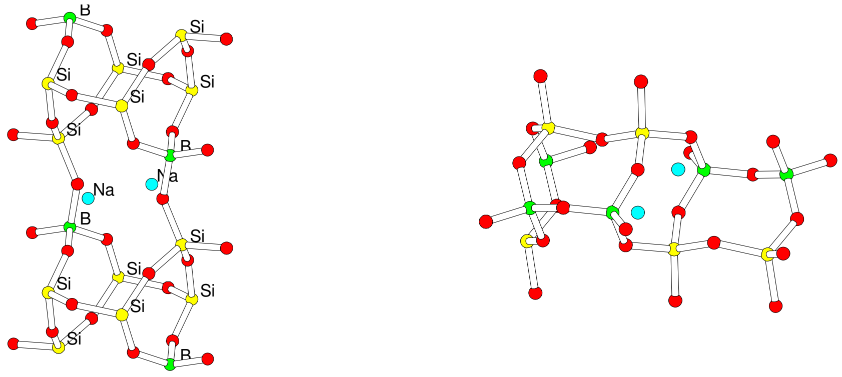

Figure 3.12 *Reedmergnerite ($NaBSi_3O_8$) and danburite ($CaB_2Si_2O_8$) structures, each with different BO_4 environments.*

3.4.2 Silicate Glass Theory

As well as N_4, another structural measure accessible using NMR relates to the silicon-29 species and its coordination in the glass network. The Si environments are described by the term Q^n, with n being the number of BO per silicon ion ($0 \leq n \leq 4$). Roderick [15,56] and Duddridge [16] (Figure 3.13) reported the changes in Q^n in borosilicate glasses used for HLW storage with the addition of various waste simulants. In conjunction with N_4 measurements, Q^n can give a measure of the number of NBOs and hence the quantity of silicon-alkali and boron-alkali bonds.

The three main Q^n groups predicted to arise in the borosilicate glasses studied in this work are (Figure 3.14);

- Q^4: $Si(OSi)_4$
- $Q^4(B)$: $Si(OSi)_{4-n}(OB)_n$
- Q^3: $Si(OSi)_3O^-R^+$ (R – Li, Na, Cs)
- Q^2: $Si(OSi)_2(O^-)_2$ (?)

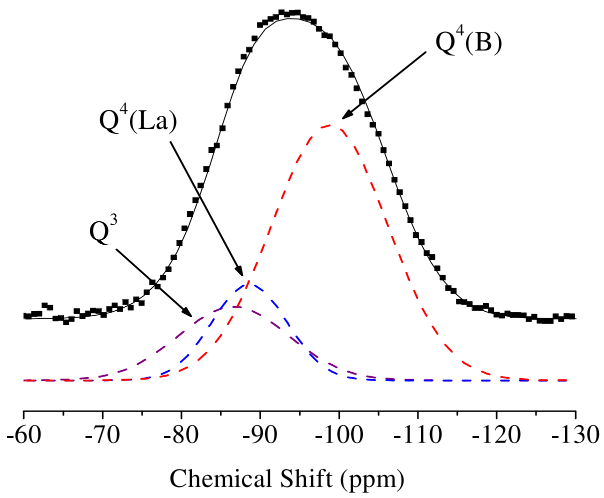

Figure 3.13 *^{29}Si MAS NMR spectrum of the various silicon Q^n groups formed in a borosilicate glass with La waste simulant. The total spectrum is a composite of peaks from the Q^4(La), Q^4(B) and Q^3 groups [16].*

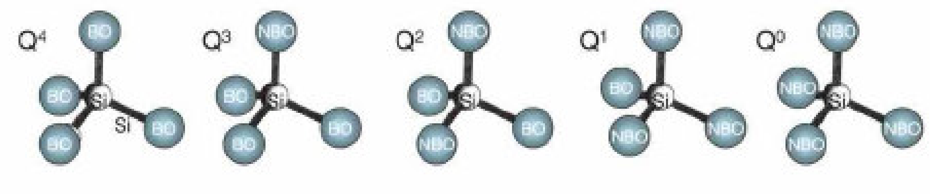

Figure 3.14 *The five possible silicate Q^n units, with n denoting the number of network bridging oxygen (BO). Non-bridging oxygen are labelled as NBO in the figure [57].*

3.4.3 Borosilicate Glass Networks – The Dell Model

Originally it was hypothesised that the networks formed by the two glass formers in borosilicate glasses were non-interacting, with the introduction of glass modifiers such as alkali and alkaline-earth oxides producing complicated structural changes, with the formation of $[BO_3]$, $[BO_3]^-$, $[BO_4]$, Q^3 and Q^4 units – all in non-trivial proportions with respect to modifier content. More recent studies have demonstrated that the two networks *are* merged [15,16]. Structural and physical values, such as N_4 and density are seen to vary in a “regional” way (unlike the smooth transitions observed in binary alkali borate and silicate glasses) with no singular function describing their values.

Dell *et al.* [58] developed a structural model based on the sodium borosilicate system which predicted N_4 across regional values of the alkali oxide/boron oxide ratio, R (Figure 3.15). This model can be summarised by the following;

- Region 1: (R < 0.5) System behaves like a binary borate system with any alkali added associates itself with the borate network alone, forming tetrahedral boron units, i.e. $N_4 \sim R$. The silicate network is unaffected. At R=0.5 $[BO_3]=[BO_4]$ and diborate units form

- Region 2: ($0.5 < R < R_{max}$) Additional alkali combines with diborate and $[SiO_4]$ to form reedmergnerite units (a boron tetrahedral unit bonded with four silica tetrahedra) R_{max} is defined as ½ + K/16

- Region 3: ($R_{max} \leq R \leq R_{dl}$) The Dell model at this point predicts that the addition of alkali to the glass forms NBOs on the silica tetrahedra. This results in the overall N_4 being unchanged

- Region 4: ($R_{d1} \leq R \leq R_{d2}$) Alkali oxide combines with the remaining diborate and reedmergnerite groups, dividing itself proportionately according to the number of boron and silicon atoms in each unit.

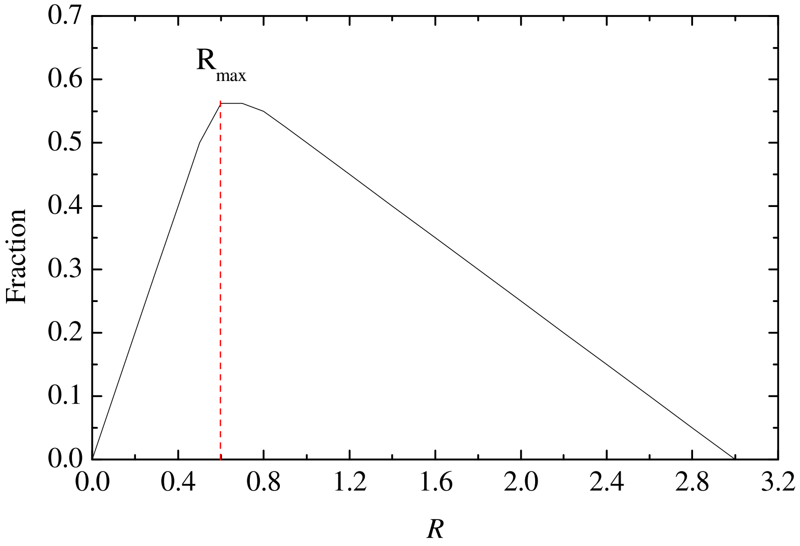

Figure 3.15 *Change in the N_4 fraction as a function of R for a K=1 glass, as predicted by Dell et al. [58].*

3.5 Structural and Physical Effects of Further Oxide Additions to Alkali Borosilicates

The effect of the addition of an oxide to the structure of alkali borosilicate glasses is a major interest in the field of HLW immobilisation. In this study the oxides Cs_2O, MgO, Al_2O_3 and La_2O_3 are added. The effect on glass structure depends on whether the oxide being added is a glass former, intermediate or modifier. Glass formers and intermediates tend to behave similarly, with their addition to a glass structure favouring bonds with alkali species, rather than to other network groups, such as boron. Hence in a borate-containing glass this results in the N_4 fraction being lowered, with four-coordinated boron sites being converted to three-coordinated sites. Glass formers and intermediates therefore cause the conversion of tetrahedral boron sites to trigonal borate units, by effectively removing alkali species from the borate network in preference to joining to the intermediate and glass forming oxides present.

Work carried out on the Al_2O_3-Na_2O-B_2O_3-SiO_2 glass system by El-Damrawi *et al.* [59] using ^{11}B, ^{29}Si and ^{27}Al MAS NMR produced a model for the sharing of the alkali oxide between the alumina, borate and silicate networks, with the model being extended to the general system X_2O_3-M_2O-B_2O_3-SiO_2, where X: Al or La. Assuming M_2O associates itself with the X_2O_3 first and borate network second, the remainder then joins the silicate network (with the condition that mol% M_2O > mol% X_2O_3). With this condition, the amount of M_2O to be incorporated in the borate and silicate networks (Ma_2^aO), left over from being associated with the X_2O_3 can be found using (3.4). From ^{11}B MAS NMR, the quantity of M_2O associated with the borate network (M_2^bO) can be found using (3.5), hence the amount of M_2O available to be used by the silicate network ($M_2^{Si}O$), can be found from (3.6).

$$[M_2^aO] = [M_2O] - [X_2O_3] \tag{3.4}$$

$$[M_2^bO] = N_4[B_2O_3] \tag{3.5}$$

$$[M_2^{Si}O] = [M_2^aO] - [M_2^bO] \tag{3.6}$$

The maximum value of N_4 was found by El-Damrawi *et al.* [59] to occur when the mol% ratio $([M_2O] - [X_2O_3]) / ([B_2O_3]) = 1$, with $N_4=0$ when $[B_2O_3] < [X_2O_3]$. The number of NBOs per silicon can therefore be determined by (3.7). ^{27}Al MAS

NMR studies also found that aluminium ions exist mainly in the form of tetrahedral $[AlO_4]^-$ units preferentially linked to the silicate network, forming Si-O-Al bonds. The amount of Si-O-Al bonds (Al_{Si}) can therefore be calculated using (3.8).

$$\mathrm{NBO/Si} = 2[\mathrm{M_2^{Si}O}]/[\mathrm{SiO_2}] \tag{3.7}$$

$$\mathrm{Al_{Si}} = [\mathrm{X_2O_3}] / ([\mathrm{SiO_2}]/4) \tag{3.8}$$

3.5.1 The Glass Transition and Crystallisation Temperatures

One unusual property of borate glasses is the non-linear variation of the glass transition temperature with increasing alkali content. For alkali borate glasses T_g increases to a maximum of 800K (527°C) at R~0.5, falling rapidly to ~500K (227°C). This is demonstrated by work conducted by Feller *et al.* [60] comparing both lithium and sodium borates glasses as well as lithium and sodium borosilicate glasses of fixed K(=1), silicon oxide/boron oxide ratio (Figure 3.16 and Figure 3.17). Further to this it was observed that a variation in the silicon content results a variation in the T_g, when R > 0.5. Instead of decreasing, as shown in Figure 3.17, the T_g begins to plateau with increasing silica content. This change with composition can be traced back to the formation of the three borate units – the symmetrical and asymmetrical $[BO_3]$ borate units and the tetrahedral $[BO_4]$ borate units, as well as the formation of the different Q^4, Q^3 and Q^2 within the glass.

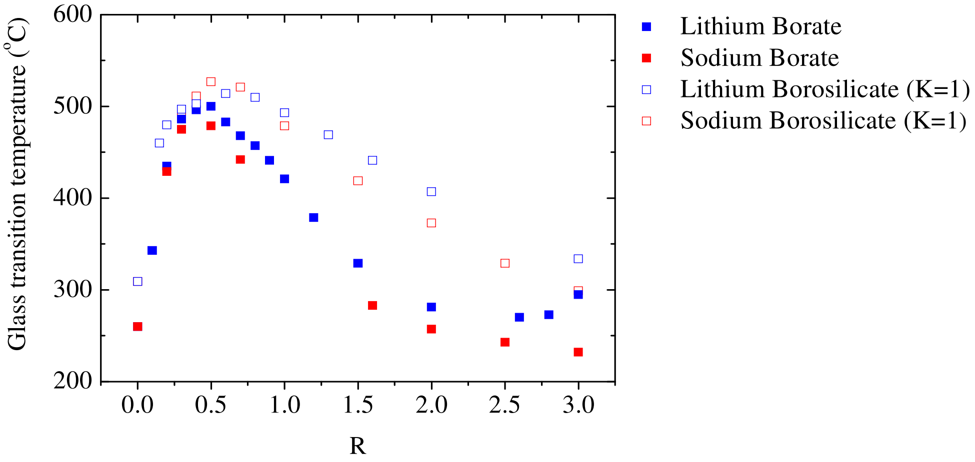

Figure 3.16 *Variation in T_g with respect to alkali and glass type. R denotes the ratio of alkali oxide to B_2O_3 content. Note the generally larger value in peak T_g in the borosilicate glasses compared to the borate glasses [60].*

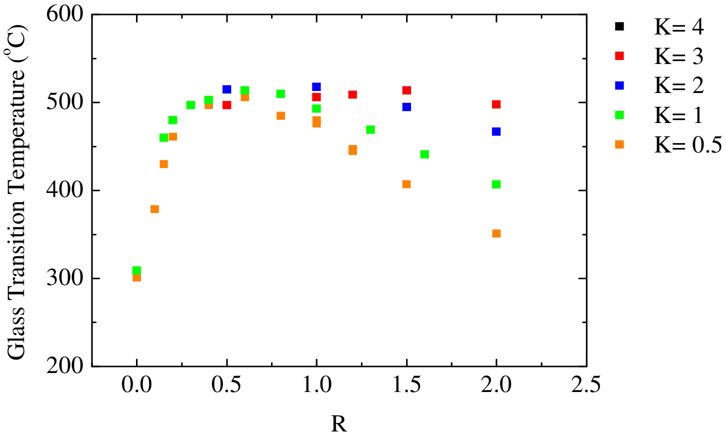

Figure 3.17 *Trends in the lithium borosilicate glass transition temperature with increasing amounts of silicon oxide [60].*

3.5.2 Borate and Borosilicate Glass Density

Density measurements on borate and borosilicate glasses although relatively simple in technique can often reveal properties and trends that on some scales are not identified through other techniques such as NMR or Raman Spectroscopy. Hence its application can be very much complementary and help to bring into light the effect of borate and silicate groups on a glass' physical structure. Work by Shibata *et al.* [61] and Karki *et al.* [62] on lithium and sodium borate glasses as well as recent work by Clarida *et al.* [4] on caesium borates has revealed quite different changes in the glass density as a function of the alkali content.

3.5.3 Glass Durability and Chemical Resistance for Waste Storage

The chemical durability and long-term structural stability of nuclear waste-containing borosilicate glasses is of prime concern in the effective design and management of glass composition. With HLW being a complex material, containing many different oxides, its effect on durability when added to an alkali borosilicate glass is of considerable importance for the safe, geographical long-term storage of HLW where different environmental factors may be present. Hence many durability studies have been carried out [63-70] with the experimental details of the topic discussed in detail in Chapter 2.

The primary reactions occurring at the glass surface-solution interfaces during corrosion tests, are described as:

- $Si–OR + H_2O \leftrightarrow Si\text{-}OH + M^+ + OH^-$ (3.9)
- $B\text{-}OH + H_2O \leftrightarrow B\text{-}OH + M^+ + OH^-$ (3.10)
- $\equiv Si\text{-}O\text{-}Si \equiv + OH^- \leftrightarrow \equiv Si\text{-}OH + \equiv Si\text{-}O^-$

  $\equiv Si\text{-}O^- + H_2O \leftrightarrow Si\text{-}OH + OH^-$ (3.11)

with M representing Li, Na or Cs.

Of the three reactions, both (3.9) and (3.10) are the most common observed in previous work [1,16,17] with the leaching of alkali groups (typically Li and Na, since these studies have not included Cs in any of their compositions). This loss is therefore predominately due to reactions (3.9) and (3.10) due to the comparatively more durable nature of the silicate network being less likely to result in the leaching of silicon groups into solution.

3.6 Summary

The study of glass systems is obviously complex, whether one or more glass networks are present, with many theories existing for different glass compounds. Because of the wide range of theories it is then understandable why so many different experimental approaches and techniques are required to understand the physiochemical properties of glass; many of these techniques are complementary to one another with distinct differences between glasses being more easily observed with one technique over another.

For example the use of NMR and thermal analysis studies in this work is very important to derive a quantitative understanding of the fraction, type and interaction between different glass units and networks and their influence on thermal properties such as volatilisation. Similarly, medium-range order in glasses, in terms of the presence of borate and borosilicate superstructural units, is observed using Raman and NMR spectroscopy and hence the two techniques assist one another in understanding the number and types of these units present.

3.7 References

[1] J. M. Roderick, *PhD Thesis, Warwick University* (2001).

[2] F. H. Stillinger, *J. Chem. Phys.* **88** (12) (1988) 7818-7825.

[3] W. H. Zachariasen, *J. Am. Chem. Soc.* **54** (1932) 3841-3851.

[4] W. J. Clarida, J. R. Berryman, M. Affatigato, S. A. Feller, S. Kroeker, J. Ash, J. W. Zwanziger, B. M. Meyer, F. Borsa, and S. W. Martin, *Phys. Chem. Glasses* **44** (3) (2003) 215-217.

[5] D. Holland, M. E. Smith, A. P. Howes, T. Davies, and L. Barrett, *Phys. Chem. Glasses* **44** (2) (2003) 59-63.

[6] M. Kodama, N. Nakashima, and T. Matsushita, *Japanese Journal of Applied Physics* **32** (1993) 2227-2229.

[7] G. E. Jellison, S. A. Feller, and P. J. Bray, *Phys. Chem. Glasses* **19** (3) (1978) 52-53.

[8] M. J. Plodinec, *Glass Technol.* **41** (6) (2000) 186-192.

[9] Y. Miura, H. Kusano, T. Nanba, and S. Matsumoto, *J. Non-Cryst. Solids* **290** (2001) 1-14.

[10] N. Ollier, T. Charpentier, B. Boizot, G. Wallez, and D. Ghaleb, *J. Non-Cryst. Solids* **341** (2004) 26-34.

[11] N. M. Vedishcheva, B. A. Shakhmatkin, and A. C. Wright, *J. Non-Cryst. Solids* **345-346** (2004) 39-44.

[12] S. Manikandan, Jagannath, V. K. Shrikhande, and G. P. Kothiyal, *Anti-Corrosion Methods and Materials* **53** (5) (2006) 303-309.

[13] D. Stentz, S. Blair, C. Goater, S. A. Feller, and M. Affatigato, *J. Non-Cryst. Solids* **293-295** (2001) 416-421.

[14] W. L. Konijnendijk and J. M. Stevels, *J. Non-Cryst. Solids* **20** (1975) 193-224.

[15] J. M. Roderick, D. Holland, A. P. Howes, and C. R. Scales, *J. Non-Cryst. Solids* **293-295** (2001) 746-751.

[16] A. Duddridge, *PhD Thesis, Warwick University* (2004).

[17] M. Islam, *PhD Thesis, Warwick University* (2005).

[18] W. Vogel, *The Chemistry of Glass*, John Wiley & Sons (1985) 108.

[19] A. H. Silver and P. J. Bray, *J. Chem. Phys.* **29** (1958) 984.

[20] O. Majerus, L. Cormier, G. Calas, and B. Beuneu, *Phys. Rev. B* **67** (20242101-024210-7) (2003).

[21] P. Beekenkamp, *Phillips Research Report Supplements* **4** (1966).

[22] M. J. Park, K. S. Kim, and P. J. Bray, *Phys. Chem. Glasses* **44** (1979) 227.

[23] M. J. Park and P. J. Bray, *Phys. Chem. Glasses* **13** (1972) 50.

[24] H. M. Kriz, M. J. Park, and P. J. Bray, *Phys. Chem. Glasses* **12** (1971) 45.

[25] S. G. Bishop and P. J. Bray, *Phys. Chem. Glasses* **7** (1966) 73.

[26] S. Greenblatt and P. J. Bray, *Phys. Chem. Glasses* **8** (1967) 190.

[27] J. Zhong and P. J. Bray, *J. Non-Cryst. Solids* **111** (1989) 67-76.

[28] M. D. Ingram, *Phys. Chem. Glasses* **44** (2) (1980) 54.

[29] S. Kroeker and J. F. Stebbins, *Inorg. Chem.* **40** (24) (2001) 6239-6246.

[30] P. M. Anguiar and S. Kroeker, *Solid State Nucl. Mag.* **27** (2005) 10-15.

[31] J. L. Shaw, A. C. Wright, R. N. Sinclair, J. R. Frueh, R. B. Williams, N. D. Nelson, M. Affatigato, S. A. Feller, and C. R. Scales, *Phys. Chem. Glasses* **44** (3) (2003) 256-259.

[32] B. P. Dwivedi, M. H. Rahman, Y. Kumar, and B. N. Khanna, *J. Phys. Chem. Solids* **54** (5) (1993) 621-628.

[33] E. I. Kamitsos and G. D. Chryssikos, *J. Mol. Struct.* **247** (1991) 1-16.

[34] A. C. Wright, N. M. Vedishcheva, and B. A. Shakhmatkin, *Materials Research Society Symp. Proc.* **455** (1997) 381-385.

[35] B. N. Meera and J. Ramakrishna, *J. Non-Cryst. Solids* **159** (1991) 1-21.

[36] J. Krogh-Moe, *Phys. Chem. Glasses* **6** (46) (1965).

[37] S. A. Feller, W. J. Dell, and P. J. Bray, *J. Non-Cryst. Solids* **51** (1982) 21-30.

[38] R. N. Sinclair, C. E. Stone, A. C. Wright, I. G. Polyakova, N. M. Vedishcheva, B. A. Shakhmatkin, S. A. Feller, B. C. Johanson, P. Venhuizen, R. B. Williams, and A. C. Hannon, *Phys. Chem. Glasses* **41** (5) (2000) 286-289.

[39] A. C. Wright, R. N. Sinclair, C. E. Stone, K. S. Knight, I. G. Polyakova, N. M. Vedishcheva, and B. A. Shakhmatkin, *Phys. Chem. Glasses* **44** (3) (2003) 197-202.

[40] R. N. Sinclair, R. Haworth, A. C. Wright, B. G. Parkinson, D. Holland, J. W. Taylor, N. M. Vedishcheva, I. G. Polyakova, B. A. Shakhmatkin, S. A. Feller, B. Rijal, and T. Edwards, *Physics and Chemistry of Glasses: European Journal of Glass Science and Technology* **Part B, 47** (4) (2006) 405-411.

[41] J. Swenson, L. Borjesson, and W. S. Howells, *Phys. Rev. B* **52** (13) (1995).

[42] L. Borjesson, L. M. Torell, U. Dahlborg, and W. S. Howells, *Phys. Rev. B* **39** (5) (1989) 3404-3407.

[43] B. P. Dwivedi and B. N. Khanna, *J. Phys. Chem. Solids* **56** (1) (1995) 39-49.

[44] W. L. Konijnendijk and J. M. Stevels, *J. Non-Cryst. Solids* **18** (1975) 307-331.

[45] S. A. Feller, *Private Communications* (2006).

[46] B. G. Parkinson, D. Holland, M. E. Smith, A. P. Howes, and C. R. Scales, *J. Non-Cryst. Solids* **351** (2005) 2425-2432.

[47] L.-S. Du and J. F. Stebbins, *J. Non-Cryst. Solids* **351** (2005) 3508-3520.

[48] L.-S. Du and J. F. Stebbins, *J. Non-Cryst. Solids* **315** (2003) 239-255.

[49] L.-S. Du and J. F. Stebbins, *Chem. Mater.* **15** (2003) 3913-3921.

[50] L.-S. Du and J. F. Stebbins, *J. Phys. Chem.* **B, 107** (2003) 10063-10076.

[51] I. V. Veksler, A. M. Dorfman, D. B. Dingwell, and N. Zotov, *Geochemica Et Cosmochimica Acta* **66** (14) (2002) 2603-2614.

[52] K. L. Geisinger, R. Oestrike, A. Navrotsky, G. L. Turner, and R. J. Kirkpatrick, *Geochemica Et Cosmochimica Acta.* **52** (1988) 2405-2414.

[53] A. A. Gurenko, I. V. Veksler, A. Meixner, R. Thomas, A. M. Dorfman, and D. B. Dingwell, *Chem. Geol.* **222** (2005) 268-280.

[54] B. G. Parkinson, *MSc Thesis, Warwick University* (2004).

[55] B. C. Bunker, D. R. Tallant, R. J. Kirkpatrick, and G. L. Turner, *Phys. Chem. Glasses* **31** (1) (1990) 30-41.

[56] J. M. Roderick, D. Holland, and C. R. Scales, *Phys. Chem. Glasses* **41** (6) (2000) 392-396.

[57] G. N. Greaves and S. Sen, *Advances in Physics* **56** (2007) 1-166.

[58] W. J. Dell, P. J. Bray, and S. Z. Xiao, *J. Non-Cryst. Solids* **58** (1983) 1-16.

[59] G. El-Damrawi, W. Muller-Warmuth, H. Doweidar, and I. A. Gohar, *Phys. Chem. Glasses* **34** (2) (1993) 52-57.

[60] S. A. Feller, J. Kottke, J. Welter, and S. Nijhawan, *Proc. 2nd Int. Conf. On Borte Glasses, Crystals and Melts.* (249) (1997).

[61] M. Shibata, C. Sanchez, H. Patel, S. A. Feller, J. Stark, G. Sumcad, and J. J. Kasper, *J. Non-Cryst. Solids* **85** (1986) 29.

[62] A. Karki, S. A. Feller, H. P. Lim, J. Stark, C. Sanhez, and M. Shibata, *J. Non-Cryst. Solids* **92** (1987) 11-19.

[63] Y. Linard, T. Advocat, C. Jegou, and P. Richet, *J. Non-Cryst. Solids* **289** (2001) 135-143.

[64] S. V. Raman, *J. Mater. Sci.* **33** (1998) 1887-1895.

[65] G. Calestani, A. Montenero, E. Ferraguti, G. Ingletto, and M. Bettinelli, *J. Non-Cryst. Solids* **84** (1986) 452-462.

[66] J. Sheng, S. Luo, and B. Tang, *Waste. Manage.* **19** (1999) 401-407.

[67] S. Sheng, S. Luo, and B. Tang, *Waste. Manage.* **19** (1999) 401-407.

[68] M. Ishida, K. Kikuchi, T. Yanagi, and R. Terai, *Nuclear and Chemical Waste Management* **6** (1986) 127-131.

[69] G. Malow, W. Lutze, and R. C. Ewing, *J. Non-Cryst. Solids* **67** (1984) 305-321.

[70] C. M. Jantzen and M. J. Plodinec, *J. Non-Cryst. Solids* **67** (1984) 207-223.

Chapter 4

4 Experimental Theory and Practice: - Glass Preparation and Characterisation

4.1 Introduction

In this chapter, theory and practice of the experimental techniques employed in the production and characterisation of the glass systems used in this study are introduced and discussed. The systems include: (a) glasses in which one of a number of oxides is added to the mixed-alkali borosilicate base-glass (MW) prior to further addition of caesium oxide (0-9.66 mol%) to investigate volatilisation at high-temperature; and (b) compositions used in the complementary study of oxygen-17 enriched mixed-alkali borosilicates. A number of experimental techniques have been used on both sets of borosilicate compositions, including differential thermal analysis (DTA) simultaneous thermal/thermogravimetric analysis (TG-DTA) - the simultaneous acquisition of DTA and thermogravimetric (TG) data as a function of temperature, volatilisation mass-loss measurements and chemical durability tests.

4.2 Glass Preparation

4.2.1 Standard Borosilicate Compositions

Four mixed-oxide borosilicate systems were prepared by a powder mix and melt-quench route, using a combination of reagent grade Wacomsil® quartz (SiO_2), sodium tetraborate ($Na_2B_4O_7$), sodium carbonate (Na_2CO_3), lithium carbonate (Li_2CO_3), caesium carbonate (Cs_2CO_3), magnesium carbonate ($MgCO_3$), aluminium oxide (Al_2O_3) and lanthanum oxide (La_2O_3).

The starting base-glass composition (MW) used by BNFL Ltd was modified according to (4.1), to include one of the following oxides (with mol%, y); aluminium oxide (0.95 mol%), lanthanum oxide (1.68 mol%) or magnesium oxide (2.55 and 10.20 mol%), to form new base-glasses ZMW (Table 4.1). These new base-glasses were then modified by the addition of caesium oxide (4.2) to form a range of compositions for each system.

$$\text{ZMW} = \text{y}[\text{Al}_2\text{O}_3,\text{La}_2\text{O}_3,\text{MgO}](100\text{-y})\text{MW} \tag{4.1}$$

$$\text{xCs}_2\text{O}(100\text{-x})\text{ZMW}, (0 < \text{x} < 10) \tag{4.2}$$

Each of these systems, unless shown otherwise, contains six compositions with increasing caesium oxide content. The ratio of free alkali oxide to boron oxide, *R*, has been modified from that given in (4.3) to that of (4.4). This modification is to take into account either the addition of further modifier in the form of MgO or the removal of one mole of alkali oxide from the glass network by one mole of Al_2O_3 or La_2O_3.

$$R = \frac{\text{mol\% alkali oxide}}{\text{mol\% boron oxide}} \tag{4.3}$$

$$R = \frac{\text{mol\% alkali oxide (I and II) - mol\% Al}_2\text{O}_3\text{, La}_2\text{O}_3}{\text{mol\% boron oxide}} \tag{4.4}$$

Two extra samples were made to investigate further the caesium-MW system studied by the author in previous work [1]. The two new compositions have increased caesium oxide concentrations of 11.0 and 13.9 mol% and their manufacture is identical to that of the four main glass systems of this study.

For each glass, 100 g batches were made with the appropriate combinations of reagent grade lithium carbonate (99.9 %), sodium carbonate (99.95 %), caesium carbonate (99.99 %), aluminium oxide (99.9 %), lanthanum oxide (99.99 %), magnesium carbonate (99.9 %), sodium tetraborate (99.5 %) and Wacomsil© quartz (99.9 %) with 0.1 mol% iron (III) oxide (99.5 %) added to reduce NMR T_1 relaxation times. The powders for each of the systems were weighed, mixed thoroughly on roller mills, placed into a 90 % platinum 10 % rhodium crucible and heated at 600°C per hour to between 1350-1370°C and maintained at temperature for 20 minutes. The melts were quenched in de-ionised water to produce a frit and allowed to dry. A small amount of the frit was taken for differential thermal analysis to obtain the glass transition temperature (T_g). The frit was then re-melted at the same temperature as the first melt and held at temperature for 20 minutes before being cast into hot moulds (~250°C).

Cylinders of the glass for leach testing (*cf.* Section 4.4) were annealed at 50°C below T_g for 6 hours. XRD studies revealed that all samples were completely amorphous.

System	mol% SiO_2	mol% B_2O_3	mol% Na_2O	mol% Li_2O	mol% Al_2O_3, La_2O_3 MgO	mol% Fe_2O_3	R
MW	60.61	18.57	10.53	10.29	-	0.1	1.12
AlMW	60.03	18.39	10.43	10.19	0.95	0.1	1.07
LaMW	59.59	18.26	10.35	10.12	1.68	0.1	1.03
MgMW	59.06	18.10	10.26	10.03	2.55	0.1	1.26
Mg'MW	54.43	16.68	9.46	9.24	10.20	0.1	1.73

Table 4.1 *Starting compositions (mol%) and R values of the initial five borosilicate base-glasses. (Note: K=3.2 for all compositions)*

For additional use in this study, sodium- and caesium-containing forms of reedmergnerite ($NaBSi_3O_8$) and danburite ($NaBSiO_4$), and a caesium-containing form of the boropollucite borosilicate glass ($CsBSi_2O_6$) [2,3] were made to the compositions outlined in Table 4.2. Previous work [4] had identified the presence of superstructural units, based on the first two of these three compositions, in the glasses, through Raman spectra of the CsMW system [5,6]. Characterisation of these glasses was intended to provide further evidence for the peak assignments made in the Raman spectroscopy and would assist in ^{11}B and ^{29}Si MAS NMR studies. These have indicated that alkali borosilicate glasses are comprised of these superstructural units, and knowledge of their fundamental properties, e.g. density and thermal properties, would help to explain the thermal and structural behaviour of the mixed-oxide alkali borosilicate compositions outlined in Table 4.1.

The boropollucite, reedmergnerite and danburite compositions outlined in Table 4.2 were made in 30 g batches, composed of sodium- or caesium-carbonate (99.95 and 99.99 % respectively), reagent grade Wacomsil® quartz (99.9 %), boron oxide (99.99%) and 0.1 mol% of iron (III) oxide (99.5 %) (to reduce NMR T_1 relaxation times). Powders were weighed, mixed thoroughly on roller mills, placed into a 90 % platinum 10 % rhodium crucible and heated at 600°C per hour to between

1250-1300°C [7] and maintained at temperature for between 1-2 hours. Due to their high viscosity, melts were not cast but were quenched by carefully dipping the base of the crucible in de-ionised water.

System	mol% Na_2O, Cs_2O	mol% B_2O_3	mol% SiO_2	mol% Fe_2O_3	R	K
danburite	25.00	25.00	50.00	0.10	1.00	2.00
caesium boropollucite	16.67	16.67	66.67	0.10	1.00	4.00
reedmergnerite	12.50	12.50	75.50	0.10	1.00	6.00

Table 4.2 *Molar compositions of the caesium boropollucite, reedmergnerite and danburite glasses, along with R and K values.*

4.2.2 Oxygen-17 Enriched Borosilicate Sample Preparation

^{17}O NMR, to enable the identification of the various oxygen sites in the glasses, required ^{17}O enriched samples due to the extremely low (~0.04 %) natural abundance of ^{17}O.

Previous ^{17}O NMR studies on borosilicate glasses by Du and Stebbins [8-16] used a synthesis route outlined by Abys *et al.* [17] which mixed silicon tetrachloride with de-ionised water (in the presence of a diethyl ether solvent, under nitrogen atmosphere) to form a silicon oxide precipitate and hydrogen chloride gas (4.5). This route was preferred over others outlined in the literature [18,19] due to both the ease of processing the resultant powder and the relative success these groups had achieved [8-16].

$$SiCl_4\ (aq.) + 2H_2{}^{17}O\ (aq.) \rightarrow SiO_2\ (s) + 4HCl\ (g) \tag{4.5}$$

The silicon oxide powder precipitate was then dried under non-oxidising conditions, using nitrogen gas, and heat-treated to remove excess water and hydroxyl groups and then used in an identical glass preparation route as the non-enriched silicon oxide powder. For K = 3.22 glasses it is easier and to produce and use ^{17}O-enriched silicon oxide rather than enriched boron oxide. To produce the ^{17}O-enriched silicon oxide, the arrangement shown in Figure 4.1 was used. Nitrogen gas was fed into a round-bottomed flask filled with approximately 10 ml of diethyl ether solvent and 3.2 ml (0.028 mol%) of silicon tetrachloride. Into this flask, at a rate of ~2 ml/min, 1 ml (0.056 mol%) of 20 % ^{17}O-enriched H_2O was syringed. The round-bottomed flask was cooled throughout the whole procedure using an ice bath, to slow the violent exothermic reaction between silicon tetrachloride and water.

Figure 4.1 *Arrangement used to prepare sol-gel silicon oxide powders, based on that used by Abys et al. [17]. Orange rubber tubes indicate the nitrogen in- and out-flow. Round-bottomed flask is sat in an ice bath, cooling the ditheyl ether solvent, which is added to the flask prior to addition of water and silicon tetrachloride.*

A single batch of ^{17}O-enriched silicon oxide powder was made using 20 % ^{17}O enriched $H_2{}^{17}O$, by the method outlined in (4.5). This produced approximately 1.7 g silicon oxide powder for the 1 ml $H_2{}^{17}O$ used – i.e. ~ 100 % yield. Both XRD and ^{29}Si MAS NMR was then carried out to check the compositional quality of the SiO_2. Removal of excess water from the SiO_2 powder, after drying under nitrogen for 12 hours, was carried out by heat-treating the powder at 200°C for 24 hours, in a horizontal tube furnace under Argon atmosphere, as outlined in [17]. Although the $Si^{17}O_2$ powder still contained some quantity of H^+ species (*cf.* ^{1}H NMR, Chapter 8), this was sufficiently small to be neglected when calculating the appropriate masses of oxides and carbonates required for each ^{17}O-enriched sample.

Five modified alkali borosilicate samples were made to the compositions outlined in Table 4.3. Two of these compositions (Na(MW) and Na(MW)') were based on modifying the base-glass MW (Table 4.1), which conventionally contains both lithium- and sodium-oxides, to contain only sodium oxide in the quantity used in the established MW composition (i.e. 20.82 mol% Na_2O rather than 10.29 mol% Li_2O and 10.53 mol% Na_2O). Similarly, the composition Cs(MW) consists of only caesium oxide, in the same quantity (20.82 mol%). The remaining two compositions, AlNa(MW) and LaNa(MW), were based on adding either Al_2O_3 or La_2O_3 (x = 0.95 and 1.85 respectively), in the form given in (4.6), to an MW composition, also containing only Na_2O. Modifying MW to contain just Na_2O (rather than both Na_2O and Li_2O) was made to simplify the analysis of the ^{17}O NMR data.

$$x(Al_2O_3, La_2O_3, Cs_2O) \bullet (100 - x) NaMW \tag{4.6}$$

Each borosilicate sample was made using approximately 0.3 g of ^{17}O-enriched SiO_2 powder and the correspondingly stochiometric and compositionally correct masses of sodium carbonate (99.9 %), caesium carbonate (99.99 %), lanthanum oxide (99.99 %), aluminium oxide (99.9 %), boron oxide (99.9 %) and iron (III) oxide (99.5 %). As with the conventional borosilicate compositions of previous studies [4,20,21], 0.1 mol% of iron (III) oxide was added to all but one composition (Na(MW)'), to reduce NMR T_1 relaxation times. The sample Na(MW)' which lacked iron (III) oxide enrichment was identical both in composition and manufacture to that of Na(MW) and was produced to check that lineshape in the ^{17}O NMR was not affected by the presence of iron (III) oxide.

Before the five ^{17}O-enriched borosilicate samples were made, a single test sodium borosilicate sample, identical to that of Na(MW) outlined in Table 4.1, was made using non-^{17}O enriched chemically prepared SiO_2 and the appropriate carbonates and oxides outlined above. This was to test the effectiveness of the manufacturing route eventually used to produce the ^{17}O-enriched borosilicate samples.

Powders were mixed for 1 hour then packed and sealed into platinum tubes and heated in a vertical tube furnace with a nitrogen atmosphere, to between 1300-1400°C for 20 minutes, before being quenched in liquid nitrogen and retrieved from the tubing. Samples were then analysed by XRD to confirm whether the resultant structures were glassy or crystalline. Energy Dispersive Analysis with X-rays (EDX) measurements were also carried out to obtain quantitative measurements of the cation and silicon species present.

Name	mol% SiO_2	mol% B_2O_3	mol% Na_2O	mol% Li_2O	mol% Cs_2O	mol% La_2O_3	mol% Al_2O_3	mol% Fe_2O_3	R
MW	60.61	18.57	10.53	10.29	-	-	-	0.1	1.12
Na(MW)	60.61	18.57	20.82	-	-	-	-	0.1	1.12
Na(MW)’	60.61	18.57	20.82	-	-	-	-	-	1.12
Cs(MW)	60.61	18.57	-	-	20.82	0.00	-	0.1	1.12
AlNa(MW)	60.03	18.39	20.62	-	-	-	0.95	0.1	1.07
LaNa(MW)	59.59	18.25	20.47	-	-	1.68	-	0.1	1.03

Table 4.3 *Compositions of the six ^{17}O enriched borosilicate compositions. Note: nominal K for all of these borosilicate compositions = 3.22.*

4.3 Characterisation Techniques

4.3.1 Introduction to X-ray Diffraction

X-ray diffraction is a technique that enables crystalline and non-crystalline structures to be characterized by the constructive interference of x-ray wave-fronts present at varying angles of incidence. The property of diffraction common to all waves is governed by the Bragg Law (4.7).

$$n\lambda = 2d\sin\theta \qquad (4.7)$$

with n being the order of reflection, λ the wavelength of the incident x-rays, d the inter-planar spacing, and θ the angle of incidence onto the sample. Signature XRD patterns are observed by the following procedures:

- The angle of incidence (and reflection) θ is changed with the use of a monochromatic beam of x-rays with a relatively defined wavelength – *rotating angle XRD*.
- The wavelength of incident x-rays is changed, hence an x-ray source with a range of x-ray energies is used along with a set angle of incidence- *Laue XRD*.

All the XRD patterns produced in this study used the method of rotating angle XRD. Production of x-rays in the Bruker D5005 was achieved through the bombardment of a Cu target with an electron beam to produce x-rays with wavelengths 0.15406 nm and 0.15444 nm. Approximately 1 % of the energy absorbed by the target goes into direct production of x-rays from excited electron states (Figure 4.2). After emission from the copper target the x-rays are directed onto the sample at the desired angle with the constructive patterns produced through the Bragg condition being satisfied. Compared to crystal structures, the XRD patterns of glassy materials cannot provide a complete analysis of the whole structure due to a lack of any long range order in the glass. The XRD pattern of glass samples can reveal whether an individual sample is an amorphous glass or whether any crystal phases exist within it.

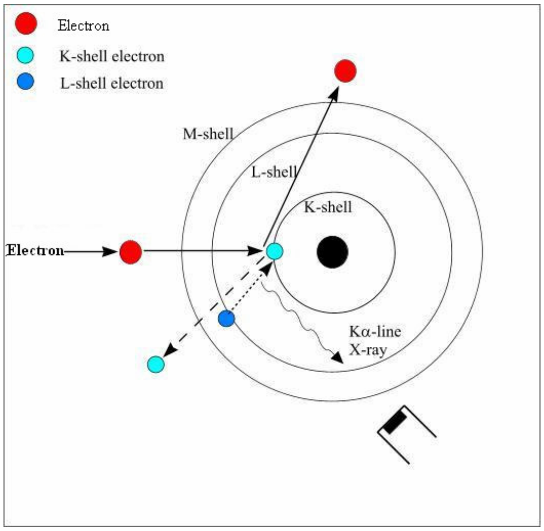

Figure 4.2 *Production of x-rays through the bombardment of a copper source with high energy electrons. (Figure modified from http://www.ikp.uni-koeln.de/jolie/Forschung/Eng/pixe_eng.htmhttp://www.indyrad.iupui.edu/public/lectures/physics/2XRAYPRO/sld008.htm)*

4.3.2 X-Ray Diffraction Method

XRD measurements were undertaken using a Bruker D5005 diffractometer, at 40kV-30 mA power. Scans were taken between 10-70^{o} with 0.02^{o} increments, 15-30 seconds/increment and with a 12 mm constant footprint. For all scans aluminium holders were used and any aluminium diffraction peaks present in results have been labelled.

4.3.3 Thermal Techniques

Thermal analysis techniques measure physical changes produced in a sample as a function of temperature; these include changes in mass (thermogravimetry - TG), enthalpy (DSC and DTA) and volume (dilatometry). The thermal studies undertaken in this work include identifying the glass transition, first crystallisation (where possible) and melting temperatures using differential thermal analysis (DTA) traces obtained from either a standard Stanton-Redcroft DTA set-up or from a simultaneous thermal/thermogravimetric analysis DTA-TG spectrometer, which also enabled thermogravimetric analysis measurements to be obtained simultaneously with differential thermal analysis measurements.

The change in mass of the glasses has also been measured using a volatilisation method developed in a previous study [4].

4.3.3.1 Differential Thermal Analysis (DTA)

The most common technique used in thermal analysis, DTA, measures the difference in temperature ($\Delta T = T_s - T_r$) between a sample (T_s) and an inert reference material (T_r). Both materials are held in separate cavities within holders of low thermal conductivity sitting inside a single furnace (Figure 4.3 (a) and (b)). Typically, solid samples are powdered and loaded into a high temperature resistant crucible (i.e. 90Pt/10Rh) with the mass of the reference used being equal to the measured mass of the analysed sample. For inorganic samples Al_2O_3 and SiO_2 are common reference materials. *Endothermic* reactions are signified by $\Delta T < 0$ and *exothermic* reactions by $\Delta T > 0$ (Figure 4.3(c)). The application of DTA to solid materials reveals important phase transitions specific to the material being analysed; these can include the crystallization temperature (T_x) and the glass transition temperature (T_g), the temperature at which the liquid passes from a glass to the supercooled state on heating.

DTA measurements in this work were conducted using both a Stanton-Redcroft DTA 673-4 and PerkinElmer Diamond DTA-TG (*cf.* Section 4.3.3.2). For both set-ups an air atmosphere was used with 90Pt/10Rh crucibles, with a ramp rate of 10^oC/minute up to 1000^oC, with the system then cooled back to room temperature. Typically 0.2 g and 20-40 g of sample were used for the Stanton-Redcroft and PerkinElmer set-ups respectively, with samples being powdered and loaded into a crucible with an equal (±0.001 g) quantity of quartz being used as a reference material. For the PerkinElmer DTA-TG measurements a 200 ml/min air purge gas was used.

For the purpose of annealing the glass disks used in chemical durability studies, T_g values were obtained from data obtained from either set-up.

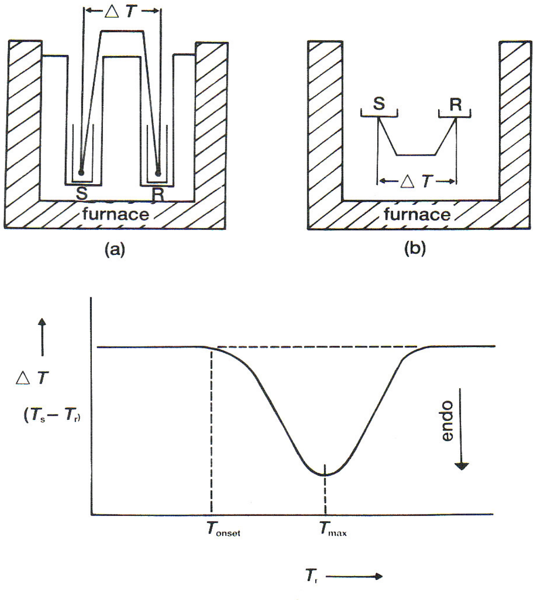

(a) (b) (c)

Figure 4.3 *In DTA, the sample (S) and reference (R) are sat in individual cavities within a single furnace (a),(b) with the temperature difference between them being measured as the differential (c) [22].*

4.3.3.2 Simultaneous Thermal/Thermogravimetric Analysis (DTA-TG)

Simultaneous thermal/thermogravimetric analysis provides a method of obtaining both DTA and thermal gravimetric analysis (TG) measurements simultaneously from a sample. TG data from this experiment provides a useful means of identifying temperatures at which mass changes, such as volatilisation, occur in a sample and linking it to thermal events in the DTA data.

4.3.3.3 Volatilisation Mass-Loss Measurements

Thermogravimetric analysis (TG) was used to identify the temperature at which volatilisation and mass-loss occurs, as well as give a quantitative value of the size of the mass-loss as a function of both temperature and caesium concentration.

Volatilisation studies of borosilicate glasses by Asano *et al.* [23-26] and Stolyarova [27] have commonly used the *Knudsen effusion* technique, which is a combination of a mass-spectrometer attached to a platinum Knudsen cell. The cell is heated across a range of temperatures, with the vapours evolved from the sample (typically 10 mg) being ionised with electrons and their mass determined. The ion species can then be identified with known mass spectra of ions. This technique allows the ion species to be identified, as well as their partial pressures and the energy/temperature of their formation. It does not typically allow the degree of mass-loss to be calculated, which is of importance in this study.

However, to obtain an accurate value of the quantity of mass-loss of each of the compositions at the temperature of volatilisation (understood to be ~1000^{o}C) the use of a method other than STA (or the Knudsen effusion technique) was required due to difficulties in integrating the total mass-loss from the sample acquired over the temperature range of the TG measurement. The third method used for this purpose was devised and used in the previous study by the author [1] and consisted of heating ~0.2 g of sample within a 90Pt/10Rh boat covered with an alumina lid, at 10^{o}C/min to 1000^{o}C and holding at temperature for 4 hours. Weight measurements of the crucible mass, initial sample mass and lid were taken before and after each experiment to give values of mass-loss from the crucible and mass gain on the lid. Of additional importance was that any condensate of volatile species evolved from the melt could be analysed by Raman spectroscopy, XRD or EDX to determine the species present.

Previous experience of this volatilisation technique [4] had shown that a limited quantity of volatilised sample had managed to condense on the alumina lid, since the temperature of lid was similar to that of the crucible. Although the amount of sample was insufficient (1-3 mg) to be removed for measurements such as NMR, it was sufficient for optical measurements such as Raman spectroscopy.

4.4 Chemical Durability

4.4.1 Leach Testing

With borosilicate glasses being chosen for HLW vitrification because of their high stability and durability to aqueous corrosion, a method is required to test and simulate the conditions under which waste-loaded glasses may be stored [28,29]. Such a method exists in the form of the international standard soxhlet test procedure [30] and it has been used in various other corrosion studies on nuclear borosilicate glasses [29-42].

Samples for the leach test are discs of 25 mm diameter and 1 mm thickness, cut from the cylinders described in Section 4.2.1 and with faces polished. For every set of experiments, each run for 14 days, four soxhlets are run in parallel (three containing one sample, and one empty soxhlet) with 300 ml of deionised water within the round-bottomed flask of each soxhlet. The deionised water is then heated to boiling so that the temperature around each sample is approximately 75°C (Figure 4.4). Before and after each experiment the pH of the water is measured (using a Hanna Instruments HI-931410 pH/mV meter) along with the sample mass and a Raman spectroscopy scan (*cf.* Chapter 5) of the disc surface. After each experiment the mass-loss of the glass disc is calculated, along with the change in pH. The resultant leachate solutions from the experiments are adjusted to a pH of 2.7 using 2.5 M nitric acid, for elemental analysis (Na, Li and Cs content) using XRF(*). Raman spectroscopy measurements on the disc surface are also repeated to observe any changes in glass structure.

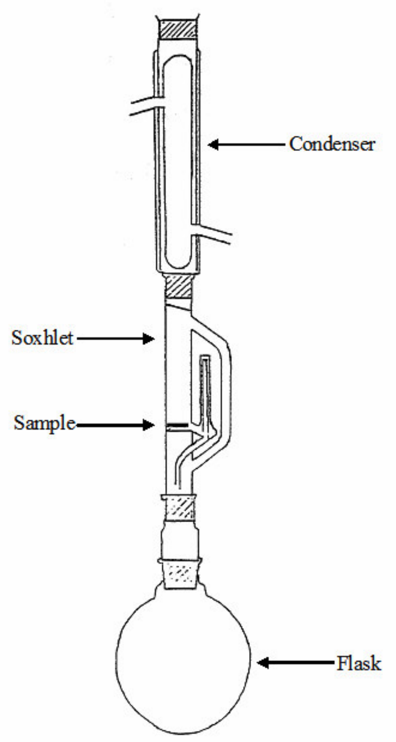

Figure 4.4 *Diagram of the arrangement used to leach test the borosilicate glass samples [30]*

(*) CERAM Research Ltd, Queens Road, Penkull, Stoke-on-Trent, ST4 7LQ, UK.

4.5 References

[1] B. G. Parkinson, *MSc Thesis, Warwick University* (2004).

[2] R. S. Bubnova, N. K. Stepanov, A. A. Levin, S. K. Filatov, P. Paufler, and D. C. Meyer, *Solid State Sci.* **6** (2004) 629-637.

[3] M. G. Krzhizhanovskaya, R. S. Bubnova, S. K. Filatov, D. C. Meyer, and P. Paufler, *Cryst. Res. Technol.* **41** (3) (2006) 285-292.

[4] B. G. Parkinson, D. Holland, M. E. Smith, A. P. Howes, and C. R. Scales, *J. Non-Cryst. Solids* **351** (2005) 2425-2432.

[5] Z. N. Utegulov, J. P. Wickstead, and G.-Q. Shen, *Phys. Chem. Glasses* **45** (3) (2004) 166.

[6] B. C. Bunker, D. R. Tallant, R. J. Kirkpatrick, and G. L. Turner, *Phys. Chem. Glasses* **31** (1) (1990) 30-41.

[7] K. L. Geisinger, R. Oestrike, A. Navrotsky, G. L. Turner, and R. J. Kirkpatrick, *Geochemica Et Cosmochimica Acta.* **52** (1988) 2405-2414.

[8] L.-S. Du and J. F. Stebbins, *J. Non-Cryst. Solids* **315** (2003) 239-255.

[9] L.-S. Du and J. F. Stebbins, *J. Non-Cryst. Solids* **351** (2005) 3508-3520.

[10] J. F. Stebbins, J. V. Oglesby, and S. K. Lee, *Chem. Geol.* **174** (2001) 63-75.

[11] J. F. Stebbins, S. Zhao, and S. Kroeker, *Solid State Nucl. Mag.* **16** (2000) 9-19.

[12] J. F. Stebbins, S. Zhao, S. K. Lee, and J. V. Oglesby, *J. Non-Cryst. Solids* **293-295** (2001) 67-73.

[13] L.-S. Du and J. F. Stebbins, *Solid State Nucl. Mag.* **27** (2005) 37-49.

[14] L.-S. Du and J. F. Stebbins, *Chem. Mater.* **15** (2003) 3913-3921.

[15] L.-S. Du and J. F. Stebbins, *J. Phys. Chem.* **B, 107** (2003) 10063-10076.

[16] L.-S. Du, J. R. Allwartdt, B. C. Schmidt, and J. F. Stebbins, *J. Non-Cryst. Solids* **337** (2004) 196-200.

[17] J. A. Abys, D. M. Barnes, S. A. Feller, G. B. Rouse, and W. M. Risen Jnr, *Material Research Bulletin* **15** (1980) 1581-1587.

[18] J. Chang, A. Yasamori, H. Kawazoe, and M. Yamane, *J. Non-Cryst. Solids* **121** (1990) 177-181.

[19] A. Osaka, M. Yuasa, Y. Miura, and K. Takahashi, *J. Non-Cryst. Solids* **100** (1988) 409-412.

[20] B. G. Parkinson, D. Holland, M. E. Smith, A. P. Howes, and C. R. Scales, *J. Non-Cryst. Solids* **353** (2007) 4076-4083.

[21] B. G. Parkinson, D. Holland, M. E. Smith, A. P. Howes, and C. R. Scales, *J. Phys.: Condens. Matter* **19** (2007).

[22] M. E. Brown, *Chapman and Hall* (1988).

[23] M. Asano, T. Kou, and Y. Mizuntani, *J. Non-Cryst. Solids* **112** (1989) 381-384.

[24] M. Asano, T. Kou, and Y. Yasue, *J. Non-Cryst. Solids* **92** (1987) 245-260.

[25] M. Asano and Y. Yasue, *J. Nucl. Mater.* **138** (1986) 65-72.

[26] M. Asano and Y. Yasue, *J. Nucl. Mater.* **151** (1988) 181-188.

[27] V. Stolyarova, *J. Nucl. Mater.* **247** (1997) 7-10.

[28] K. D. Crowley, *Physics Today* (June Issue) (1997) 32-39.

[29] G. Calestani, A. Montenero, E. Ferraguti, G. Ingletto, and M. Bettinelli, *J. Non-Cryst. Solids* **84** (1986) 452-462.

[30] B.N.F.L., *BNFL Research and Technology, Operating Instruction* **HTP 07** (2) (1999).

[31] T. Akai, C. D., D. Masui, and T. Yazawa, *Glass Technol.* **44** (2) (2003) 71-74.

[32] O. Menard, T. Advocat, J. P. Ambrosi, and A. Michard, *Appl. Geo.* **13** (1998) 105-126.

[33] G. Malow and W. Lutze, *J. Non-Cryst. Solids* **67** (1984) 305-321.

[34] S. V. Raman, *J. Mater. Sci.* **33** (1998) 1887-1895.

[35] J. Sheng, S. Luo, and B. Tang, *Waste. Manage.* **19** (1999) 401-407.

[36] M. Islam, *PhD Thesis, University of Warwick* (2005).

[37] K. B. Harvey and C. D. Jenson, *Nucl. Chem. Waste. Manag.* **3** (1982) 43-50.

[38] D. D. Walker, J. R. Wiley, M. D. Dukes, and J. H. LeRoy, *Nuclear and Chemical Waste Management* **3** (1982) 91-94.

[39] L. L. Hench, D. E. Clark, and J. Campbell, *Nuclear and Chemical Waste Management* **5** (1984) 149-173.

[40] D. M. Strachan, K. M. Krupa, and B. Grambow, *Nuclear and Chemical Waste Management* **5** (1984) 87-99.

[41] M. Ishida, K. Kikuchi, T. Yanagi, and R. Terai, *Nuclear and Chemical Waste Management* **6** (1986) 127-131.

[42] M. I. Ojovan, R. J. Hand, N. V. Ojovan, and W. E. Lee, *J. Nucl. Mater.* **340** (2005) 12-24.

Chapter 5

5 Experimental Theory and Practice: - Structural Determination

5.1 Introduction

This chapter describes the different structural experimental techniques used in this study, such as density measurements, NMR and Raman spectroscopy (RS) and where possible their relationship and use on the glass systems used in this study.

5.2 Density Measurements

5.2.1 Introduction

Density studies have often been used in combination with more complex experiments such as NMR, RS and neutron diffraction as an indication of the structural changes in alkali borates and borosilicate glasses with respect to varying composition [1-3]. Often, when translated to changes of the molar volume, non-linear or regional effects based on the formation of different medium-range order units, are observed that are characteristic of borate, silicate and borosilicate glasses.

5.2.2 Experimental Method – Archimedes Method and Pycnometer

Measurements of glass densities in this study were typically undertaken using Archimedes' method, which involves weighing a solid sample in both air (M_{AIR}) and a chosen displacement fluid (M_{LIQ}). Since the samples in this work are heavily doped with alkali oxides, which are sensitive to water, a suitable non-aqueous based displacement fluid was used in the form of glycerol (99 % pure). It is essential to know the density of the displacement fluid at room temperature ($\rho_{LIQ}(T)$) and so the weight of a known volume of glycerol was measured on each occasion to calculate this. The density of glycerol was found to be 1.25 ± 0.06 g/cm^3 when measuring the glass densities at the typical temperature of 24 ± 2^{o}C. The density of the fluid (glycerol), mass of sample in air and mass of sample in fluid give the density of the solid through (5.1).

$$\rho_{SOLID}(T) = \frac{\rho_{LIQ}(T) M_{AIR}}{M_{AIR} - M_{LIQ}} \tag{5.1}$$

For the oxygen-17 enriched glass powder compositions, the use of Archimedes' method was not possible due to powders being destroyed in the displacement fluid. The alternative approach was to use a *pycnometer*, which, through changes of pressure of a known volume of gas in a reference cell, can be used to calculate material density of a bulk, powder or liquid composition. The pycnometer measures the change in pressure of a known volume of gas that is passed through a reference volume into a cell, where the sample is held. Initially, the gas pressure in the cell is given by

$$P_{gas} = \frac{n_{gas} R T_{gas}}{V_c - V_p} \tag{5.2}$$

Where V_c and V_p are the cell and sample volumes respectively, n_{gas} the number of moles of gas, R the gas constant and $\underline{T_{gas}}$ the cell temperature. The reference volume V_{ref}, when pressurised to P_1 is defined as

$$V_{reference} = \frac{n_1 R T_{gas}}{P_1} \tag{5.3}$$

When the valve between the reference and sample volumes is opened, allowing gas flow between the sample cell and the pressurised reference volume, the pressure lowers to P_2.

$$P_2 = \frac{R T_{gas}(n_{gas} + n_1)}{V_{cell} - V_p + V_{reference}} = \frac{P_{gas}(V_{cell} - V_p) + P_1 V_{reference}}{(V_{cell} - V_p + V_{reference})} \tag{5.4}$$

Hence, with P_{gas} initially set to zero, the sample volume can be expressed by

$$V_p = V_{cell} - V_{refernce}((P_1 / P_2) - 1) \tag{5.5}$$

V_{cell} and $V_{reference}$ are known from calibration, with both the cell volume and stainless steel sphere reference, of accurately known volume. The mass of the sample of study is measured prior to experiment and therefore density can be calculated, when combined with V_p. Before measurements were carried out, the system was purged for 10-15 minutes.

5.3 Nuclear Magnetic Resonance Spectroscopy [4-8]

5.3.1 Introduction

The property of NMR arises from transitions between nuclear spin energy levels brought about through the quantization of spin angular momentum *P* that arises from the total spin quantum number *I*.

$$P = \hbar\left[I(I-1)\right]^{1/2} \tag{5.6}$$

The degeneracy of the spin energy levels for a nucleus is removed (*Zeeman splitting*) in a magnetic field that defines the z-direction, into the values I, I–1, I–2,…, –I. For example, a spin-1/2 and spin-3/2 nuclei possess the nuclear energy levels 1/2 and –1/2 and 3/2, 1/2, –1/2, –3/2 respectively, corresponding to the z-component of the angular momentum (Figure 5.1).

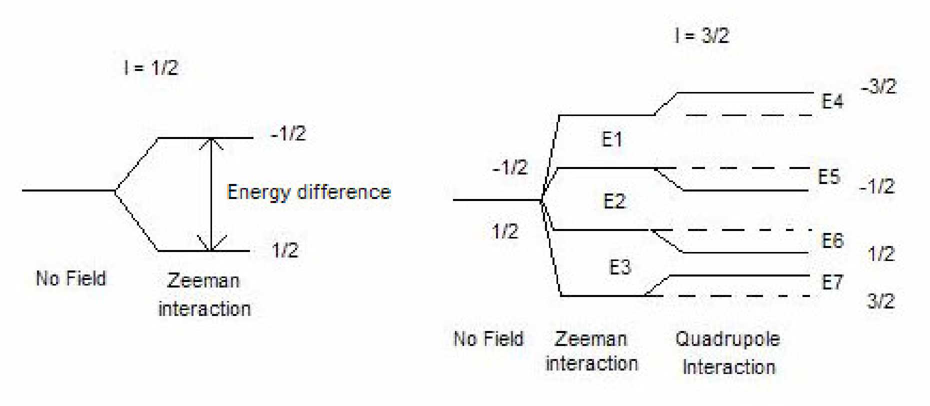

Figure 5.1 *Zeeman splitting for a spin-1/2 and spin-3/2 nucleus. Nuclei with I>1/2 possess additional contributions to the energy levels splitting due to the quadrupole effect (E4, E5, E6 and E7). Note: For the I=3/2 nuclei,* $E_1 = E_2 = E_3$, $E_4 = E_5 = E_6 = E_7$ *and energy differences E1 and E3 do not equal the first Zeeman energy splitting band of E2 when the quadrupole interaction is non-zero.*

Nuclei with I > 1/2 are known to possess an electric quadrupole moment, with the resultant NMR lines in the spectrum often being broader. This effect is of special consideration in this work since ^{23}Na, ^{11}B and ^{17}O are all quadrupole nuclei. The quadrupole moment can introduce a second set of effects that determine the energy on top of the original Zeeman splitting, with the energy differences between levels (other than the central energy band) differing from the initial energy separation caused by the Zeeman interaction.

Not all nuclei can be studied with NMR and the conditions required can be summarised in three rules:

- Nuclei with odd mass number have half-integer spin (e.g. ^{29}Si)
- Nuclei with even mass number and an even charge number have zero spin and therefore cannot be studied by NMR (e.g. ^{16}O).
- Nuclei with even mass number but an odd charge number have integer spin and can be studied, but usually with some difficulty (e.g. ^{10}B).

NMR is achieved through promoting more spins into a higher nuclear energy state (*saturation*) than the original equilibrium energy states. For example, when a spin-1/2 nucleus is placed in an external magnetic field the nuclei align themselves either parallel or anti-parallel to the field, with lower and higher energies respectively. The fraction of spins in each of the levels is at this point approximately equal and so saturation is achieved through the absorption of energy from an RF pulse, promoting a fraction of the spins to a higher energy.

5.3.2 The NMR signal – spin relaxation and RF pulses

The nuclear spin energy of the nucleus in a magnetic field is described by (5.7) with $\boldsymbol{\mu}$ being the magnetic moment of the nucleus (μ_Z the component of the magnetic moment in the z-direction) and **B** the applied magnetic field vector (B_0 is the actual applied magnetic field strength). Substitution of μ_Z by the factors g_N and m_I in (5.8) arises from the quantization of angular momentum with m_I = –I, –I+1,…..,+I and nuclear g-factor g_N. This in turn can be converted to another form to give the magnetogyric ratio - γ(5.9).

$$U = -\mu.B = -\mu_Z B_0 \tag{5.7}$$

$$= -\gamma\hbar m_I B_0 \tag{5.8}$$

$$\gamma = \frac{g_N \mu_N}{\hbar} \tag{5.9}$$

Furthermore the Larmor frequency of a nucleus can be found using (5.9) and this gives a value of the resonant frequency for a particular nucleus in a magnetic field, B (5.10).

$$\nu = \left|\gamma / 2\pi\right| B \tag{5.10}$$

5.3.3 Nuclear Spin Energy and the Larmor frequency

Excitation of the nucleus to higher energies is generated by RF pulses applied at the sample's Larmor frequency. The rotation of the spins either transversely ($\pi/2$) or longitudinally (π) to the external magnetic field, with sufficiently long pulse lengths, are two approaches to achieving saturation and population inversion respectively. Relaxation in the transverse plane (spin-spin relaxation) is measured as the time T_2, with relaxation from the longitudinal state measured as T_1. Naturally $T_1 \geq T_2$, with $T_1 >> T_2$ being typical for solids due to the increased interaction in the solid state. Often though in solid state NMR, because nuclei have "long" (T_1) relaxation times, the most efficient means of obtaining a given signal-to-noise is with a pulse length less than that required to rotate nuclei by 90^o [5,6].

For the application of NMR for chemical spectroscopy, the interaction of the nuclear magnetic field plus the magnetic field generated by the surrounding electrons is taken into account. The precession of the surrounding electrons produces an opposing diamagnetic field at the nucleus with various interactions through electronic bonding, such as spin-spin coupling or J-coupling, and the magnetic field observed by the nucleus differs by very specific values. Classically the magnetic field as 'seen' by the nucleus is not B_0, but instead that described by (5.11) with σ representing the shielding constant, a value usually of the order of ppm.

$$B = B_0(1 - \sigma) \tag{5.11}$$

From this shielding, or 'magnetic screening', the notion of the chemical shift is brought into play whereby the resonant frequency, of the particular nucleus being studied, changes from that of a bare nucleus with no electrons (5.10) to that of (5.12).

$$\nu = \left|\gamma / 2\pi\right| B_0 (1-\sigma) \tag{5.12}$$

At this stage it must be taken into account that chemical shifts are relative to the type of compound being studied because of the measured signal being a collective value brought about from the bulk of the sample. It must also be noted that the chemical shift is a useful quantity only when it is compared to a secondary sample or *reference* and it is from this that the value for the chemical shift (δ) is described by (5.13). The reference is a material of known concentration and molecular configuration, hence it is dependent on the element and material. For NMR experiments carried out in Section 5.3.6, the reference material is stated. Units may be stated in either Hz or ppm.

$$\delta = \frac{\nu_{SAMPLE} - \nu_{REFERENCE}}{\nu_{REFERENCE}} \tag{5.13}$$

The NMR spectrum also reveals details of the inter-atomic bonds between the nucleus being studied and its neighbouring atoms through the dipole-dipole and the spin-spin interaction, an interaction brought about between each of the two nuclear sites and B_0; the quadrupole coupling interaction, brought about through interaction between nuclei with $I > 1/2$ and the surrounding electrons; and J-coupling interactions (present through nuclei interacting with each other via their shared electrons).

5.3.4 Heteronuclear spins, dipole-dipole coupling, magic angle spinning and quadrupolar line broadening

With solid state NMR the atoms are linked within a rigid framework which results in any dipole-dipole interactions having a non-zero value (unlike the case of liquids). Therefore, considering a two spin system with nucleus A under examination through NMR at Larmor frequency ν_A influenced by neighbouring nuclear spin X with frequency ν_B, the (truncated) dipolar Hamiltonian for the heteronuclear spin system is described by (5.14).

$$h^{-1}\hat{H} = -(\nu_A m_A + \nu_X m_X) - R m_A m_X (3\cos^2\theta - 1) \tag{5.14}$$

With, h being Planck's constant and m_A and m_X the spins for nuclei A and X respectively. R represents the splitting, or dipolar z, constant.

From this equation the second term in the Hamiltonian represents a geometric factor of the form $(3\cos^2\theta - 1)$ which is non-zero for solids and is zero for liquids because of the motional averaging brought about through the inherent dynamics of a liquid. Through the application of magic angle spinning (MAS) an identical kind of motional averaging can be achieved in solids by spinning the solid sample about its own axis which is inclined at an angle of $\cos^{-1}\theta = (1/3)^{1/2} = 54.7^{\circ}$ to the primary B_0 magnetic field (Figure 5.2).

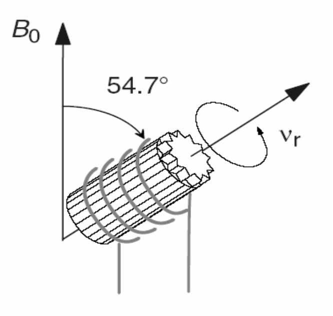

Figure 5.2 *Magic Angle Spinning (MAS) reduces signal broadening brought about through dipole – dipole interactions between the nucleus being studied and its neighbouring nuclei [4].*

About this angle, the anisotropic term (5.15) expanded from the general spin Hamiltonian [5] reduces to zero for $\theta = 54.7^{\circ}$, leaving the isotropic solution-like part of the Hamiltonian described in (5.14) [5].

$$\frac{(3\cos^2\theta - 1)}{2}\Delta A[(3\cos^2\beta - 1) + \eta\sin^2\beta\cos 2\gamma] \qquad (5.15)$$

where A is a constant [5], β and γ are angles in the principal axis of the sample (Figure 5.3) and η is the asymmetry parameter (5.16) with V_{ii} the electric potential in the i$^{\text{th}}$ direction.

$$\eta = \frac{V_{xx} - V_{yy}}{V_{zz}} \qquad (5.16)$$

Typically for MAS, solids are spun at a rate of several kHz (e.g. ^{11}B samples in a 14.1 T field are spun between 12-15 kHz in this study) with the spacing of MAS sidebands being proportional to the MAS rate (Figure 5.4).

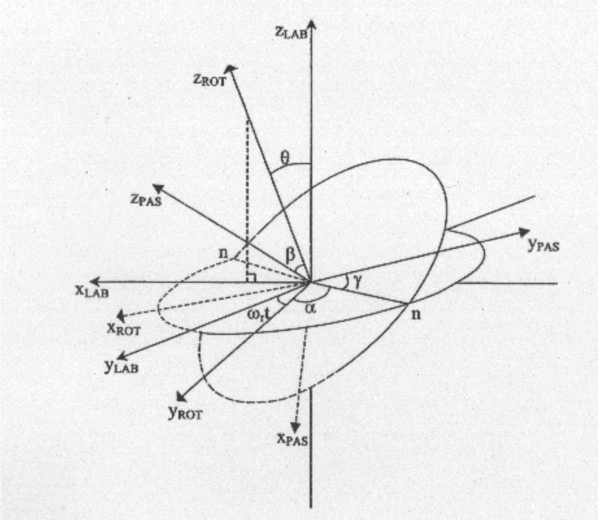

Figure 5.3 *Relative orientations of the principal axis system, rotor and laboratory frame [5].*

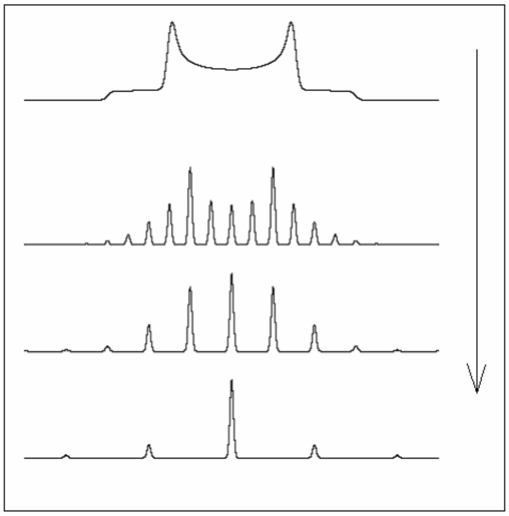

Figure 5.4 *The effect of increasing the MAS rate (indicated by arrow) is to increase the resolution of each peak with the appearance of spinning sidebands around the central peak [4]. MAS removes the dipole-dipole, chemical shift anisotropy and the first-order quadrupole interactions, narrowing the resonance lines [4,5] of the spectrum, with the spacing between MAS peaks related to the spinning speed used.*

A convenient way of describing the electrical charge of the nucleus is to consider it as a composite of a series of charges or electric poles. In this respect we can describe the electric charge of the nucleus *C(**r**)* as:

$$C(\underline{r}) = C^{(0)}(\underline{r}) + C^{(1)}(\underline{r}) + C^{(2)}(\underline{r})\ldots \tag{5.17}$$

Here $C^{(0)}(\underline{r})$ represents a spherical charge distribution, $C^{(1)}(\underline{r})$ a dipolar electric charge distribution (i.e. the electric dipole moment) and $C^{(2)}(\underline{r})$ re-introduces the concept of a quadrupole electric charge distribution (electric quadrupole moment) which affects quadrupole nuclei with I > 1/2, leading to the formation of the quadrupole coupling constant C_Q (5.18).

$$C_Q = \frac{e^2 qQ}{4I(2I-1)h} \tag{5.18}$$

where eQ is the quadrupole moment and $eq = V_{zz}$, the principal (i.e. largest) value of the electric field gradient. Unlike for an isotropic liquid where the quadrupole effect is zero due to motional averaging, solids with I > 1/2 exhibit the quadrupole effect with a frequency of (5.19).

$$v_Q = \frac{3eQj}{4I_j(2I_j-1)} V_{zz}^{j} \tag{5.19}$$

with subscript j denoting the spin I, quadrupole moment Q and electric potential V_{zz} of the charge j.

For quadrupole nuclei in the solid state however, the width of the central resonance can be reduced by increasing the strength of the applied magnetic field. This result arises from the fact that both the second-order quadrupole-induced shift and the line-width of the resonance are inversely proportional to the Zeeman frequency - which increases with field-strength [8].

Although partially removed by MAS at the angle of 54.7°, the unwanted effect of the quadrupole interaction is not totally removed, due to the angular variation of the *second-order* quadrupole effect. The second-order quadrupole interaction can however be removed by spinning at a second angle of either 30.56° or 70.15°, complementary to the initial magic-angle of 54.7°, using the technique of Double Angle Rotation (DOR) NMR [5,6]. This second angle through which the sample is spun simultaneously to the initial magic-angle, is found from the second-order quadrupole energy of interaction, described by (5.20) being a solution of $P_4(\cos\theta) = 0$ [5].

$$E_Q^{(2)}\left|m,m-1\right\rangle = \frac{1}{\nu_0}\left[\frac{3\chi_Q}{2I(2I-1)}\right]^2 \begin{bmatrix} C_0(I,m)F_0(\eta) + \\ C_2(I,m)P_2(\cos\theta_1)F_2(\beta,\gamma,\eta) + \\ C_4(I,m)P_4(\cos\theta_2)F_4(\beta,\gamma,\eta) + \end{bmatrix} \tag{5.20}$$

where crucially, the second-order angular-dependant term is

$$P_4(\cos\theta_2) = \frac{1}{8}(35\cos^4\theta_2 - 30\cos^2\theta_2 + 3) \tag{5.21}$$

with

$$F_0(\eta) = 1 + \frac{\eta^2}{3} \tag{5.22}$$

$$F_2(\beta,\gamma,\eta) = -\left(1 - \frac{\eta^2}{3}\right)P_2(\cos\beta)\eta\sin^2\beta\cos 2\gamma \tag{5.23}$$

$$\begin{aligned} F_4(\beta,\gamma,\eta) &= \left(1 + \frac{\eta^2}{18}\right)P_4(\cos\beta) + \\ &\frac{5\eta}{96}(7\cos 4\beta - 4\cos 2\beta - 3)\cos 2\gamma + \\ &\frac{35\eta^2}{1152}(\cos 4\beta - 4\cos 2\beta + 3)\cos 4\gamma \end{aligned} \tag{5.24}$$

From which the important result is that neither $P_2(\cos\theta)$ or $P_4(\cos\theta)$ could equal zero for a single value of θ. Hence, the magic-angle of 54.7° removes the first-order effects ($P_2(\cos\theta)$) and partially reduces the contribution from the second-order quadrupolar $P_4(\cos\theta)$ term. Complete removal of the second-order, $P_4(\cos\theta)$, term is carried out by spinning an inner rotor within the first at a second angle found from (5.21), to be either 30.56° or 70.15° (Figure 5.5).

The DOR NMR technique lends itself well to crystalline samples with dominant quadrupolar interactions, such as minerals [9-12] but in cases where medium-range order (MRO) exists, in traditionally-viewed disordered materials such as borate and borosilicate glasses, the technique provides the opportunity for resolving more detail of the structure. In much the same way as multiple quantum (MQ) MAS NMR, described later in this chapter, DOR NMR can separate the different sites of quadrupole nuclei, but by using a much simpler one-pulse experiment that, unlike MQMAS, is quantitative.

For borosilicate glasses therefore this technique could be applied in the form of ^{17}O DOR NMR to quantifiably resolve the different ^{17}O sites in Si-O-Si, Si-O-Al, Si-O-B etc. groups. Where MRO units are concerned, ^{11}B DOR NMR could also be used to more easily resolve and quantify $^{11}B_3$ in network units and, more interestingly, $^{11}B_4$ sites with different next nearest neighbours, i.e. reedmergnerite units with B_4 surrounded by 4Si, and danburite units containing B_4 surrounded by 1B and 3Si (*cf.* Chapter 3).

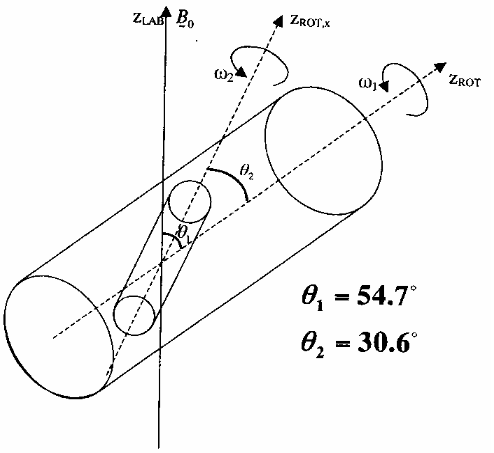

Figure 5.5 *Example of the rotor set-up within a DOR probe, with rotors spinning at angles* θ_1 *and* θ_2 *[5].*

Similarly, the second-order quadrupole effect can also be reduced by the application of the somewhat technically simpler, but less-quantitative technique of MQMAS NMR, which by exciting multiple quantum transitions, outside of the central (1/2, −1/2) transition, in a two-dimensional experiment can reveal greater detail of quadrupolar nuclei.

5.3.5 Multiple Quantum Magic Angle Spinning NMR

Multiple quantum MAS NMR (MQMAS NMR) provides a highly useful tool for studying non-integer quadrupole spins with I > 1/2 (i.e. ^{11}B - 3/2 and ^{17}O - 5/2) whereby removal of the second-order quadrupole interaction occurs [13]. The MQMAS technique enables the resolution of inequivalent chemical sites, distinguishing isotropic chemical from quadrupolar shifts as well as providing a single magnetic field route to locating individual parameters, such as the quadrupolar coupling constant (C_Q) and the asymmetry parameter η, which would otherwise require experiments and fits from multiple experiments at different fields [7].

Differing from single quantum (i.e. single pulse) experiments MQMAS enables the magnetism from multiple transitions in quadrupolar nuclei to be excited through multiple pulses being applied to the analysed system. In the simplest form of an MQMAS NMR experiment, i.e. 2D MAS NMR, initially a single high powered rf pulse is applied to produce the transition MQ. After MQ coherence has evolved (in time t_1) a second pulse is applied to convert the MQ coherence to $p = -1$ (observed in time t_2). Immediately after this second pulse the signal is acquired, with an echo forming at the time given in Equation (5.25) [7,13].

$$t_2 = |k| \bullet t_1 \tag{5.25}$$

where k is the ratio of the (fourth-rank) coefficients of the I > 1/2 and I = 1/2 transitions [7]. By varying t_1, only the intensity of the lineshape is varied. 2D Fourier transformation will then show the resonances as ridges in the quadrupole anisotropy (QA) axis, with the isotropic spectrum observed by projection of the 2D spectrum on the line $\upsilon_1 = \upsilon_2 = 0$, perpendicular to the QA-axis. In a similar approach 3Q and 5Q MAS NMR have also been used on non-integer spin nuclei to obtain information on the interactions of heteronuclear spins.

For example, for a quadrupolar nucleus, the observed shift in the MQMAS is given by (5.26).

$$\delta^{\mathrm{MQMAS}} = (-17/31)\delta^{\mathrm{CS}} + (30/31)\delta^{\mathrm{2Q}} \tag{5.26}$$

where

$$\delta_{iso}^{2D} = \frac{-3\times10^{6}}{40}\frac{I(I+1)-(3/4)C_Q^2(1+\eta^2/3)}{I^2(2I-1)^2\omega_0^2} \qquad (5.27)$$

is the second-order quadrupolar shift and δ^{CS} is the isotropic chemical shift. C_Q and η are the quadrupolar coupling constant and asymmetry parameter, respectively. Hence for sites with different C_Q values, different 2D isotropic shifts are observed. This proves useful, especially with glasses, where oxygen sites can have dramatically different local environments (i.e. different δ and C_Q).

5.3.5.1 Application of ^{17}O MQMAS NMR to Disordered Materials

MQMAS NMR has been used in the study of various glass systems, most notably alkali borosilicates, where both ^{11}B [14-17] and ^{17}O [14,15,18,19] MQMAS NMR has been used to provide more information than initial single-pulse MAS NMR techniques. Of importance in this study however, is the use of ^{17}O MQMAS NMR in conjunction with both single pulse ^{17}O MAS NMR, for revealing information on network connectivity.

Oxygen-17 NMR is an ideal technique for understanding physical characteristics of both organic and inorganic compounds, due to its sensitivity to local environment. This leads to a broad range of chemical shift values based on nearest-neighbour combinations and therefore is a powerful tool in glass science for understanding network connectivity and its relation to physical and chemical glass properties. Unfortunately though, its widespread use is limited by several factors; the natural abundance of ^{17}O is ~0.04 % and its nuclear spin of 5/2, often resulting in a large quadrupolar broadening effect. The first of these problems, the low natural abundance, can be reduced by the use of enrichment (*cf.* preparation of oxygen-17 enriched glasses in Chapter 4) with the second being reduced by the use of both (MQ) MAS and/or DOR NMR [9,20]. In this study, ^{17}O MQMAS NMR is used to identify heteronuclear bonds, such as Si-O-Si, Si-O-B, Si-O-alkali and B-O-alkali bonds [14,15] present.

5.3.6 ^{23}Na, ^{27}Al, ^{11}B, ^{29}Si and ^{17}O NMR Acquisition Conditions

^{23}Na MAS NMR was carried out on a Varian/Chemagnetics Infinity 600 NMR spectrometer at 159.03 MHz with 4 mm rotors. For each sample, acquisitions were taken at room temperature using a 15 kHz MAS frequency, a pulse delay of 1 s and pulse length of 0.7 μs (45° tip angle). A sodium chloride (solid) reference was used at 7.2 ppm.

For measurements of the aluminium sites in the CsAlMW glasses, ^{27}Al MAS NMR spectra were obtained on a Varian/Chemagnetics Infinity 600 NMR spectrometer operating at 156.03 MHz with a Chemagnetics MAS 4 mm probe spinning at 12 kHz. For each sample 1000 acquisitions were taken with a pulse delay of 1 s and a 0.5 μs pulse length (45° tip angle). Samples were referenced against YAG solid using the AlO_6 resonance, taken at 0.7 ppm. Peak fractions were calculated using the Origin program.

All ^{11}B MAS NMR measurements were obtained on a Varian/Chemagnetics Infinity 600 NMR spectrometer at 192.04 MHz with 4 mm rotors. For each sample 1000 acquisitions were taken at room temperature using a 12-15 kHz MAS frequency, a pulse delay of 1 s and pulse length of 0.7 μs (B_1 ~ 60 kHz). Previous studies [21] of ^{11}B in borates and borosilicates have used Pyrex® as a reference, but all spectra in this study were referenced against boron phosphate (99.994 %) at −3.3 ppm (equivalent to referencing to $Et_2O{:}BF_3$ at 0 ppm), this change has been made because of the non-standard stoichiometric composition of Pyrex®.

Note: ^{11}B MAS NMR spectra were obtained at 14.1T (rather than at lower fields) due to the optimal spectral width obtained at this field, allowing clear separation and resolution of the two peaks in the ^{11}B MAS NMR spectra.

^{29}Si MAS NMR was carried out using a 360 Varian NMR spectrometer operating at 71.25 MHz with 6 mm rotors, 5 s pulse delay, 2 μs pulse length (30° tip angle) with 1000 acquisitions, and a line broadening of 50 Hz. Spectra were obtained at 5-6 kHz MAS frequency. Tetramethylsilane (TMS) was used as a primary reference at 0 ppm.

^{17}O NMR $^{(*)}$ spectra were recorded on a Bruker Avance II+ spectrometer at 14.1 T operating at a frequency of 81.37 MHz for ^{17}O. A 4 mm MAS probe was used for ^{17}O MAS and 3QMAS experiments.

^{17}O MAS NMR spectra were acquired with a whole Hahn echo experiment [22] with a 2.5 and 5.0 μs pulse-width used with an interpulse delay of ~1 ms (10 x rotor-period). ^{17}O 3QMAS NMR spectra were recorded with a whole-echo phase-modulated split-t_1 3QMAS experiment [23]. The optimized excitation and conversion pulse-widths were 5 and 2.25 μs, respectively, with a radiofrequency of 125 kHz. 27 μs was set for the selective 180° pulse with a solid rf pulse of 18.5 kHz.

All ^{17}O NMR spectra were acquired with sample spinning at 10000 ± 2 Hz, and with a recycle delay of 1-10 s. No difference in the lineshape was observed between recycle delays of 1 s and 10 s. All spectra were referenced to H_2O at 0 ppm. One dimensional ^{17}O MAS NMR plots are represented in the conventional manner, with peak positions denoted by ppm. MQMAS NMR plots, with peaks requiring two coordinates to locate their positions, are represented by the horizontal scale being the MAS dimension (x) and the vertical representing the isotropic dimension (y). In this study, the position of peaks in the MQMAS NMR maps are abbreviated to the form (x, y), i.e. a peak at 60 MAS ppm and 40 isotropic ppm would be denoted by (60, 40).

5.4 Raman Spectroscopy

5.4.1 Introduction

Raman spectroscopy (RS) is an approach based on the polarisability of a molecule induced through a laser source incident on the sample (Figure 5.6). Similar in its approach to IR spectroscopy RS often allows transitions which are forbidden by the IR selection rules and so the two techniques are complementary, with one technique often producing results unobtainable by the other.

In the majority of cases the application of a photon source with frequency ν onto a sample produces scattered photons with the same frequency (*Rayleigh scatter*) but about 1 in 10^7 photons produces scattered radiation of a different frequency,

---

(*) All ^{17}O NMR experiments in this study, including single pulse- and MQMAS- NMR, were carried out in direct collaboration with Dr Alan Wong of the Warwick Nuclear Magnetic Resonance Group.

mostly to a lower one (*Stokes Shift*) and to a smaller degree to higher frequencies (*anti-Stokes shift*) (Figure 5.7) [21].

From the excitation and detection of photons, arising from vibrations of the molecule, identifiable peaks in the form of an intensity spectrum as a function of frequency difference (Raman shift, cm^{-1}) can be obtained that can be used to deduce the type of molecule and its atomic grouping. Hence this technique is a useful way to construct a picture of the structure of borates and borosilicate glasses that contain strong structural groupings such as boroxol rings etc.

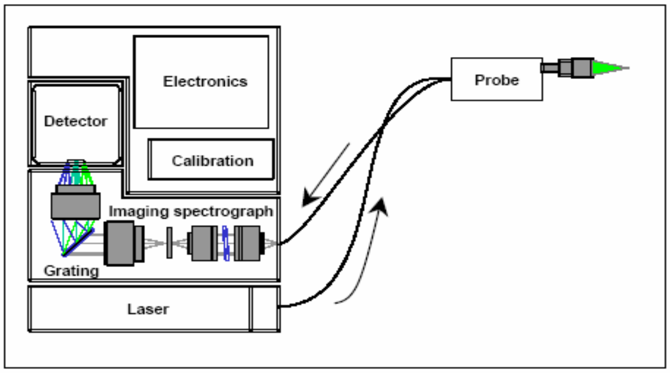

Figure 5.6 *The Raman spectroscopy set-up consists typically of a laser light source in conjunction with a probe focussed through a microscope onto the sample. The probe then relays the detected signal back to an imaging spectrograph and the relevant electronics [24].*

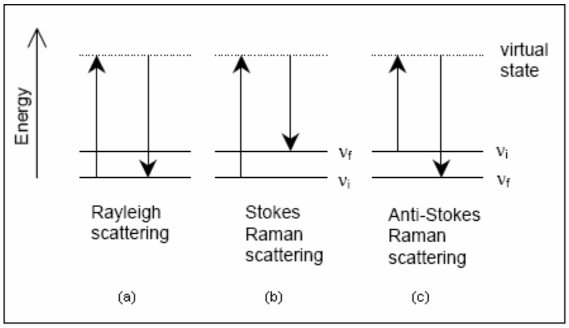

Figure 5.7 *Schematic of the three main scattering processes produced in Raman spectroscopy. An incident photon of frequency ν_0 excites an electron which then either: relaxes back to its initial state releasing a photon of frequency ν_0 (a); relaxes to an excited state releasing a photon with a lower frequency (b) or induces photon emission with a higher frequency (i.e. higher energy) (c) [24].*

Classically the theory of Raman spectroscopy is very similar to the Compton scattering of X-rays with the change in frequency between the incident and emitted photon from a molecule being described by (5.28) with the two energies E_m and E_n being initial and excited energy states (with h – Planck's constant). Note; for the technique of IR spectroscopy, $\Delta v = v_0$. From this it can be seen that:

- Rayleigh scattering $\Delta v = 0$
- Stokes-Raman scattering $\Delta v > 0$
- Anti-Stokes-Raman scattering $\Delta v < 0$.

with the energy differences being zero, positive and negative respectively (5.28) .

$$\Delta v = v_0 - v = \frac{E_m - E_n}{h} \tag{5.28}$$

5.4.2 Raman spectroscopy of glassy materials

Important to the study of borate and borosilicate glasses using RS, is the fact that there is a spectrum of molecular groupings, such as from borate [25] and borosilicate [26] superstructures. Examples include the boroxol, pentaborate and metaborate superstructures present in alkali borates (Figure 5.8) [27] and, for borosilicate glasses, vibrational units present include the reedmergnerite and danburite superstructures and, throughout the range of the silicate and borosilicate compositions, the whole range of silicon Q^n units (*cf.* Chapter 3). Hence the vibrational excitations detected across the range of compositions produce a spectrum of frequency shifts. The results from a crystal sample however differ, in that a crystal structure is built around a single molecular group and so the photon excitations stimulate different modes from the same group.

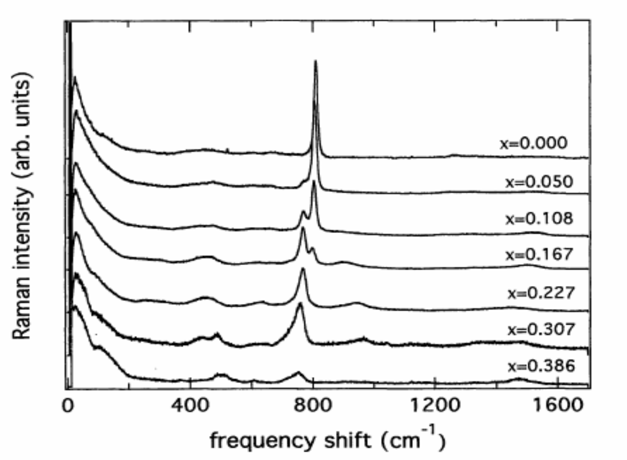

Figure 5.8 *Structural molecular groups present in a borate glass with their Raman frequency in brackets; (a) boroxol group (808 cm^{-1}), (b) pentaborate group (525-530, 603-655, 767 and 930-967 cm^{-1}), (c) dipentaborate group (757 cm^{-1}) [27].*

5.4.3 Quantitative Raman Spectroscopy of Glassy Materials

Unlike for NMR, the use of Raman spectroscopy (RS) as a quantitative method for measuring structural quantities is both limited and in some cases contentious. As a quantitative technique RS would be ideal since it is non-destructive, rapid in its acquisition of data and the results show clear changes across samples that have distinctly different thermal and physical properties, as well as more subtle properties such as sample preparation techniques.

The greatest drawback with using the technique in a quantitative measurement however arises from the problem that the Raman spectrum can contain a number of details greater than just features directly related to the structures and units present in the glass. These include peaks in the spectrum from polarisation effects and from multiple symmetries of the same unit.

Some work has however been carried out using RS quantitatively (Figure 5.9 and Figure 5.10), most notably on silicate [28-30] and aluminosilicate [31] glasses. All of these papers utilise the Raman spectra to obtain fractions of the silicon Q^3 and Q^4(B) units, as functions of temperature and composition respectively. The paper by Mysen [31] brings to attention one further problem with using RS - that being the removal of any background signal collected during data acquisition. Mysen [31] found the background signal to be exponential in form up to high (> 1000 cm^{-1})

wavenumbers and that it was possible to subtract the background before performing peak fitting to the data with Gaussian peaks. Most notably though, for both papers, peak fitting was carried out only around regions of the Raman spectrum where it was confidently thought that any peaks present were due to vibrations directly from individual units, and not because of any other optical effects.

If quantitative RS of a borosilicate glass spectrum could be repeatedly achieved in HLW-borosilicate glasses (with simulated and non-simulated loads), the calculation of the silicon Q^n fractions, especially in cases where glasses containing significant (~2 mol%) proportions of a NMR-unfriendly paramagnetic species (such as HLW containing glasses) then an alternative method of measuring Q^n units would be possible. The technique would also lend itself well in situations where destruction of the sample was not favourable, such as for measuring the Q^n fraction in chemically leached glass disks, and where the quantity of sample available is unrealistic to use in ^{29}Si MAS NMR (i.e. the condensates of volatile species collected from mass-loss measurements).

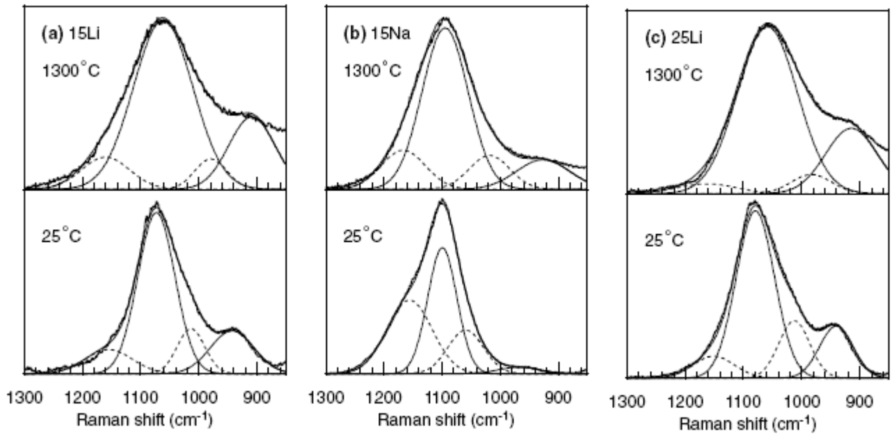

Figure 5.9 *Examples of peak fitting the Raman spectra of lithium and sodium silicate glasses, carried out over the region of the spectra where labelling of the peaks could be confidently undertaken [28].*

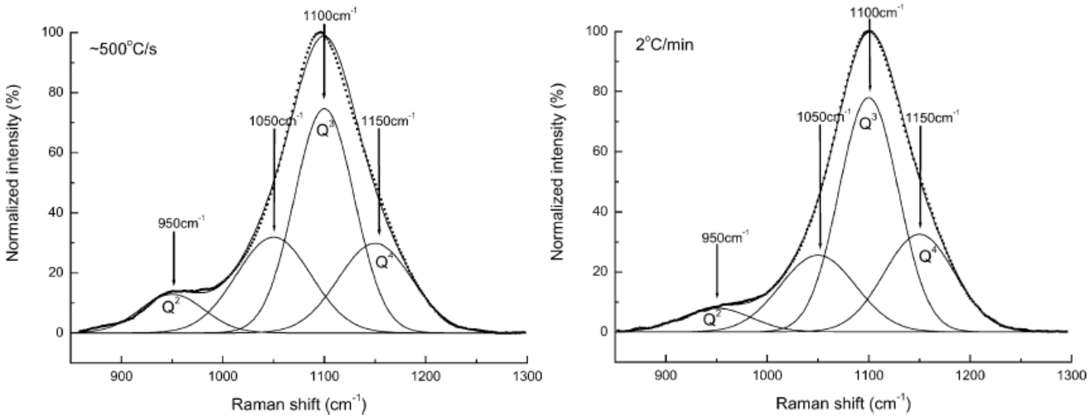

Figure 5.10 *Peak fitting of Raman spectra from sodium silicate glass that have been prepared at different quenching rates [29].*

5.4.4 Raman Spectroscopy – Experimental Method

Raman spectra on the silicate and borosilicate (including the leach disk samples) glass compositions were obtained at room temperature with a 10 mW laser source, x50 magnification with between 50-100 acquisitions across the range 100-3200 cm^{-1} to obtain data for high wavenumbers to which any background signal could clearly be identified and removed. The removal of the background signal from the Raman spectra was carried using a technique adapted from Mysen [31], by fitting an exponential curve up to the high wavenumber region of the spectrum and subtracting it from the data [32].

Quantitative analysis of borosilicate glass Raman spectra was carried out by the fitting of an appropriate number of Gaussian peaks (typically four) to the region of the Raman spectrum associated with the silicon Q^n unit breathing modes (~850-1260 cm^{-1}) [29,32-34]. The half-widths of all but the central peak (assigned to be from a Q^3 unit resonance [29,33]) were constrained to approximately 70 cm^{-1}. Three iron-borosilicate glasses from a previous study by Duddridge [35] were also analysed with this method in order to calculate Q^3 [32] since ^{29}Si MAS NMR is not possible because of the high (>1 mol%) iron content in these samples.

5.5 References

[1] J. M. Roderick, D. Holland, A. P. Howes, and C. R. Scales, *J. Non-Cryst. Solids* **293-295** (2001) 746-751.

[2] D. Feil and S. A. Feller, *J. Non-Cryst. Solids* **119** (1990) 103-111.

[3] N. L. Laberge, P. K. Gupta, and P. B. Macedo, *J. Non-Cryst. Solids* **17** (1975) 61-70.

[4] M. H. Levitt, *Spin Dynamics - Basics of Nuclear Magnetic Resonance*. (John Wiley and Sons Ltd., 2001).

[5] K. J. D. Mackenzie and M. E. Smith, *Multinuclear Solid-State NMR of Inorganic Materials*. Pergamon (2002).

[6] M. Duer, *Introduction to Solid-State NMR Spectroscopy*, 1st ed. (Blackwell Publishing, Oxford, 2004).

[7] A. Medek and L. Frydman, *J. Bra. Chem. Soc.* **10** (4) (1999) 263-277.

[8] A. P. M. Kentgens, *Geoderma* **80** (1997) 271-306.

[9] K. Pike, V. Lemaitre, A. Kukol, T. Anupold, A. Samoson, A. P. Howes, A. Watts, M. E. Smith, and R. Dupree, *J. Phys. Chem.* **108** (2004) 9256-9263.

[10] B. F. Chmelka, K. T. Mueller, A. Pines, J. F. Stebbins, Y. Wu, and Zwanziger, *Nature* **339** (1989).

[11] U.-T. Pingel, J.-P. Amoureux, T. Anupold, F. Bauer, H. Ernst, C. Fernadez, D. Freude, and A. Samoson, *Chem. Phys. Lett.* **294** (1998).

[12] L. M. Bull, B. Buessemer, T. Anupold, A. Reinhold, A. Samoson, J. Sauer, A. K. Cheetham, and R. Dupree, *J. Am. Chem. Soc.* **122** (2000) 4948-4958.

[13] G. Wu, S. Kroeker, R. E. Wasylishen, and R. G. Griffin, *J. Magn. Reson.* **124** (1997) 237-239.

[14] L.-S. Du and J. F. Stebbins, *J. Non-Cryst. Solids* **315** (2003) 239-255.

[15] L.-S. Du and J. F. Stebbins, *J. Non-Cryst. Solids* **351** (2005) 3508-3520.

[16] L. van Wullen and W. Muller-Warmuth, *Solid State Nucl. Mag.* **2** (1993) 279-284.

[17] L.-S. Du and J. F. Stebbins, *J. Phys. Chem.* **B, 107** (2003) 10063-10076.

[18] S. Wang and J. F. Stebbins, *J. Non-Cryst. Solids* **231** (1998) 286-290.

[19] F. Angeli, T. Charpentier, S. Gin, and J. C. Petit, *Chem. Phys. Lett.* **341** (2001) 23-28.

[20] A. P. Howes, T. Anupold, V. Lemaitre, A. Kukol, A. Watts, A. Samoson, M. E. Smith, and R. Dupree, *Chem. Phys. Lett.* **421** (2006) 42-46.

[21] S. K. Giri, E. R. Hemesath, C. J. Olson, S. A. Feller, and M. Affatigato, *Phys. Chem. Glasses* **44** (3) (2003) 230-233.

[22] A. C. Kunwar, G. L. Turner, and E. Oldfield, *J. Magn. Reson.* **69** (1986) 124.

[23] S. P. Brown and S. Wimperis, *J. Magn. Reson.* **128** (1997) 42.

[24] *Raman Spectroscopy - An overview, Raman Products Technical Note Number 1101*. (2001).

[25] A. C. Wright, N. M. Vedishcheva, and B. A. Shakhmatkin, *Materials Research Society Symp. Proc.* **455** (1997) 381-385.

[26] B. C. Bunker, D. R. Tallant, R. J. Kirkpatrick, and G. L. Turner, *Phys. Chem. Glasses* **31** (1) (1990) 30-41.

[27] S. Kojima and M. Kodama, *Japanese Journal of Applied Physics* **33** (1994) 2886-2889.

[28] T. Maehara, T. Yano, and S. Shibata, *J. Non-Cryst. Solids* **351** (2005) 3685-3692.

[29] J. Tan, S. Zhao, W. Wang, G. Davies, and X. Mo, *Material Science and Engineering B* **106** (2004) 295-299.

[30] L. G. Soltay and G. S. Henderson, *Phys. Chem. Glasses* **46** (4) (2005) 381-384.

[31] B. O. Mysen, *Am. Mineral.* **75** (1990) 120-134.

[32] B. G. Parkinson, D. Holland, M. E. Smith, C. Larson, J. Doerr, M. Affatigato, S. A. Feller, A. P. Howes, and C. R. Scales, *J. Non-Cryst. Solids* **Accepted, awaiting publication** (2007).

[33] W. L. Konijnendijk and J. M. Stevels, *J. Non-Cryst. Solids* **20** (1975) 193-224.

[34] H. Maekawa, T. Maekawa, K. Kawamura, and T. Yokokawa, *J. Non-Cryst. Solids* **127** (1991) 53-64.

[35] A. Duddridge, *PhD Thesis, Warwick University* (2004).

Chapter 6

6 Results: - Glass Preparation and Characterisation

6.1 Introduction

In this chapter the experimental results from sample preparation, characterisation (including x-ray diffraction) and thermal analysis measurements, for both the four main borosilicate systems and the reedmergnerite, danburite and boropollucite glasses are presented. Chemical durability measurements, including mass-loss and leachate analysis results, are also presented at the end of this chapter for the mixed-oxide alkali borosilicate glasses.

6.2 Glass Characteristics

6.2.1 X-Ray Diffraction

A selection of samples from each of the modified mixed-alkali borosilicate systems were checked to confirm their amorphous character and identify any crystalline phases formed during casting. Figure 6.1 is typical for all of the borosilicate systems in this study. None of the compositions showed crystallisation during quenching, with all compositions confirmed to be amorphous within the limits of XRD, with no optical phase separation [1,2]. This was expected, since R values for these compositions are outside the zone of immiscibility ($0.2 \leq R \leq 0.3$) where phase separation is found to occur.

Similarly for the reedmergnerite, danburite and boropollucite compositions, all were confirmed to be amorphous and with no visible phase separation, despite the range of K (2-6) throughout the three compositions.

Despite the high use of alkali carbonates in the production of these glasses CO_2 retention is not thought to be a significant problem, based on work by Feller et al. [3-5]. These publications showed that, for alkali borate glasses with $R < 2$ (as studied here), the percentage of CO_2 retained was approximately 0.

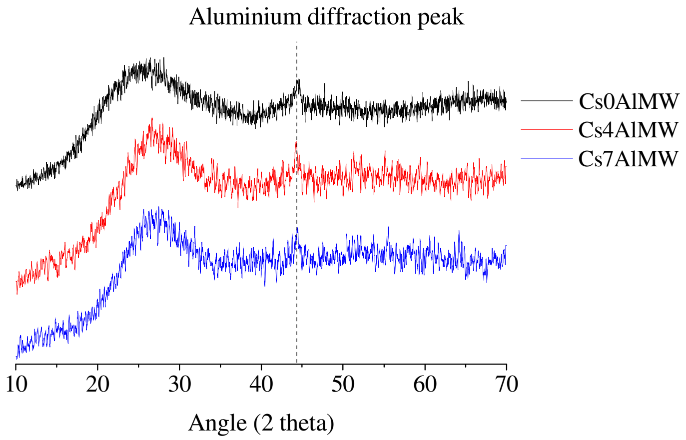

Figure 6.1 *XRD diffractograms for a selection of samples in the CsAlMW system. These XRD diffractograms are typical for all the modified mixed-alkali borosilicate compositions of this study.*

6.3 Thermal Analysis Techniques

6.3.1 Differential Thermal Analysis

6.3.1.1 Borosilicate Glasses

From the differential thermal analysis (DTA) traces obtained for all the compositions in the four-borosilicate glass systems, the glass-transition temperatures (T_g) were obtained (Figure 6.2). Measurements of the melting temperature (T_m) were less clear from these sets of data and so were obtained from further TG-DTA measurements (*cf.* Section 6.3.2).

As predicted from previous work on the caesium containing borosilicate glass system, CsMW [6], T_g for all the borosilicate systems is dominated by the addition of Cs_2O [1]. The increasing Cs_2O content in all the glass systems has the effect of lowering T_g (Figure 6.2) which is explained by the weaker bonding of Cs_2O within the glass network, relative to other oxides present. The heat of formation (ΔH_f) for Cs_2O is smaller at −346 kJ/mol compared to the Group I oxides; −414 kJ/mol and −598 kJ/mol for Na_2O and Li_2O respectively [7] (Table 6.1).

Comparing values of T_g from all the modified mixed-alkali borosilicate glass systems [1] shows measurements to be consistent within error ($\pm 10^{o}$C) with those for the CsMW system measured previously [6]. For identical Cs_2O contents, the CsLaMW compositions have the largest T_g values of the four glass systems.

Oxide	ΔH_f (kJ mol^{-1})
La_2O_3	−1916.3
Cs_2O	−317.8
Al_2O_3	−1675.7
MgO	−602.2
SiO_2	−860.0
Na_2O	−416.2
Li_2O	−596.2
B_2O_3	−1246.0

Table 6.1 *Heat of formation values for the oxides present across the range of borosilicate glass systems [8].*

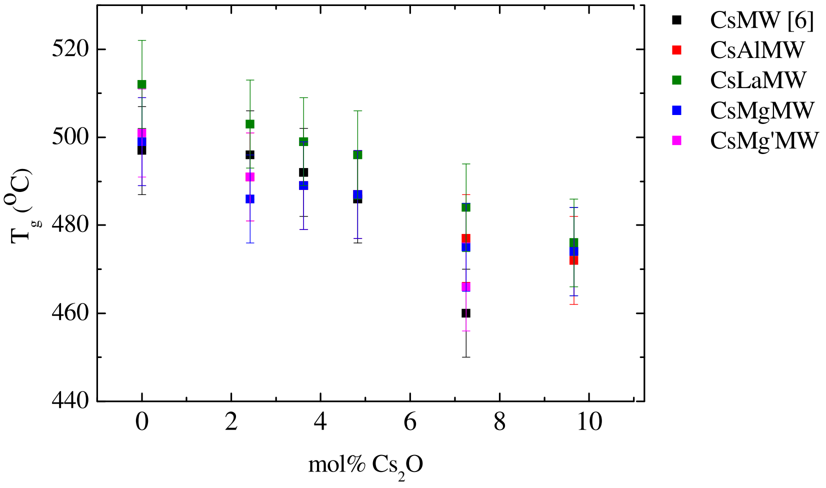

Figure 6.2 *Glass transition temperatures for the four borosilicate systems [1], compared against previous measurements for the CsMW system [6].*

6.3.2 Simultaneous Thermal/Thermogravimetric Analysis

From the TG-DTA measurements acquired from the four modified borosilicate glass systems, both T_g and T_m were identified from the DTA trace, and T_v, the temperature at which mass-loss begins, was identified from the TG trace. A typical plot from one of the borosilicate glasses is shown in Figure 6.3, showing all three temperatures of interest. Measurements of T_g, from the TG-DTA data, agree within error (±10°C) with those from the standard DTA measurements in Section 6.3.1.1 and so measurements of T_v can be regarded as having a similar error.

Values of T_g are shown to decrease approximately linearly with Cs_2O content (Figure 6.4), agreeing with the trend observed in Figure 6.2 from the initial standard DTA measurements in Section 6.3.1. Within error (±10°C) T_g values agree for samples of equal Cs_2O content, although this is not observed for values of T_m, with there being clear separation in the resolved, non-linearly decreasing values of the four borosilicate systems (Figure 6.5).

For all but one of the compositions (Cs2MgMW), the MgO-containing glasses have the lowest values of T_m, with T_m for the CsMg'MW system being lower than those for the CsMgMW, and CsLaMW and CsAlMW systems having increasing T_m respectively. The addition of the intermediates Al_2O_3 or La_2O_3 can therefore be seen to weaken the structure of the glass (on addition of Cs_2O) from that of the original CsMW system, where the absence of these oxides leads to the more stable Si-O-Si, Si-O-B and B-O-B network units. The addition of MgO to CsMW is observed to have the largest detrimental effect to glass stability, not by the weakening of the network units by the formation of less favourable groups, but rather by the more significant formation of a larger number of NBO/Si.

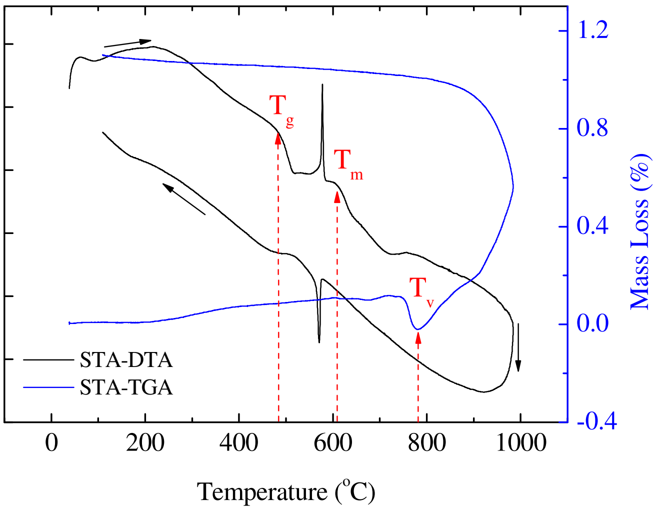

Figure 6.3 *TG-DTA plot for one of the borosilicate glasses (Cs4AlMW) showing both the DTA (-) and TG (-) data.* T_g *is observed at ~450°C, with* T_m *and the temperature of volatilisation (*T_v*) observed at 610°C and ~800°C respectively. Note: arrows indicate direction of heating and eventual cooling.*

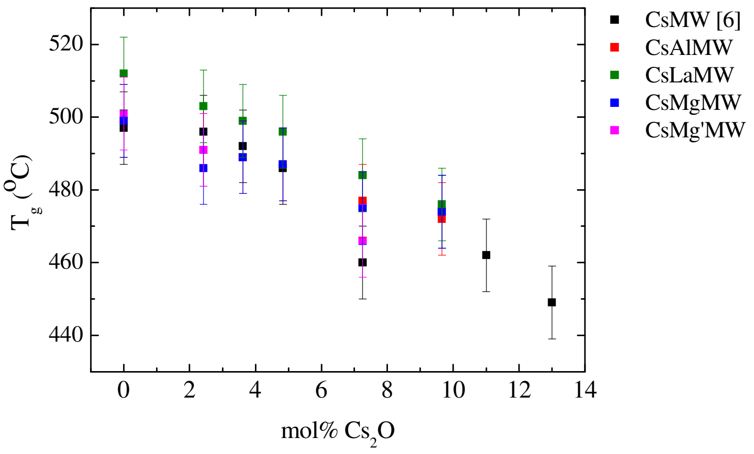

Figure 6.4 *TG-DTA glass transition temperatures (T_g) for the borosilicate glasses, compared against previous measurements [6].*

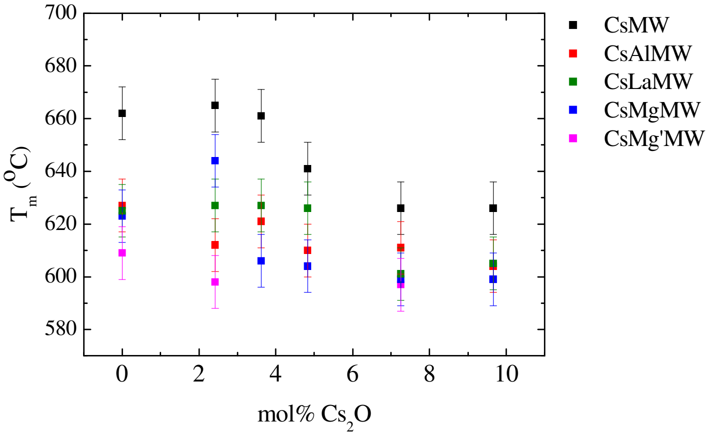

Figure 6.5 *TG-DTA Melting temperatures (T_m) for the borosilicate glasses, compared against (new) STA-DTA measurements taken on the CsMW system.*

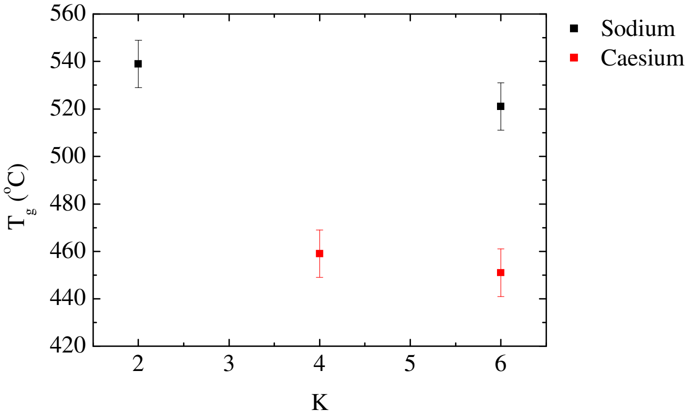

Figure 6.6 *Glass-transition temperatures for the danburite (K = 2), caesium boropollucite (K = 4) and reedmergnerite (K = 6) glasses (sodium and caesium analogues).*

For the reedmergnerite, danburite and boropollucite glasses, which all have R=1, T_g is observed to decrease slightly with increasing K and with replacement of sodium oxide by Cs_2O (Figure 6.6). Within the limited number of measurements and the error (±10°C) it is not possible for this result to be accurately compared with Roderick's study [9] which showed T_g to *increase* as a function of increasing K.

From the TG data of the borosilicate glass systems, the point at which a mass-loss occurs (T_v) appears to vary considerably as a function of composition (Figure 6.7 and Figure 6.8). In the initial study on the CsMW glass system [6,10] the temperature at which this was thought to occur (since TG-DTA measurements were not available at that time) was ~1000°C. This however is not the case across the range of systems in this current study, with T_v observed to vary non-linearly as a function of caesium oxide content and across the range 700-950°C; lower than the initial presumed temperature of volatilisation.

Although there appears to be little trend to the data in Figure 6.8, the observation of a range of temperatures at which mass-loss occurs, agrees with the work of Asano *et al.* [11] which revealed various alkali borate groups to evolve from the melt throughout a similar distribution of temperatures, depending on the initial glass composition (Table 6.2). These results of Asano *et al.* [11] interestingly also show that the temperatures at which Na/Cs-BO_2 and $NaCs(BO_2)_2$ vapour species form decrease as the ratio of Cs/(Cs+Na) increases, highlighting the dominant effect of Cs_2O on the thermal properties of a glass.

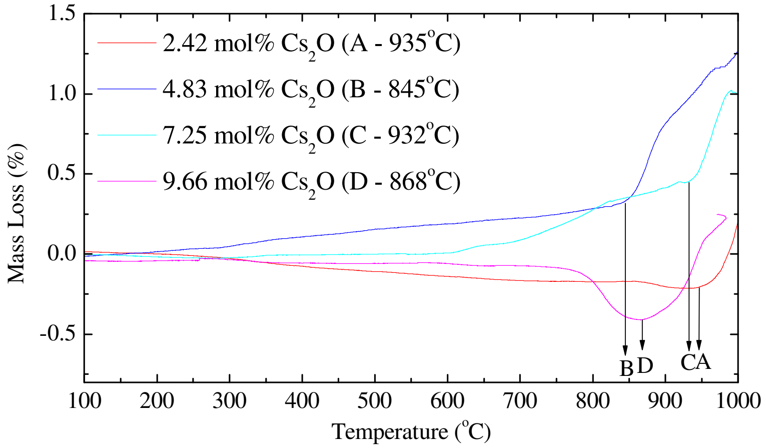

Figure 6.7 *STA-TG plots for a selection of the CsMW glasses with different caesium oxide contents showing the different values of resolved T_v (A-D).*

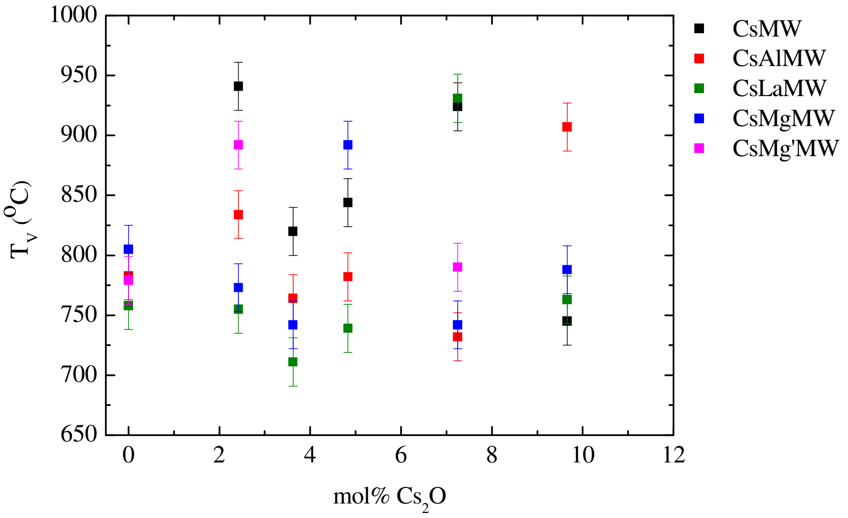

Figure 6.8 *Temperatures of volatilisation (T_V) for the borosilicate glasses.*

Glass Composition	Glass R, K	Ratio Cs/(Na+Cs)	Temperature Range of Formation (^oC)	Vapour Species Evolved	Vapour R (N.B. K=0)
$1Na_2O$-$1B_2O_3$-$3SiO_2$	1.0, 3.0	0	642-827	$NaBO_2$	1.0
			772-899	$Na_2(BO_2)_2$	1.0
$1Na_2O$-$0.15Cs_2O$-$1B_2O_3$-$3SiO_2$	1.15, 3.0	0.13	732-877	$NaBO_2$	1.0
			763-877	$Na_2(BO_2)_2$	1.0
			732-847	$CsBO_2$	1.0
			800-877	$NaCs(BO_2)_2$	1.0
$0.85Na_2O$-$0.15Cs_2O$-$1B_2O_3$-$3SiO_2$	1.0, 3.0	0.15	729-849	$NaBO_2$	1.0
			729-849	$Na_2(BO_2)_2$	1.0
			729-849	$CsBO_2$	1.0
			755-849	$NaCs(BO_2)_2$	1.0
$1Cs_2O$-$1B_2O_3$-$3SiO_2$	1.0, 3.0	1.0	572-763	$CsBO_2$	1.0

Table 6.2 *Range of temperatures at which rapid mass-loss was observed to begin in the study carried out by Asano et al. [11]. The compositions of the vapour species formed, which are of further interest in Chapter 7, are also given.*

6.3.3 Volatilisation Measurements

Volatilisation measurements showed a large degree of scatter and non-linear behaviour throughout the range of systems, as a function of increasing Cs_2O content (Figure 6.9). Typically mass-losses of up to 40 % were observed, with the CsAlMW and CsLaMW systems being the most volatile of the four modified borosilicate glass systems. Mass-losses were observed to increase from 3 % to 30 %, as the length of time for which the glasses were heated at 1000°C was increased from 30 minutes to 4 hours. The decision to increase heating time was based on the requirement to obtain larger deposits of the volatile species than those obtained in the previous study [6]. These deposits would then be used for further analysis with Raman spectroscopy and EDX, to determine their composition and structure.

The effects of glass surface area on the resultant mass-loss, as highlighted in Harbour's volatilisation study on borosilicate glasses containing simulated quantities of American HLW [12], were minimised where possible by using an even distribution of glass powder over the base of the platinum boat. Values for the mass-gain on the alumina substrate, placed over the crucible of the volatilisation experiment, are not given due to the greater uncertainty associated with this measurement.

Mass-losses were observed for all four systems, at all compositions (excluding MW), confirming the observation made by Asano *et al.* [13] that mass-loss occurs when $R > 1$, independent of alkali oxide present. Based on this result (Figure 6.9), and previous studies [6,11,13-15], it can be deduced that the presence of Cs_2O is not crucial for mass-loss to occur (Figure 6.9). Additions of other oxides can produce significant increase in volatilisation loss. The compositions Cs0AlMW, Cs0LaMW, Cs0MgMW and Cs0Mg'MW all have non-zero mass-losses even though no Cs_2O is present. The relationship between mass-loss and silicon Q^3 content is made in the following chapter.

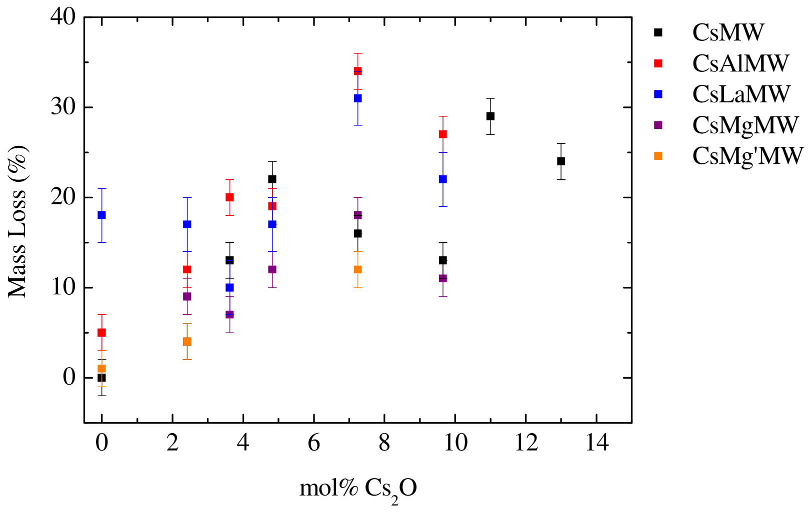

Figure 6.9 *Mass-loss measurements on all of the borosilicate glass systems, including new measurements, with the longer 4 hour heating time, on the CsMW system.*

Volatilisation measurements on the four reedmergnerite and danburite glasses, containing either sodium or caesium (Table 6.3), show that the degree of mass-loss is inversely related to K; with the danburite glass showing a larger mass-loss than the reedmergnerite composition. This result transpires to be an important factor in explaining the mass-loss results for the four borosilicate systems (Figure 6.9) when related to the presence of two medium-range order (MRO) structures based on danburite and reedmergnerite as measured using ^{11}B MAS NMR [16-18] (*cf.* Chapter 5).

One possible explanation for the difference in volatility between reedmergnerite and danburite, could be the presence in the danburite structure of the boron-oxygen-boron bond (B-O-B), which is energetically unfavourable compared to B-O-Si or Si/B-O-X (X: Li, Na, Cs, Mg).

Structure	K	Na-containing mass-loss (±2 %)	Cs-containing mass-loss (±2 %)
reedmergnerite	6.0	1	4
danburite	2.0	12	12

Table 6.3 *Mass-loss (%) results from the four reedmergnerite (K=6.0) and danburite (K=2.0) glasses (containing either sodium or caesium).*

6.4 Chemical Durability - Leach Testing

6.4.1 pH and elemental analysis of leachates

The differences in the measured leachate pH after the 14 day tests, are shown in Figure 6.10. The most significant result is the increase in leachate pH as a function of Cs_2O content for the CsAlMW glass system. This is in contrast to results for the CsMW, CsLaMW and CsMg'MW systems where the observed pH decreases to a more alkaline pH, as Cs_2O content is increased. For the remaining CsMgMW system, the pH increases slightly upon the addition of caesium oxide to the glass, and then proceeds to plateau, a trend similar to that for the CsAlMW system.

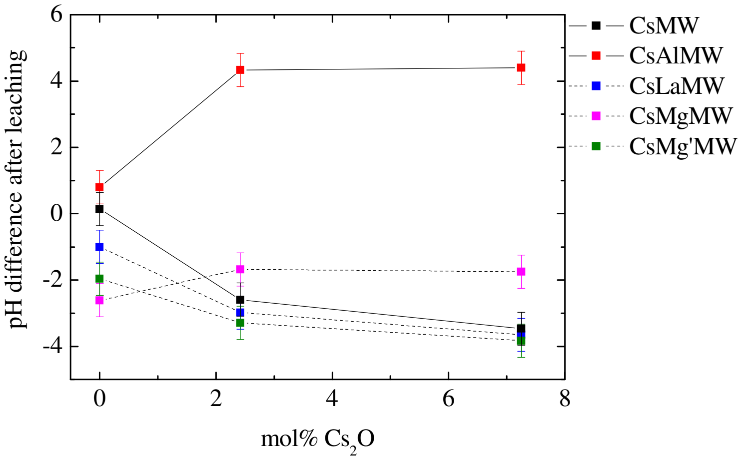

Figure 6.10 *Change in water pH as a function of caesium oxide content, for the four borosilicate glasses and CsMW system.*

A limited number of leachate solutions from the four glass systems, including the caesium-sodium-lithium borosilicate (CsMW) system of a previous study [6], were analysed(*) for Cs, Na and Li content. Table 6.4 shows the results of these measurements, with leached Cs, Na and Li contents (ppm) and the rate of increase of leached alkali content (ppm per mol% Cs_2O) for the CsMW system and aluminium-, lanthanum- and magnesium-containing mixed alkali borosilicate glasses. Where

---

(*) ICP alkali leachate analysis carried out by CERAM Reseach Ltd, Queens Road, Penkhull, Stoke-on-Trent, Staffordshire ST4 7LQ, United Kingdom, Tel +44 (0)1782 764444 possible, errors have been quoted based on measurements carried out on a control solution (deionised water).

For all four glass systems, the quantity of leached Cs and Na is greater than that of Li, which can be explained by the greater reactivity of Cs and Na. Of the four base-glasses (i.e. glasses with 0 mol% Cs_2O content) the leachate solution from the Mg-containing base-glass (Cs0MgMW) contained the greatest quantity of Li and Na; 13 and 30 ppm respectively, compared to < 1 and < 5 ppm for the remaining three glass systems.

The addition of Al_2O_3 or L_2O_3 to the CsMW glass system increases the rate at which Cs and Na are leached in the presence of water, with the La-containing system showing the greatest rate of corrosion with Cs and Na leach rates of 4.6±0.8 and 6.6 ppm/mol% Cs_2O respectively, compared to 3.4±0.4 and 3.9 ppm/mol% Cs_2O for the aluminium-containing system, which has a Na leach rate similar to that of the CsMW glass system (3.3 ppm/mol% Cs_2O).

Sample	mol% Cs_2O	Leached Alkali content			Rate of increase of leached alkali content (ppm/mol% Cs_2O)		
		Cs (± 2 ppm)	Li	Na	Cs	Li	Na
MW	0	0.24	0.2	2	9.8 ± 0.4	2.4	3.3
Cs4MW	4.83	47.5	12	18			
Cs0AlMW	0	19.5*	0.7	3	3.4 ± 0.4	2.3	3.9
Cs4AlMW	4.83	35.7	12	22			
Cs0LaMW	0	0.17	0.2	3	4.6 ± 0.8	3.2	6.6
Cs2LaMW	2.42	11.4	8	19			
Cs0MgMW	0	2.48	13	30	-		

Table 6.4 *Leached caesium, lithium and sodium contents (ppm) and rate of increase of leached caesium, lithium and sodium content (ppm per mol% Cs_2O) for a limited number glasses from the CsMW, CsAlMW, CsLaMW and CsMgMW glass systems. Base-glass compositions (i.e. glasses with 0 mol% Cs_2O) are highlighted (red). (* Dubious result).*

6.4.2 Mass-Loss Measurements

The mass-loss of the glasses is displayed as a function of Cs_2O addition in Figure 6.11. For the CsAlMW and CsLaMW systems, the percentage mass-loss increases significantly more than for the CsMgMW, CsMg′MW and CsMW systems. The reduction in Al_2O_3 and La_2O_3 content leads in this study to greater mass-loss as a function of increasing Cs_2O content.

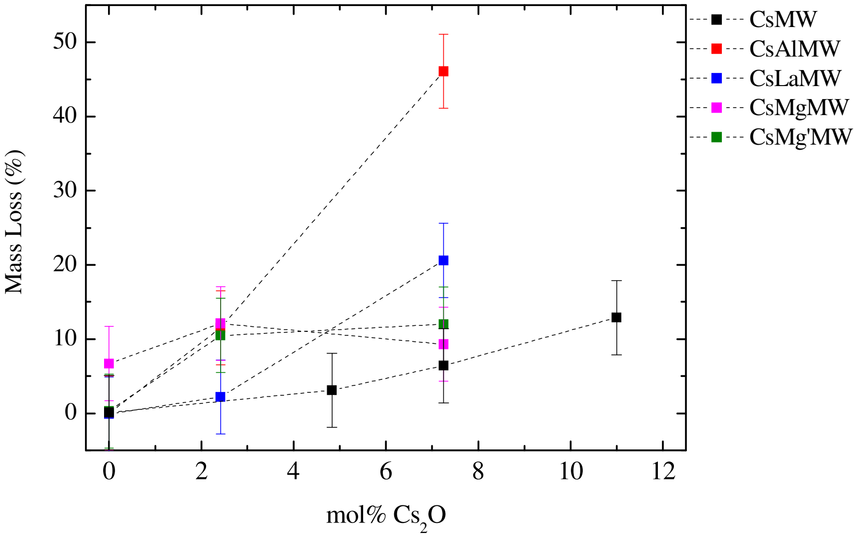

Figure 6.11 *Mass-loss (%) of leached glasses as a function of caesium oxide content, compared with measurements taken on the CsMW glass system.*

6.4.3 Leached Glass Structure

Structural measurements of the leached glasses are reported in the following chapter, in the form of Raman spectroscopy measurements.

6.5 Summary

A range of thermal analysis measurements; DTA, TG-DTA and a custom designed mass-loss experiment have been used on the four modified mixed-alkali borosilicate glasses, to obtain glass transition- and melting-temperatures, as well as values for the degree of mass-loss from each of the compositions, all as a function of increasing Cs_2O content. The temperature at which rapid mass-loss is observed, obtained from TG measurements, is also reported.

DTA measurements from both standard-DTA and TG-DTA experiments show that both the glass transition- and melting-temperatures decrease with increasing Cs_2O content, a consequence of both the weaker bonding and the lower heat of formation of Cs_2O compared to the remaining oxides present in the different compositions.

For the two Cs- and Na-containing reedmergnerite glasses, with identical R and K, the glass transition temperatures are lower in compositions where Cs rather than Na is present - confirming the dominant effect the presence of caesium oxide has on the thermal properties of the different glass systems.

Measurements of the melting temperature show a similar result, with values decreasing with increasing Cs_2O content, with the melting temperatures for the MgO-containing glasses being lower than those for both the Al- and La-containing glasses and the original caesium-sodium-lithium borosilicate system from the previous study [6]. This result suggests that the formation of non-bridging oxygens on the silicate network by modifier-MgO groups has a greater effect on thermal stability than the introduction of intermediate oxides, such as Al_2O_3 or La_2O_3.

Values of T_V vary unsystematically with Cs_2O content. The range of temperatures over which volatilisation occurs is typically between 700-950^{o}C, which is lower than the temperature of ~1000^{o}C at which it was originally thought species were evolving from the melt. This result compares well with results from the study by Asano *et al.* [11] which, although on much simpler one or two alkali oxide borosilicate glasses, showed alkali borate vapour species to form across a similar range. The notion of this being a high temperature problem must therefore also be reviewed in light of this result, since many of the volatilisation temperatures are within 150^{o}C of the melting temperatures of these glasses - typically 650^{o}C.

Non-zero values of mass-loss were observed for all four glass systems, even in the absence of Cs_2O; confirming previous results [6,11,13-15] which showed that the presence of Cs_2O is not essential for mass-loss to occur, and other factors, such as the addition of intermediate oxides (such as Al_2O_3, La_2O_3 or TeO_2) or modifiers (e.g. MgO) to the base-glass composition MW are potentially more detrimental to glass thermal stability and the formation of volatile species at ‘high’ temperature. The observation by Asano *et al.* [13] that volatilisation occurs for $R>1$ is also confirmed in these results.

Results from the two reedmergnerite glasses shows that the observed mass-loss is four-times greater when the glass contains Cs_2O rather than Na_2O. For the two danburite glasses however (one containing Na_2O and one with Cs_2O) the mass-loss values were identical at 12 %, highlighting a further factor; this being the presence of B-O-B links in the danburite glass, that are not present in the reedmergnerite composition, effecting volatility. Comparing the caesium-containing reedmergnerite and danburite glasses, with identical R but K=6 and 2 respectively, the mass-loss was three times greater for the danburite glass. These B-O-B links are energetically less favourable then other network links, and therefore an important factor affecting glass volatility. This is discussed further in Chapter 7, in conjunction with quantitative results of the fraction of B-O-B and non-B-O-B units in all four borosilicate glasses obtained from ^{11}B MAS NMR measurements.

Chemical durability measurements in the form of leach corrosion tests show pH values of the resultant leachate solutions to increase and then plateau as a function of caesium oxide content for the CsAlMW and CsMgMW glass systems but to decrease for the CsMW, CsLaMW and CsMg'MW systems. In terms of the alkali content of the leachate solutions, all show Cs, Na and Li to be present, with increasing Cs_2O content in the glasses leading to a greater increase in the quantity of leached Cs. The introduction of Al_2O_3, La_2O_3 and MgO to the caesium-sodium-lithium borosilicate glass composition results in a greater quantity of alkali being leached from each of the glasses, with La_2O_3 having the greatest affect.

Mass-loss from the leached glasses increases with Cs_2O content, consistent with the hygroscopic nature of Cs. The introduction of Al_2O_3, La_2O_3 or MgO increases mass-loss, with the Al_2O_3 containing glass system showing the greatest increase, from ~5 % at 0 mol% Cs_2O to ~50 % with 7.25 mol% Cs_2O.

6.6 References

[1] B. G. Parkinson, D. Holland, M. E. Smith, A. P. Howes, and C. R. Scales, *J. Non-Cryst. Solids* **353** (2007) 4076–4083.

[2] B. G. Parkinson, D. Holland, M. E. Smith, A. P. Howes, and C. R. Scales, *J. Phys.: Condens. Matter* **19** (2007).

[3] A. Karki, S. A. Feller, H. P. Lim, J. Stark, C. Sanhez, and M. Shibata, *J. Non-Cryst. Solids* **92** (1987) 11-19.

[4] M. Shibata, C. Sanchez, H. Patel, S. A. Feller, J. Stark, G. Sumcad, and J. J. Kasper, *J. Non-Cryst. Solids* **85** (1986) 29.

[5] J. Kasper, S. A. Feller, and G. Sumcad, *Journal of American Ceramics Society* **67** (4) (1984).

[6] B. G. Parkinson, D. Holland, M. E. Smith, A. P. Howes, and C. R. Scales, *J. Non-Cryst. Solids* **351** (2005) 2425-2432.

[7] R. D. Harrison, *Revised Book of Data,* (Longman, 1972).

[8] R. C. Weast, *Handbook of Chemistry and Physics*, 55 ed. (CRC Press, 1974).

[9] J. M. Roderick, *PhD Thesis, Warwick University* (2001).

[10] B. G. Parkinson, *MSc Thesis, Warwick University* (2004).

[11] M. Asano, T. Kou, and Y. Yasue, *J. Non-Cryst. Solids* **92** (1987) 245-260.

[12] J. R. Harbour, *Journal of American Ceramics Society* **75** (3) (1992) 507-513.

[13] M. Asano and Y. Yasue, *J. Nucl. Mater.* **138** (1986) 65-72.

[14] M. Asano, T. Kou, and Y. Mizuntani, *J. Non-Cryst. Solids* **112** (1989) 381-384.

[15] M. Asano and Y. Yasue, *J. Nucl. Mater.* **151** (1988) 181-188.

[16] L.-S. Du and J. F. Stebbins, *Chem. Mater.* **15** (2003) 3913-3921.

[17] L.-S. Du and J. F. Stebbins, *J. Phys. Chem.* **B, 107** (2003) 10063-10076.

[18] L.-S. Du and J. F. Stebbins, *J. Non-Cryst. Solids* **315** (2003) 239-255.

Chapter 7

7 Results and Discussion: - Standard Borosilicate Glass Structural Determination

7.1 Introduction

Chapter 7 presents structural results for the four modified mixed-alkali borosilicate glass systems, obtained from density measurements, NMR and Raman spectroscopy. NMR results include the boron N_4 and silicon Q^3 fractions resolved from ^{11}B and ^{29}Si MAS NMR respectively, as well as resolved Q^3 fractions from Raman spectroscopy. Structural details for all the systems are outlined and where possible compared against similar compositions, models and studies. Raman spectra and EDX measurements of the condensed species evolved during mass-loss measurements are also presented.

7.2 Density Measurements

For all the four systems, density and molar volume values increase linearly with caesium oxide content (Figure 7.1 and Figure 7.2). This result is consistent with previous work [1] with the dominant overall factor being the greater density of caesium oxide (4.25 g/cm^3) compared to the other four 'core' oxides (Table 7.1); sodium-, lithium-, boron-, and silicon-oxide, and all but one of the three remaining additive oxides, lanthanum oxide. Although of significantly greater density than the remaining oxides present in glasses of the CsLaMW system, the addition of lanthanum oxide to the CsMW system makes a negligible difference to the overall density due to its relatively small molar quantity (1.68 mol%) in the initial composition of the glass. This is also true for the CsAlMW system, with the comparatively dense aluminium oxide (3.97 g/cm^3) contributing only ~1 mol% to the starting composition, before the addition of the more significant caesium oxide.

Oxide	Density (g/cm^3)
La_2O_3	6.51
Cs_2O	4.21
Al_2O_3	3.97
MgO	3.58
SiO_2	2.20
Na_2O	2.27
Li_2O	2.01
B_2O_3	1.81

Table 7.1 *Densities [2] of all the oxides present throughout the borosilicate glass systems, listed in order of decreasing density.*

Dopant ion	Bond length: 4-coordination (Å)	Bond length: 6-coordination (Å)	Bond length: 8-coordination (Å)
La^{3+}	2.28	2.43	2.54
Al^{3+}	1.76	1.91	-
Mg^{2+}	1.69	-	-

Table 7.2 *X-O bond lengths for a number of co-ordination states of the additive ions from [3].*

Molar volumes (V_m) for the four systems, calculated from density measurements, are shown to increase as a function of caesium oxide content. This is consistent in part with the larger ionic size of caesium compared to lithium, sodium and the remaining borosilicate oxide components [1]. The molar volume is equal within error for the CsAlMW and CsMgMW systems, reflecting the approximately equal M-O bond lengths in 4-coordination (Table 7.2). For the CsLaMW glasses V_m is approximately equal to the CsAlMW and CsMgMW systems up to the composition Cs3LaMW with 3.63 mol% Cs_2O content, whereupon V_m increases from 30 to 32 cm^3/mol, before again being equal to both the CsAlMW and CsMgMW compositions for glasses containing 9.66 mol% Cs_2O. For the CsMg′MW system, the molar volume is consistently greater than the remaining three glass systems, based on the much larger quantity (~10 mol%) of the relatively less dense magnesium oxide throughout the glass compositions.

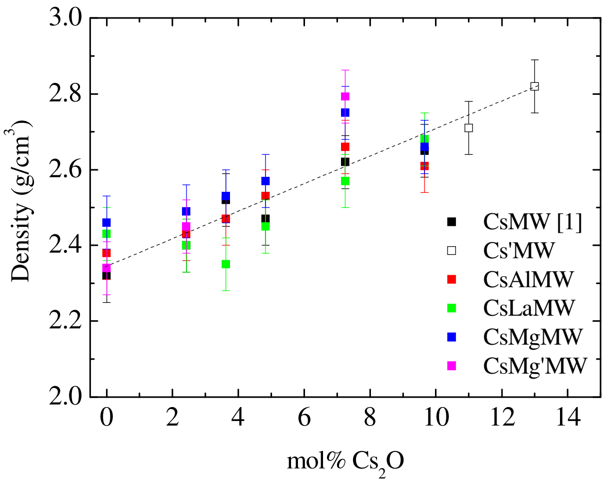

Figure 7.1 *Density values for all the borosilicate glasses, compared against values measured on the CsMW system [1]. Note: line is a guide to the eye.*

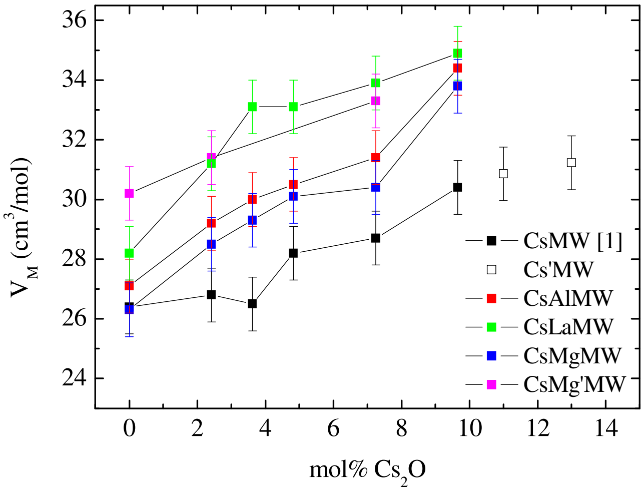

Figure 7.2 *Molar volumes for the borosilicate glasses compared against values for the CsMW system [1].*

For the reedmergnerite, danburite and boropollucite glasses, glass density is observed to decrease as a function of increasing K for both caesium- and sodium-containing glasses (Figure 7.3), consistent with the study by Roderick [4] and is explained by the longer bond to oxygen of silicon compared to boron, resulting in a less dense glass network for the same value of R. For identical values of R, the density and V_m are greater for caesium-containing glasses. Figure 7.4 shows that, for both alkali-analogues, V_m decreases as a function of K, but does so much more rapidly for the larger Cs^+ ion, raising interesting questions about the accommodation of large cations in the borate and silicate networks.

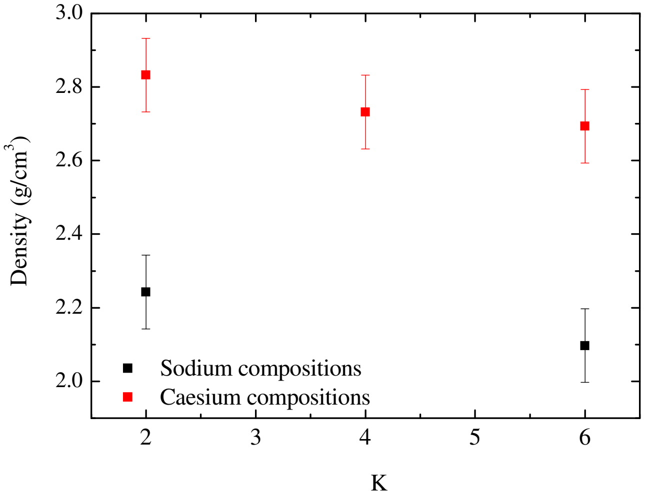

Figure 7.3 *Densities for the danburite (K=2), caesium boropollucite (K=4) and reedmergnerite (K=6) glasses, as a function on K and composition. Note: all compositions have R=1.0.*

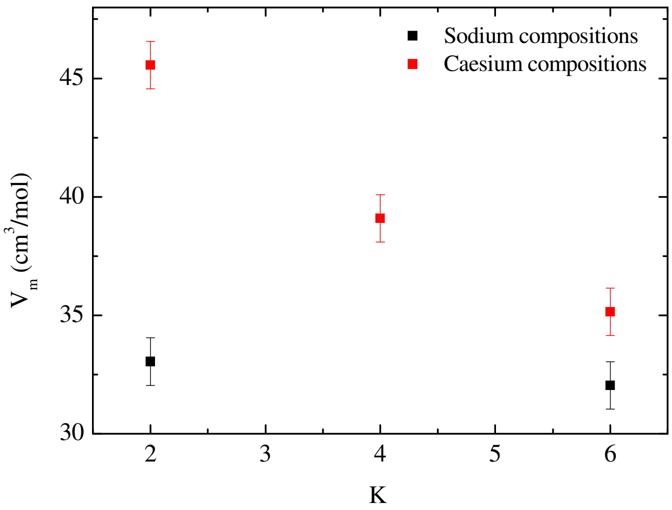

Figure 7.4 *Molar-volume values for the danburite (K=2.0), caesium boropollucite (K=4.0) and reedmergnerite (K=6.0) glasses as a function on K and composition. Note: all compositions have R=1.*

7.3 Nuclear Magnetic Resonance

7.3.1 Borosilicate Glasses

In this section, the results are presented for ^{23}Na, ^{27}Al, ^{11}B and ^{29}Si MAS NMR and the structural implications are discussed; including N_4 and Q^n values. The fractions of the medium-range order (MRO) structures and non-MRO silicon units, resolved from ^{11}B and ^{29}Si MAS NMR are also presented.

7.3.2 ^{23}Na MAS NMR

^{23}Na MAS NMR spectra from the four borosilicate glass systems showed a broad resonance (Figure 7.5), similar to that previously observed in sodium borosilicate glasses [5]. The asymmetry in the lineshape is due to the residual second-order quadrupolar broadening of a distribution of quadrupole interactions [6]. Although no attempt has been made to fit the ^{23}Na MAS NMR lineshape, peak half-width measurements (Table 7.3) show an increase of approximately 4 ppm across the range of caesium oxide contents for all four glass systems, implying an increase in the range of environments and/or an increase in the field gradient at the nucleus.

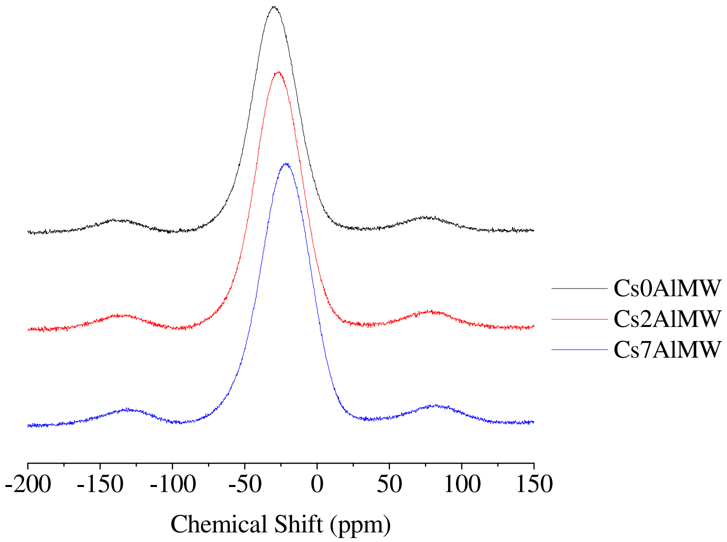

Figure 7.5 *Example of ^{23}Na MAS NMR data for the modified mixed-alkali borosilicate glasses.*

Figure 7.6 shows the peak maximum chemical shift of the peak resonance for each of the spectra (δ_{peak}), with shifts ranging from −28 to −10 ppm. For all four systems, δ_{peak} increases linearly with caesium oxide content(*) with the CsAlMW, CsLaMW and CsMgMW systems showing an increase from approximately −15 ppm at 0 mol% Cs_2O, to −10 ppm at 7.25 mol% Cs_2O. For the CsMg′MW system, the initial δ_{peak} (–27 ppm) is significantly lower than for the first three systems and increases to −15 ppm as Cs_2O is added.

This linear increase agrees with measurements by Ratai *et al.* [7,8] who suggest that this increase in shift originates from increasing charge transfer to the borate and silicate networks, indicating that the overall charge density is more important than the nature of the glass network or alkali ions.

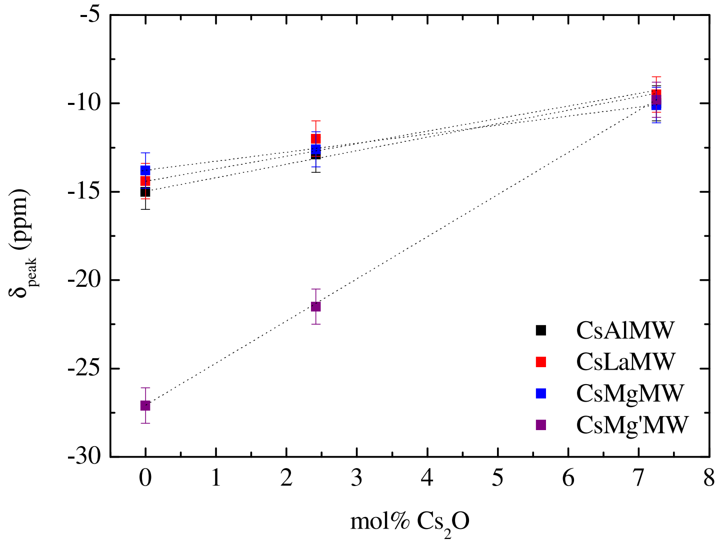

Figure 7.6 *Peak maximum chemical shift values for the four borosilicate glass systems. Note: lines are a guide to the eye.*

mol% Cs_2O	CsAlMW Δ ±0.5 ppm	CsLaMW Δ ±0.5 ppm	CsMgMW Δ ±0.5 ppm	CsMg'MW Δ ±0.5 ppm
0	33.8	35.4	35.4	36.3
2.42	36.3	36.3	37.0	36.3
7.25	38.7	37.9	37.9	37.1

Table 7.3 *Half-widths (Δ ppm) of the ^{23}Na MAS NMR spectra for the four borosilicate systems.*

---

[*] Note that the absolute content of Na_2O will decrease with addition of Cs_2O although its quantity relative to the other components remains constant.

7.3.3 ^{27}Al MAS NMR

The ^{27}Al MAS NMR spectra in Figure 7.7 show two or more peaks: one at approximately 55 ppm associated with 4-coordinated sites and one/two between 10 and −3 ppm, which arise from 6-coordinated sites [9]. It is clear that the majority of Al are in 4-coordinated sites. In the 0 mol% and 9.66 mol% Cs_2O samples, 6-coordinated Al gives a single sharp peak at ~ −3 ppm, superimposed on a broader peak (complicated by the spinning sideband, denoted by *) whereas, in the 2.42 mol% and 4.83 mol% Cs_2O samples, there is a second sharp peak at ~10 ppm which is of similar intensity. The total percentage of 6-coordinated Al is ~10 %, with slightly more in the 4.83 mol% Cs_2O sample [9].

El-Damrawi *et al.* [10] showed that Al^{3+} exists in $[AlO_4]^-$ units and imply that the tetrahedral aluminium is associated with the silicate network exclusively. Duddridge [11], studying an alkali-aluminoborosilicate glass system, concluded that Al^{3+}, in glasses with K=3.2, exist mainly as $[AlO_4]^-R^+$ units, indicating that alkali ions associate with Al_2O_3 in preference to B_2O_3. This would agree with the ^{11}B MAS NMR N_4 data presented later in this chapter, where N_4 for the CsAlMW system is found to be lower than for the CsMW system [1,12], for compositions with identical R, confirming the network intermediate role of aluminium.

In Figure 7.7 the position of the 4-coordinated Al peak of ~55 ppm is typical of $[Al(OSi)_4]$ rather than $[Al(OB)_4]$ (~40-45 ppm) units and means that the Al_2O_3 addition is associating specifically with silicate polyhedra. It is possible that $[AlO_4]$ units substitute for $[BO_4]$ units in reedmergnerite or danburite. However, there is overwhelming evidence that $[AlO_4]^-$ units avoid each other in aluminosilicates. Therefore, we would not expect $[AlO_4]^-$ to substitute for $[BO_4]^-$ in the danburite units. Du and Stebbins [13] found that the mutual avoidance of $[AlO_4]$ and B_4 in aluminoborate glasses is less pronounced than for B_4-B_4 or $[AlO_4]$-$[AlO_4]$. In a subsequent study on aluminoborosilicate glasses [14], Du *et al.* observed that $[AlO_4]$-B_4 avoidance is a major factor where only monovalent cations are available for charge balancing. The origin of the 6-coordinated Al units is not known. The sharper features may arise from a crystalline impurity phase(s) - possibly aluminosilicate in nature. Their overall abundance is too low for crystalline peaks to be detected by the X-ray diffraction measurements reported in Chapter 6. Alternatively, they may correspond to $[Al(OM)]_6$ units with different next nearest neighbour M atoms.

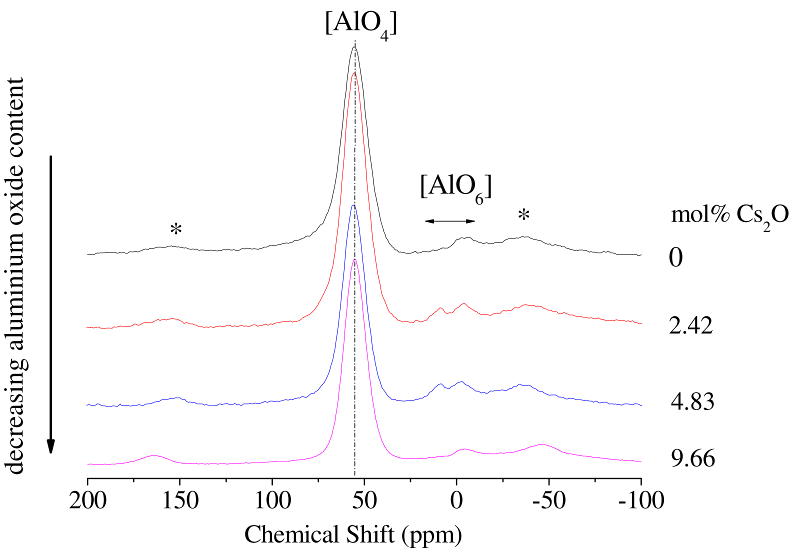

Figure 7.7 *^{27}Al MAS NMR spectra for the CsAlMW system [9].*

7.3.4 ^{11}B MAS NMR

Boron-11 MAS NMR measurements from all four borosilicate glass systems (Figure 7.8, Figure 7.9 and Figure 7.10) were initially used to calculate the fraction of four-coordinated boron (N_4) in each system for comparison against previous measurements in the literature [1,15] including the Dell model of N_4 for K=3.0 borosilicate glasses [16] (Figure 7.11 and Figure 7.12). In addition, fits to the ^{11}B MAS NMR spectra were used a) to calculate the fraction of different resolved BO_4 peaks [17-19] and hence the fraction of different borosilicate superstructures present, and b) in conjunction with ^{29}Si MAS NMR measurements to calculate the fraction of MRO and non-MRO silicon units.

Du *et al.* [18] deduced the possibility of up to three [BO_4] sites (each separated by ~1.6 ppm) with different next nearest neighbours (NNN); (0B, 4Si), (1B, 3Si) and (2B, 2Si) (Figure 7.10). The first two of these sites can be related to the presence of the reedmergnerite and danburite-like superstructural units respectively, which have [BO_4] sites with these surrounding environments, i.e. [$B(OSi)_4$] and [$B(OB)(OSi)_3$]. In the Du studies, clearer evidence for the presence of all these three [BO_4] sites in the ^{11}B lineshape can be found in compositions of varying R (0 < R < 1) and K (0.5 < K < 4), with the symmetry of the [BO_4] peak shifting through the centre line of –2 ppm as a function of K (Figure 7.10) [17,18]. Resolving the two [BO_4] peaks in the ^{11}B lineshape showed them to be separated by a chemical shift of ~1.6 ppm throughout the range of compositions, and peak fitting of the data in this current study is consistent within error with that in the literature.

The ^{11}B MAS NMR spectra (Figure 7.8) show a large, relatively narrow peak from [BO_4] at ~0 ppm and a smaller, broader peak from [BO_3] at ~13 ppm, with Figure 7.9 being representative of the ^{11}B MAS NMR spectra for all four systems. Peak fitting of the ^{11}B MAS NMR spectra assumed the presence of two [BO_3] sites (symmetric and asymmetric) as well as two [BO_4] sites (Figure 7.9), though the range of possible NNN mean that more than two [BO_3] sites are possible. Fitting of two [BO_4] peaks to alkali borate [20,21] and borosilicate [18] (Figure 7.10) ^{11}B MAS NMR data is a relatively new approach, since the ^{11}B MAS NMR lineshapes observed in previous studies, of borosilicate glasses, in particular [1,4,11,15], had not suggested the existence of multiple [BO_4] sites, and therefore only single peaks had been fitted. In this current study however, the [BO_4] peak at ~0 ppm, was fitted using two 50% Gaussian-50% Lorentzian peaks (a good approximation, since the quadrupolar coupling constant is small for the B_4 site). To obtain a physically sensible fit the η values for the [BO_3] peaks were constrained to be 0.28.

Only two peaks were fitted under the [BO_4] peak for the four systems, corresponding to two superstructural units - reedmergnerite and danburite, since the value of R for this set of glasses does not produce significant quantities of the third (2Si, 2B) B_4 site. Although this third peak was fitted in the study by Du *et al.* [19], its contribution to the total area of the [BO_4] lineshape was found to be insignificant compared to the resolved area of the (0B, 4Si) and (1B, 3Si) B_4 peaks and its fraction was found to decrease with increasing R, and K, where it decreased from ~40 % to 7 % as K was increased from 0.5 to 2 [9]. Hence, although K (= 3.2) values for the compositions is this current study exist in the compositional range of glasses used by Du *et al.* [19] ($2 < K < 4$) the presence of a (2B, 2Si) site is diminished by the much greater values of R used here ($1 < R < 2$, compared to $0.25 < R < 0.75$).

In fitting the two B_4 peaks, the positions were initially fixed to mean values reported by Du and Stebbins [18] and the fitting procedure run to see if peaks of realistic half-widths were obtained. Fits were judged to be unrealistic if the resolved half-width for the smaller peak (at approximately −2 ppm) was greater than 2 ppm. After this check, the peak positions were allowed to vary. The danburite peak was found at ~ −0.2 ± 0.5 ppm and the reedmergnerite peak at ~ −1.7 ± 0.5 ppm, giving a separation of ~1.5 ± 0.5 ppm, with peak-widths of ~2.7 ± 0.5 ppm and ~2.0 ± 0.5 ppm respectively. The fraction of danburite-like units was obtained by dividing the fractional intensity by 2 to allow for the presence of twice as many B atoms in the danburite unit as the reedmergnerite unit [9].

N_4 fractions calculated from the DMfit2002 program [22] were corrected with the resolved $[BO_3]$ fraction being increased by 4 %. This increase is necessary due to the loss, under MAS, of the central (1/2, −1/2) transition intensity from the $[BO_3]$ centre-band into the spinning sidebands. This does not happen for the $[BO_4]^-$ sites with their much smaller quadrupole interaction, so that all the central (1/2, −1/2) transition intensity appears in the centre-band [6].

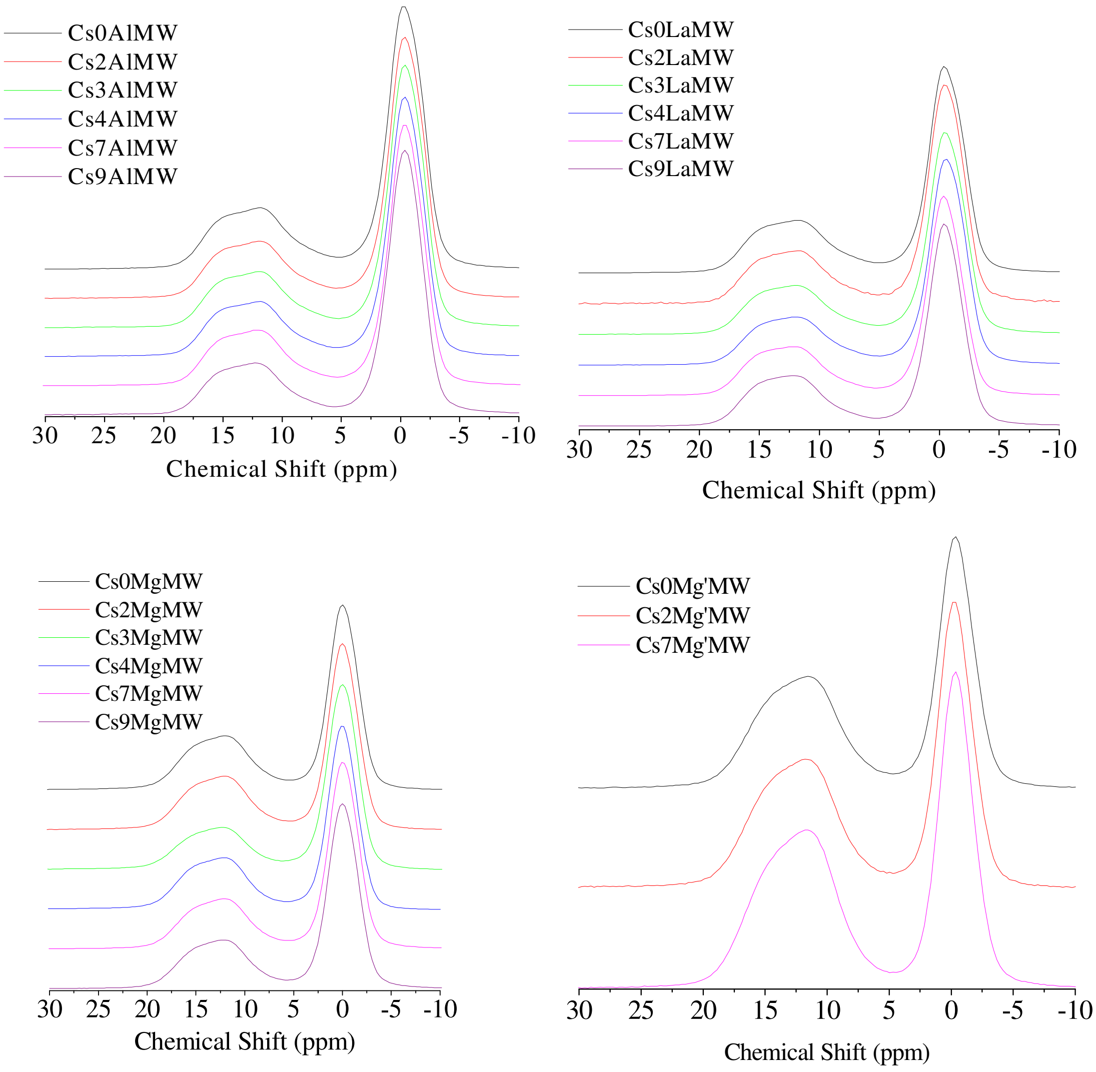

Figure 7.8 ^{11}*B MAS NMR spectra for the four modified mixed-alkali borosilicate glass compositions.*

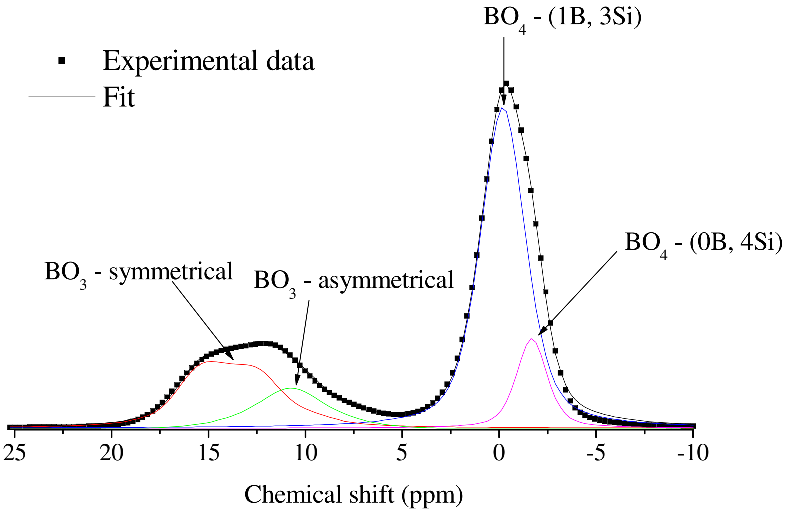

Figure 7.9 *Four peak fit of the Cs7LaMW ^{11}B MAS NMR spectra, with two [BO_4] peaks fitted to the [BO_4] region of the spectrum at ~0 ppm [9].*

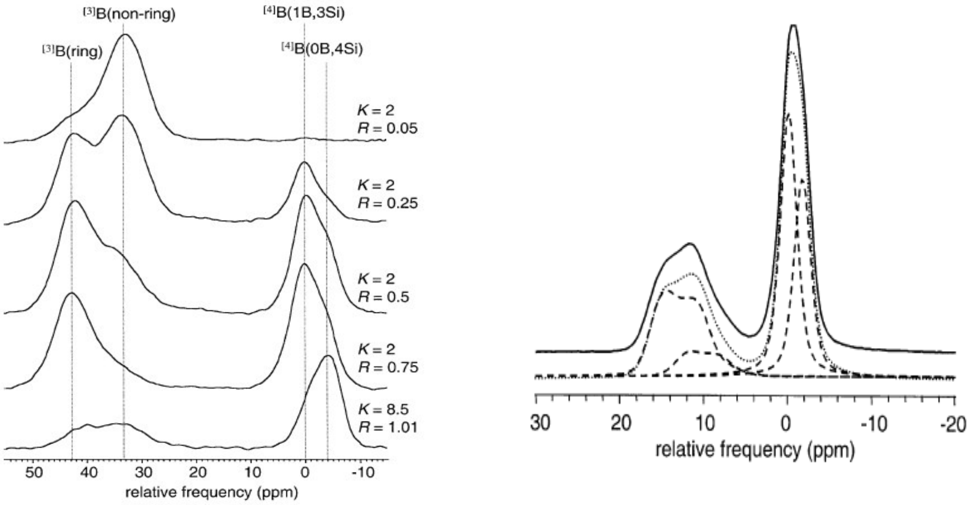

Figure 7.10 *Clear asymmetry in the [BO_4] region of the ^{11}B MAS NMR spectra, for a range of sodium borosilicate glasses (left) with an example fit from Du et al. of multiple BO_4 peaks fits under the BO_4 [18].*

The changes in N_4 fraction as a function of R for the CsAlMW and CsLaMW systems and for the CsMgMW and CsMg′MW systems are shown in Figure 7.11 and Figure 7.12 respectively. In the systems containing intermediate oxides, R is calculated on the basis that every mole of intermediate present (i.e. Al_2O_3 and La_2O_3) removes one mole of alkali oxide to form $[ZO_n]^{-}Y^{+}$ network units, where n is 4 for Al and 6 or 7 (including some BOs) for La. MgO is treated as a modifier for the purpose of calculating R, adding to the total molar contribution from the Group I oxides present. N_4 values [9] are compared in Figure 7.11 with those obtained by Roderick [4], the Dell model [16] and the previous study on Cs_2O additions to MW [1]. For similar values of R, N_4 values for the four systems containing intermediate oxides are lower than both the prediction of the Dell model [16] and the values observed from the borosilicate system composed of entirely Group I alkali oxides, CsMW [1]. Therefore, the simple argument of removal of alkali as a charge compensating cation for the intermediate species is insufficient to explain the reduction of the fraction of four-coordinated borate units. A major consequence of the addition of these oxides is the promotion of the transfer of modifier alkali to the silicate network [23].

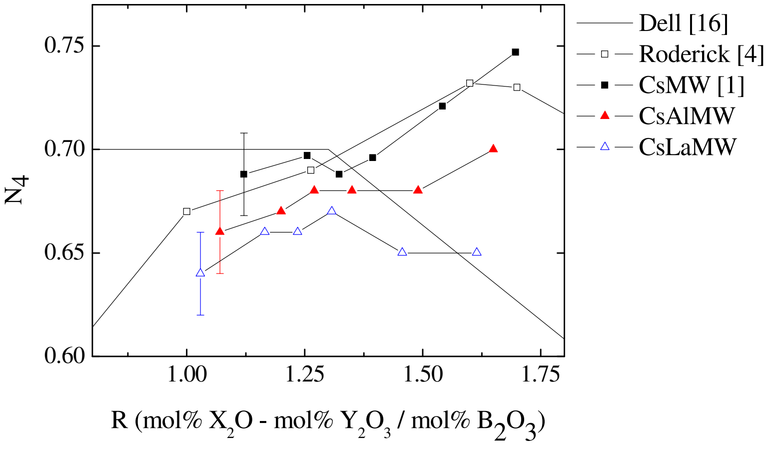

Figure 7.11 *N_4 as a function of R for the intermediate-containing borosilicate glasses [9], compared against previous measurements.*

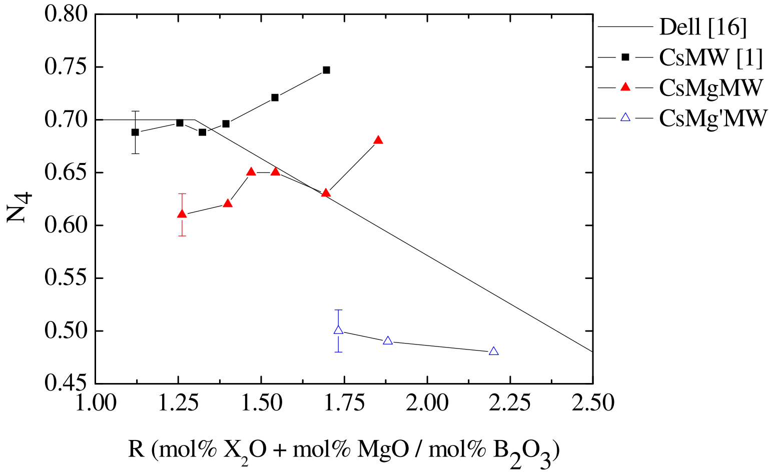

Figure 7.12 *N_4 as a function of R for the magnesium-containing borosilicate glasses [9]. Values are compared with previous work [1,15] and theory [16].*

The danburite fraction obtained from the two resolved peaks under the [BO_4] region of the ^{11}B MAS NMR spectrum (Figure 7.13) decreases from approximately 0.60 to 0.35, for the Al_2O_3 and La_2O_3 containing systems, and increases from 0.50 to 1.1, for the Group I alkali [1] and MgO-containing borosilicate systems (Figure 7.14) [9,24]. The presence of danburite-like units, with their B_4-O-B_4 connections, is surprising, given the usual tendency for charged units to avoid each other. Similar results have also been obtained by Du *et al.* [17] in sodium borosilicate glasses with a range of K values, with the fraction of danburite units increasing (0 to 0.4) with R ($0 \leq R \leq 0.7$).

On adding Cs_2O to the AlMW glass, N_4 increases in parallel with the CsMW data (Figure 7.11), the displacement reflecting the modifier removed to charge compensate $[AlO_4]^-$. A similar situation arises for the La_2O_3 addition. In both of these cases there is also an increase in the fraction of danburite units compared to reedmergnerite units. This is consistent with an increase in N_4, since danburite units contain twice as many boron atoms compared to reedmergnerite units. Addition of MgO in small quantities produces a large reduction in N_4 initially, but subsequent addition of Cs_2O again produces an increase in N_4 which parallels that of CsMW. However, in this case, the amount of danburite decreases relative to reedmergnerite.

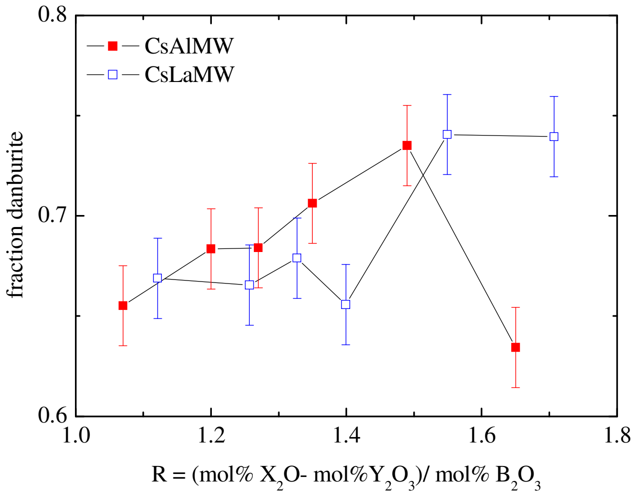

Figure 7.13 *Fraction of danburite units resolved in the ^{11}B MAS NMR spectra for the trivalent oxide-containing borosilicate glass systems [9].*

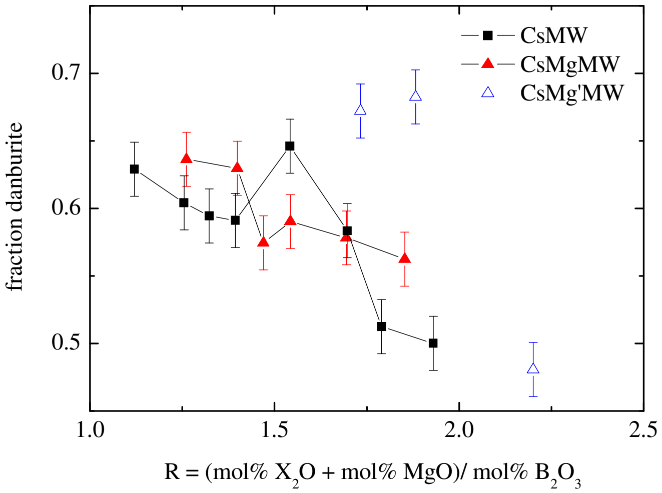

Figure 7.14 *Fraction of danburite units resolved from the* ^{11}*B MAS NMR spectra for the alkaline- and earth alkaline-containing borosilicate glass systems [9].*

The ^{11}B MAS NMR spectra of the danburite, caesium boropollucite and reedmergnerite glasses (Figure 7.15) resemble the spectra shown in Figure 7.11, with a broad [BO_3] peak at ~12 ppm and a sharper [BO_4] peak at ~0 ppm. Peak fitting of the reedmergnerite and danburite spectra, was carried out using a three-peak fit; two [BO_3] quadrupolar peaks and a single [BO_4] peak (Figure 7.15) based on the justification that each superstructural-like group has just one single [BO_4] site with unique surrounding NNN environment. The boropollucite glass spectrum was fitted with the four-peak fit, as used for the previous four borosilicate systems (Figure 7.15) with the chemical shift separation of the two [BO_4] peaks found to be 1.3±0.5 ppm, consistent with the separation observed in the four-borosilicate glasses above and the literature [17,19].

For the reedmergnerite and danburite glasses, fits revealed the two glass systems to have high (>0.60) N_4 fractions (Table 7.4). N_4 values are also shown to remain constant (within error) even with an increase in K, for the reedmergnerite and danburite glasses (since R=1 for both glasses). From the Dell model, N_4 for the reedmergnerite and danburite glasses are calculated to be 0.85 and 0.57 respectively, greater than those found from ^{11}B MAS NMR. Similarly, for the caesium boropollucite glass, N_4 is 0.81±0.02, which is less than the value of 0.98 predicted from the Dell model for a R=1, K=4.0 borosilicate glass [16]. It should be pointed out that N_4 is equal to 1 in the crystalline analogues.

Sample	N_4 (± 0.02)	K
danburite (Na)	0.71	2.0
danburite (Cs)	0.66	2.0
boropollucite	0.81	4.0
reedmergnerite (Na)	0.69	6.0
reedmergnerite (Cs)	0.66	6.0

Table 7.4 *Resolved N_4 fractions for the danburite, caesium boropollucite and reedmergnerite glasses. The molar ratio of alkali oxide to boron oxide (R) is constant (=1) for both all four glasses.*

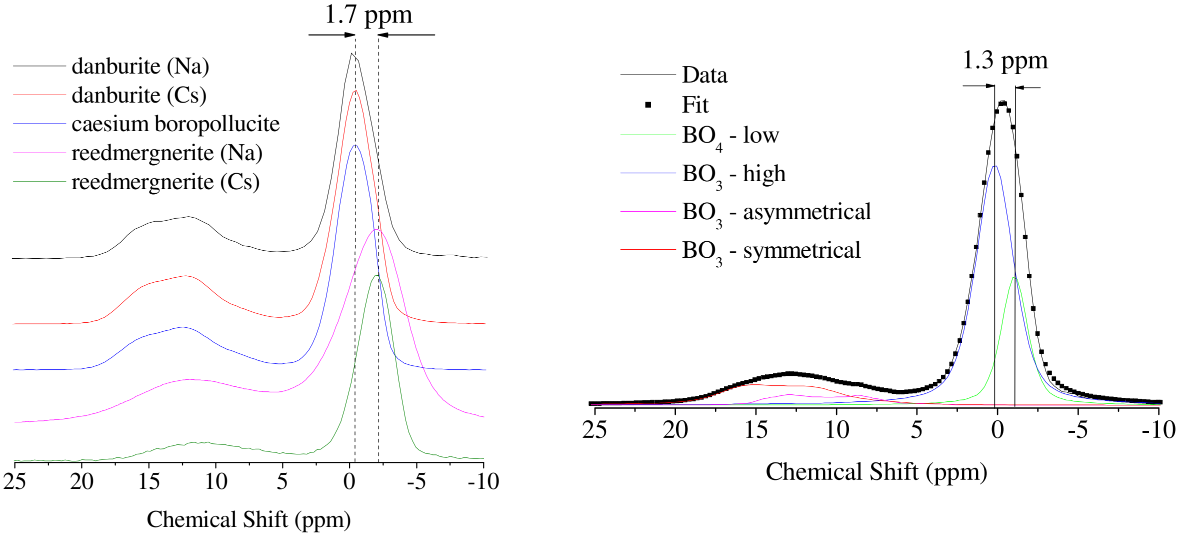

Figure 7.15 *^{11}B MAS NMR spectra for the five borosilicate crystal based glasses (left) with the fit for the ^{11}B MAS NMR spectrum of the caesium boropollucite glass (right).*

Mass-loss measurements obtained in Chapter 6 were plotted as a function of the fraction of danburite units resolved across the four modified alkali borosilicate glasses (Figure 7.16). This shows mass-loss to decrease for the Mg-containing glasses, where there is a decreasing danburite fraction and inversely for the Al- and La-containing glasses were mass-loss increases as a function of increasing danburite content.

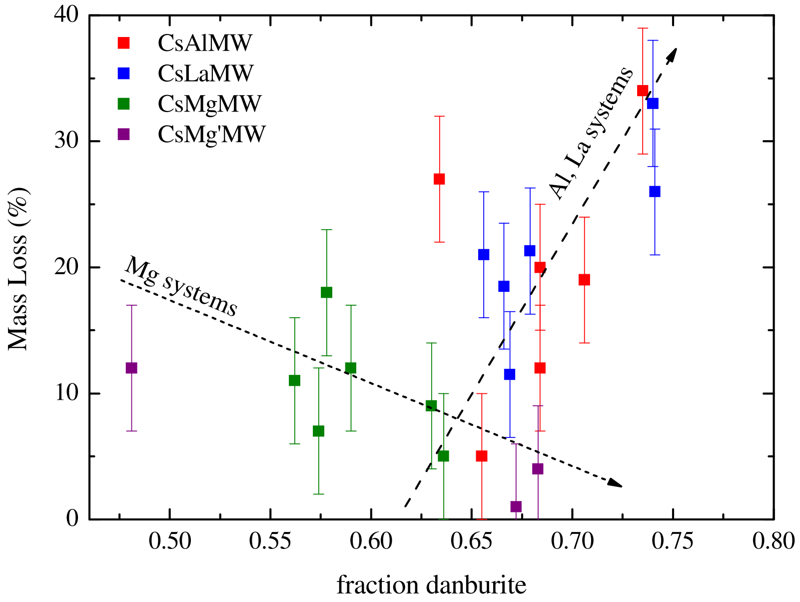

Figure 7.16 *Mass loss (%) as a function of resolved danburite fraction from ^{11}B MAS NMR, for the four borosilicate glass systems. Note: dotted lines are a guide to the eye.*

7.3.5 ^{29}Si MAS NMR

The fraction of Q^3 silicon units for each of the borosilicate glass compositions was resolved from ^{29}Si MAS NMR measurements (Figure 7.17, Figure 7.18 and Figure 7.19). Across the four borosilicate glass systems the ^{29}Si MAS NMR lineshape changes continuously with caesium oxide content (Figure 7.18). The ^{29}Si MAS NMR spectra were fitted in most cases with two Gaussian lines: one Q^3 peak and one Q^4(B) peak, a silicon with one or more boron NNN (Figure 7.17). Contributions from Q^2 units were negligible for all but typically the highest Cs_2O content and the high-MgO series, CsMg′MW. Raman spectroscopy data and fits later in this chapter however (*cf.* Section 7.4.1) suggest the presence of Q^2 for high caesium contents. Fits were carried out using a constraint, based where possible on the predicted fraction of NBO/Si (i.e. Q^3 fraction) calculated using Equation 7.1. $M_{2/z}O$ refers to modifiers Na_2O, Li_2O, Cs_2O and MgO whilst X_2O_3 refers to intermediates Al_2O_3, Fe_2O_3 and La_2O_3, with N_4 values obtained from ^{11}B MAS NMR measurements.

$$\text{NBO/Si} = Q^3(\text{predicted}) = \frac{2\times(\Sigma\ \text{mol\%}\ M_{2/z}O - \Sigma\ \text{mol\%}\ X_2O_3 - N_4\times\text{mol\%}\ B_2O_3)}{\text{mol\%}SiO_2} \quad (7.1)$$

$$Q^4(B) = 1 - Q^3 \tag{7.2}$$

Resolved Q^3 values (Figure 7.19) agree within error (±10 %) with predicted NBO/Si values, with Q^3 for all four systems increasing linearly with caesium oxide content [9,24,25]. Chemical shifts for the Q^3 and Q^4(B) units were found to be −88±1 and −100±1 ppm respectively, corresponding well with previous measurements carried out by Roderick [15] and Duddridge [11].

The Q^3 fractions for all four borosilicate systems are greater than those for the CsMW system [1], at equivalent values of R (Figure 7.19). This complements the ^{11}B MAS NMR results, which suggest that the introduction of Al_2O_3 and La_2O_3 into the CsMW system not only reduces the amount of alkali modifier bonded to the borate network, which lowers N_4, but also results in transfer of alkali species to the silicate network, increasing the fraction of Q^3 units.

For the MgO-containing CsMgMW system, the resolved Q^3 fraction is initially 0.4 increasing to 0.6, before decreasing to 0.50 [9,24,25]. This decrease can most easily be explained by the formation of Q^2 units at higher caesium-content. Similarly, the resolved Q^3 fraction for the CsMg′MW system is larger than for the remaining three systems ($0.80 < Q^3 < 0.75$) - a large discrepancy compared with the predicted NBO/Si fraction, suggesting the model of NBO/Si formation, outlined in Equation 7.1, to be inadequate for this system.

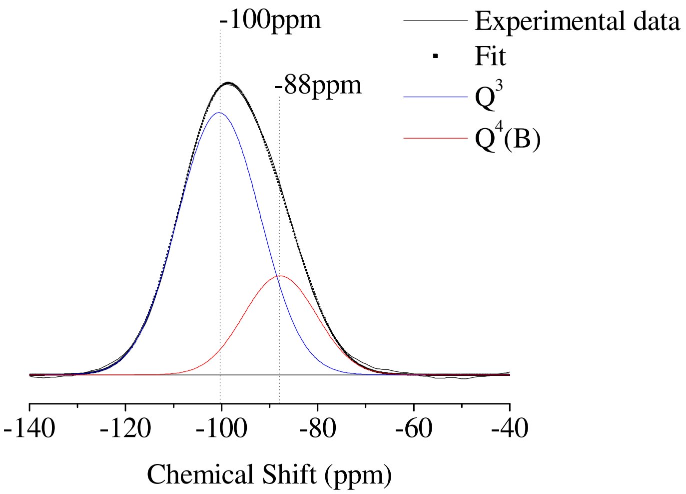

Figure 7.17 *Typical ^{29}Si MAS NMR fit for one of the borosilicate glasses, using a constrained two peak fit [24,25].*

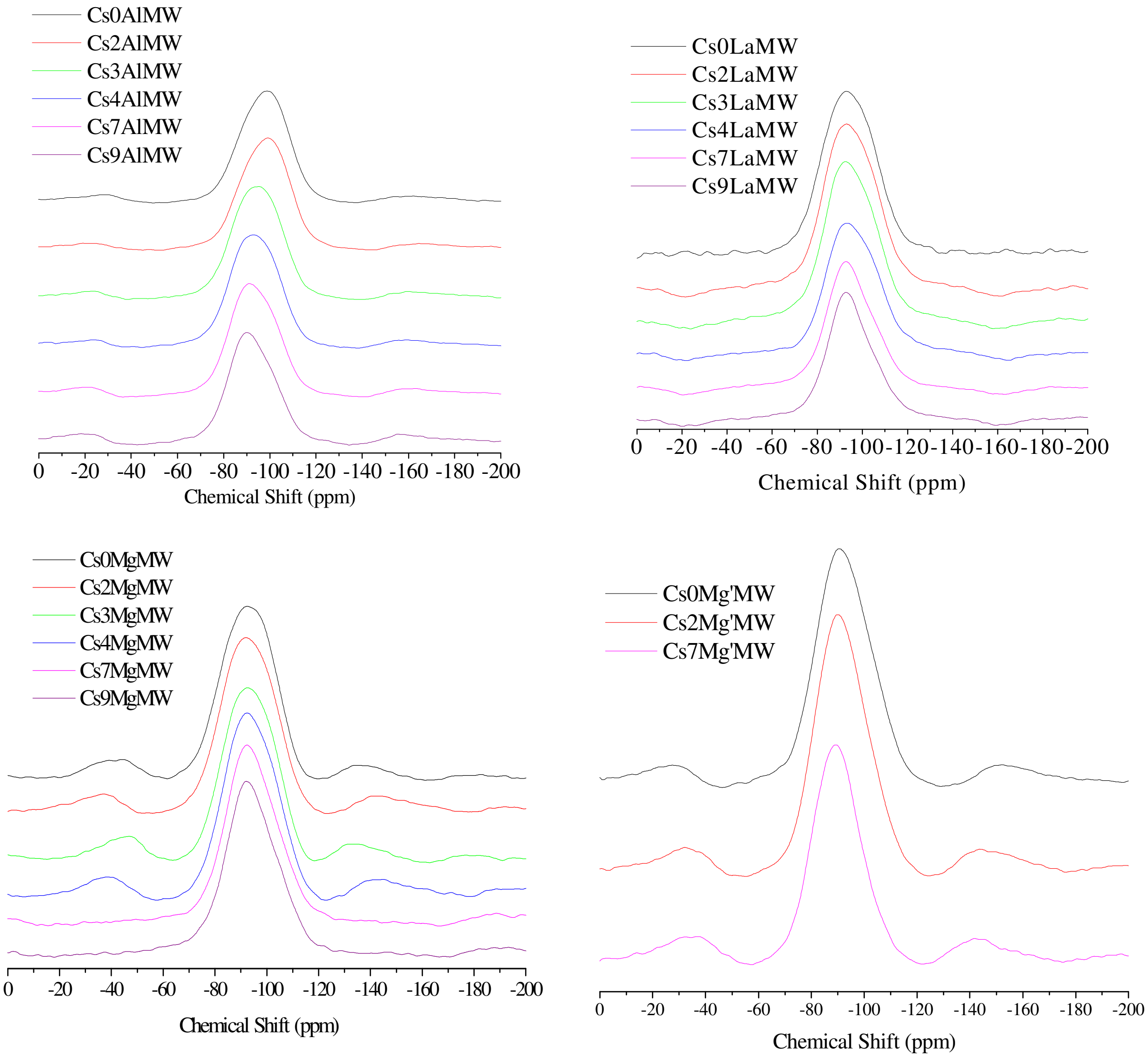

Figure 7.18 *^{29}Si MAS NMR spectra for the four borosilicate glass systems.*

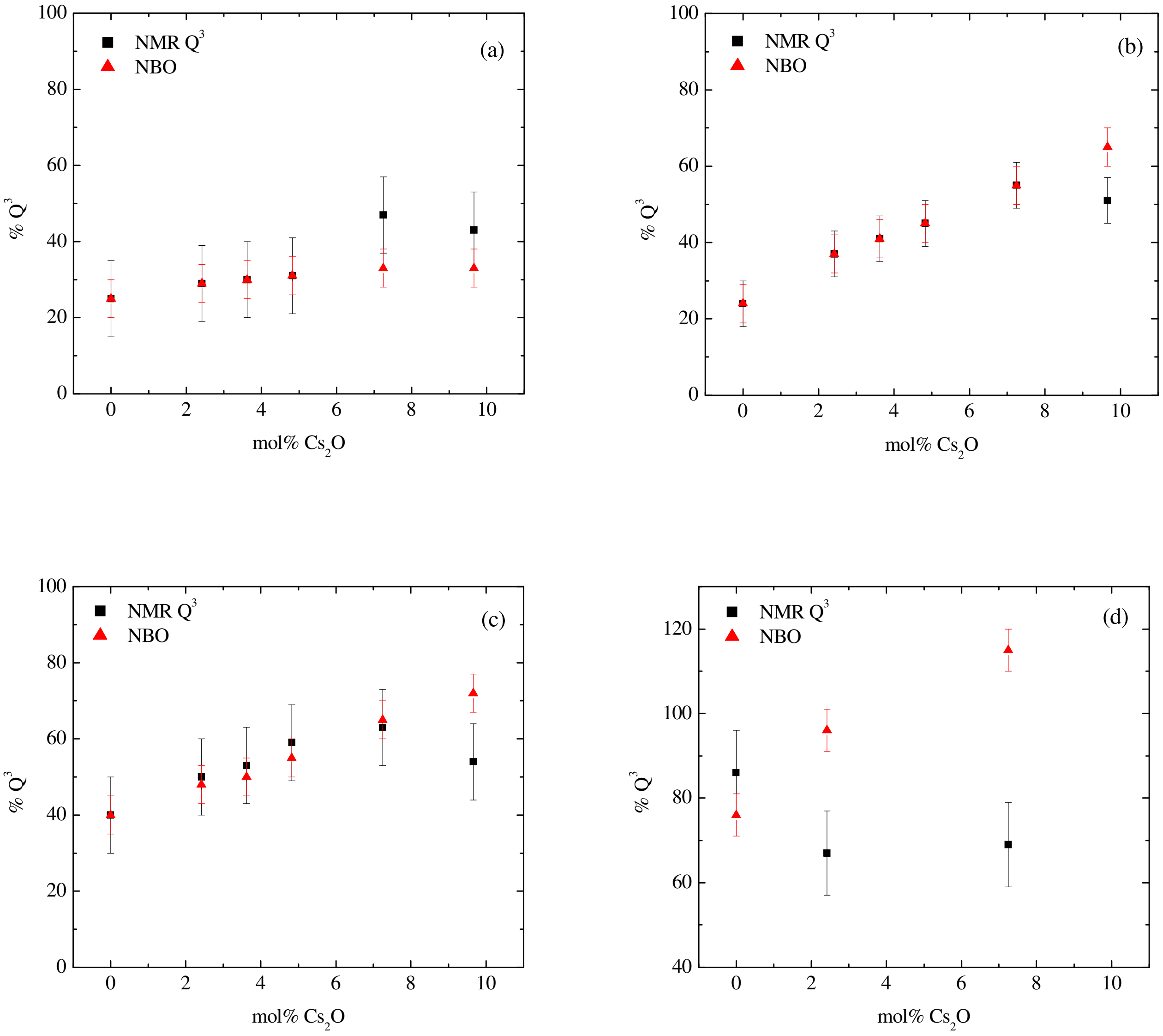

Figure 7.19 *Resolved ^{29}Si MAS NMR Q^3 fractions for the (a) CsAlMW, (b) CsLaMW (c) CsMgMW and (d) CsMg'MW borosilicate glass systems compared against predicted values of Q^3 (NBO) [9,24,25].*

Coupled with the ^{11}B NMR data obtained in Section 7.3.4, ^{29}Si MAS NMR has also been used to calculate the relative amounts of the reedmergnerite and danburite MRO units present, which have been identified in previous studies using Raman spectroscopy [5,23] and NMR [18]. This information can be used further, in conjunction with the fraction of Q^4 units obtained from ^{29}Si MAS NMR, to calculate the proportion of Q^4 units which are *not* associated with these MRO units.

If there are *b* moles of B_2O_3 and *s* moles of SiO_2 in glass, with N_4 (four-coordinated boron), f_D (fraction of danburite) and Q^3 (fraction of Q^3 units) experimentally measured from both ^{11}B and ^{29}Si MAS NMR, then the number of boron atoms in danburite units (B_4D) is given by

$$B_4D = 4*b*N_4*[f_D/(1 + f_D)] \tag{7.3}$$

and the number of boron atoms in reedmergnerite units is given by

$$B_4R = B_4 - B_4D \tag{7.4}$$

The boron NNNs are 4Si for reedmergnerite borons and 1B + 3Si for the danburite borons. Assuming there is B_4/Q^3 avoidance, because of their charges, then the number of Si (= Q^4) connected to the boron atoms in the MRO units is given by

$$0.75*B_4D + B_4R \tag{7.5}$$

Some of these Q^4 will be members of the MRO units. The number of Q^4 not connected to MRO boron atoms (referred to as non-MRO Q^4) is then given by

$$\text{Non-MRO } Q^4 = s*(1-Q^3) - (0.75*B_4D + B_4R) \tag{7.6}$$

Note that this does not exclude Q^4 connected to ring silicon atoms and presumes that Q^2 silicon units are not formed across the range of R values used in the glass systems of this study. The model also makes the assumption that no third B_4 site, with 2B, 2Si NNN are formed, based on the two B_4 site peak fits obtained from the ^{11}B MAS NMR spectra in Section 7.3.4.

The percentages of Q^4 units which are not connected to MRO boron atoms are compared with those in the MRO units as a function of R for the various systems in Figure 7.20. The following, Figure 7.21, compares the amounts of non-MRO Q^4 for the various systems. The high-MgO system, CsMg′MW, has not been included in these calculations because of the large fraction of Q^2 units which are present in these samples. Figure 7.20 shows that the fractions of Q^4 units which are associated with the MRO units remain remarkably constant as R changes and it is the non-MRO Q^4 units which decrease, indicating that it is these which are preferentially converted to Q^3. Figure 7.21 shows that the rate of removal of the non-MRO Q^4 units is largely independent of the minor additions of Al_2O_3 and La_2O_3 compared to the basic system CsMW, the main difference being an initial offset. The upturn at the end of three of the curves reflects the production of Q^2 at these R values (i.e. the breakdown of the model described in Equation 7.6) and is not the formation of more Q^4 units outside of MRO units.

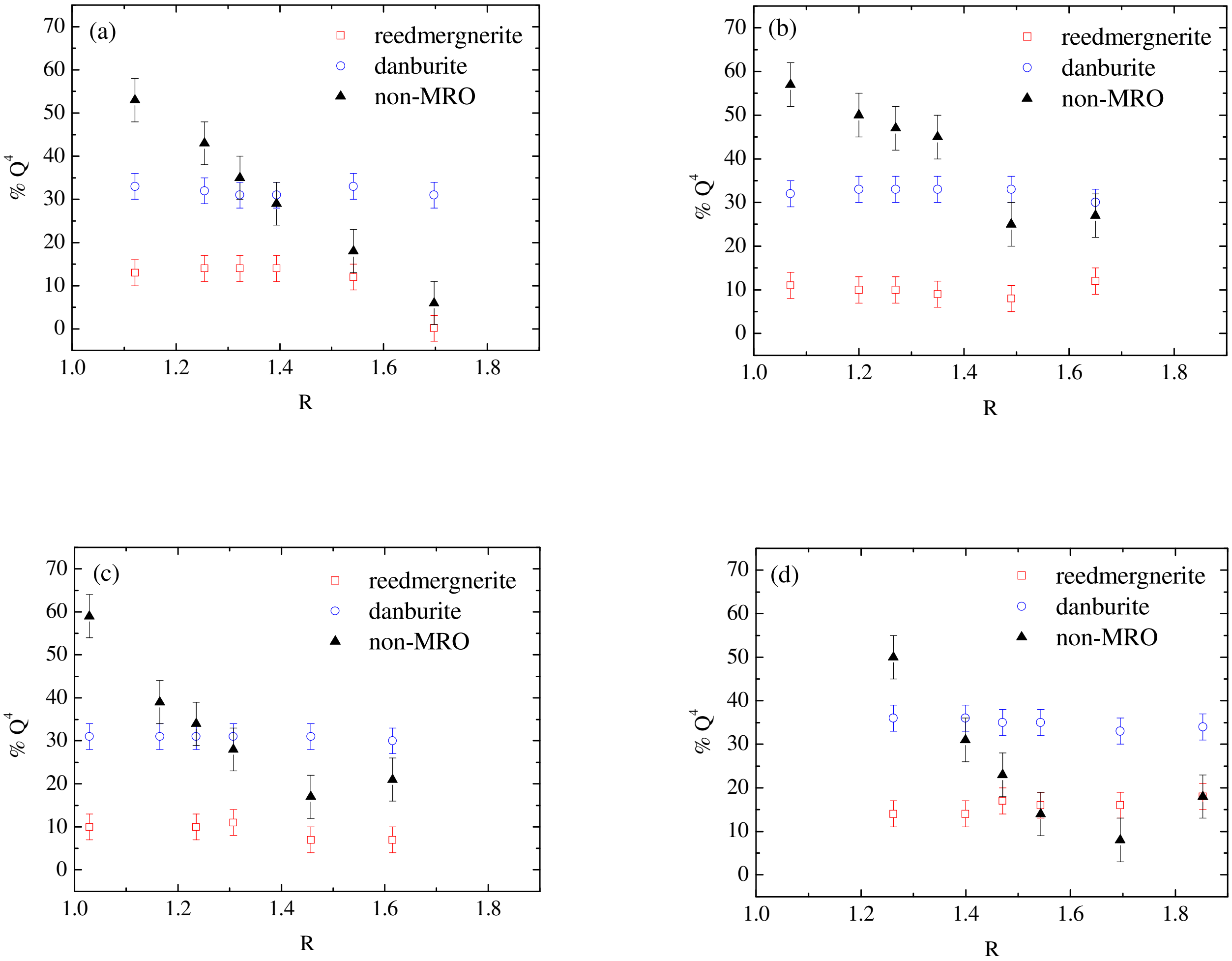

Figure 7.20 *Resolved Q^4 fractions (reedmergnerite, danburite and non-MRO Q^4 units) for (a) CsMW, (b) CsAlMW, (c) CsLaMW and (d) CsMgMW glass systems [9].*

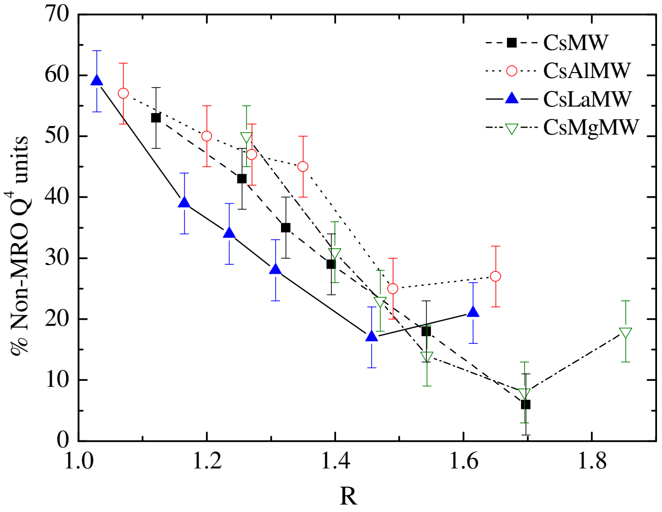

Figure 7.21 *Comparison of the percentage of non-MRO Q^4 units for the CsMW, CsAlMW, CsLaMW and CsMgMW systems [9]. Note: lines are drawn to guide the eye.*

The similarity of these curves (Figure 7.20) is in contrast to the differences seen in the Q^3 v R plots (Figure 7.19) which reflect the corrosion and volatilisation tendencies of these systems [17].

A result of importance to the heart of this investigation is shown in Figure 7.22, which links the resolved Q^3 fractions from ^{29}Si MAS NMR and the volatilisation mass-loss measurements from the previous chapter. Here mass-loss is observed to increase with increasing Q^3 (=NBO), but also the rate of increase of mass-loss with Q^3 varies significantly depending on the additive oxide (i.e. Al_2O_3, La_2O_3 or MgO) present in the composition [24]. The CsAlMW and CsLaMW systems have greater mass-loss and rate of increase of mass-loss, compared to the MgO-containing glass systems. These systems are also those with *increasing* quantities of danburite units, in contrast to the less volatile MgO-containing systems which have *decreasing* quantities of danburite groups, and *increasing* reedmergnerite contents (*cf.* Figure 7.13 and Figure 7.14) [24].

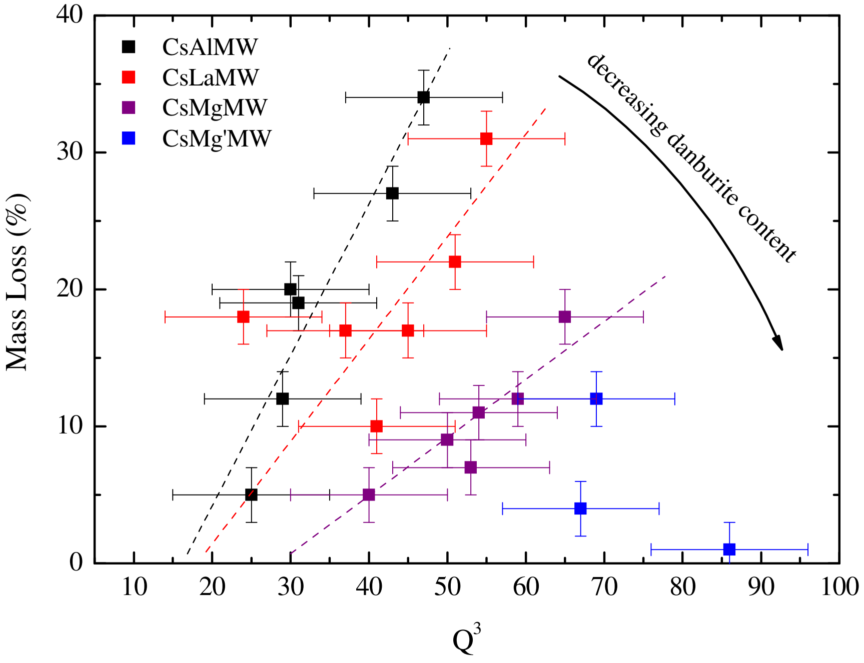

Figure 7.22 *Mass-loss measurements from Chapter 6 as a function of resolved Q^3 fraction. Arrow indicates decreasing danburite population in glass resolved from ^{11}B MAS NMR (cf. Section 7.3.4) [24]. Note: dashed lines are a guide to the eye.*

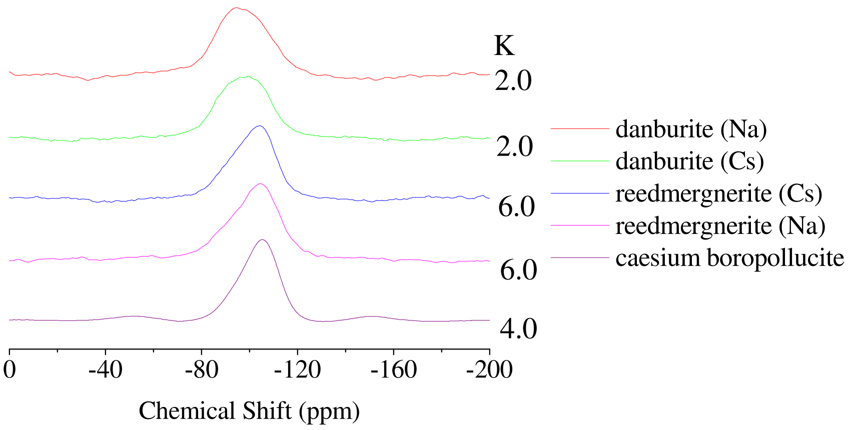

Figure 7.23 *^{29}Si MAS NMR spectra for the five borosilicate crystal based glasses.*

Q^3 values from the caesium- and sodium-containing reedmergnerite (0.39), danburite (0.103) and caesium boropollucite glass (0.095) ^{29}Si MAS NMR spectra (Figure 7.23) agree with NBO/Si predictions made using Equation 7.1 (NBO/Si = 0.390, 0.103 and 0.095 respectively). The fraction of Q^3 units increases with increasing K on going from the danburite to the reedmergnerite glass and is independent of alkali type present.

7.4 Raman Spectroscopy

7.4.1 Borosilicate Glasses

The Raman spectra (Figure 7.24 to Figure 7.25) for the borosilicate glass systems [9,25], including three high (> 1 mol%) iron-content borosilicate glasses(*) [11] (Table 7.5), can be clearly divided into two regions. The first, from 400 to 850 cm^{-1}, includes the vibrational modes of the two MRO superstructures, reedmergnerite $[BSi_3O_8]^-$ and danburite $[B_2Si_2O_8]^{2-}$. The second region, from 850 to 1250 cm^{-1}, includes peaks from silicon Q^n vibrational modes and it is this region which is of primary interest in this study. Before peak fitting to this region was carried out, the background for each Raman spectrum was subtracted by fitting an exponential curve to the data in a technique adapted from Mysen [26]. The corrected spectrum was then fitted with Gaussian peaks which were assigned to individual vibrations according to the literature. Peaks originating from vibrations arising solely from SRO boron units are not resolvable.

Peak fitting of the data for all the borosilicate glasses, in the Q^n region used four Gaussian peaks at approximately 925 cm^{-1}, 970 cm^{-1}, 1065 cm^{-1} and 1150 cm^{-1} (Figure 7.26). Peak half-widths for all but the peak at ~1065 cm^{-1} (assigned as the central Q^3 peak [27,28]) were accepted as being realistic when between 60-80 cm^{-1} [25]. Previous work [27] suggested that the peak at 925 cm^{-1} is due to a vibrational mode of the Q^2 unit. However it should be noted that the fraction of the Q^2 units resolved in the ^{29}Si MAS NMR data is generally negligible, except for the highest caesium oxide content in the borosilicate glasses and the high-MgO content system. The peak at approximately 1060 cm^{-1} has been assigned to the Q^3 vibrational unit, with the remaining peaks at 970 cm^{-1} and 1150 cm^{-1} to $Q^4(B)$ groups. The Raman spectra from the iron oxide-containing borosilicate glasses are shown in Figure 7.25 and were fitted in an identical manner to that described above.

---

[*] Manufactured in a previous study ([11] A. Duddridge, *PhD Thesis, Warwick University* (2004).) but used in this current study to test the effectiveness of Raman spectroscopy to resolve Q^3 fractions in glasses, when NMR was not possible (due to the presence of a high (>1 mol%) quantity of paramagnetic species)

For all the Raman spectra, Q^3 fractions were obtained by summing the areas of all the resolved Q^3 peaks and dividing by the total peak area in the range 850 to 1250 cm^{-1} [25]. These fractions are then compared with those obtained by ^{29}Si MAS NMR in Figure 7.27. This approach uses the assumption that the oscillator strengths for the different Q^n units are equal.

For the four borosilicate glass systems, the trend is for the Q^3 fraction to increase with caesium oxide concentration, when Q^4(B) groups are converted to Q^3 units. Relatively small additions of aluminium-, lanthanum- or magnesium- oxides to the CsMW system alter the Q^3 fraction significantly for compositions of identical caesium oxide content, with Al_2O_3 and La_2O_3 effectively behaving as network intermediates, whilst MgO behaves as a modifier. This behaviour is discussed in more detail in [9]. In Figure 7.27, the Q^3 values resolved from Raman spectroscopy are compared with those obtained from ^{29}Si MAS NMR and also with the NBO/Si values predicted by Equation 7.1. These agree within experimental error (±10 %) for all of the systems, except the high-MgO system, where the modifier content is sufficiently large that significant amounts of Q^2 species are generated [25].

Values of the Q^3 fractions obtained by peak fitting of the Raman spectra from the three iron-containing mixed-alkali borosilicate glasses are plotted against R in Figure 7.28 [25]. When calculating R, assumptions are made about the structural role of the iron oxide added to these glasses. This requires knowledge of the oxidation state of the iron ions in the glass. It is well known that the Fe^{3+}/Fe^{2+} ratio depends on glass composition, as well as the temperature and atmosphere during melting. Mössbauer measurements on these glasses give the Fe^{3+}/Fe^{2+} ratios listed in Table 7.5 [11]. It is generally accepted that Fe^{2+} behaves as a modifier in glass, whilst Fe^{3+} forms $[FeO_4]^-$ network polyhedra, which require charge balancing M^+ ions, as is the case for Al^{3+} ions. In Figure 7.28, the data points plotted for the iron-containing glasses have R values calculated using the oxidation ratio from the Mössbauer measurements such that $R = (M_2O+FeO-Fe_2O_3)/B_2O_3$. The line drawn in Figure 7.28 is the linear least squares fit to the AlMW system. The Raman data from the FeMW system are within experimental error of this line.

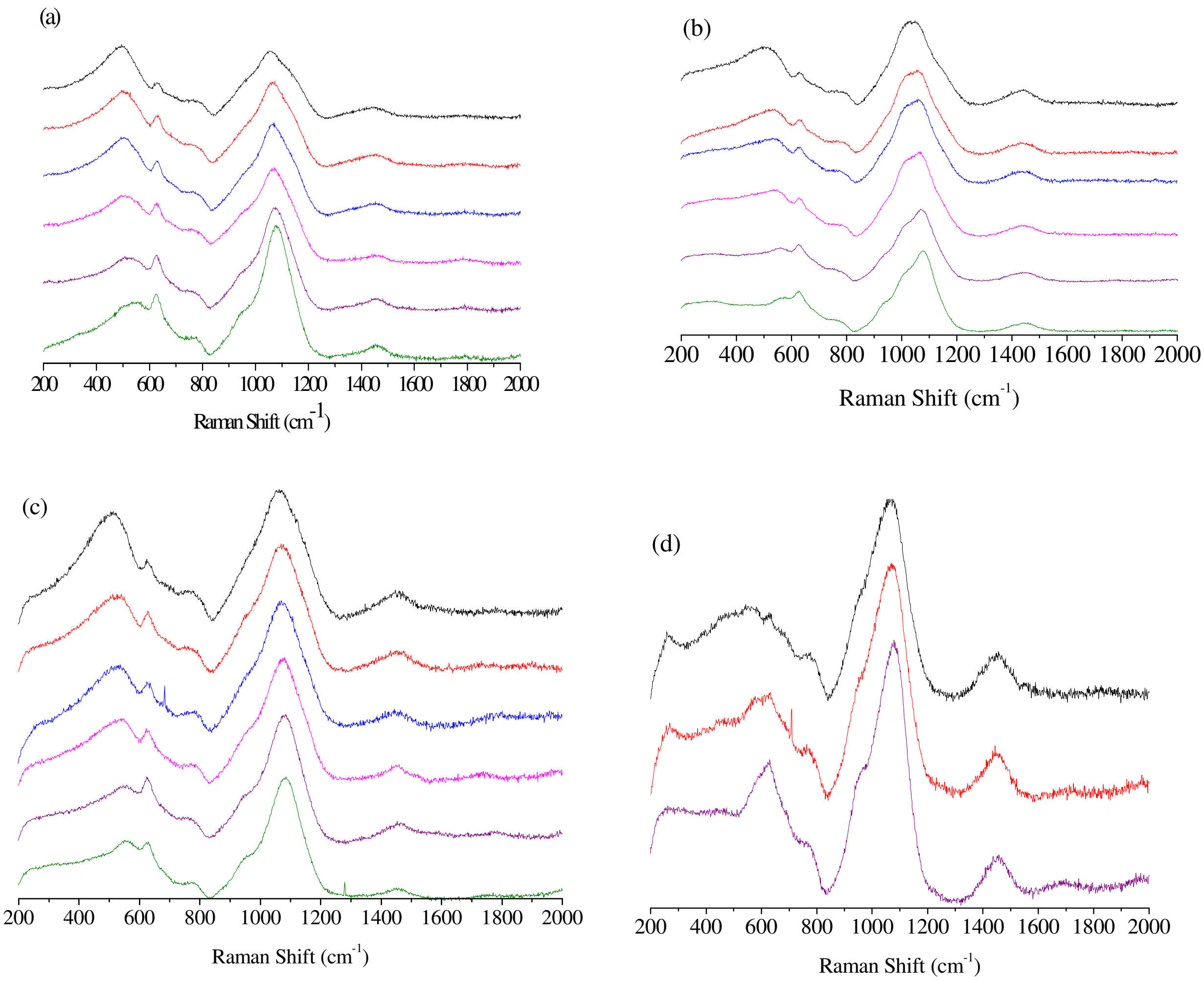

Figure 7.24 *Raman spectra for the four alkali borosilicate glasses: (a) CsAlMW, (b) CsLaMW, (c) CsMgMW and (d) CsMg'MW, with caesium oxide contents; - 0 mol% Cs$_2$O - 2.42 mol% Cs$_2$O - 3.62 mol% Cs$_2$O - 4.83 mol% Cs$_2$O - 7.25 mol% Cs$_2$O - 9.66 mol% Cs$_2$O [9,25].*

Sample	mol% SiO$_2$	mol% B$_2$O$_3$	mol% Na$_2$O	mol% Li$_2$O	mol% Fe$_2$O$_3$	R	[Fe^{3+}]/[Fe^{2+}] [11]
Fe2MW	59.10	18.1	10.31	10.07	2.42	1.08	3.5
Fe9MW	54.70	16.77	9.55	9.32	9.66	0.79	6.1
Fe12MW	53.34	16.34	9.28	9.06	11.98	0.65	7.3

Table 7.5 *Compositional details for the three iron-alkali borosilicate glasses used to calculate Q^3 from Raman spectrometer, where conventional ^{29}Si MAS NMR measurements are not available due to the high (>1 mol%) iron contents [25].*

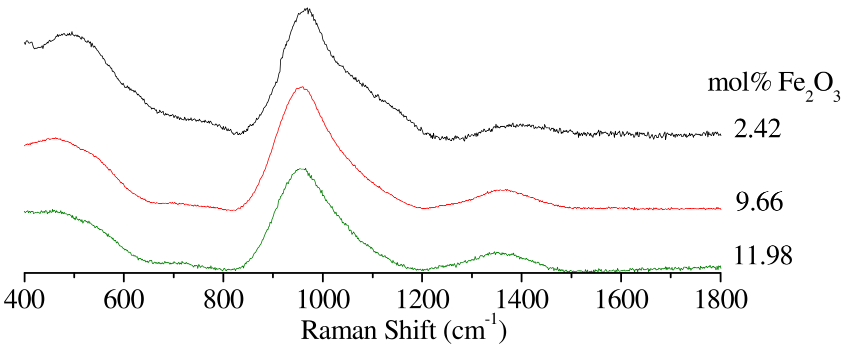

Figure 7.25 *Raman spectra for three iron alkali borosilicate glasses [25].*

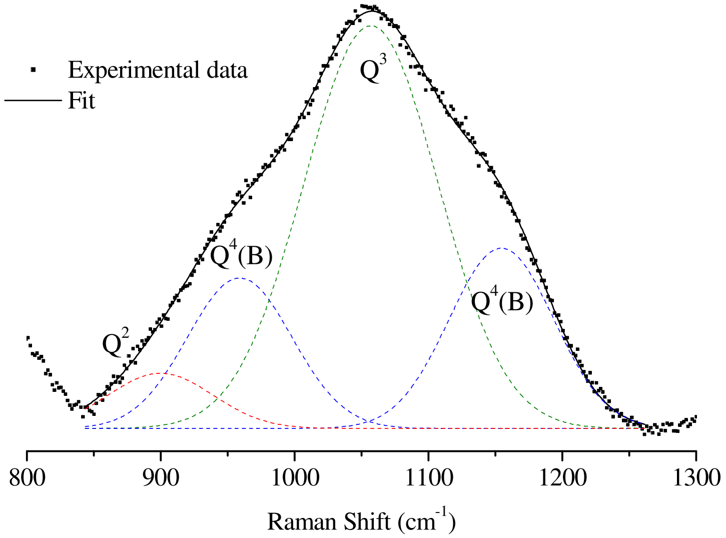

Figure 7.26 *Example of the fitted Q^n region of a borosilicate Raman spectrum [25].*

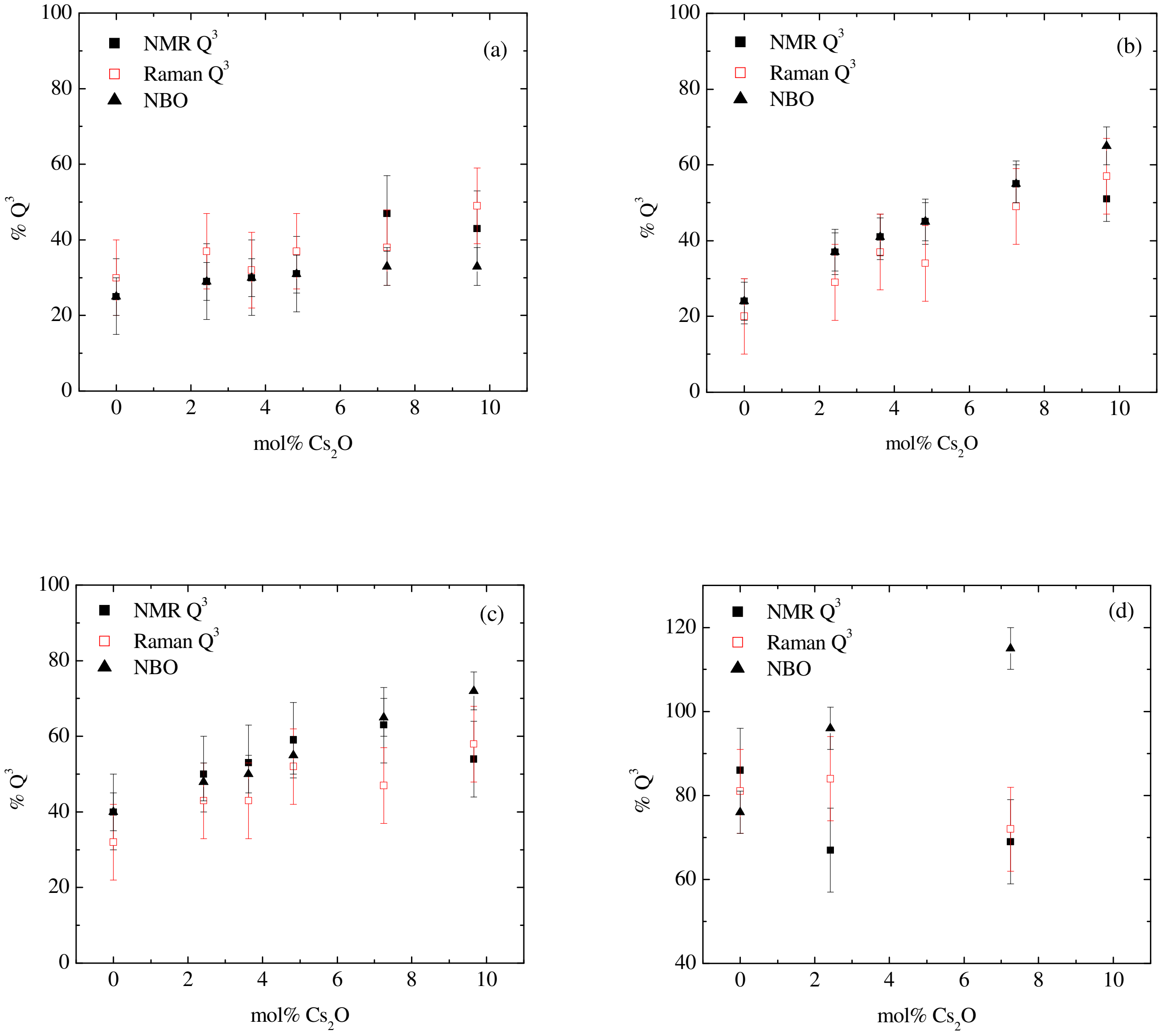

Figure 7.27 *Resolved Q^3 fractions of Raman spectroscopy data compared against ^{29}Si MAS NMR Q^3 data for the (a) CsAlMW, (b) CsLaMW, (c) CsMgMW and (d) CsMg'MW glass systems [25]. Note: values labelled "NBO" have been calculated from stoichiometry using Equation 7.1 in Section 7.3.5.*

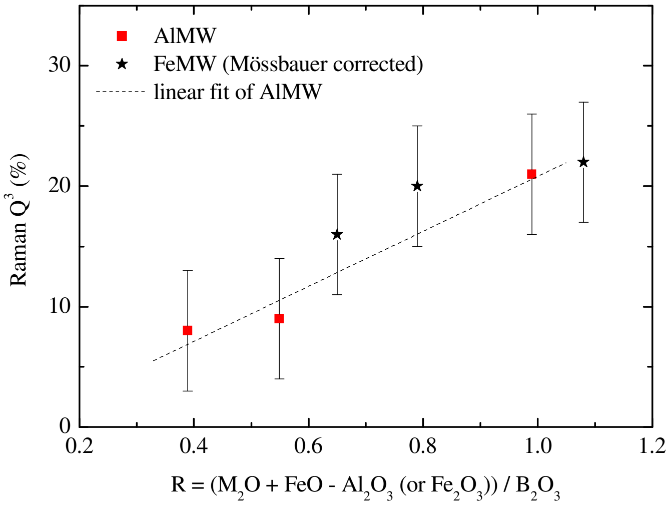

Figure 7.28 *Measured Q^3 fractions from Raman spectroscopy for the FeMW glass system, compared with predicted NBO/Si for the AlMW system. The dotted line is a linear least squares fit to the AlMW data [25].*

For the three superstructural glasses, the Raman spectrum obtained (Figure 7.29 and Figure 7.30) are characteristic of the Raman spectra for the mixed-oxide-borosilicate glasses shown above. Silicon Q^n units are present in the 800-1300 cm^{-1} region of the spectrum, with boron units in the form of tetrahedral and trigonal BO_3 units observed at 800 and 1500 cm^{-1} respectively [5,23,29]. The larger, reedmergnerite (500 cm^{-1}) and danburite (600 cm^{-1}) MRO structures present in the boropollucite glasses are also observed, confirming results from both ^{11}B and ^{29}Si MAS NMR earlier in this chapter.

Based on a method that was originally planned for calculating the fraction of four-coordinated boron units (N_4) in borate glasses; by using borate crystals known to be containing single borate superstructures (i.e. from which N_4 can then be predicted), resolving the fraction of reedmergnerite and danburite units in the mixed alkali borosilicate glasses in this study was thought possible by using Raman spectra from crystal forms of these two units. This technique however was abandoned when it became clear the detail in the Raman spectra from both borate and borosilicate crystals (Figure 7.31 and Figure 7.32) was far too great to resolve in terms of the resonances from just superstructural groups.

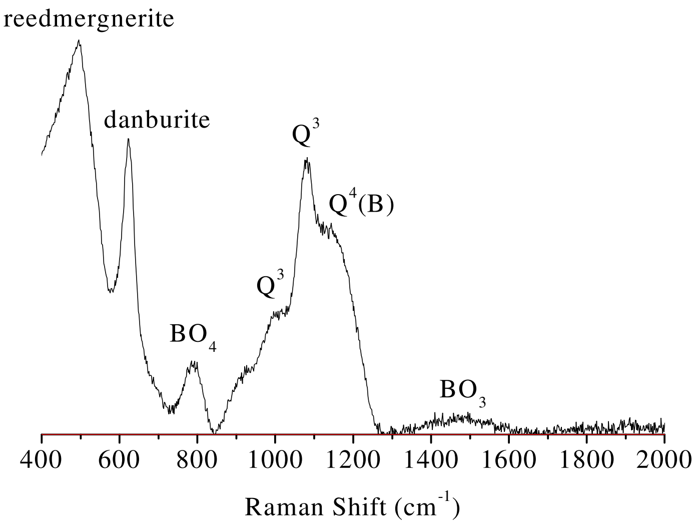

Figure 7.29 *Caesium boropollucite glass Raman spectrum with labelled peak units [5,23,29].*

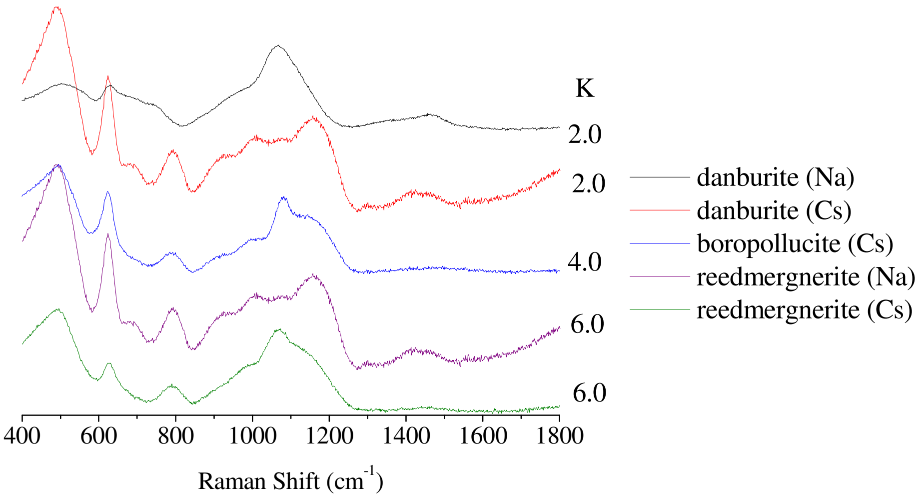

Figure 7.30 *Raman spectra for the five different borosilicate superstructural glasses.*

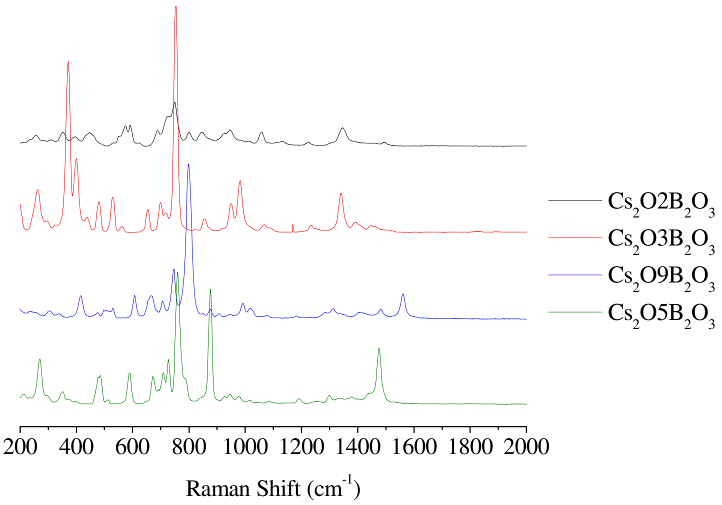

Figure 7.31 *Raman spectra for a range of caesium borate crystals [30].*

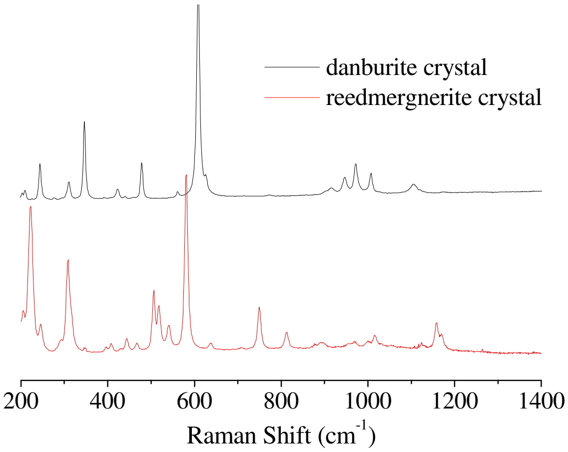

Figure 7.32 *Raman spectra for the danburite ($CaB_2(SiO_4)_2$) and reedmergnerite ($NaBSi_3O_8$) crystalline minerals [31].*

7.4.2 Volatilisation Deposits and Residual Material

Raman spectra of the deposits collected from the volatilisation measurements are shown in Figure 7.33. Only four spectra were obtainable (from the Cs3MgMW, Cs7MgMW, Cs3AlMW and Cs2LaMW samples) from the volatilisation measurements (*cf.* Chapter 4) because of the small masses of volatile material collected (~1-10 mg). Peak assignments suggest the volatile species contain metaborate (642 cm^{-1}), dipentaborate (747 cm^{-1}), boroxol (792 cm^{-1}) and possibly Q^2 (946 cm^{-1}) units based on comparison with borate [32] and borosilicate [29] glass Raman peak assignments from the literature. The presence of these units compares well with the borosilicate volatilisation work by Archakov *et al.* [33] who found vapours from borosilicate melts to also consist of silicate, borate and alkali borate species.

The Raman spectra of the deposits are approximately independent of the starting composition of glass. The only clear difference between the four spectra in Figure 7.33 is the additional peak at 792 cm^{-1} in the Cs3AlMW sample. The three additive oxides are not detected with Raman spectroscopy and so further analysis with EDX later in this chapter provides in more detail on the composition of the volatile species.

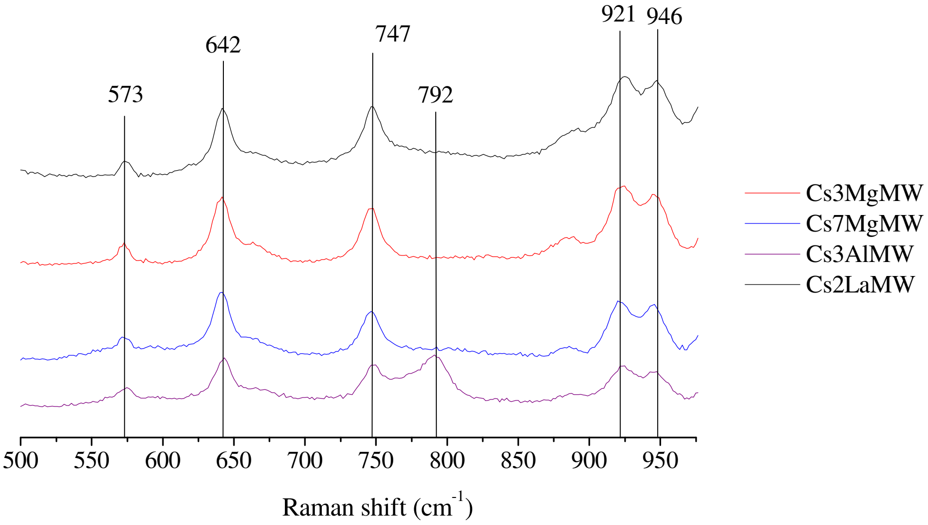

Figure 7.33 *Raman spectra of the deposit on the volatilisation lid from three of the borosilicate glass volatilisation experiments.*

7.4.3 Leached Borosilicate Glasses

Raman spectra were obtained from borosilicate glasses before and after the 14 day leach tests (Figure 7.34). Q^3 fractions from the Raman spectra (Figure 7.35) were resolved in an identical manner to those in Section 7.4.1. With the exception of the Cs7AlMW and Cs2MgMW disks (where the Q^3 fraction is larger for the leached compositions) values are seen to remain approximately constant (within error) between leached and non-leached compositions. Although a previous study by Islam [34] suggested increasing Q^3 fraction leads to increasing corrosion and therefore mass-loss, the mechanism by which this takes place is not confidently known.

The lack of any significant change in the resolved Q^3 fraction suggests that loss of alkali is from the borate network of the glass, resulting in tetrahedral borate groups being converted back to trigonal units. This result has been observed in work by Roderick [4] where ^{11}B MAS NMR measurements found a reduction in N_4 after corrosion tests were conducted on variants of MW. Like the quantitative Raman measurements in this study, these effects were subtle, with N_4 lowering by only 0.04 after leaching. This is supported by the understanding that alkali silicate glasses are typically more resistant to chemical corrosion than alkali borates.

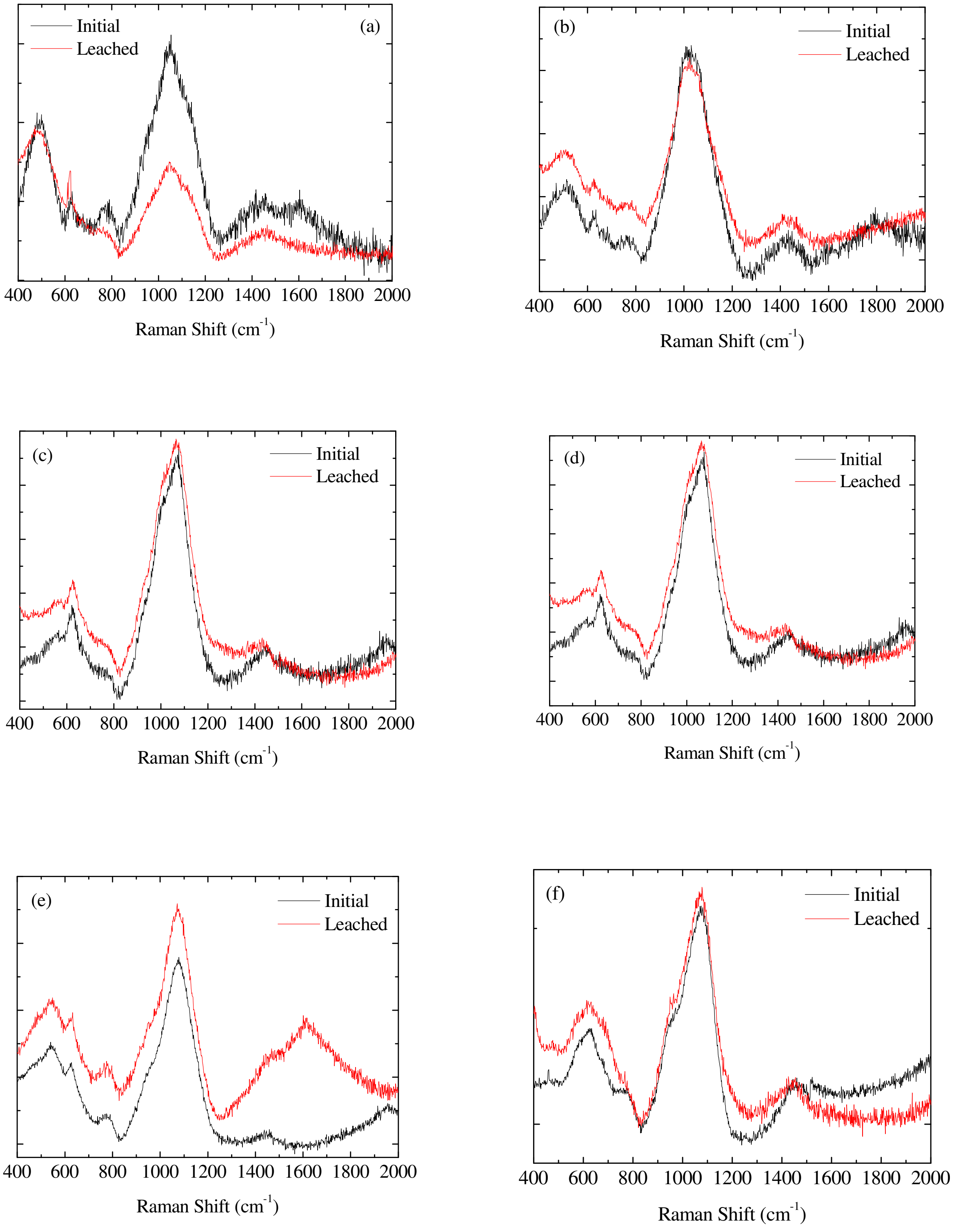

Figure 7.34 *Examples of Raman spectra from leached and non-leached borosilicate glass disks: (a) Cs0AlMW, (b) Cs0LaMW, (c) Cs7AlMW, (d) Cs7LaMW, (e) Cs7MgMW and (f) Cs7Mg'MW. Note: Spectra are background subtracted.*

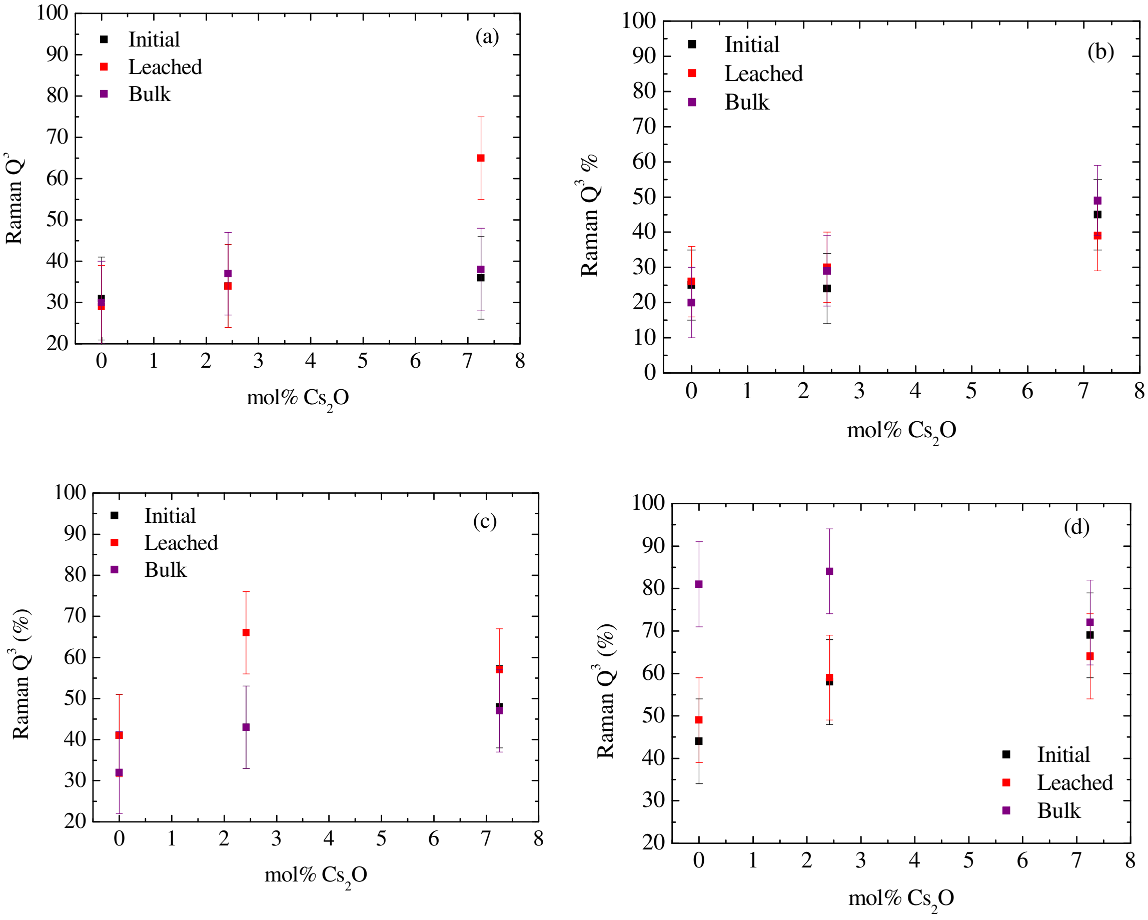

Figure 7.35 *Resolved* Q^3 *fractions from Raman Spectroscopy measurements of the (a) CsAlMW, (b) CsLaMW, (c) CsMgMW and (d) CsMg′MW leach disks (before and after leaching). Measurements from leached glass discs are compared with those from identical unleached discs (initial) and resolved fractions from the bulk glasses (cf. Section 7.4.1).*

7.5 Energy Dispersive Analysis with X-rays (EDX)

7.5.1 Volatile Species from Volatilisation Measurements

EDX measurements of deposits from the three most volatile samples, representative of all four borosilicate systems, showed the deposit contained caesium, sodium, boron and silicon (Figure 7.36) [24]. This is identical to previous EDX measurements on the CsMW system [1] (Figure 7.36). Both calcium, magnesium and aluminium are also present in the spectra due to the alumina substrate on which the volatile compound is collected, and the interaction between the substrate and the lining of the furnace at high temperature during the volatilisation experiment, also observed in the previous study [1].

The alkali borosilicate compositional form of the volatile species evolved from the melt, interestingly does not match the results by Asano *et al.* [35-38] or Stolyarova *et al.* [39]. These studies have all observed vapour species to be lacking any silicon component and therefore consisted of either alkali or alkali-borate species (*cf.* Table 6.2 in Chapter 6) or in the cases where they are present, vapours of additional oxides added to the glasses, i.e. Te_2, TeO or TeO_2 in the study of Asano *et al.* [38]. A possible reason for this result is the higher temperature (1000°C) at which the samples in this study were held, and it was this that promoted the release of silicon-containing groups from the melt, in addition to alkali and alkali borate species; a result supported by similar results in the study carried out by Archakov *et al.* [33]. The presence of silicon in the EDX results is supported by the Raman measurements on the same material (*cf.* Section 7.4.2), which also revealed the presence of silicon (Q^2) groups.

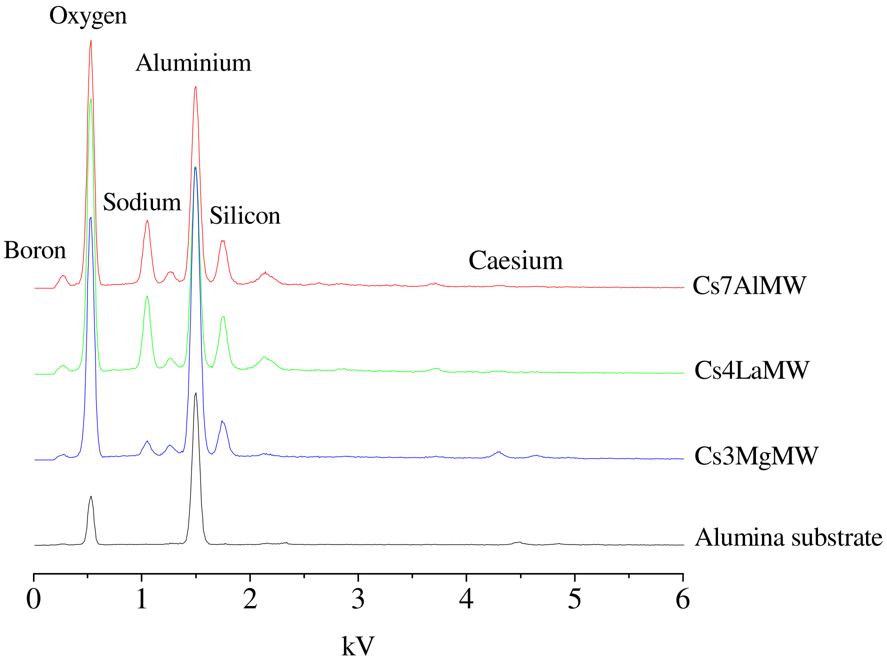

Figure 7.36 *EDX spectra of the volatile species formed from three borosilicate compositions, representing the four borosilicate systems [24], compared against the spectra obtained from the CsMW system [1].*

7.6 Summary

Density measurements on all the borosilicate glasses have been shown to be dominated by the increasing caesium content, with the addition of either aluminium-, lanthanum- or magnesium-oxide having negligible effect on overall increasing glass density as a function of caesium oxide. Glass density is seen to increase from approximately 2.4 g/cm^3 to 2.6 g/cm^3 and within error is approximately equal for all four glass systems. Molar volume measurements show a clear separation between the different systems. All are shown to increase as a function of caesium oxide content, due to the relatively large size of Cs^+ ions being added to the glass network.

^{23}Na MAS NMR measurements revealed a typically broad asymmetric peak due to quadrupole interactions of the 3/2 spin ^{23}Na site. The peak maximum moved to less negative ppm values with caesium oxide addition; characteristic of an increasing charge transfer to the borate and silicate networks. ^{27}Al MAS NMR spectra showed both Al^{3+} sites and Al^{6+} sites were seen to exist, with the four-coordinated alumina units found to associate themselves preferentially with the silicate network giving $[Al(OSi)_4]$ groups.

^{11}B MAS NMR measurements showed spectra with a broad quadrupolar lineshape due to trigonal planar B_3 units, and a sharper Gaussian resonance due to tetrahedral four-coordinated boron units. Asymmetry in the B_4 peak of the NMR spectra allowed, using two Gaussian peaks separated by ~1.5 ppm, two BO_4 sites with different next-nearest neighbour (NNN) environments to be resolved; one B_4 surrounded by 4Si and one B_4 surrounded by $1B_{(4)}$ and 3Si. These two sites are present because of two different medium-range order (MRO) units – reedmergnerite and danburite, present across all four glass systems, which contain unique B_4 environments. The presence of danburite units, containing B_4 sites with 1B, 3Si NNN, is interesting because of the double B_4-B_4 present which is energetically less stable.

Both N_4 (the fraction of four-coordinated boron units) and the fraction of the two MRO units were resolved for the four glass systems. As a function of R, N_4 was found to increase from 0.6 to 0.75, for the CsAlMW, CsLaMW and CsMgMW systems, but to decrease from 0.5 to 0.45 for the CsMg'MW system. For the Al- and La-containing systems, the fraction of danburite units was found to increase as a function of R, and to decrease for the Mg-containing glasses. Comparing the resolved fractions of danburite units with mass-loss measurements from Chapter 5 suggests that, along with the formation of greater numbers of silicon Q^3 units, the increasing presence of danburite units, as a function of R, is also related to greater volatility.

^{29}Si MAS NMR measurements allowed the resolving of the fraction of silicon Q^3 units, and were found within error to agree with theory. For all the systems, apart from the high-magnesium content system, where the theory of Q^3 formation is found to be inaccurate, the resolved Q^3 fraction was found to increase as a function of R. Using N_4 and Q^3 values obtained from ^{11}B and ^{29}Si MAS NMR respectively and known compositional details, the percentage of silicon Q^4 units outside of MRO units was calculated as a function of R and was found to decrease from ~60 % to ~15 %.

From Raman spectroscopy, the presence of the danburite and reedmergnerite MRO units was confirmed, supporting the observations made by ^{11}B MAS NMR. Quantitative peak fitting of the region of the Raman spectra between 800-1100 cm^{-1}, enabled the fraction of Q^3 units to be resolved for all systems apart from CsMg'MW. These were found to agree with both theory and values obtained from ^{29}Si MAS NMR. This technique was also applied to the selective number of glass disks used in the chemical durability corrosion measurements, where it was found that Q^3 remained approximately constant before and after leaching.

EDX measurements on the volatilised species, obtained from the mass-loss measurements described in Chapters 5 and 6, show the composition of the species to contain sodium, caesium, boron and silicon; supporting studies by other authors that at high temperature alkali borate and alkali silicate groups are volatilised from the melts of alkali borosilicate glasses of varying compositions. Interestingly the composition of the EDX spectra appears to be independent from the additional oxide (i.e. Al_2O_3, La_2O_3 or MgO) present in the initial borosilicate glass.

7.7 References

[1] B. G. Parkinson, D. Holland, M. E. Smith, A. P. Howes, and C. R. Scales, *J. Non-Cryst. Solids* **351** (2005) 2425-2432.

[2] R. C. Weast, *Handbook of Chemistry and Physics*, 55 ed. (CRC Press, 1974).

[3] N. E. Brese and M. O'Keeffee, *Acta Crystallogr.* **B47** (1991) 192-197.

[4] J. M. Roderick, *PhD Thesis, Warwick University* (2001).

[5] B. C. Bunker, D. R. Tallant, R. J. Kirkpatrick, and G. L. Turner, *Phys. Chem. Glasses* **31** (1) (1990) 30-41.

[6] K. J. D. Mackenzie and M. E. Smith, *Multinuclear Solid-State NMR of Inorganic Materials*, (Pergamon, 2002).

[7] E.-M. Ratai, J. C. C. Chan, and H. Eckert, *Phys. Chem. Glasses* **4** (2002) 3198-3208.

[8] E.-M. Ratai, M. Janssen, J. D. Epping, J. C. C. Chan, and H. Eckert, *Phys. Chem. Glasses* **44** (2) (2003) 45-53.

[9] B. G. Parkinson, D. Holland, M. E. Smith, A. P. Howes, and C. R. Scales, *J. Phys.: Condens. Matter* **19** (2007).

[10] G. El-Damrawi, W. Muller-Warmuth, H. Doweidar, and I. A. Gohar, *Phys. Chem. Glasses* **34** (2) (1993) 52-57.

[11] A. Duddridge, *PhD Thesis, Warwick University* (2004).

[12] B. G. Parkinson, *MSc Thesis, Warwick University* (2004).

[13] L.-S. Du and J. F. Stebbins, *Solid State Nucl. Mag.* **27** (2005) 37-49.

[14] L.-S. Du and J. F. Stebbins, *J. Non-Cryst. Solids* **351** (2005) 3508-3520.

[15] J. M. Roderick, D. Holland, and C. R. Scales, *Phys. Chem. Glasses* **41** (6) (2000) 392-396.

[16] W. J. Dell, P. J. Bray, and S. Z. Xiao, *J. Non-Cryst. Solids* **58** (1983) 1-16.

[17] L.-S. Du and J. F. Stebbins, *J. Phys. Chem.* **B, 107** (2003) 10063-10076.

[18] L.-S. Du and J. F. Stebbins, *J. Non-Cryst. Solids* **315** (2003) 239-255.

[19] L.-S. Du and J. F. Stebbins, *Chem. Mater.* **15** (2003) 3913-3921.

[20] S. Kroeker, S. A. Feller, M. Affatigato, C. P. O'Brien, W. J. Clarida, and M. Kodama, *Phys. Chem. Glasses* **44** (2) (2003) 54-58.

[21] P. M. Anguiar and S. Kroeker, *Solid State Nucl. Mag.* **27** (2005) 10-15.

[22] D. Massiot, F. Fayon, M. Capron, I. King, S. Le Calve, B. Alonso, J. O. Durand, B. Bujoli, Z. Gan, and G. Hoatson, *Magnetic Resonance Chemistry* **340** (76) (2002).

[23] Z. N. Utegulov, J. P. Wickstead, and G.-Q. Shen, *Phys. Chem. Glasses* **45** (3) (2004) 166.

[24] B. G. Parkinson, D. Holland, M. E. Smith, A. P. Howes, and C. R. Scales, *J. Non-Cryst. Solids* **353** (2007) 4076–4083.

[25] B. G. Parkinson, D. Holland, M. E. Smith, C. Larson, J. Doerr, M. Affatigato, S. A. Feller, A. P. Howes, and C. R. Scales, *J. Non-Cryst. Solids* **Accepted, awaiting publication** (2007).

[26] B. O. Mysen, *Am. Mineral.* **75** (1990) 120-134.

[27] J. Tan, S. Zhao, W. Wang, G. Davies, and X. Mo, *Material Science and Engineering B* **106** (2004) 295-299.

[28] W. L. Konijnendijk and J. M. Stevels, *J. Non-Cryst. Solids* **18** (1975) 307-331.

[29] W. L. Konijnendijk and J. M. Stevels, *J. Non-Cryst. Solids* **20** (1975) 193-224.

[30] R. N. Sinclair, R. Haworth, A. C. Wright, B. G. Parkinson, D. Holland, J. W. Taylor, N. M. Vedishcheva, I. G. Polyakova, B. A. Shakhmatkin, S. A. Feller, B. Rijal, and T. Edwards, *Physics and Chemistry of Glasses: European Journal of Glass Science and Technology* **Part B, 47** (4) (2006) 405-411.

[31] http://rruff.info/index.php

[32] B. N. Meera and J. Ramakrishna, *J. Non-Cryst. Solids* **159** (1991) 1-21.

[33] I. Y. Archakov, V. L. Stolyarova, and M. M. Shultz, *Rapid Commun. Mass Spectrom.* **12** (1998) 1330-1334.

[34] M. Islam, *PhD Thesis, Warwick University* (2005).

[35] M. Asano, T. Kou, and Y. Mizuntani, *J. Non-Cryst. Solids* **112** (1989) 381-384.

[36] M. Asano, T. Kou, and Y. Yasue, *J. Non-Cryst. Solids* **92** (1987) 245-260.

[37] M. Asano and Y. Yasue, *J. Nucl. Mater.* **138** (1986) 65-72.

[38] M. Asano and Y. Yasue, *J. Nucl. Mater.* **151** (1988) 181-188.

[39] V. Stolyarova, *J. Nucl. Mater.* **247** (1997) 7-10.

Chapter 8

8 Results and Discussion: - ^{17}O Enriched Borosilicate Systems

8.1 Introduction

This chapter presents the sample characterisation and structural results for the oxygen-17 enriched borosilicate compositions; including XRD, EDX and thermal analysis results together with density, ^{11}B, ^{29}Si and ^{17}O NMR and Raman spectroscopy measurements.

8.2 Characterisation of the ^{17}O-Enriched Borosilicate System

8.2.1 X-ray Diffraction measurements

Both the ^{17}O- and non-^{17}O enriched SiO_2 precipitates, dried at 200°C, were white and XRD analysis of the non-^{17}O enriched SiO_2 powder showed it to be non-crystalline with a broad amorphous XRD signature (Figure 8.1).

When removed from their platinum tubes, all of the resultant borosilicate samples were black or dark grey in colour; this is assumed to be due to retention of some carbon from the carbonate precursors (Figure 8.2). This colouration is not observed when melting in air when carbonate gases can escape before the melts are quenched [1,2]. Samples were stored in a desiccator to reduce attack by atmospheric moisture.

XRD spectra for all but the Cs(MW) sample (Figure 8.3), show the samples to be amorphous within the limits of detection of XRD. The addition of relatively small amounts of intermediate oxides Al_2O_3 and La_2O_3 (0.95 and 1.68 mol% respectively) to Na(MW) to form AlNa(MW) and LaNa(MW), makes negligible difference to the glass-forming characteristics of their resultant compositions.

The XRD spectrum of Cs(MW) (Figure 8.4), shows sharp Bragg diffraction peaks, characteristic of a crystalline structure. Peak matching using the Crystallographica XRD database showed the sample to be crystalline $Cs_2O.B_2O_3.2SiO_2$ (PDF x-ray diffraction pattern code 37-1347). This crystal phase, with composition R=1 and K=2, can be compared to the intended glassy composition with R=1.12 and K=3.2. The amorphous background visible in the XRD pattern is therefore likely due to the excess SiO_2 in the glass composition compared to the crystal stoichiometry – probably as a silicon-rich caesium borosilicate.

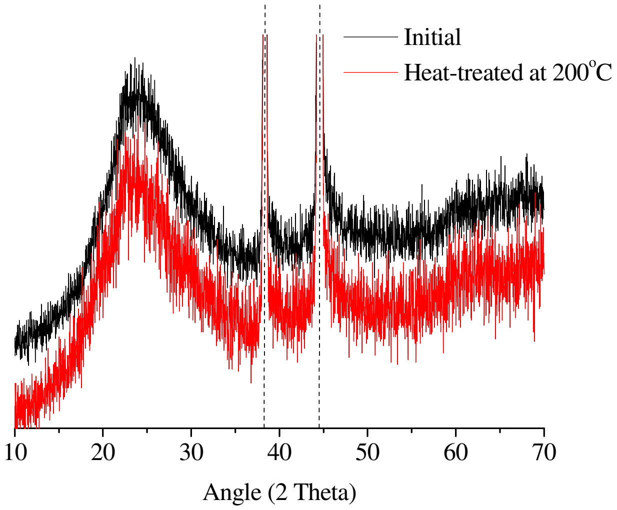

Figure 8.1 *XRD spectrum of the ^{17}O-enriched SiO_2 powder. Note: Dashed lines indicated diffraction peaks from the aluminium sample holder.*

Figure 8.2 *Example of the black colouring of the oxygen-17 enriched borosilicate samples. This being the Cs(MW) sample.*

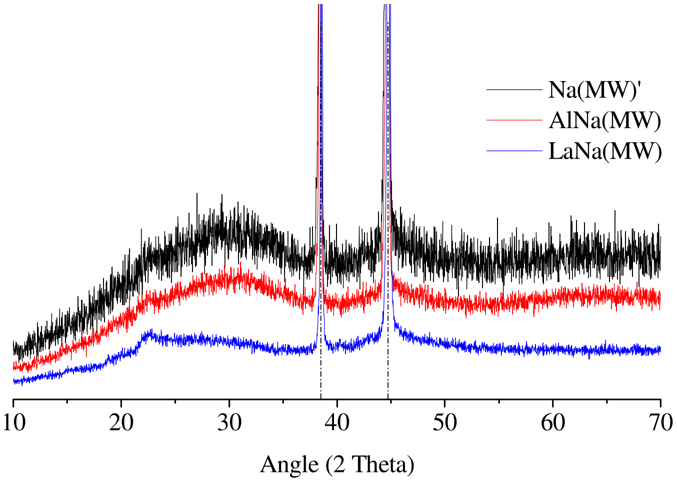

Figure 8.3 *XRD spectra for the (a) Na(MW)', (b) Cs(MW), (c) AlNa(MW) and (d) LaNa(MW) ^{17}O enriched samples. Note: Diffraction peaks at 38° and 45° in all spectra are from the aluminium sample holder. Note: dashed lines indicate diffraction peaks from the aluminium sample holder.*

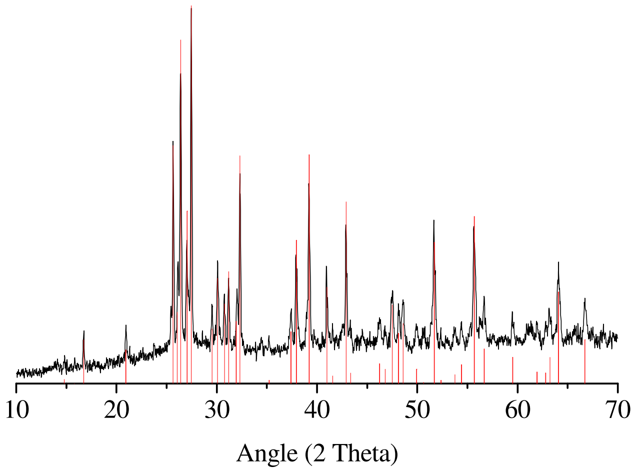

Figure 8.4 *XRD spectrum (black) and match (red) for the Cs(MW) ^{17}O-enriched sample.*

8.2.2 Energy Dispersive Analysis with X-rays (EDX)

EDX spectra obtained for the six borosilicate compositions (Figure 8.5) are similar to alkali borosilicate EDX measurements obtained in a previous study [1]. In each of the six spectra, peaks from O and Si are present at 0.53 and 1.75 kV respectively. For every spectrum, except the Cs(MW) crystal, a peak is present at 1.1 kV due to Na. For the Cs(MW) crystal, a triplet of peaks at 4.3, 4.6 and 5.0 kV is present, confirming the presence of Cs. Similarly, for LaNa(MW), La peaks are observed at 4.7 and 5.1 kV. The presence of Al is confirmed in AlNa(MW) with a relatively small peak at 1.5 kV. The existence of carbon, retained at the stage of sample manufacture, is confirmed by a large peak at 0.27 kV in all the EDX spectra, apart from those for AlNa(MW) and LaNa(MW) where the peak is still present but with reduced intensity. Although the EDX sample holders contain carbon, typically the carbon background signal is significantly smaller than that observed in Figure 8.5.

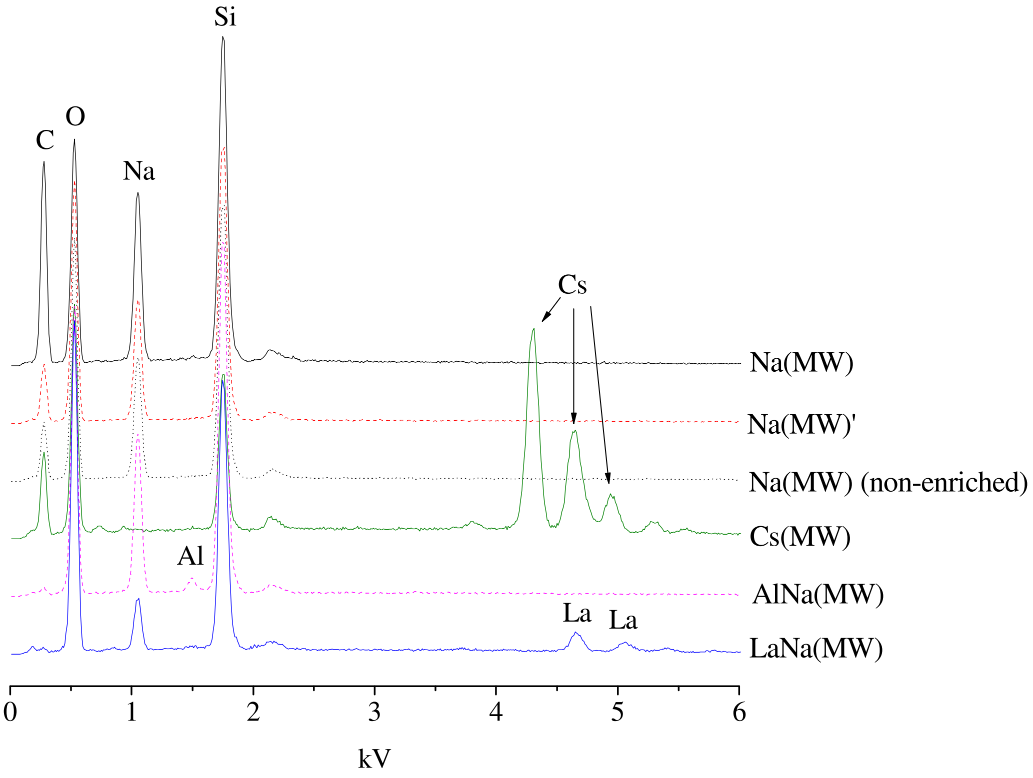

Figure 8.5 *EDX spectra for the borosilicate compositions, including the non-*^{17}*O enriched sodium borosilicate glass.*

Averaged[*] ZAF corrected total cation atomic % to silicon atomic % ratios, Π, obtained from EDX, for Na(MW), Na(MW)', Cs(MW), AlNa(MW) and LaNa(MW) are given in (Table 8.1). Values deviate significantly from theory (8.1) apart from Na(MW)' and AlNa(MW). For the Cs(MW) crystal, Π was found to be 1.05±0.10 compared to the calculated value of 0.69.

---

[*] Averaging over two values; one correcting and one not correcting for the presence of the strong carbon signal in the EDX measurements.

$$\Pi = \frac{2\times mol\%Cs_2O + 2\times mol\%Na_2O + 2\times mol\%Al_2O_3, La_2O_3}{mol\%SiO_2} \qquad (8.1)$$

	Total Cation / Silicon atomic% Ratio	
Sample	Averaged ZAF Corrected EDX (± 0.10)	Theory (Π)
Na(MW)	0.82	0.69
Na(MW)'	0.73	0.69
Cs(MW)	1.05	0.69
AlNa(MW)	0.75	0.73
LaNa(MW)	0.69	0.77

Table 8.1 *Cation atom % to silicon atom % ratios for the six borosilicate compositions calculated from averaged ZAF corrected EDX, compared against values calculated from theory.*

8.2.3 Thermal Analysis Measurements

The combined DTA and TG traces from the non-^{17}O enriched, sol-gel prepared SiO_2 precursor are shown in Figure 8.6. Negligible mass-loss was observed in the TG trace, indicating minimal residual hydroxyl groups in the powder, present from the sol-gel process. If hydroxyl groups were present the mass-loss TG curve would show a much larger response from 100^{o}C. This indicated that the sol-gel manufacture process outlined in Chapter 4 (including heat-treating the powder at 200^{o}C) was successful for use in producing $Si^{17}O_2$. Note: DTA-TG measurements were not carried out on the ^{17}O-enriched SiO_2 powder due to the high cost and the limited quantity available.

Combined DTA-TG plots for the Na(MW), AlNa(MW) and LaNa(MW) ^{17}O-enriched glasses are shown in Figure 8.7. All DTA traces are relatively featureless, which is characteristic for borosilicate glasses with these compositions [1], with only subtle changes in all but the Cs(MW) sample, indicating glass transition and melt-temperatures (T_g and T_m respectively). Positive mass-loss is observed between 200-1000^{o}C in the TG traces for all the samples (Figure 8.7); this is thought to originate from both the removal of atmospheric water, obtained during powdering of the samples, starting at approximately 200^{o}C and eventually through the volatilisation of alkali borate/silicate species at higher temperatures (> 800^{o}C).

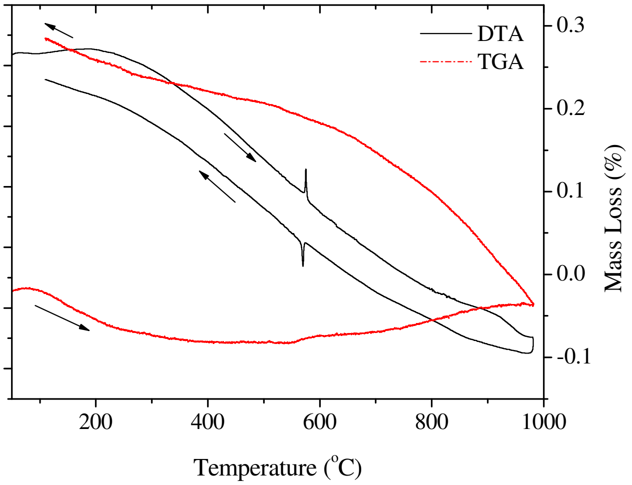

Figure 8.6 *DTA-TG data for the sol-gel prepared non-enriched* SiO_2 *powder, to check for any residual water in the sample. Note: arrows indicate the direction of heating and eventual cooling.*

Sample	T_g (± 10°C)	T_m (± 10°C)
MW [1]	497	662
Na(MW)	460	670
Na(MW)'	520	670
Cs(MW)	-	-
AlNa(MW)	-	649
LaNa(MW)	-	682

Table 8.2 *Glass transition and melting temperatures for the* ^{17}*O-enriched compositions and MW [1].*

Glass transition- and melt-temperatures resolved from DTA-TG measurements are given in Table 8.2. For the Cs(MW) crystal, the DTA-TG trace (Figure 8.7) shows no clear T_m. A large mass-loss is observed between 800-1000°C, which is not observed for Na(MW) and AlNa(MW), where there is no Cs_2O (*). Neither AlNa(MW) or LaNa(MW) show any clear T_g in their DTA traces (Figure 8.7). Na(MW) and Na(MW)', show surprisingly different TG results (Figure 8.7(a) and (b)). Na(MW) shows a larger loss of material (~5 % compared to < 1 % for the

---

[*] *It was not possible to conduct mass spectrometry to help conclude the composition of the volatilised material from the Cs(MW) sample.*

Na(MW)' glass) observed from 200^{o}C. This disparity could only to be due to different quantities of unwanted atmospheric moisture obtained during powdering of the samples since both samples are effectively identical in composition.

The TG plots for Na(MW) and Cs(MW) (Figure 8.7(a) and (c)) initially show mass-losses of ~2 % and 5 % respectively (consistent with the greater moisture sensitivity of Cs(MW)), before the rate of mass-loss increases for both samples at 1000^{o}C and 800^{o}C respectively. This is characteristic of the volatilisation of alkali borate/silicate material from these types of glasses at these temperatures [1,3]. By 1300^{o}C, the maximum mass-losses observed for these two samples are ~7 % and 45 % respectively, which is consistent with Cs being more volatile than Na [1].

An increasing rate of mass-loss from ~1000^{o}C is also observed for both AlNa(MW) and LaNa(MW) in Figure 8.7(d) and (e). In the region 200-1000^{o}C, both glasses show minimal mass-loss (~2 %), before volatilisation of material begins at ~1000^{o}C resulting in a more rapid rate of mass-loss. Presumably the volatilised material is also alkali borate/silicate in composition which supports the earlier finding that the presence of Cs_2O is not essential for the volatilisation of species to occur [1,3].

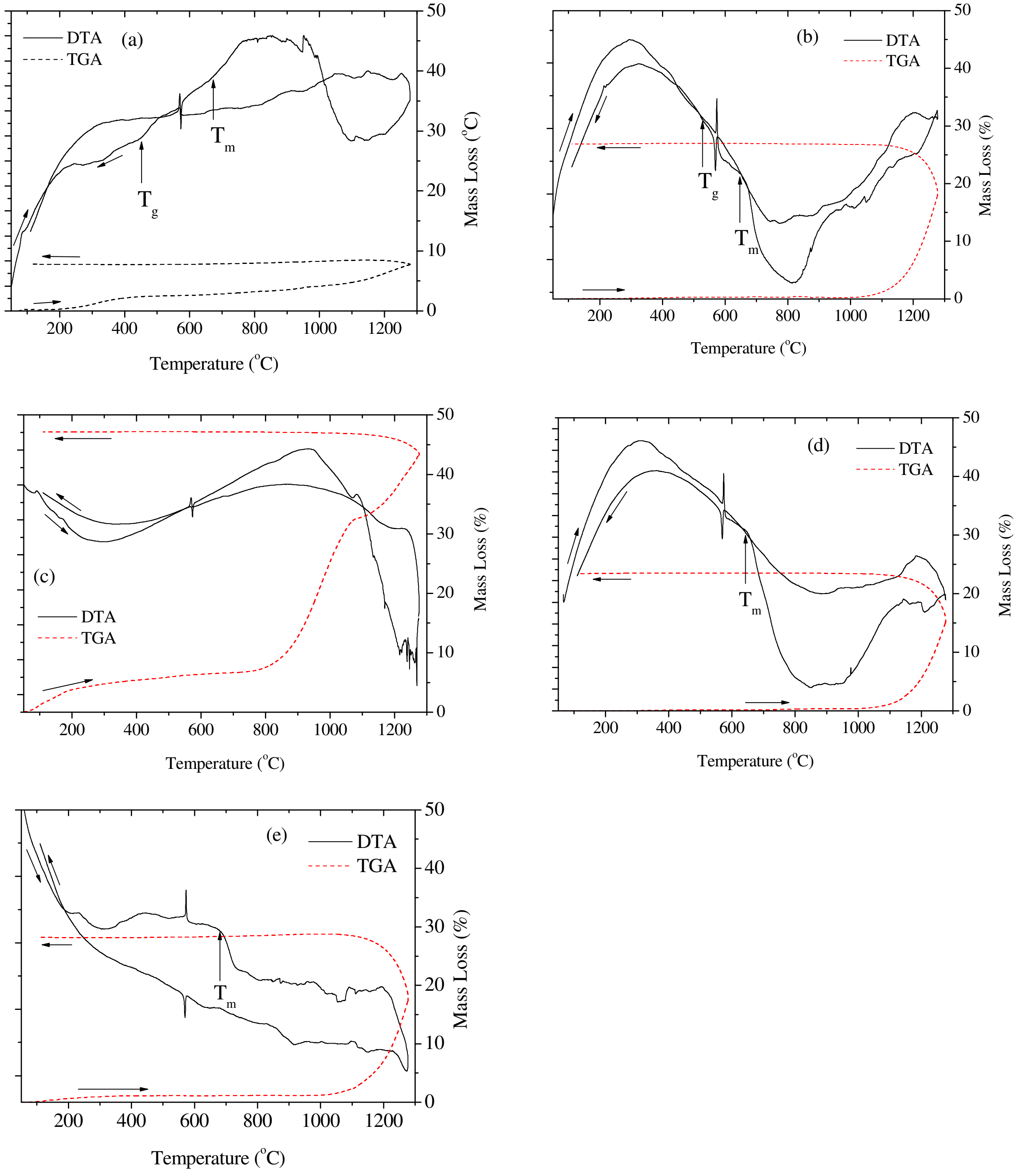

Figure 8.7 *TG-DTA plots for the (a) Na(MW), (b) Na(MW)' (c) Cs(MW), (d) AlNa(MW) and (e) LaNa(MW) compositions, showing both DTA and TG data for all systems. Note: Arrows indicate the direction of heating and eventual cooling.*

8.3 Structural Measurements

8.3.1 Density Measurements

Densities of the ^{17}O-enriched borosilicate glasses are plotted in Figure 8.8. Where possible, values are compared with those from standard borosilicate glasses of similar composition (*cf.* Chapter 7). These comparisons are only approximate, since the ^{17}O-enriched compositions are MW with only one alkali species (i.e. Na_2O) combined with either Al_2O_3 or La_2O_3. Hence, if the structure remains the same, the replacement of Li_2O by Na_2O in the compositions should result in an increase in density [1,2].

For approximately equivalent compositions, within error the densities of the ^{17}O-enriched glasses are equal to non-enriched glasses of comparable composition (*cf.* Chapter 7). For the MW compositions, the density of the Na(MW)' glass is larger than for the mixed-alkali MW [1]. This is consistent with the replacement of Li_2O increasing the overall density of the glass (Table 8.3). Interestingly the sample Na(MW)', which does not contain 0.1 mol% Fe_2O_3, has a greater density than both MW [1] and Na(MW), by 0.23 g/cm^3 and 0.50 g/cm^3 respectively. This may be due to a greater amount of Na being lost at the manufacturing stage of the Na(MW) glass, which supports the TG result (Figure 8.7) where less mass is lost compared to Na(MW)' - because of mass being lost earlier during sample manufacture. The measured density (3.4 g/cm^3) of the Cs(MW) crystal is greater than that for its Na_2O-analogue, Na(MW) (2.0 g/cm^3), due to the much larger density of Cs_2O compared to Na_2O (Table 8.3).

Resolved values of the molar volumes (V_m) for each of the samples (Figure 8.9), show that within error (±1 cm^3), V_m for the LaNa(MW) and AlNa(MW) glasses compare well with values calculated for the similar standard modified borosilicate glasses of this study (*cf.* Chapter 7). Interestingly V_m for the Na(MW) glass is much greater than that of both Na(MW)' and MW [1] (32 cm^3/mol compared to 24 and 26 cm^3/mol respectively). Calculated V_m values for the Na(MW)', AlNa(MW) and LaNa(MW) glasses, are all lower than V_m values calculated for the mixed alkali compositions; a consequence of the replacement of Li_2O in the ^{17}O-enriched samples, which therefore must involve some structural changes. Interestingly, resolved V_m values from the LaNa(MW) glass and its equivalent (Cs0LaMW) from the main section of this study, are (within error) equal – even though later structural measurements show little similarity between the two samples.

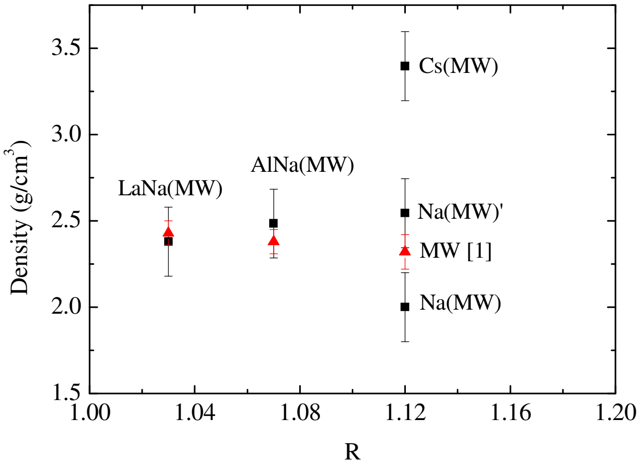

Figure 8.8 *Density measurements for the ^{17}O-enriched borosilicate glasses (black), compared against standard melt-quenched borosilicate glasses of similar composition from this study; Cs0LaMW, Cs0AlMW and MW [1].*

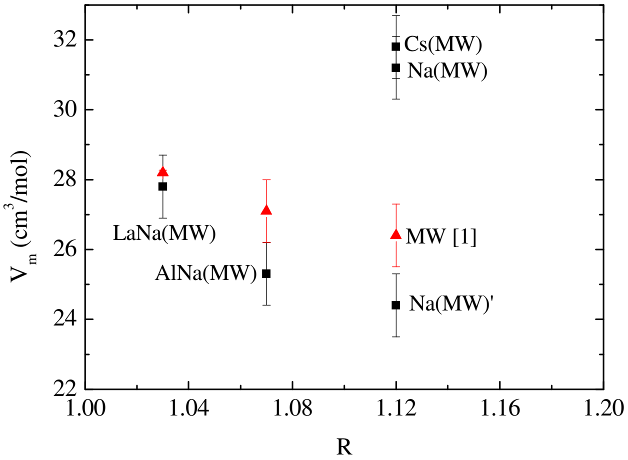

Figure 8.9 *Molar volume measurements for the ^{17}O-enriched borosilicate glasses (black), compared against standard melt-quenched borosilicate glasses of similar composition from this study; Cs0LaMW, Cs0AlMW and MW [1].*

Oxide	Density (g/cm^3)
La_2O_3	6.51
Cs_2O	4.21
Al_2O_3	3.97
SiO_2	2.20
Na_2O	2.27
Li_2O	2.01
B_2O_3	1.81

Table 8.3 *Densities [4] of all the oxides present throughout the borosilicate glass systems, listed in order of decreasing density.*

8.3.2 ^{1}H NMR

The static, unreferenced ^{1}H NMR spectra (Figure 8.10) consist of a relatively broad resonance. Heat-treating the sol-gel prepared SiO_2 powder is seen to reduce the hydrogen content by 50 % from 0.002 to 0.001 mol H per mol SiO_2.

The greater presence of hydrogen in the Cs(MW) crystal compared to the remaining samples is due to the greater hygroscopic nature of Cs compared to Na. This effect is also translated across the range of samples, where the different hydrogen contents for the different samples indicates different reactivities towards atmospheric moisture, depending on composition. Similarly the Na-containing samples will be more water sensitive than the mixed-alkali composition MW.

Difficulties in obtaining more accurate measurements of the hydrogen content arose through the large ^{1}H background of the NMR rotor and probe (Figure 8.10). Note: the quoted error in Table 8.4 is based on repeated ^{1}H NMR measurements on the Na(MW)’ glass.

The increased ^{1}H contents (0.026-0.23 mol H per mol sample) of the samples, compared to that for the heat-treated SiO_2 powder (0.001 mol H per mol SiO_2) (Table 8.4) indicates that ^{1}H is obtained by the samples at the stage of the samples being powdered and not from the initial SiO_2 source. ^{1}H could also be present from ^{1}H in the other initial oxide and carbonate powders – along with the carbonates formed (*cf.* Section 8.2.1) this would also not be lost at the melt stage since the melts are formed in closed crucibles.

Sample	mol H per mol sample (± 0.001)	N_4 (± 0.02)
SiO_2 (initial)	0.002	-
SiO_2 (heat-treated)	0.001	
MW	-	0.67
Na(MW)	0.039	0.86
Na(MW)’	0.016	-
Cs(MW)	0.228	0.80
AlNa(MW)	0.022	0.73
LaNa(MW)	0.026	0.31

Table 8.4 *^1H contents and N_4 fractions for MW [1], the initial and heat-treated SiO_2 powders, ^{17}O-enriched glasses and crystal.*

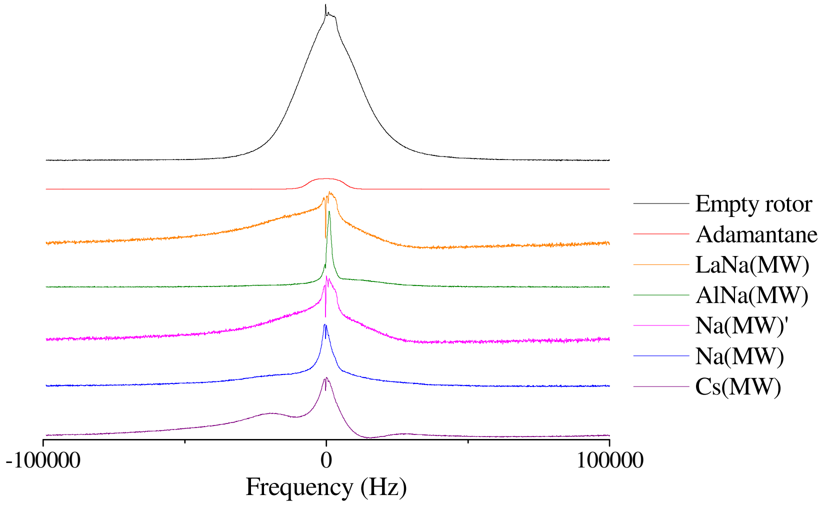

Figure 8.10 *^1H NMR of the ^{17}O-enriched borosilicate glasses. Also included are the spectra from the NMR rotor and the Adamantane reference used for quantitative analysis. Note: the ^1H NMR signal has been subtracted from the sample data and the Adamantane ^1H spectrum has been scaled down in comparison to the remaining samples.*

8.3.3 ^{11}B MAS NMR

The ^{11}B MAS NMR for the Na(MW) and Na(MW)’ compositions are shown in Figure 8.11 with the spectra for the remaining compositions shown in Figure 8.12. ^{11}B MAS NMR spectra for both the ^{17}O-enriched and non-enriched Na(MW) glasses show a Gaussian B_4 peak at ~2 ppm and a broader quadrupolar lineshape from the trigonal planar B_3 boron units, at 12 ppm. This is consistent with the spectra observed for alkali borosilicate glass systems of similar compositions in this and previous studies [1,5-7]. The ^{11}B MAS NMR spectra for the remaining two glasses and crystal (Figure 8.12) show comparable features.

The asymmetric B_4 peak in the Cs(MW) ^{11}B MAS NMR spectrum (Figure 8.12), suggests that the crystalline structure contains three, rather than two, B_4 sites with different next nearest neighbours (NNN) environments; (0B, 4Si), (1B, 3Si) and (2B, 2Si), marked on at −1.7, −0.2 and 1.5 ppm respectively. The presence of three B_4 sites is also observed in the four ^{17}O-enriched borosilicate glasses – a result which although uncommon, is supported by ^{11}B MAS NMR measurements by Du *et al.* [6,8] where three distinct B_4 sites were also found across a range of borosilicate glass compositions.

Resolved N_4 fractions (Figure 8.13 and Table 8.4) were found to be 0.81±0.02 and 0.86±0.02 for the enriched and non-^{17}O-enriched Na(MW) samples respectively. For the same value of R, these two N_4 values are approximately 0.1 greater than for the conventional MW glass [1,9], and is thought to be due to modifying H^+ groups in the samples. The lower than predicted [10] N_4 value for the LaNa(MW) composition (0.31±0.02) indicates the possible loss of material during the sample manufacture, due to the presence of La which previous volatilisation results in this study [3] have shown to result in greater mass-loss compared to solely alkali-containing glasses. Loss of mass would also account for the reduced ^{17}O signal observed in later NMR measurements (*cf.* Section 8.3.5) due increased oxygen exchange. Alkali loss is consistent with the mass-loss measurement from the un-enriched alkali-lanthanum borosilicate glass (with 0 mol% Cs_2O) of this study (*cf.* Chapter 6) [3], which gave an 18 % mass-loss. Loss of material at the stage of sample manufacture would therefore result in the minimal further mass-loss in subsequent TG experiments, observed in Figure 8.7.

For the Cs(MW) crystallised sample, N_4 is found to be 0.80±0.02, greater than that predicted by the Dell model for an R=1, K=3 composition glass [10]. This may be due to water attack during sample powdering – reflected by its large hydrogen content (*cf.* Section 8.3.2). There is no crystal structure available from which to calculate the actual N_4 value.

For the AlNa(MW) glass, N_4 is 0.73±0.02 compared to the predicted value from the Dell model of 0.70. From a previous study [3], for a similar composition of alkali aluminoborosilicate glass (R=1.07) the N_4 fraction was found to be 0.66±0.02 - lower than the Dell model value of 0.67.

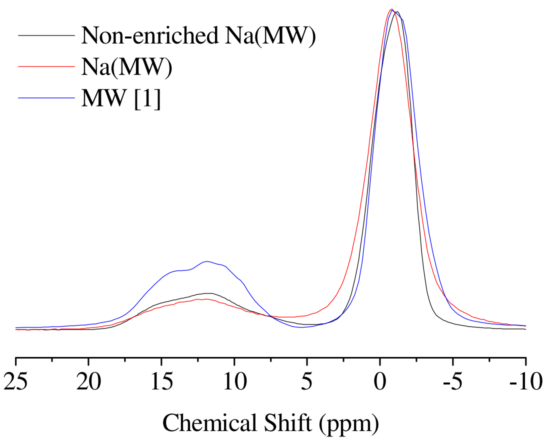

Figure 8.11 *^{11}B MAS NMR spectra for the enriched and non-enriched Na(MW) glasses, compared against a spectrum, for the same composition (MW) [1].*

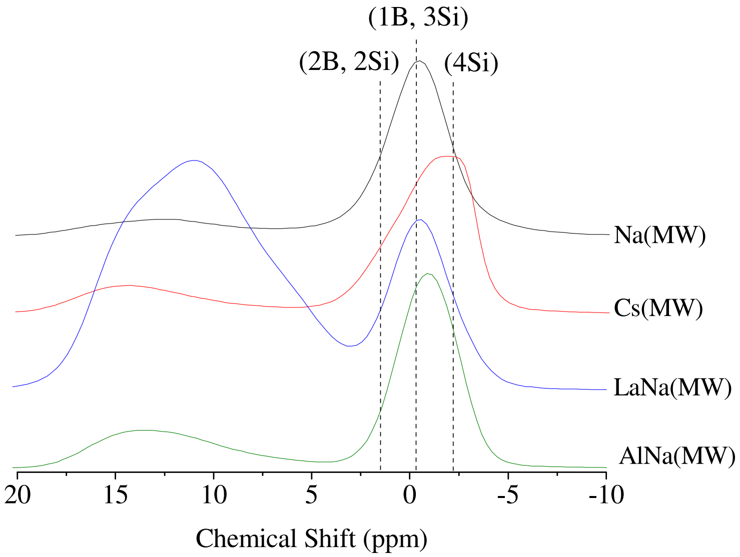

Figure 8.12 *^{11}B MAS NMR spectra for the ^{17}O-enriched borosilicate glasses with positions of the three different possible four-coordinated boron sites with different next-nearest neighbours marked by dashed lines [6].*

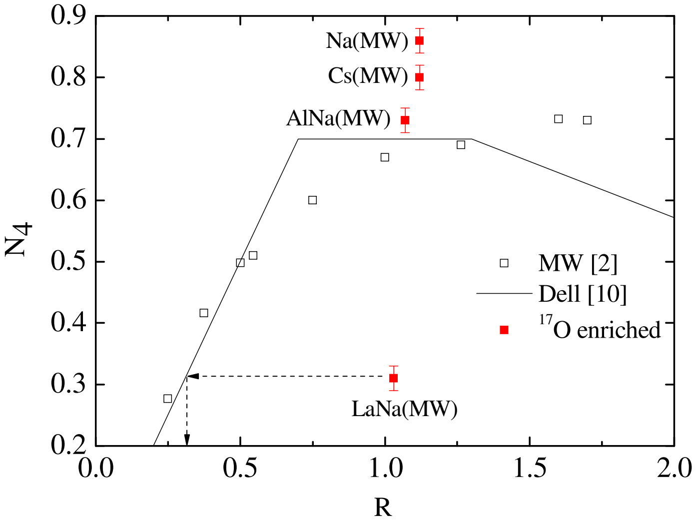

Figure 8.13 *N_4 values for the ^{17}O-enriched borosilicate glasses and crystal, compared against previous measurements [2] and theory [10].*

8.3.4 ^{29}Si MAS NMR

^{29}Si MAS NMR spectra for the sol-gel prepared SiO_2 powder, before and after heat-treating, are shown in Figure 8.14, with spectra for the three glasses shown in Figure 8.15. The ^{29}Si MAS NMR spectrum for the Cs(MW) crystal is shown in Figure 8.16.

The ^{29}Si MAS NMR spectrum for the initial pre-heat-treated non-^{17}O enriched SiO_2 powder (Figure 8.14) is shown to be complex, with peaks at −78, −86, −93 and −102 ppm due to Q^1, Q^2, Q^3 and Q^4 units respectively [5,11]. Heat-treating the SiO_2 powder at 200°C for 24 hours in an argon atmosphere [12] resulted in the ^{29}Si MAS NMR lineshape changing to a peak consisting predominantly of Q^3 and Q^4 groups. In relation to the ^{1}H NMR data (*cf.* Section 8.3.2) and the low ^{1}H content for the initial SiO_2 powder (0.002 mol H per mol SiO_2) few Q^3, Q^2 and Q^1 species should be present. This indicates that the T_1 used was perhaps too short, hence a larger signal was obtained from the H^+-containing Q^3 units present which have shorter T_1 times than Q^4 units.

In Figure 8.15, a broad asymmetric resonance, with centre of gravity at approximately −103 ppm, is observed for the three glasses, comparable to the spectra observed in previous studies [2,3,11] of alkali borosilicate glasses of similar composition. Although the spectra obtained was of insufficient signal-to-noise to use for quantitative measurements, it is clear through the asymmetry of the resonance that Q^4(B) and Q^3 silicon units are present in all of the three glasses, marked in Figure 8.15 at −102 and −93 ppm respectively. This is consistent with previous measurements on similar glasses [1,2].

The presence of Q^3 groups supports results in the preceding ^{17}O MQ MAS NMR 2D spectra (*cf.* Figure 8.18 in Section 8.3.5.2), which show a strong signal from NBO groups, due to the large population of NBO-containing Q^3 units. The ^{29}Si MAS NMR spectrum in Figure 8.16, is largely crystalline showing clearly defined peaks at −87 and −105 ppm, with a third peak, a shoulder on the −87 ppm peak, at approximately −92 ppm. Within the error of measurement (±5 ppm) these would be equivalent to: Q^2 (−87 ppm), Q^3 (−92 ppm) and Q^4(B) (−105 ppm) – probably with an underlying broad peak from residual glass. Note: the exact identification of these peaks is not possible due to the crystal structure being unknown.

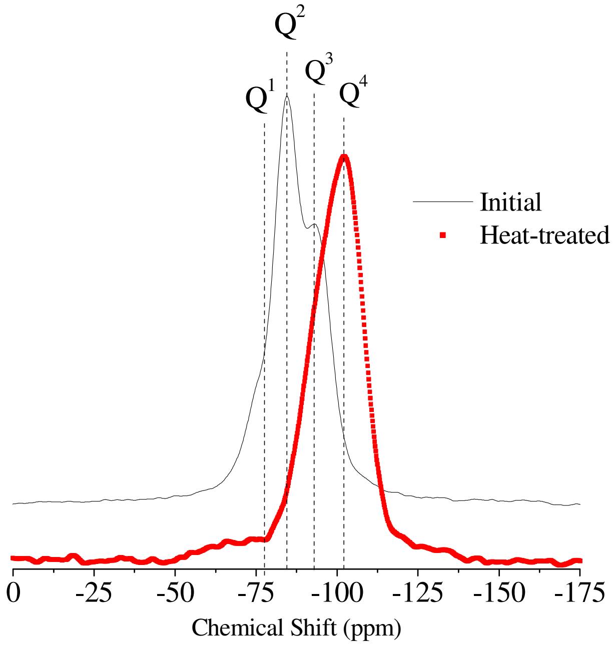

Figure 8.14 *^{29}Si MAS NMR spectra of the sol-gel prepared non-enriched SiO_2 powder, before and after heat-treating to remove remnant hydroxyl groups.*

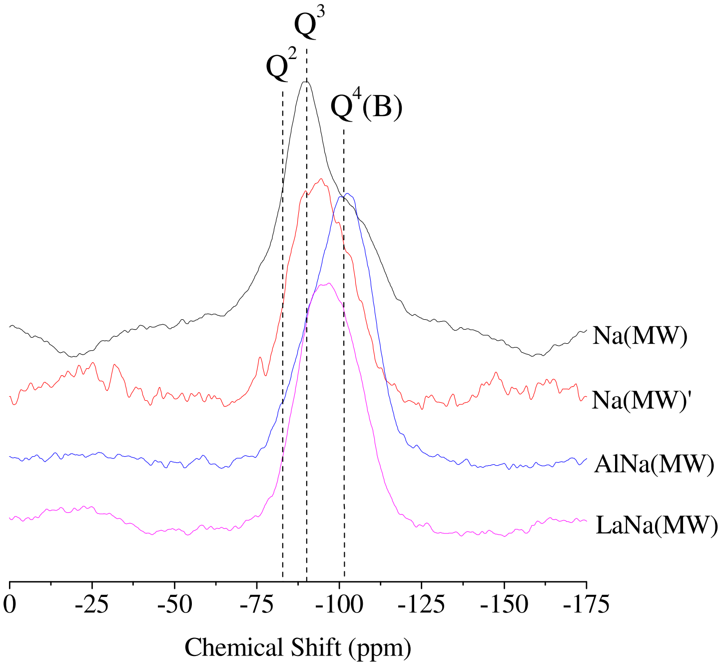

Figure 8.15 ^{29}*Si MAS NMR spectra for the oxygen-17 enriched borosilicate compositions.*

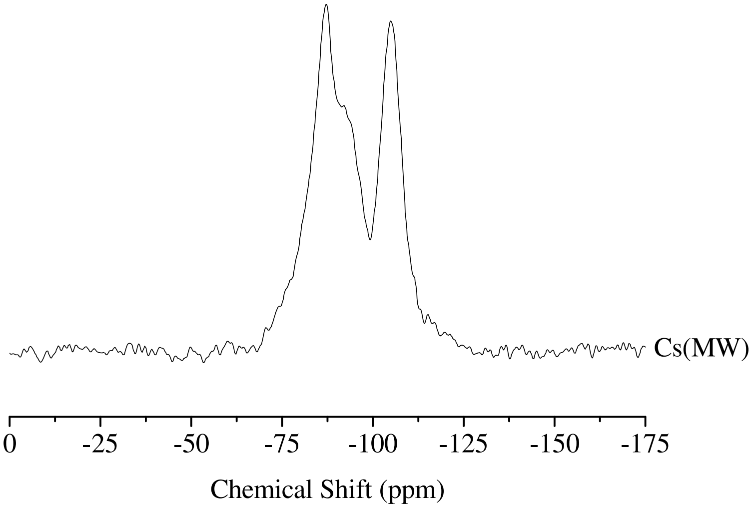

Figure 8.16 ^{29}*Si MAS NMR spectrum for the Cs(MW) crystal.*

8.3.5 ^{17}O NMR Measurements

8.3.5.1 ^{17}O MAS NMR

One-dimensional ^{17}O MAS NMR data for the five ^{17}O-enriched samples; Na(MW), Na(MW)', AlNa(MW), Cs(MW) and LaNa(MW), are shown in Figure 8.17. On each spectrum, magic angle spinning sidebands are clearly present and are denoted by *. The ^{17}O MAS NMR spectra for the Na(MW), Na(MW)' and AlNa(MW) glasses consist of a relatively sharp asymmetric peak at ~40 ppm, with a shoulder at ~10 ppm. The main resonance, by comparison with previous studies [13,14], is assigned to NBO sites on Si or Al units, i.e. Si/Al-^{17}O-Na^{+}, with the shoulder at 10 ppm arising from BO sites within the three glasses.

For Cs(MW) and LaNa(MW), the ^{17}O MAS NMR spectra consist of much broader asymmetric resonances. The asymmetric peak of the Cs(MW) crystal contains both silicon NBO as well as boron NBO, at 25 ppm and 60 ppm respectively. The broad asymmetric resonance for the LaNa(MW) glass contains peaks at 20, 40 and 95 ppm due to BO, Si-NBO, B-NBO and La-NBO (for the LaNa(MW) glass) respectively. The lower quality ^{17}O NMR signal from the Cs(MW) crystal was initially thought to be due to a longer T_1 relaxation time, compared to the remaining glasses. Measurements however showed this not to be the case.

A comparison between the ^{17}O MAS NMR spectra for the Na(MW) and Na(MW)' glasses indicates little change in the lineshape due to the presence of iron (III) oxide. The large, sharp resonance at ~40 ppm in Na(MW) and NaAl(MW) due to ^{17}O in NBO sites, is consistent with the ^{29}Si MAS NMR measurements which shows predominantly Q^3 at –93 ppm. This similarity is carried through to the ^{17}O MQMAS NMR results (*cf.* Section 8.3.5.2) where peaks from NBO and BO sites are clear for both glasses. The addition of the relatively small quantity of Al_2O_3 (0.95 mol%) results in the much broader BO resonance, through the formation of Si-O-Al units which distorts the original BO site centred around (25, 90).

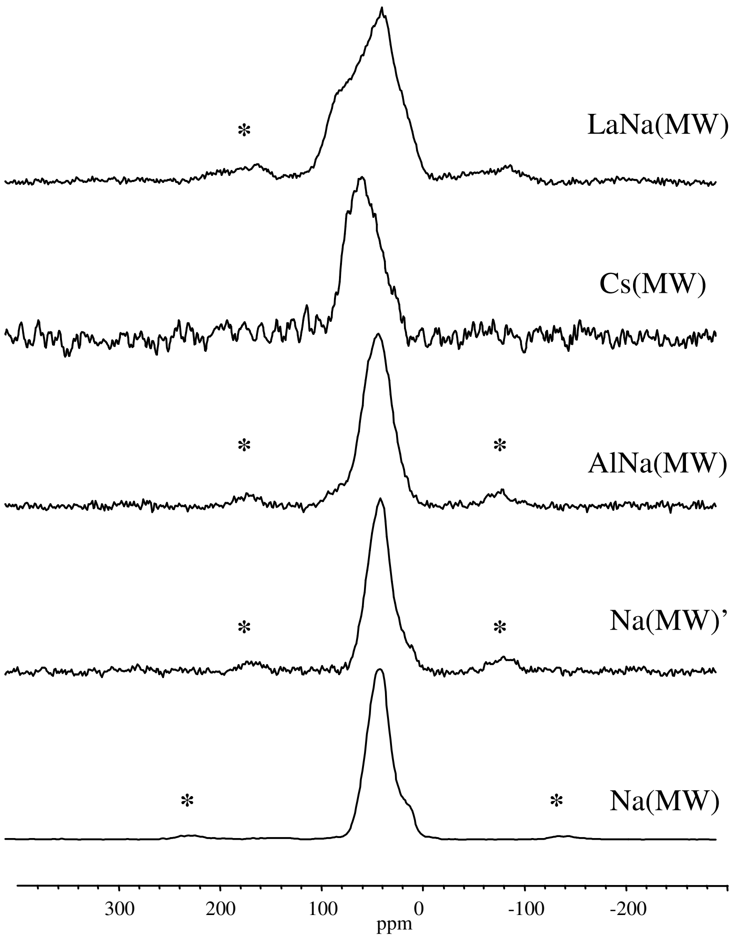

Figure 8.17 *One dimensional ^{17}O MAS NMR plots for the five ^{17}O-enriched borosilicate samples. Note: magic angle spinning sidebands are denoted by **

8.3.5.2 ^{17}O MQMAS and DOR NMR

^{17}O MQMAS NMR plots (Figure 8.18) complement and support the 1D ^{17}O MAS NMR data in Figure 8.17. For the Na(MW) glass, the MQ map consists of a well defined elliptical region at (30 ,60), as well as a larger region at (22, 100). These two main regions, by comparison with previous work [14], have been identified as ^{17}O in NBO and network Si-^{17}O-Si and Si-^{17}O-B sites respectively. For the AlNa(MW) glass, the MQ map is similar, with a less well defined region at (20, 100) due to the presence of ^{17}O sites in both Si-^{17}O-Si, Si-^{17}O-B and Si-^{17}O-Al groups. This region is even less well defined for the LaNa(MW) glass, where there exist network ^{17}O sites Si-^{17}O-Si and Si-^{17}O-La units. The Cs(MW) crystal MQ plot is significantly different from the MQ plots for the three glasses, consisting of a large distorted region with two approximate centres at (53, 100) and (29, 80), present from ^{17}O in B-^{17}O-B and B-NBO sites. The broad spectrum for the LaNa(MW) glass suggests multiple ^{17}O sites exist but are not resolvable.

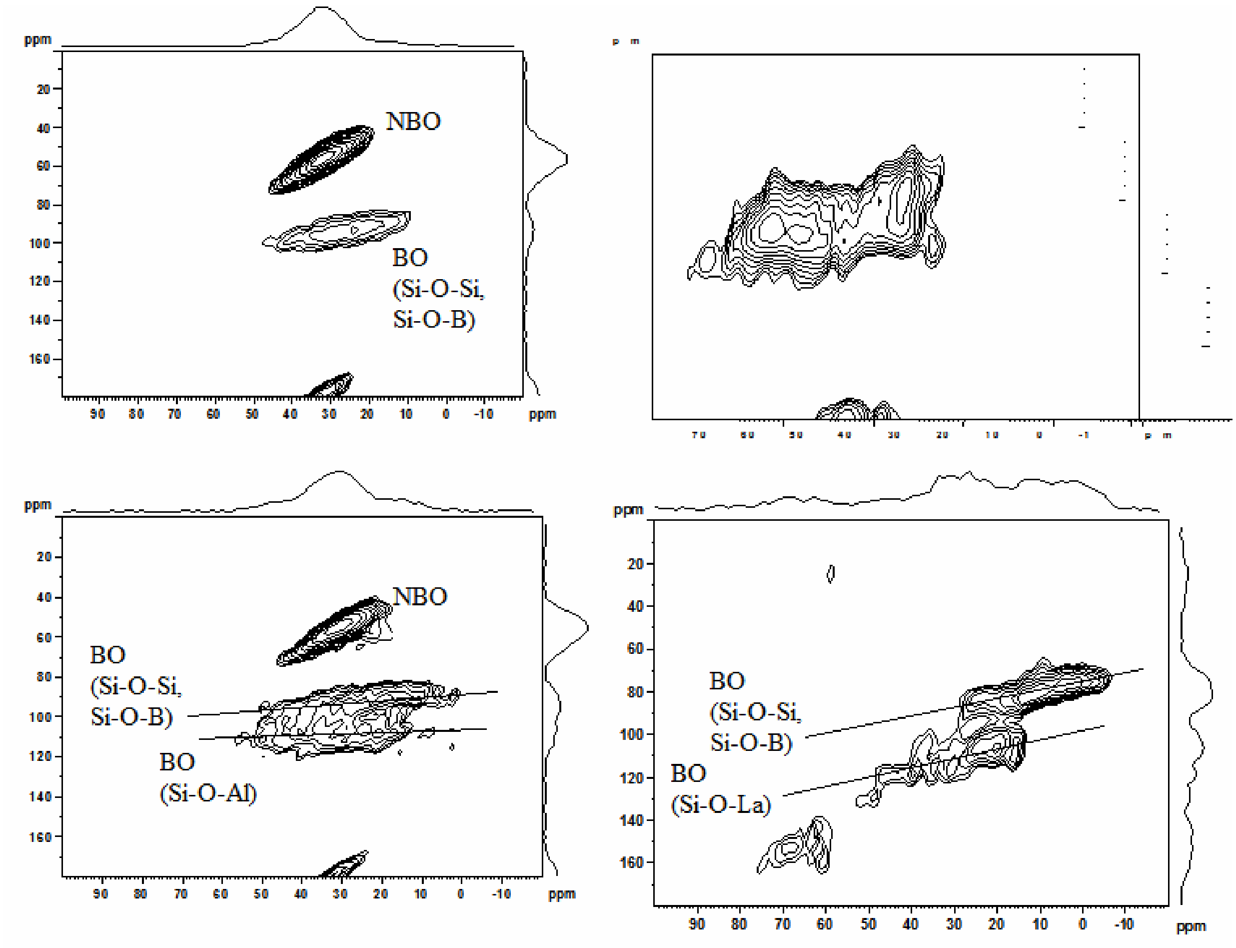

Figure 8.18 *^{17}O MQMAS NMR 2D spectra for the Na(MW) glass (top left), Cs(MW) crystal (top right), AlNa(MW) glass (bottom left) and LaNa(MW) glass (bottom right). Note: the isotropic dimension, free of any quadrupole interactions, is displayed as the y-axis.*

The fraction of NBO and BO, resolved from the isotropic ^{17}O spectra of the Na(MW) and AlNa(MW) glasses (top left and bottom left in Figure 8.18, respectively) are shown in Table 8.5. Further measurements on any of the remaining glasses and Cs(MW) crystal were not possible due to difficulty in resolving two distinct NBO and BO peaks.

Preliminary ^{17}O DOR NMR (DOuble angle Rotation NMR, *cf.* Chapter 5) on the simplest of the ^{17}O-enriched compositions, the Na(MW) glass, gave the spectrum shown in Figure 8.19. Resolving the NBO and BO peaks in the spectrum gave values, quoted in Table 8.5, that compare within error to those obtained from the isotropic ^{17}O MQMAS NMR spectrum of the same glass. The BO site was found to have a longer T_1. These results highlight the benefits of ^{17}O DOR NMR (over the more complicated ^{17}O MQMAS NMR experiments) which although is mechanically more difficult to conduct, is easier to both obtain spectra and resolve and quantify peaks within them.

Sample	NBO (± 0.1)		BO (± 0.1)	
	MQMAS	DOR	MQMAS	DOR
Na(MW)	0.65	0.73	0.35	0.27
AlNa(MW)	0.48	-	0.53	-

Table 8.5 *NBO and BO fractions for the Na(MW) and AlNa(MW) glasses, resolved from the isotopic ^{17}O MQMAS NMR spectra and, for the Na(MW) glass, from ^{17}O DOR NMR. Measurements included data obtained from the MAS sidebands of the MQMAS- and DOR-NMR spectra.*

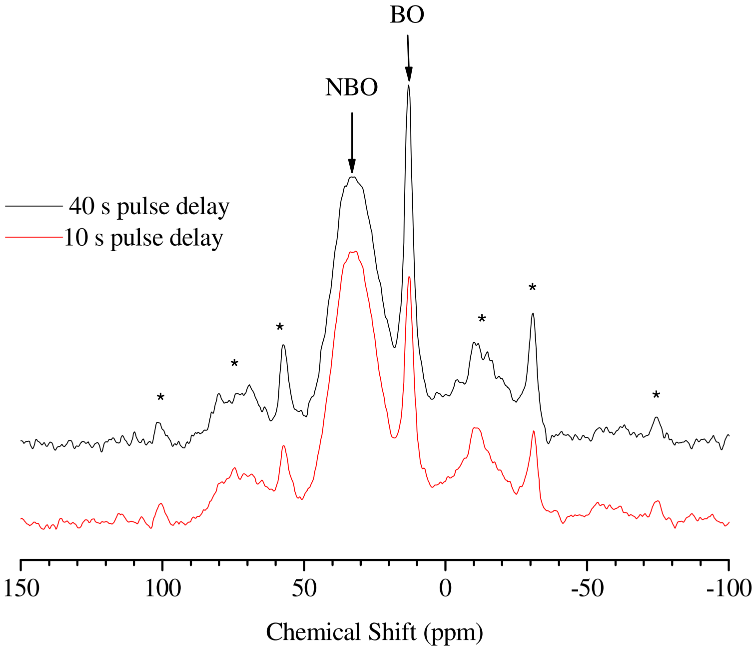

Figure 8.19 *^{17}O DOR NMR spectra (at different pulse delays) for the Na(MW) glass obtained at 14.1T. Arrows indicate oxygen sites, with * indicating MAS sideband positions.*

8.3.6 Raman Spectroscopy

Raman spectra for the Na(MW), Cs(MW), AlNa(MW) and LaNa(MW) samples are shown in Figure 8.20 and Figure 8.21. The Raman spectrum of the non-^{17}O-enriched Na(MW) glass (Figure 8.20) shows features comparable with the standard alkali borosilicate samples [1,3,15]. Akin to previous studies [1,11,15] the spectrum consists of two regions; region 1: 400-1000 cm^{-1} and region 2: 1000-1800 cm^{-1}. Region 1 contains peaks from the two MRO reedmergnerite and danburite units, at approximately 500 cm^{-1} and 630 cm^{-1} respectively, with a smaller peak from boron tetrahedra at ~800 cm^{-1}. Within region 2, a large asymmetric peak exists between 1000 cm^{-1} and 1300 cm^{-1} due to resonances from the different silicon Q^n units. Based on previous Raman measurements of borosilicate glasses, the positions of the three Q^n units are marked on Figure 8.20.

Quantitative peak fitting of the non-enriched Na(MW) Raman spectrum, give Q^3 and Q^4 fractions of 0.62±0.1 and 0.38±0.1 respectively, which agree within error with the Q^3 fraction obtained for MW using ^{29}Si MAS NMR (0.57 ± 0.07) [1]. Both qualitative and quantitative details from the spectrum give confidence to the method of glass production of these sol-gel samples.

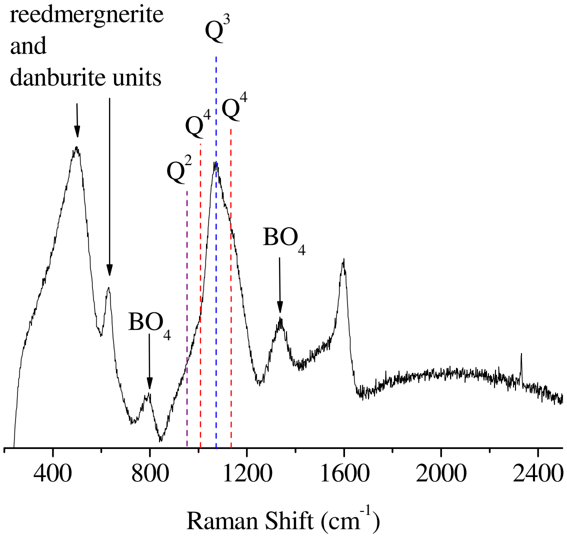

Figure 8.20 *Raman spectrum of the non-enriched sodium-borosilicate glass.*

The Raman spectra for the Cs(MW), AlNa(MW) and LaNa(MW) samples (Figure 8.21) show limited similarity with the Raman spectra typically observed from both alkali borosilicate glasses and crystals of previous studies [1,3,15] and from the non-^{17}O enriched Na(MW) glass (Figure 8.20). The most common similarity in the Raman spectra of these three samples and that observed in Figure 8.20, are the two peaks observed at ~1344 cm^{-1} and 1595 cm^{-1} (marked on Figure 8.21 by dashed lines); the first of which is identified as being from BO_4 units with the samples. It is also observable in all Raman spectra, bar that for the Na(MW) glass, that peaks exist in varying positions throughout the region 800-1200 cm^{-1}, which is typically the region across which Raman peaks from silicon Q^n units occur [11,16]. It must also be noted however that the Raman spectra for the Na(MW) and Na(MW)' glasses are not comparable and the reason for this cannot currently be explained.

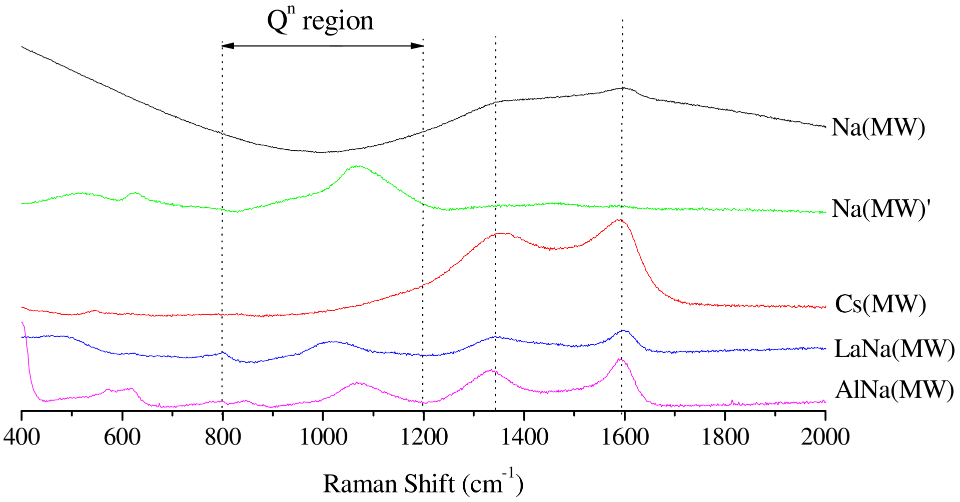

Figure 8.21 *Raman spectra for the four ^{17}O enriched borosilicate compositions. Peaks from silicon Q^n units are observed across the region 800-1200 cm^{-1}, with additional peaks common in the Raman spectra of borosilicates found at ~1344 and 1595 cm^{-1}.*

8.4 Summary

Four ^{17}O-enriched modified sodium borosilicate glasses and one caesium-borosilicate crystal were successfully manufactured using standard alkali carbonates and oxides combined with $Si^{17}O_2$ obtained from hydrolysing silicon tetrachloride with 20 % enriched $H_2{}^{17}O$ in a nitrogen atmosphere. Two *modified* sodium borosilicate glasses were produced, containing relatively small additions of Al_2O_3 (0.95 mol%) and La_2O_3 (1.68 mol%), in quantities comparable to those used in the standard mixed-alkali borosilicate glasses of this study.

Both XRD and thermal analysis measurements gave confidence in the manufacturing route used to produce the ^{17}O-enriched compositions, based on comparable results to standard borosilicate glasses in this study. TG measurements also gave results comparable to those obtained from the standard modified alkali borosilicates in the remainder of this study, with significant mass-losses observed at ~1000^{o}C and above.

^{11}B MAS NMR measurements on the borosilicate compositions showed N_4 to differ from that predicted by the Dell model [10], with N_4 being greater than the Dell model [10] for the Cs(MW), Na(MW) and AlNa(MW) compositions; due to atmospheric moisture absorbed during sample preparation. For the LaNa(MW) glass however, the resolved N_4 fraction is significantly lower than that predicted, due to the loss of alkali borate/silicate material from its melt at the stage of sample manufacture, which is supported by TG results in this study and other studies [3]. Confusingly, although the ^{11}B MAS NMR N_4 measurement on the LaNa(MW) glass clearly shows a strong deviation from that expected by initial composition, suggesting a severe change in R from that originally planned, density and EDX measurements are consistent with nominal composition. From EDX, the total cation to silicon (atomic %) ratios from experiment and theory were found to be 0.69 and 0.77 respectively – the difference being within acceptable limits for EDX measurements.

^{29}Si MAS NMR measurements on the five compositions indicate that Q^4, Q^3 and some Q^2 units are present.

Importantly, ^{17}O MAS- MQMAS- and DOR-NMR measurements show the presence of various BO and NBO environments whose quantities depend on glass composition. This supports the previous findings, that the addition of relatively small (< 2 mol%) quantities of these oxides to the alkali borosilicate base-glass MW results in significant changes to the resultant glass structure and thermal character [3,7]. Both MQMAS- and DOR-NMR have been used quantitatively in resolving the fraction of NBO and BO units in the Na(MW) glass, with DOR, despite being experimentally challenging, giving better resolution and simpler quantification.

8.5 References

[1] B. G. Parkinson, D. Holland, M. E. Smith, A. P. Howes, and C. R. Scales, *J. Non-Cryst. Solids* **351** (2005) 2425-2432.

[2] J. M. Roderick, *PhD Thesis, Warwick University* (2001).

[3] B. G. Parkinson, D. Holland, M. E. Smith, A. P. Howes, and C. R. Scales, *J. Non-Cryst. Solids* **353** (2007) 4076-4083.

[4] R. C. Weast, *Handbook of Chemistry and Physics*, 55 ed. (CRC Press, 1974).

[5] J. M. Roderick, D. Holland, A. P. Howes, and C. R. Scales, *J. Non-Cryst. Solids* **293-295** (2001) 746-751.

[6] L.-S. Du and J. F. Stebbins, *J. Phys. Chem.* **B, 107** (2003) 10063-10076.

[7] B. G. Parkinson, D. Holland, M. E. Smith, A. P. Howes, and C. R. Scales, *J. Phys.: Condens. Matter* **19** (2007).

[8] L.-S. Du and J. F. Stebbins, *Chem. Mater.* **15** (2003) 3913-3921.

[9] J. M. Roderick, D. Holland, and C. R. Scales, *Phys. Chem. Glasses* **41** (6) (2000) 392-396.

[10] W. J. Dell, P. J. Bray, and S. Z. Xiao, *J. Non-Cryst. Solids* **58** (1983) 1-16.

[11] B. G. Parkinson, D. Holland, M. E. Smith, C. Larson, J. Doerr, M. Affatigato, S. A. Feller, A. P. Howes, and C. R. Scales, *J. Non-Cryst. Solids* **Accepted, awaiting publication** (2007).

[12] J. A. Abys, D. M. Barnes, S. A. Feller, G. B. Rouse, and W. M. Risen Jnr, *Material Research Bulletin* **15** (1980) 1581-1587.

[13] J. F. Stebbins, S. Zhao, S. K. Lee, and J. V. Oglesby, *J. Non-Cryst. Solids* **293-295** (2001) 67-73.

[14] L.-S. Du and J. F. Stebbins, *J. Non-Cryst. Solids* **351** (2005) 3508-3520.

[15] W. L. Konijnendijk and J. M. Stevels, *J. Non-Cryst. Solids* **20** (1975) 193-224.

[16] P. McMillan, *Am. Mineral.* **69** (1984) 622-644.

Chapter 9

9 Conclusions and Further Work

9.1 Introduction

This chapter summarises the conclusions made from the results chapters, 6 to 8. Finally, a number of suggestions are made for further work that would both complement and extend the work carried out in this study.

9.2 Characterisation of the Modified Mixed-Alkali Borosilicate System

9.2.1 Introduction

A range of modified mixed-alkali modified borosilicate glasses were made based on the base-glass composition (MW) used by BNFL in the vitrification of high level nuclear waste (HLW). Four new initial base-glass systems were made by adding either aluminium oxide (0.95 mol% Al_2O_3), lanthanum oxide (1.68 mol% La_2O_3) and magnesium oxide (2.55 and 10.2 mol% MgO) in quantities realistic to their quantity in HLW. Caesium oxide was then added to each base-glass in increasing quantities (0 to 9.66 mol% Cs_2O) to investigate the problem of caesium-volatilisation at high temperature. In order to study this problem a variety of different thermal and structural techniques have been employed in for the form of density, differential thermal- and thermogravimetric-analysis, mass-loss, nuclear magnetic resonance and Raman spectroscopy measurements.

9.2.2 Thermal and Structural properties and their relationship to Volatilisation

The addition of Cs_2O, coupled with the initial introduction of one of three oxides; Al_2O_3, La_2O_3 or MgO to the mixed-alkali borosilicate base-glass MW, is shown to affect dramatically both the thermal and structural properties of each resultant glass system.

All four systems are shown to form glasses readily, within the limits of detection, highlighting the important reliability of these compositions to form amorphous structures given a variety of oxide loads [1-3]. Both the glass transition- and melt-temperatures are shown to be dominated by the addition of Cs_2O, where it is thought the smaller heat of formation of Cs_2O, compared to the remaining oxides, leads to weaker bonds within the glass structure [1].

Similarly, density measurements are also dominated by the presence of Cs_2O, with the linear increase in density due to the relative high-density of Cs_2O compared to the other oxides. Although both Al_2O_3 and La_2O_3 possess relatively high densities, their quantities in the respective systems are small compared to the quantity of Cs_2O added. Again, molar volume calculations also show a linear increase as a function of Cs_2O, with the glass structure expanding to accommodate the large Cs^+ ions added.

^{11}B MAS NMR measurements show the fraction of four-coordinated boron (N_4) to increase as a function of Cs_2O or R, the ratio of alkali oxide to boron oxide [1,2]. Compared to the original caesium-sodium-lithium borosilicate glass system from a previous study [4], N_4 fractions for the four new glass systems are lower, indicating the preferential association of alkali species with the additive or with the silicate- rather than the borate-network.

The fitting of two peaks under the BO_4 region of the ^{11}B MAS NMR spectrum has enabled the fraction of two medium-range order (MRO) units present in all the glass systems to be calculated [2]. These two MRO structures, reedmergnerite and danburite, are borosilicate mineral-like units containing B_4 sites with different next-nearest neighbour (NNN) arrangements. Reedmergnerite contains B_4 surrounded by four silicon sites, with danburite shown to contain B_4 surrounded by three silicon sites and one further boron site. For Al_2O_3- and La_2O_3-containing systems the fraction of danburite was found to increase and for MgO-containing glasses decrease, as a function of Cs_2O. The increasing presence of danburite units with B_4-B_4 bonds is particularly interesting and significant since this bond is energetically less stable.

^{29}Si MAS NMR measurements have been used to resolve the fraction of silicon Q^3 units, which increases as a function of Cs_2O content in all four systems [1-3]. The mass-loss % for all four systems increases linearly as a function of Q^3 (Figure 9.1) [1]. However, the rate of increase differs, depending on fraction of danburite present, being lower for the MgO-containing glasses compared to the Al_2O_3- and La_2O_3-containing systems [1]. This represents progress from the previous study by the author [4] where it was concluded that volatilisation depended solely on the silicate network, whereas now it becomes clear that the increasing presence of B_4-B_4 (in danburite units) also assists in the formation of volatilisation from the glass.

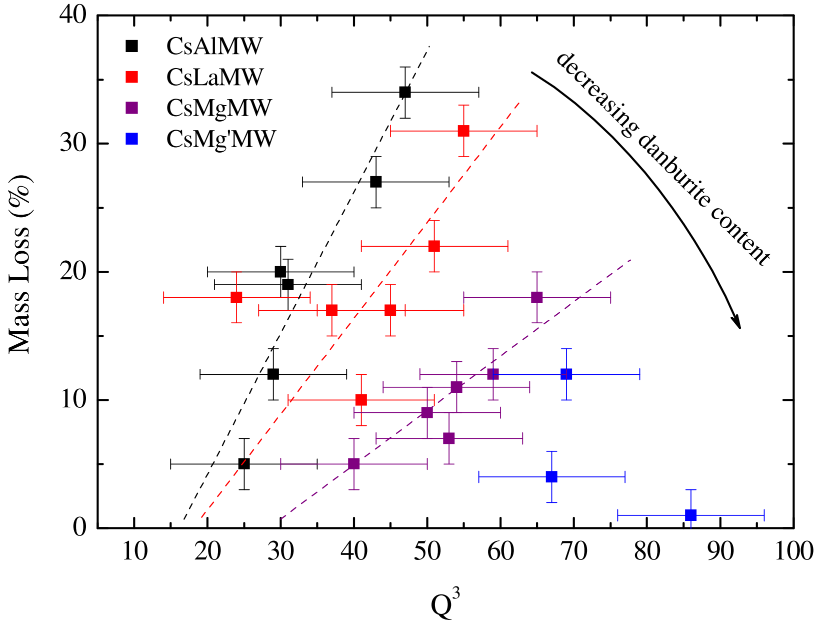

Figure 9.1 *Mass-loss measurements from Chapter 6 as a function of resolved Q^3 % [1]. Arrow indicates decreasing danburite population in glass resolved from ^{11}B MAS NMR. Note: Dashed lines are a guide to the eye.*

Based on N_4 and Q^3 measurements from ^{29}Si and ^{11}B MAS NMR, the fraction of Q^4 units *not* in MRO units has been calculated and shown to decrease as a function of R [2]. This equates to the addition of Cs_2O reducing the number of non-MRO Q^4 units, converting them into non-MRO Q^3 units and leading to greater volatilisation of material at high temperature.

Raman spectroscopy has been used to quantify silicate units, as well as supporting the presence of MRO units in all the glasses [2,3]. Resonances from borate groups are not typically observed in any of the Raman spectra. Quantitative measurements of the silicon Q^3 units were made possible using the technique outlined by McMillan *et al.* [5] which peak fitted to the region between ~900-1100 cm^{-1}. For all but the CsMg'MW glass system, within error, the Q^3 fraction resolved from Raman spectroscopy compares well with values from ^{29}Si MAS NMR [1-3], providing a alternative route for obtaining information on the silicate network when

NMR is not possible, i.e. when the presence of paramagnetic species common in HLW, renders NMR difficult or impossible.

9.2.3 Composition and Structural details of Volatilised Material

Compositional measurements of the volatile species, although limited to *qualitative* EDX measurements, (because boron and lithium cannot be measured quantitatively with EDX), show that the oxide composition of the volatile species is largely independent of the oxide addition [1]. Results (Figure 9.2) show the volatile species to contain caesium, sodium, boron and silicon suggesting the composition to be mixed-alkali borosilicate in form [1]. Studies by Asano *et al.* [6-8] and Bonnell *et al.* [9] found the vapour composition to be alkali (meta-)borate in form, devoid of any silicate groups, however these measurements were typically carried out at temperatures lower (< 1000^{o}C) than that used in this study. Mass spectroscopy measurements carried out by Archakov *et al.* [10] at higher temperatures (1200-1800^{o}C) than those used in the Asano and Bonnell studies (< 1000^{o}C) found silicon to be present in the evolved vapour. Hence, on comparison with the work by Archakov *et al.* [10], at the temperature (1000^{o}C) used in this current study by the author, it is likely that the vapour species formed also contained both alkali borate *and* alkali silicate groups, rather than predominantly alkali borosilicate groups, which in the previous study [4] was originally thought to be the case. Raman measurements of the volatilised deposits support this result, showing the presence of a variety of alkali borate and alkali silicate groups, based on comparisons with other Raman borate and borosilicate studies [11,12].

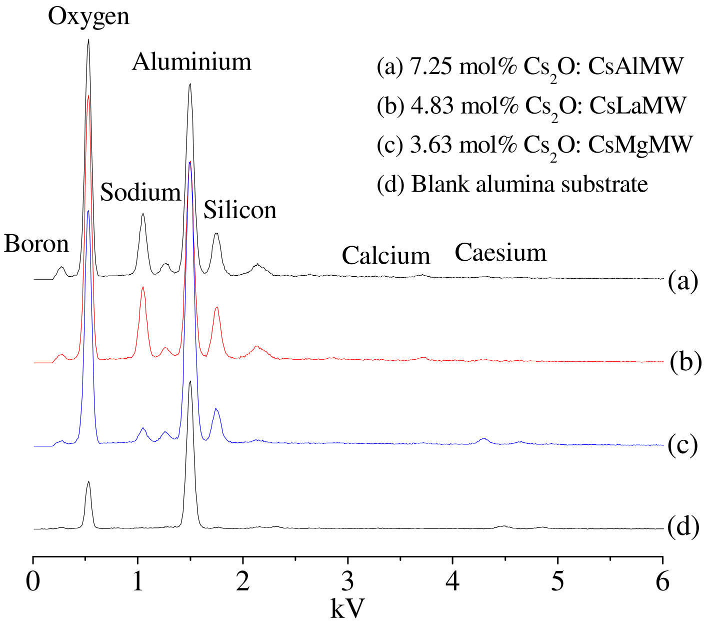

Figure 9.2 *EDX spectra of three selected deposits from volatilisation mass-loss experiments. (a) 7.25mol% Cs_2O, CsAlMW, (b) 4.83 mol% Cs_2O CsLaMW, (c) 3.63 mol% Cs_2O CsMgMW and (d) blank alumina substrate [1].*

9.3 Characterisation of the Oxygen-17 Enriched Modified Alkali Borosilicate System

9.3.1 Introduction

Sodium- and caesium-borosilicate (Na(MW) and Cs(MW) respectively), sodium-aluminoborosilicate (AlNa(MW)) and sodium lanthanum-borosilicate (LaNa(MW)) samples, with comparable compositions to those glasses in the main of this study, were made with enriched quantities of ^{17}O. This enabled the study, using ^{17}O MAS and MQMAS NMR, of the varying oxygen environments within these glasses, which combined with ^{11}B and ^{29}Si MAS NMR and density measurements allowed further structural information to be obtained. This was then compared with thermal analysis measurements to assist in attaining a clearer relationship between structure and volatilisation of material from borosilicate glasses.

9.3.2 General Physical and Thermal Characteristics

A single batch of ^{17}O-enriched SiO_2 (~1.3 g) powder was successfully made using a hydrolysis route outlined by Abys *et al.* [13], using 20 % ^{17}O-enriched H_2O.

Manufacture of $Si^{17}O_2$ rather than $B_2{}^{17}O_3$, was the more beneficial route to undertake due to the greater quantity of SiO_2 compared to B_2O_3 (K=3.2) in these glasses. From this single batch of $Si^{17}O_2$ powder and the compositionally appropriate alkali carbonates and oxides, five ^{17}O-enriched borosilicate samples were made under non-oxidising melt conditions, to limit the amount of oxygen exchange. Resultant samples were found to be black/dark grey in appearance due to the retention of carbon, from the initial alkali carbonate powders, upon quenching.

Using X-ray diffraction, all of the samples, apart from the Cs(MW) sample, were found to be glassy, displaying typical broad diffraction peaks. The caesium borosilicate crystal was identified as having the composition Cs_2O-B_2O_3-$2SiO_2$, with R=1 and K=2; indicating the loss of alkali silicate material during the melt stage which reduced both R and K from the initial values of R=1.12 and K=3.22. This result was predictable given the initial high (~20 mol%) content of volatile Cs_2O in the sample. DTA revealed typically featureless traces, with a limited number of T_g and T_m resolved across the ^{17}O samples. TG showed different responses across the compositions, with the Na(MW), AlNa(MW) and LaNa(MW) glasses displaying results similar to the standard non-enriched glasses of this study, with mass-loss occurring at high (~1000-1300°C) temperature. Since Cs is not present in all but one of the samples, this supports the result observed in other volatilisation studies [6-10,14] that the presence of Cs in alkali borosilicate glasses is not essential for high-temperature volatilisation to occur.

9.3.3 Structural Characteristics from Density and NMR Spectroscopy

Density measurements showed the Na(MW), AlNa(MW) and LaNa(MW) glasses to have comparable densities to the non-enriched borosilicate glasses in the main part of this study. ^{11}B MAS NMR measurements gave results which differed from the main study, with the B_4 peak being broader, suggesting the presence of three, rather than two, B_4 sites. This was especially true for the Cs(MW) Cs_2O-B_2O_3-$2SiO_2$ crystal which displayed a broad asymmetric B_4 peak, strongly suggesting the presence of a B_4 site with 2B, 2Si next nearest neighbour environment – typical for a borosilicate composition with this value of K (=2). N_4 values for all but one sample (LaNa(MW)) were greater (> 0.70) than those predicted by the Dell model [15] suggesting the presence of further modifying species, in the form of H^+. The lower than predicted N_4 fraction for the LaNa(MW) glass is thought to be due to the volatilisation of alkali material at the melt stage of the glass. The presence of modifying H^+ species was supported by quantitative ^{1}H NMR which showed all the samples to have hydrogen contents of between 0.02-0.2 mol H per mol sample. It is thought that these H^+ species are collected at the melt stage of sample manufacture, rather than being residual hydrogen retained from the hydrolysis reaction used to make $Si^{17}O_2$. ^{29}Si MAS NMR also confirmed the presence of these H^+ modifying species with the presence of Q^2 units observed in ^{29}Si MAS NMR spectra - typically not observed in the previous ^{29}Si MAS NMR measurements in this study.

Crucially in this section of the study, one dimensional ^{17}O MAS NMR showed the clear presence of NBO and BO sites. 3Q ^{17}O MAS NMR gave further evidence of this with a strong presence of NBO sites, as well as BO in Si-O-Si and Si-O-B, and Si-O-Al and Si-O-La environments in the respective Al- and La-containing glasses. From the isotropic ^{17}O MAS NMR and DOR NMR spectra for the Na(MW) glass, the fraction of BO and NBO units were found to agree within error.

Together with the different trends in mass-loss observed in the DTA-TG measurements for these samples, and coupled with results from the main borosilicate glasses in the majority of this study, this ^{17}O NMR work again shows the large effect that the relatively small addition (< 2 mol%) of Al_2O_3 and La_2O_3 has on glass structure and thermal character. Further ^{17}O NMR work, in the form of DOR- rather than MQMAS-NMR, on these and other glasses in future studies, as a function of more systematic change in composition (i.e. as a function of Al_2O_3, La_2O_3, MgO or alkali oxide content), would be highly beneficial in obtaining a quantitative measure of the different NBO and BO sites,

9.4 Future Work

Although a considerable quantity of work has been carried out on a wide range of different borosilicate glasses, including those designed for applications in the nuclear industry, the amount of work focussed on the problem of volatilisation has been limited. Previous volatilisation studies used only relatively simple binary and ternary alkali borosilicate compositions. Expanding upon these compositions, as this study has initially aimed to do, using all available structural and thermal techniques, would be an obvious area of development to gain further knowledge and ability in limiting the unwanted volatilisation of material.

A useful measurement would be the effect of composition on viscosity as a function of temperature; and lowering the temperature at which adequate viscosity for pouring could be maintained would also potentially result in lowering the amount of volatilisation from the melt.

Determining the effect of varying K on volatility would have potential technological benefit, though there could be detrimental effects on other properties of the glass such as waste-loading ability, thermal properties, radiation and chemical resistance. The addition of further simulate-waste oxides, such as molybdenum, technetium and thorium [16] to MW, followed by the standard and structural) measurements would also be a highly beneficial piece of work.

As well as additions and expansions of the glass systems used in this and other studies, the application of more sophisticated complementary experimental techniques would also be of great assistance in this area of work for the nuclear industry. Although attempted during the course of this study, high temperature ^{11}B MAS NMR (a relatively infrequently applied NMR technique [17,18] given its potential benefits in understanding glass behaviour) was not successful in providing information on how changes to the glass structure affected the resulting thermal properties due to problems with experimental equipment. Applying this technique with the equipment soon to be available at Warwick University, not only retrospectively to glasses used in this study but to more complicated systems would provide a unique and important insight into the link between structure and thermal behaviour. If possible, since thermal properties (e.g. volatility) are affected by both modifier and network species, this would be carried out through high-temperature ^{11}B and ^{29}Si NMR, enabling changes in N_4 and Q^n fractions to be mapped as a function of temperature, with additional ^{6,7}Li and/or ^{23}Na NMR providing information on ion mobility as a function of temperature. Limited high temperature NMR work has already been carried out globally and so the successful development of this technique would be highly advantageous.

Similarly, the use of high-temperature Raman spectroscopy would also be an exciting development, especially through the further use of the quantitative Raman spectroscopy technique used in this study in obtaining measurements of the silicon Q^n units as a function of temperature, not only on ‘typical’ modified mixed-alkali borosilicate compositions, such as those used in this study, but on compositions with high (>1 mol%) of paramagnetic species such as iron and cobalt, commonly found in HLW, where any NMR is not possible.

It would be beneficial if future ^{17}O NMR work was carried out on more complicated mixed-oxide borosilicates, to identify the role of oxides in an amorphous material, where their behaviour (i.e. as modifiers or intermediates) is not fully understood. Initially this would be an expensive exercise, due to the high financial cost of producing ^{17}O-enriched borosilicate samples, but a great number of highly informative NMR experiments are possible, especially with the availability of DOR NMR at Warwick University.

9.5 References

[1] B. G. Parkinson, D. Holland, M. E. Smith, A. P. Howes, and C. R. Scales, *J. Non-Cryst. Solids* **353** (2007) 4076-4083.

[2] B. G. Parkinson, D. Holland, M. E. Smith, A. P. Howes, and C. R. Scales, *J. Phys.: Condens. Matter* **19** (2007).

[3] B. G. Parkinson, D. Holland, M. E. Smith, C. Larson, J. Doerr, M. Affatigato, S. A. Feller, A. P. Howes, and C. R. Scales, *J. Non-Cryst. Solids* **Accepted, awaiting publication** (2007).

[4] B. G. Parkinson, D. Holland, M. E. Smith, A. P. Howes, and C. R. Scales, *J. Non-Cryst. Solids* **351** (2005) 2425-2432.

[5] P. McMillan, *Am. Mineral.* **69** (1984) 622-644.

[6] M. Asano, T. Kou, and Y. Yasue, *J. Non-Cryst. Solids* **92** (1987) 245-260.

[7] M. Asano and Y. Yasue, *J. Nucl. Mater.* **138** (1986) 65-72.

[8] M. Asano, T. Kou, and Y. Mizuntani, *J. Non-Cryst. Solids* **112** (1989) 381-384.

[9] D. W. Bonnell, E. R. Plante, and J. W. Hastie, *J. Non-Cryst. Solids* **84** (1986) 268-275.

[10] I. Y. Archakov, V. L. Stolyarova, and M. M. Shultz, *Rapied Communications in Mass Spectrometry* **12** (1998) 1330-1334.

[11] B. N. Meera and J. Ramakrishna, *J. Non-Cryst. Solids* **159** (1991) 1-21.

[12] W. L. Konijnendijk and J. M. Stevels, *J. Non-Cryst. Solids* **20** (1975) 193-224.

[13] J. A. Abys, D. M. Barnes, S. A. Feller, G. B. Rouse, and W. M. Risen Jnr, *Material Research Bulletin* **15** (1980) 1581-1587.

[14] M. Asano and Y. Yasue, *J. Nucl. Mater.* **151** (1988) 181-188.

[15] W. J. Dell, P. J. Bray, and S. Z. Xiao, *J. Non-Cryst. Solids* **58** (1983) 1-16.

[16] R. K. Mishra, P. Sengupta, C. P. Kaushik, A. K. Tyagi, G. B. Kale, and K. Raj, *J. Nucl. Mater.* **360** (2007) 143-150.

[17] J. F. Stebbins and S. E. Ellsworth, *Journal of American Ceramics Society* **79** (9) (1996) 2247-2256.

[18] A. R. Jones, R. Winter, P. Florian, and D. Massiot, *J. Phys. Chem. B* **109** (2005) 4324-4332.

Appendix A

Abstracts of Publications

Effect of minor additions on structure and volatilisation loss in simulated nuclear borosilicate glasses

Journal of Non-Crystalline Solids 353 (2007) 4076–4083

B. G. Parkinson, D. Holland, M. E. Smith and A. P. Howes
Department of Physics, University of Warwick, Coventry, CV4 7AL, UK.
C. R. Scales
Nexia Solutions, Sellafield, Seascale, Cumbria, U.K.

Structural and thermal properties are reported for a range of caesium oxide-containing alkali borosilicate glasses, of the form $xCs_2O(100-x)ZMW$ ($0 < x < 10$), where ZMW represents a variety of simulated base-glasses. Glass densities increase and glass transition temperatures decrease with increase in caesium oxide concentration. Mass-loss from the melt is found to depend on composition in the same manner as the fraction of silicon Q^3 units, resolved from ^{29}Si MAS NMR, and is related to the presence of danburite medium-range order units, resolved from ^{11}B MAS NMR. Volatilisation is shown to occur even in the absence of caesium oxide and the mixed alkali borosilicate composition of the volatile species, evolved from the melt at high temperature, is independent of the starting composition of the glass.

The effect of oxide additions on medium range order structures in borosilicate glasses

Journal of Physics: Condensed Matter 19 (2007)

B. G. Parkinson, D. Holland, M. E. Smith and A. P. Howes
Department of Physics, University of Warwick, Coventry, CV4 7AL, UK.
C.R. Scales
Nexia Solutions, Sellafield, Seascale, Cumbria, U.K.

Boron-11 MAS NMR and Raman spectroscopies have been used to study four families of glasses**:** $xCs_2O(100-x)ZMW$, $(0 < x < 10)$ where ZMW represents the borosilicate glass MW to which oxides Z (Al_2O_3, La_2O_3 and MgO) are added such that, overall, $1.0 \leq R$ (= $[\text{modifier}]/[B_2O_3]$) ≤ 2.5; K (= $[SiO_2]/[B_2O_3]$) = 3.2. These glasses are related to the system used for the vitrification of high-level nuclear waste. The spectra reveal the presence of reedmergnerite and danburite medium-range order structural units in the glasses. The fraction of danburite units increases with caesium oxide addition when Al_2O_3 or La_2O_3 are present, and decreases when MgO is present.

Quantitative measurement of Q^3 species in silicate and borosilicate glasses using Raman spectroscopy

Journal of Non-Crystalline Solids (2007) (Awaiting Further publication details)

B. G. Parkinson, D. Holland, M. E. Smith, A. P. Howes
Department of Physics, University of Warwick, Coventry, CV4 7AL, UK.
C. Larson, J. Doerr, M. Affatigato, S. A. Feller
Physics Department, Coe College, Cedar Rapids, IA 52402, USA
C. R. Scales
Nexia Solutions, Sellafield, Seascale, Cumbria, CA20 8PG, UK

Raman spectroscopy has been used to measure the fraction of tetrahedral silicate units connected at three corners into the network (Q^3) in binary lithium silicate glasses and also in the more complex borosilicate glasses used for waste immobilisation. Agreement within experimental error was obtained with ^{29}Si MAS NMR measurements

of the same samples. Raman provides an alternative method of structural determination for silicon-containing glasses with a high content of paramagnetic species where NMR loses resolution. Analysis was performed on borosilicate glasses containing up to 11.98 mole % Fe_2O_3 and the Q^3 values obtained by Raman spectroscopy agree within error with the published ^{29}Si NMR results from borosilicate glasses containing the equivalent quantity of Al_2O_3.

Appendix B

Data

Summarised in these tables are the sample details and resolved data from thermal analysis, density, ^{11}B and ^{29}Si MAS NMR and Raman measurements. *Note: The silicon oxide to boron oxide ratio (K) for all glass compositions is 3.22.*

1.1 CsMW System

Sample	mol% Cs_2O	R	Molar Mass (g/mol)	ρ (1)	N_4 (2)	Danburite Fraction (2)	Reedmergnerite Fraction (2)	NMR Q^3 (3)	Mass Loss (±5%)	T_g (4)
Cs0MW	0.00	1.12	64.0	2.32	0.69	0.63	0.37	0.27	0	494
Cs2MW	2.42	1.26	73.6	2.40	0.70	0.60	0.40	0.33	4	478
Cs3MW	3.62	1.32	76.8	2.52	0.69	0.59	0.41	0.39	13	467
Cs4MW	4.83	1.39	83.3	2.47	0.70	0.59	0.41	0.43	22	463
Cs7MW	7.25	1.54	89.7	2.62	0.72	0.65	0.35	0.50	16	454
Cs9MW	9.66	1.70	64.0	2.65	0.75	0.58	0.42	0.58	13	453

Table 1

(1) ± 0.07 g/cm^3

(2) ± 0.02

(3) ± 0.1

(4) ± 10°C

1.2 CsAlMW System

Sample	mol% Cs_2O	R	Molar Mass (g/mol)	ρ (1)	N_4 (2)	Danburite Fraction (2)	Reedmergnerite Fraction (2)	NMR Q^3 (3)	Raman Q^3 (3)	Mass Loss (±5%)	T_g (4)
Cs0AlMW	0.00	1.07	64.5	2.38	0.66	0.66	0.34	0.25	0.30	5	499
Cs2AlMW	2.42	1.20	70.9	2.43	0.67	0.68	0.32	0.29	0.37	12	491
Cs3AlMW	3.62	1.27	74.0	2.47	0.68	0.68	0.32	0.3	0.32	20	489
Cs4AlMW	4.83	1.35	77.2	2.53	0.68	0.71	0.29	0.31	0.37	19	487
Cs7AlMW	7.25	1.49	83.5	2.66	0.68	0.74	0.26	0.47	0.38	34	477
Cs9AlMW	9.66	1.65	89.8	2.61	0.70	0.63	0.37	0.43	0.49	27	472

Table 2

(1) ± 0.07 g/cm^3

(2) ± 0.02

(3) ± 0.1

(4) ± 10°C

1.3 CsLaMW System

Sample	mol% Cs_2O	R	Molar Mass (g/mol)	ρ (1)	N_4 (2)	Danburite Fraction (2)	Reedmergnerite Fraction (2)	NMR Q^3 (3)	Raman Q^3 (3)	Mass Loss (±5%)	T_g (4)
Cs0LaMW	0.00	1.03	68.6	2.43	0.64	0.67	0.33	0.24	0.20	12	512
Cs2LaMW	2.42	1.17	74.8	2.40	0.66	0.67	0.33	0.37	0.29	19	503
Cs3LaMW	3.62	1.24	77.9	2.35	0.66	0.68	0.32	0.41	0.37	21	499
Cs4LaMW	4.83	1.31	81.0	2.45	0.67	0.66	0.34	0.45	0.34	21	496
Cs7LaMW	7.25	1.46	87.2	2.57	0.65	0.74	0.26	0.55	0.49	26	484
Cs9LaMW	9.66	1.62	93.4	2.68	0.65	0.74	0.26	0.51	0.57	33	476

Table 3

1.4 CsMgMW System

Sample Name	mol% Cs_2O	R	Molar Mass (g/mol)	ρ (1)	N_4 (2)	Danburite Fraction (2)	Reedmergnerite Fraction (2)	NMR Q^3 (3)	Raman Q^3 (3)	Mass Loss (±5%)	T_g (4)
Cs0MgMW	0.00	1.26	64.7	2.46	0.61	0.64	0.36	0.40	0.32	5	499
Cs2MgMW	2.42	1.40	71.0	2.49	0.62	0.63	0.37	0.50	0.43	9	486
Cs3MgMW	3.62	1.47	74.2	2.53	0.65	0.57	0.43	0.53	0.43	7	489
Cs4MgMW	4.83	1.54	77.3	2.57	0.65	0.59	0.41	0.59	0.52	12	487
Cs7MgMW	7.25	1.69	83.6	2.75	0.63	0.58	0.42	0.63	0.47	18	475
Cs9MgMW	9.66	1.85	89.9	2.66	0.68	0.56	0.44	0.54	0.58	11	474

Table 4

(1) ± 0.07 g/cm^3

(2) ± 0.02

(3) ± 0.1

(4) ± 10°C

1.5 CsMg’MW System

Sample Name	mol% Cs_2O	R	Molar Mass (g/mol)	ρ (1)	N_4 (2)	Danburite Fraction (2)	Reedmergnerite Fraction (2)	NMR Q^3 (3)	Raman Q^3 (3)	Mass Loss (±5%)	T_g (4)
Cs0Mg’MW	0.00	1.73	70.7	2.34	0.50	0.67	0.33	0.86	0.81	1	501
Cs2Mg’MW	2.42	1.88	76.9	2.45	0.49	0.68	0.32	0.67	0.84	4	491
Cs7Mg’MW	7.25	2.20	89.2	2.79	0.48	0.48	0.52	0.69	0.72	12	466

Table 5

(1) ± 0.07 g/cm^3

(2) ± 0.02

(3) ± 0.1

(4) ± 10°C

1.6 Reedmergnerite and Danburite Glasses

Note: The ratio of alkali oxide to boron oxide (R) for all reedmergnerite and danburite glasses is 1.0.

Sample Name	mol% Cs_2O Or Na_2O	K	Molar Mass (g/mol)	ρ (1)	N_4 (2)	NMR Q^3 (3)	Mass Loss (±5%)
Reedmergnerite (Sodium)	12.5	6.0	71.75	2.09	0.69	0.39	1
Reedmergnerite (Caesium)	12.5	6.0	94.53	2.69	0.66	0.39	4
Danburite (Sodium)	25.0	2.0	69.38	2.24	0.61	0.10	12
Danburite (Caesium)	25.0	6.0	129.25	2.83	0.66	0.10	12

Table 6

(1) ± 0.07 g/cm^3

(2) ± 0.02

(3) ± 0.1

(4) ± 10°C

Appendix C

Borosilicate Glass Compositional Details

Note: All glasses have a silicon oxide to boron oxide ratio (K) of 3.22.

Name	mol% SiO_2	mol% B_2O_3	mol% Na_2O	mol% Li_2O	mol% Al_2O_3	mol% Cs_2O	mol% Fe_2O_3	R
Cs0ALMW	60.03	18.39	10.43	10.19	0.95	0.00	0.1	1.07
Cs2ALMW	58.58	17.95	10.18	9.95	0.93	2.42	0.1	1.20
Cs3ALMW	57.86	17.73	10.05	9.82	0.92	3.62	0.1	1.27
Cs4ALMW	57.13	17.59	9.93	9.70	0.90	4.83	0.1	1.35
Cs7ALMW	55.68	17.06	9.67	9.45	0.88	7.25	0.1	1.49
Cs9ALMW	54.24	16.62	9.42	9.21	0.86	9.66	0.1	1.65

Table 1

Name	mol% SiO_2	mol% B_2O_3	mol% Na_2O	mol% Li_2O	mol% La_2O_3	mol% Cs_2O	mol% Fe_2O_3	R
Cs0LaMW	59.59	18.26	10.35	10.12	1.68	0.00	0.1	1.03
Cs2LaMW	58.15	17.82	10.10	9.87	1.64	2.42	0.1	1.17
Cs3LaMW	57.44	17.60	9.98	9.75	1.62	3.62	0.1	1.24
Cs4LaMW	56.71	17.38	9.85	9.63	1.60	4.83	0.1	1.31
Cs7LaMW	55.27	16.93	9.60	9.38	1.56	7.25	0.1	1.46
Cs9LaMW	53.84	16.49	9.35	9.14	1.52	9.66	0.1	1.62

Table 2

Name	mol% SiO_2	mol% B_2O_3	mol% Na_2O	mol% Li_2O	mol% MgO	mol% Cs_2O	mol% Fe_2O_3	R
Cs0MgMW	59.06	18.10	10.26	10.03	2.55	0.00	0.1	1.26
Cs2MgMW	57.64	17.66	10.01	9.79	2.49	2.42	0.1	1.40
Cs3MgMW	56.93	17.44	9.89	9.67	2.46	3.62	0.1	1.47
Cs4MgMW	56.21	17.22	9.77	9.54	2.43	4.83	0.1	1.54
Cs7MgMW	54.78	16.78	9.52	9.30	2.37	7.25	0.1	1.69
Cs9MgMW	53.36	16.35	9.27	9.06	2.30	9.66	0.1	1.85

Table 3

Name	mol% SiO_2	mol% B_2O_3	mol% Na_2O	mol% Li_2O	mol% MgO	mol% Cs_2O	mol% Fe_2O_3	R
Cs0Mg’MW	54.43	16.68	9.46	9.24	10.20	0	0.1	1.73
Cs2Mg’MW	53.11	16.27	9.23	9.02	9.95	2.42	0.1	1.88
Cs7Mg’MW	50.48	15.47	8.77	8.57	9.46	7.25	0.1	2.20

Table 4

Name	mol% SiO_2	mol% B_2O_3	mol% Na_2O	mol% Li_2O	mol% Cs_2O	mol% Fe_2O_3	R
Cs11MW	53.94	16.53	9.37	9.15	11.00	0.1	1.79
Cs13MW	52.73	16.16	9.16	8.95	13.00	0.1	1.93

Table 5

Appendix D

^{11}B MAS NMR Fits

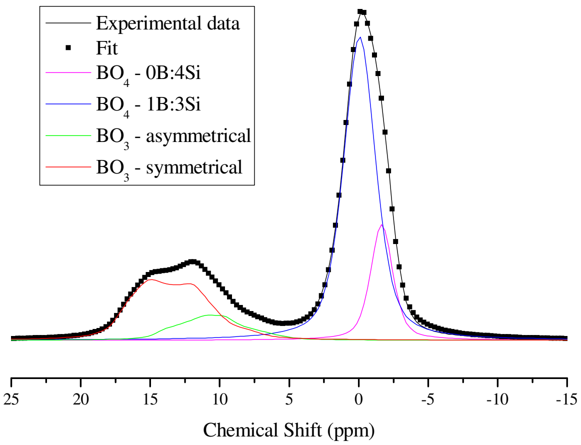

Figure 1 Cs0AlMW

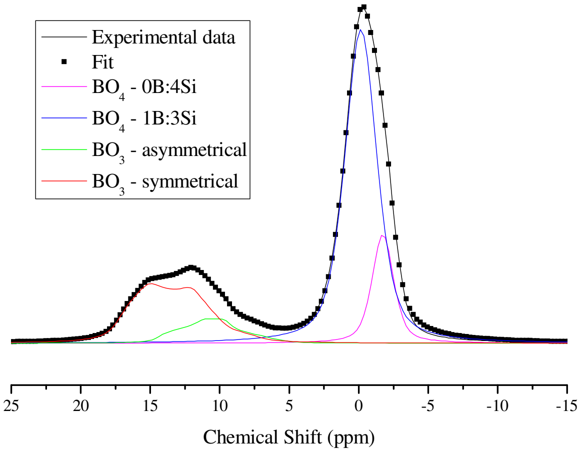

Figure 2 Cs2AlMW

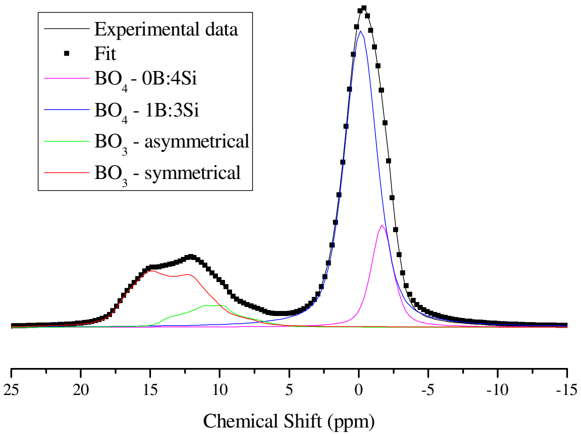

Figure 3 Cs3AlMW

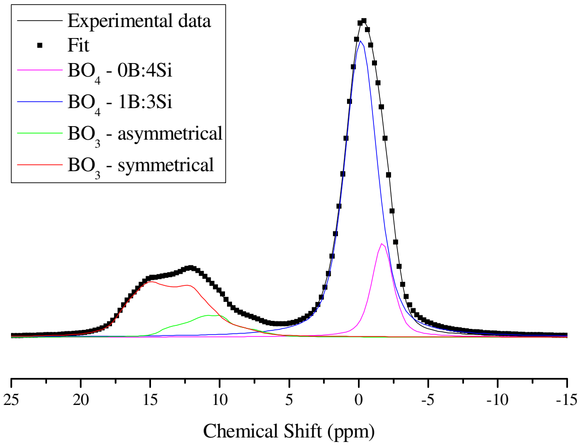

Figure 4 Cs4AlMW

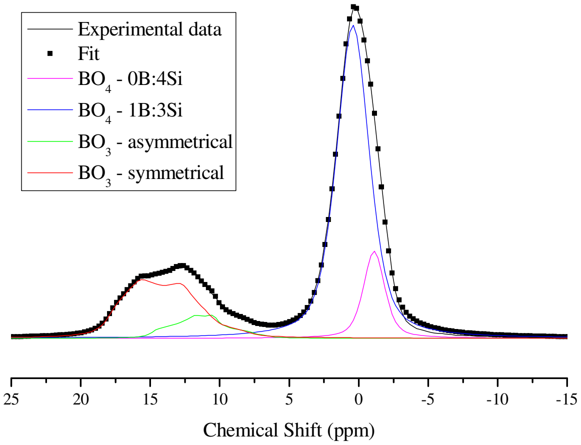

Figure 5 Cs7AlMW

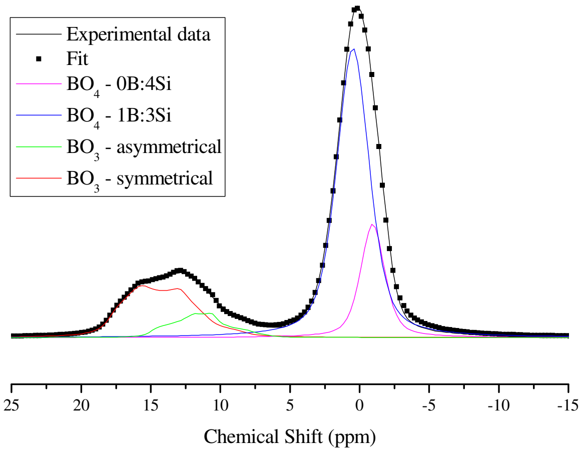

Figure 6 Cs9AlMW

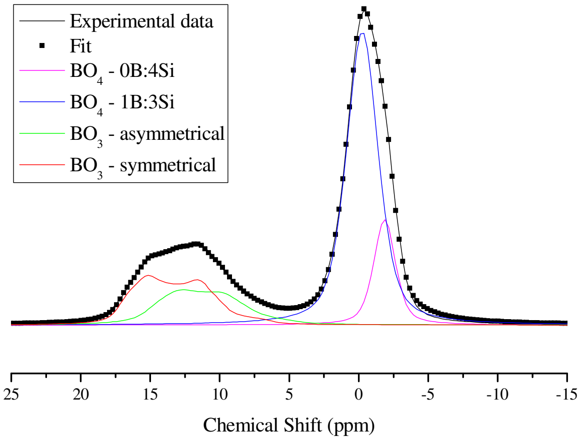

Figure 7 Cs0LaMW

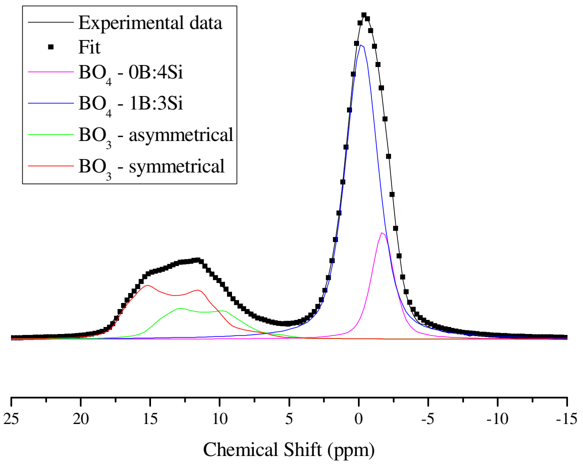

Figure 8 Cs2LaMW

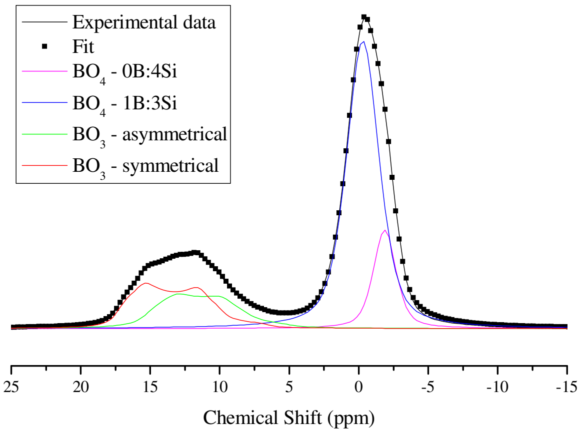

Figure 9 Cs3LaMW

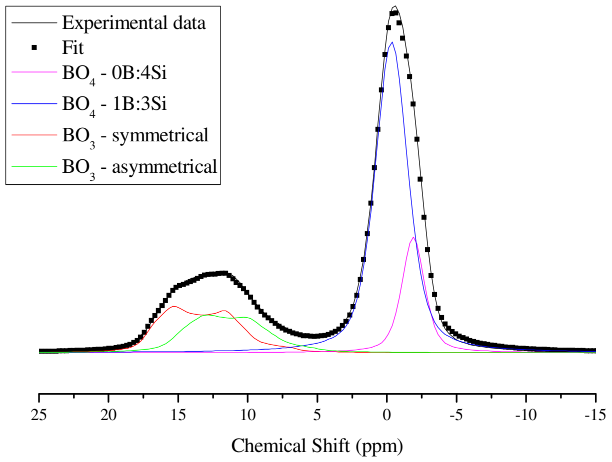

Figure 10 Cs4LaMW

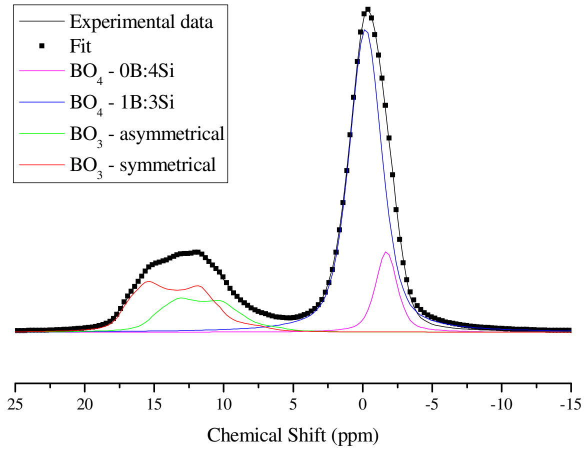

Figure 11 Cs7LaMW

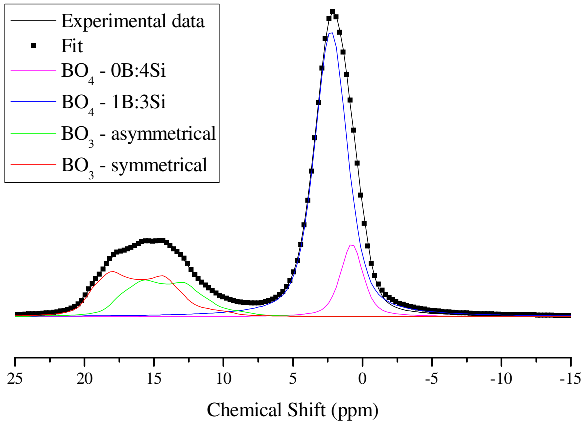

Figure 12 Cs9LaMW

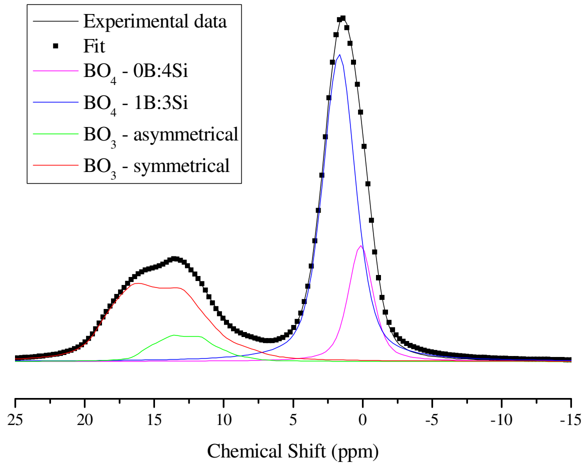

Figure 13 Cs0MgMW

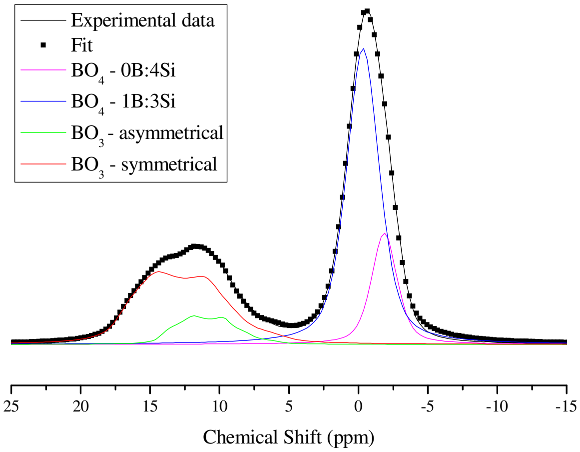

Figure 14 Cs2MgMW

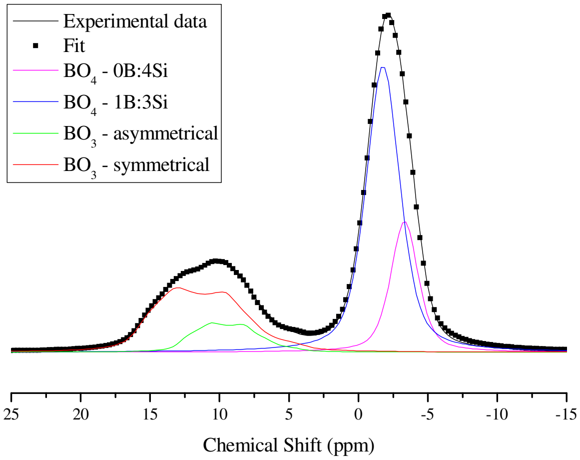

Figure 15 Cs3MgMW

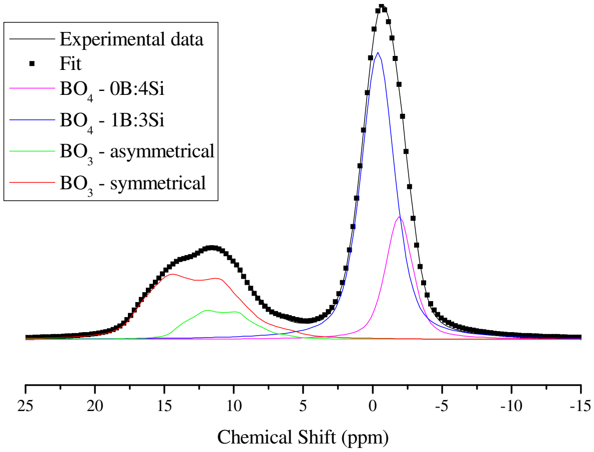

Figure 16 Cs4MgMW

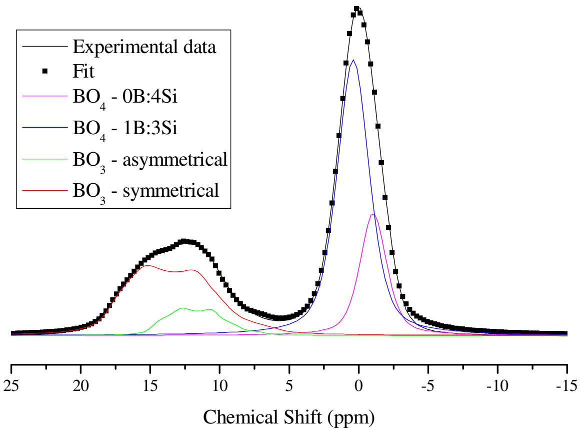

Figure 17 Cs7MgMW

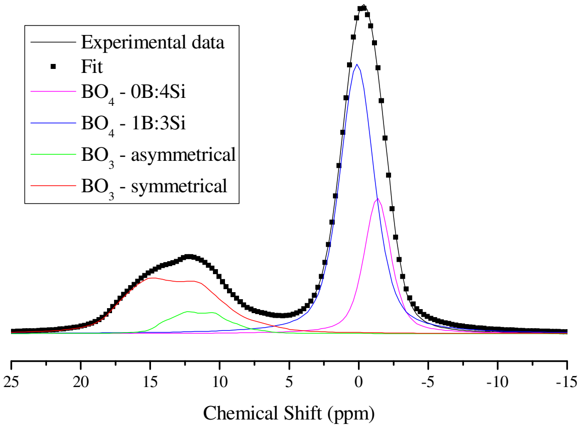

Figure 18 Cs9MgMW

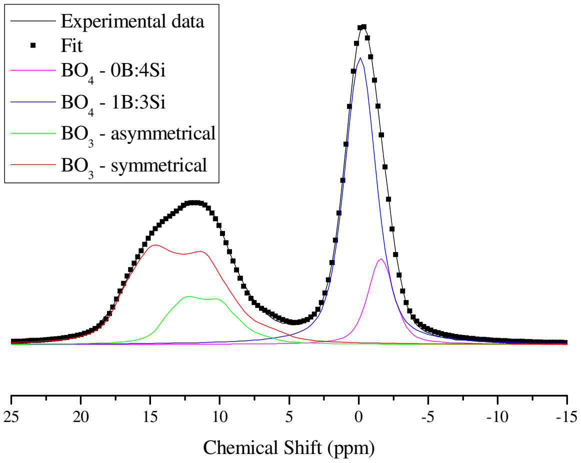

Figure 19 Cs0Mg'MW

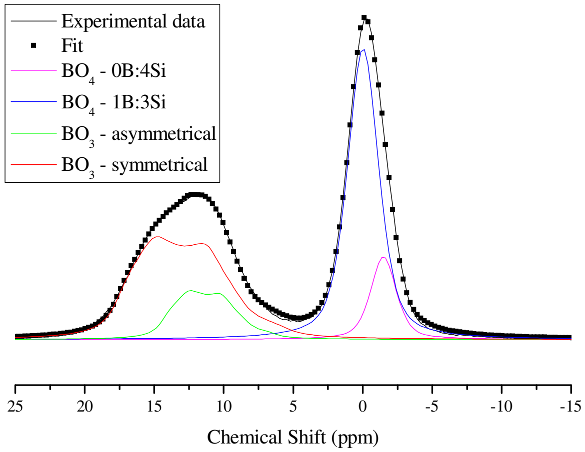

Figure 20 Cs2Mg'MW

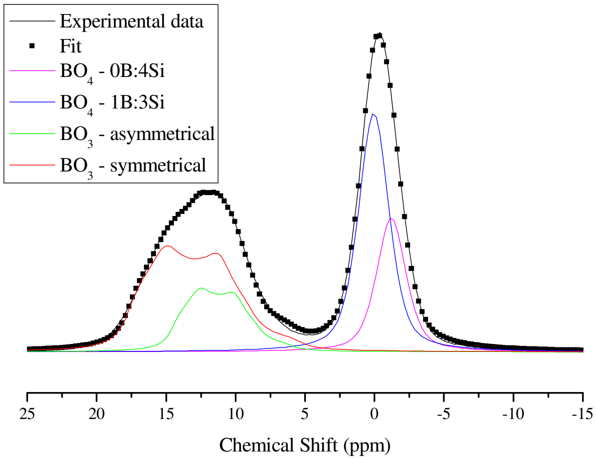

Figure 21 Cs7Mg'MW